universität wien

DISSERTATION

Titel der Dissertation

„Analysis of *Tle* genes in medaka embryonic development“

Verfasserin

DI (FH) Gerlinde Jung

angestrebter akademischer Grad

Doktorin der Naturwissenschaften (Dr. rer. nat.)

Wien, 2013

Studienkennzahl lt. Studienblatt:	A 091 490
Dissertationsgebiet lt. Studienblatt:	Molekulare Biologie
Betreuerin / Betreuer:	Univ. Prof. Dr. Erwin Heberle-Bors

“The most exciting phrase to hear in science, the one that heralds new discoveries, is not 'Eureka!' but 'That's funny...' ”

Isaac Asimov

ABSTRACT

Groucho/Transducine-like Enhancers of Split (Gro/TLE) belong to a conserved protein family of co-repressors. They mediate repression through interaction with various DNA-binding proteins by multiple molecular mechanisms, making them important players during developmental processes and in several diseases. The main part of this thesis focuses on their role in the embryonic development of medaka. For this, the function of Gro/TLE proteins was impaired by misexpressing their antagonist Amino-terminal Enhancer of Split (Aes) in heat shock inducible transgenic lines. The embryos developed smaller eyes that were tilted towards the midline where they fused to a cyclopic eye or were even lost in severe cases. To confirm these results individual members of this multigene family were knocked down. As expected, eye phenotypes like cyclopia appeared confirming the results of the misexpression experiments.

Tcf3 is an interaction partner of Gro/TLE and an important determinant of anterior-posterior development. In zebrafish, lack of *tcf3* function resulted in eye-less embryos. zThe single medaka *tcf3* gene is expressed in a pattern comparable to its zebrafish orthologous *headless* and *tcf3b*. Loss of function experiments with PNA and morpholino antisense molecules resulted in anophthalmia and showed an anterior shift of the expression markers *pax2*, *pax6* and *gbx1*. These results are in good agreement with zebrafish data. The phenotypes of gain of function experiments resembled those of *aes*-induced embryos. However, injection of *tcf3* versions lacking the Gro/TLE interaction domain showed strongly reduced eye phenotypes, indicating a role of Gro/TLE corepressors in this process.

The application of antisense molecules is an efficient way of gene inactivation in fish. Since microinjection generates varying results, methods with better reproducibility were explored. Compared to zebrafish, medaka have a substantially reduced sensitivity for chemicals (e.g. lithium chloride) and it is commonly assumed that this is due to the rigid chorion surrounding the embryo. Indeed, closer inspection of the chorion showed that larger molecules were not able to cross the chorionic barrier whereas small fluorescing tracer molecules readily passed into the perivitellin space. Interestingly, dechorionation only slightly improved the uptake into the embryos; instead inner membranes were identified as the limiting structure for diffusion. Adding detergents improved the diffusion effectively but also affected the internal distribution of the chemicals. Finally, electroporation could be established as a suitable method to enhance the uptake of small molecules into medaka embryos.

ZUSAMMENFASSUNG

„Groucho/Transducin-like enhancer of split“ (Gro/TLE) Proteine gehören zu einer konservierten Familie von Korepressoren. Durch die Interaktion mit DNA gebundenen Proteinen hemmen sie die Transkription auf mehrere verschiedene Arten. Dadurch hat Gro/TLE eine Schlüsselrolle in verschiedensten entwicklungsbiologischen Prozessen, aber auch in der Entstehung von Krankheiten. Der Hauptteil dieser Arbeit konzentriert sich auf die Rolle von Gro/TLE in der frühen embryonalen Entwicklung von Medakafischen. Für diese Analyse wurde die Funktion durch ihren Antagonisten, “Amino-terminal Enhancer of Split“ (Aes) in einer Hitze induzierbaren transgenen Fischlinie gehemmt. Die Embryonen entwickelten kleinere Augen, deren anteriores Ende nach medial kippte, wo es zu einem zyklopischen Auge zusammen wuchs. In schweren Fällen wurde die Augenentwicklung zur Gänze gehemmt. „Knock-down“ von einzelnen Mitgliedern dieser großen Genfamilie bestätigten die Ergebnisse.

Tcf3 ist einer der Interaktionspartner von Gro/TLE dem eine wichtige Rolle in der anterio-posterior Entwicklung zugeschrieben wird. Zebrafischembryonen ohne Tcf3 entwickelten keine Augen. Eine Expressionsanalyse des einzigen Medaka *tcf3* Gens zeigte ähnliche Muster wie eine Kombination der zwei Zebrafisch Orthologe *headless* und *tcf3*. Embryonen, deren *tcf3* Funktion durch PNA Moleküle oder Morpholino Oligonucleotide ausgeschaltet wurde, entwickelten kleine oder gar keine Augen. Zusätzlich war das Expressionsmuster der molekularen Marker *pax2*, *pax6* und *gbx1* anterior verschoben. Auch diese Beobachtungen waren vergleichbar mit Zebrafisch Resultaten. Die Überexpressionsphänotypen ähnelten wiederum denen der Aes-induzierten Embryonen. Injektionen mit *tcf3* Versionen, deren Gro/TLE Interaktionsdomäne fehlte, zeigten eine deutlich reduzierte Zahl an Phänotypen, ein weiteres Indiz dafür, dass Gro/TLE eine Rolle in diesem Prozess spielt.

Oft werden Antisensemoleküle für die Inaktivierung von Genen in Fischen verwendet. Sie werden mittels Mikroinjektion in den Embryo appliziert. Variierende Ergebnisse dieser Methode machen Alternativen mit höherer Reproduzierbarkeit interessant. Medakaembryonen reagieren weniger empfindlich auf Chemikalien (z.B. Litiumchlorid) als Zebrafische. Eine Erklärung dafür ist, dass die Embryonen durch eine starre Außenhülle, dem sogenannten Chorion, geschützt werden. Genauere Analysen des Chorions zeigten, dass große Moleküle diese Barriere wirklich nicht passieren konnten, kleine jedoch ungehindert bis in den Perivitellinraum vordringen konnten. Das Entfernen des Chorions brachte nur wenig Verbesserung. Es scheint deshalb, dass nicht, wie bisher angenommen, die harte Außenhülle, sondern ein weiteres Membransystem im Inneren des Embryos der Ausschlussgrund für viele Moleküle ist. Die Zugabe von Detergentien verbesserte die Durchlässigkeit wesentlich, hatte jedoch auch Auswirkungen auf die interne Verteilung der jeweiligen Chemikalien. Elektroporation dagegen steigerte nur deren Aufnahme, ohne ihre Verteilungseigenschaften zu ändern und stellt damit eine effiziente Methode für die Aufnahme kleiner Moleküle in Medaka Embryonen dar.

ACKNOWLEDGEMENT

No matter how much effort you put into your work, the success of any project depends largely on the suggestions and encouragement of many others. Therefore, I take this opportunity to express my deepest gratitude to the people who have been vital for the successful completion of this thesis.

I would like to show my greatest appreciation to FH-Prof. Dr. Thomas Czerny. Thank you for giving me the possibility to work in such a wonderful team. Thank you for your guidance and support, for your suggestions and brilliant yet sometimes crazy ideas and most of all for all the endless discussions that helped putting the pieces together. Thank you for chocolate Easter bunnies in the waterbath, scientific Christmas treasure hunts and the exhilarating tales of Rambi and the three Ice-Ladies.

I would also like to express my gratitude to the University of Applied Life Sciences FH Campus Wien for providing such a beautiful new laboratory and Univ. Prof. Dr. Erwin Heberle-Bors for being my advisor at the University of Vienna

Thanks to all the "Czernys": Viktoria, Lisi, Stefan, Laura, Adrian (Thomas), Adriane, Alfred, Andrea, Barbara, Baubi, Carmen, Chris, Christian, Christine, Fiona, Gemma, Kathi, Markus, Markus (Mäxchen), Markus Holzer, Narges, Noreen, Sebastian, Sylvia, Thomas H., Thomas P., Yvonne. Together we were a wonderful team. I would like to thank Baubi and Narges for introducing me to the topic and all the fish methods. To all my Diploma, Bachelor and Master students, I learned so much from you. Especially Laura, your motivation and enthusiasm were so inspiring.

I cannot express how much I thank my fellow labmates Viktoria and Lisi. We have had such a great time. Thank you for all the fun we have had in the last six years, for inspiring discussions, for helping hands, for unwavering support, for keeping me harmonious during challenging times and for the big C's (coffee, coke, cake and chocolate). No matter what, together we managed every project and every problem and made a lot out of so very little. Six years ago we were three labmates and now we are really great friends. GVL forever!

An old proverb says. "True friends can be counted on one hand". Well, luckily I need two hands to count those who were so (almost always) patient in all these years: Marion, Dani, Oliver, Manfred, Babsi, Mark, Sarah, Viktoria and Lisi.

I would like to thank my parents who are always there for me, who help whenever I need them and encourage me to do everything my way.

To Benny, my best friend and love of my life, who lived with this thesis as much as I did and who supported me in all these years without questioning. Now we will go on holidays, I promise!

THANK YOU!

TABLE OF CONTENTS

ABSTRACT ..... **I**

ZUSAMMENFASSUNG ..... **III**

ACKNOWLEDGEMENT ..... **V**

TABLE OF CONTENTS ..... **VII**

LIST OF FIGURES ..... **XI**

LIST OF TABLES ..... **XIII**

NOMENCLATURE ..... **XV**

1 INTRODUCTION **1**

1.1 MEDAKA (*ORYZIAS LATIPES*) 1

1.1.1 Medaka Biology *1*

1.1.2 Medaka as a Model Fish *2*

1.1.3 Chorion *3*

1.1.4 Medaka in Toxicity Testing *4*

1.2 GROUCHO/TLE CO-REPRESSORS 5

1.2.1 Structure *6*

WD-Repeat Domain 6

Q Domain 8

Non-Conserved Region 10

1.2.2 Aes *10*

1.2.3 Mechanisms of Gro/TLE-Mediated Repression *12*

1.2.4 The Regulation of Gro/TLE-Mediated Repression *13*

1.2.5 The Role of Gro/TLEs in Development *16*

1.2.6 The Role of Gro/TLEs in Diseases *17*

1.2.7 Tle And Aes in Medaka *18*

1.3 TCF TRANSCRIPTION FACTORS 19

1.3.1 Tcf3 ..... *21*

1.3.2 The Wnt/β-Catenin Pathway, Tcf/Lef and Gro/TLE *21*

2 MATERIALS AND METHODS **25**

2.1 MATERIALS 25

2.1.1 Laboratory Equipment *25*

2.1.2 Consumables *25*

2.1.3 Chemicals and Reagents *26*

2.1.4 Buffers and Solutions *28*

2.1.5 Enzymes *28*

2.1.6 Antibiotics *29*

2.1.7 Oligonucleotides *29*

2.1.8 Plasmids *29*

2.1.9 Cell Lines *31*

2.1.11 Medaka Stocks *32*

2.1.12 Software ... *32*
2.2 METHODS ... 32
2.2.1 DNA and RNA Methods ... *32*
Polymerase chain reaction (PCR) ... 32
DNA/RNA gel electrophoresis ... 33
DNA gel purification ... 33
Calf intestinal phosphatase (CIP) dephosphorylation ... 34
A-tailing ... 34
Ligation ... 34
Transformation ... 34
Mini-preparation of plasmid DNA ... 35
Midi-preparation of plasmid DNA ... 35
RNA probe synthesis for *in situ* hybridization ... 35
2.2.2 Protein Methods ... *36*
Antibody pre-adsorbtion for *in situ* hybridization ... 36
Dual luciferase assay ... 37
2.2.3 Cell Culture Methods ... *37*
Coating ... 37
Transfection ... 37
2.2.4 Fish Methods ... *38*
Fixation and dechorionation of medaka embryos ... 38
Microinjection of medaka embryos ... 38
Whole mount *in situ* hybridization in medaka ... 39
Heat shock ... 40
Diffusion and electroporation ... 40

3 RESULTS ... 41

3.1 ANALYSIS OF GRO/TLE IN MEDAKA EMBRYONIC DEVELOPMENT ... 41
3.1.1 Loss of Function Through a Dominant-Negative Approach ... *41*
A single Q-Domain Represses Gro/TLE Function ... 46
Aes Mediates the Repression of Tle1 and Tle4 ... 47
Characterization of the Aes/Q Phenotype ... 49
3.1.2 Knock Down With Antisense Morpholino Oligonucleotides ... *51*
3.2 CHARACTERIZATION OF MEDAKA TCF3 ... 58
3.2.1 Isolation and Expression of the Medaka Tcf3 Gene ... *58*
3.2.2 Morpholino Knock Down of the Medaka Tcf3 Gene ... *60*
3.2.3 Medaka Tcf3 Gain of Function ... *65*
3.3 ELECTROPORATION OF SMALL MOLECULES ... 69
3.3.1 Diffusion Into Medaka Embryos ... *69*
Fluorescein Reference ... 70
Fluorescein Uptake and Distribution in Medaka Embryos ... 71
Diffusion Kinetics ... 72
Diffusion Barriers within the Medaka Egg ... 72
Triton X-100 Affects the Membrane Behavior ... 74
3.3.2 Electroporation of Small Molecules Into Medaka Embryos ... *76*
Electroporation Improves the Uptake of Small Molecules into Medaka Embryos 76
Lithium Induces Deficiencies in Anterior-Posterior Development ... 77

4 DISCUSSION ... 79

4.1 ANALYSIS OF GRO/TLE LOSS OF FUNCTION IN MEDAKA ... 79
4.2 CHARACTERIZATION AND ANALYSIS OF MEDAKA TCF3 ... 83
4.3 ELECTROPORATION IMPROVES THE UPTAKE OF SMALL MOLECULES INTO MEDAKA EMBRYOS ... 85

5 REFERENCES.....89

APPENDIX I: TLE PROTEIN SEQUENCES.....103

APPENDIX II: SCIENTIFIC PUBLICATIONS.....105

VITA.....170

LIST OF FIGURES

Figure 1| Medaka fish..... 1

Figure 2| Morphological differences between male and female medaka..... 2

Figure 3| Medaka embryos are surrounded by a chorion.. 3

Figure 4| The structure of Gro/TLE proteins. 6

Figure 5| Schematic presentation of the Gro/TLE WD-repeat domain. 7

Figure 6| Gro/TLE tetramerization. 9

Figure 7| The structure of Aes/Grg5 proteins. 11

Figure 8| Mechanisms of Gro/TLE-mediated repression. 12

Figure 9| The regulation of Gro/TLE-mediated repression. 14

Figure 10| Schematic structure of human Tcf/Lef proteins and their splice variants. ... 20

Figure 11| The canonical Wnt/β-catenin signaling pathway..... 23

Figure 12| Standard PCR program using Phusion polymerase. 33

Figure 13| PCR cycler program for standard heat treatment. 40

Figure 14| Gro/TLE loss of function through a dominant-negative approach. 42

Figure 15| Schematic protein structure of Gro/TLE deletion mutants. 43

Figure 16| Overview of Aes/Q misexpression phenotypes. 46

Figure 17| Q-domain multimerization. 47

Figure 18| Schematic picture of the mammalian two-hybrid setup. 48

Figure 19| Two-hybrid analysis of Tle1 and Tle4 with Aes..... 49

Figure 20| Genotypic characterization of the Aes/Q-induced Gro/TLE loss of function phenotype..... 50

Figure 21| Gro/TLE antisense morpholino oligonucleotide design..... 52

Figure 22| Gro/TLE antisense morpholino-induced loss of function phenotypes. 53

Figure 23| Whole mount in situ hybridization experiments with Gro/TLE knock down embryos. 54

Figure 24| Analysis of the Gro/TLE knock-down phenotype at late gastrula. 56

Figure 25| Clustal alignment of medaka and zebrafish Tcf3 protein sequences. 59

Figure 26| Expression pattern of tcf3 during medaka embryonic development. 60

Figure 27| Tcf3 antisense morpholino oligonucleotide design. 60

Figure 28| Overview of tcf3 loss of function phenotypes during early medaka development. 61

Figure 29| Tcf3 antisense morpholino induced phenotypes. 62

Figure 30| Comparison of tcf3 loss of function with Gro/TLE morpholino and Aes/Q-induced phenotypes. 63

Figure 31| Genotypic analysis of the tcf3 loss of function phenotype. 64

Figure 32| Schematic protein structure of Tcf3 and Tcf3 mutants. 65

Figure 33| Ectopic otic vesicle formation in Tcf3 mutants lacking the GBS. 66

Figure 34| The tcf3 gain of function phenotype is enhanced in younger developmental stages. 67

Figure 35| Comparison of tcf3 loss of function with tcf3 gain of function phenotypes. .. 68

Figure 36| Fluorescein in beads. 70

Figure 37| Fluorescein reference. To quantify the amount of fluorescein within the embryos, a reference was calculated from the pixel intensities measured in the cellulose sulfate beads in Figure 36. 71

Figure 38| Fluorescein uptake during early medaka development. 71

Figure 39| Disrupted membrane systems of a dechorionated embryo. 73

Figure 40| Fluorescein uptake into medaka embryos after pre-incubation with de-ionized water. 74

Figure 41| Fluorescein uptake into medaka embryos after co-incubation with Triton X-100.. 75

Figure 42| Improvement of fluorescein uptake. 76

LIST OF TABLES

Table 1| List of consumables and companies they were purchased from. 25

Table 2| List of consumables and companies they were purchased from. 26

Table 3| List of chemicals and companies they were purchased from. 27

Table 4| List of enzymes. 28

Table 5| Oligonucleotides and their sequences. 29

Table 6| Vectors and inserts. 30

Table 7| Plasmids and their origin. 31

Table 8| Software and its origin/developer. 32

Table 9| Transfection mix for 2-hybrid transfection. 38

Table 10| Time of Proteinase K digestion. 39

Table 11| Dominant-negative effects of Tle1 containing C-terminal amino acid substitutions. 44

Table 12| Misexpression of the WRPW motif and the WD40-repeat domain have no effect on medaka embryonic development. 45

Table 13| Medaka heat-inducible transgenic lines. 46

Table 14| Statistical overview of marker gene expression in Aes/Q-induced Gro/TLE loss of function phenotypes. 50

Table 15| Statistical overview of the Gro/TLE antisense morpholino-induced loss of function phenotypes. 53

Table 16| Statistical overview of whole mount in situ hybridization experiments with Gro/TLE morpholino oligonucleotide injected embryos. 55

Table 17| Statistical overview of the Gro/TLE kock-down phenotype at late gastrula. 57

Table 18| Statistical overview of the genotypic analysis of tcf3 loss of function. 64

Table 19| Gain of function phenotypes of the medaka tcf3 gene. 66

NOMENCLATURE

Aes	Amino-terminal Enhancer of Split
AH	Amphipathic α-helix
AP	Anteroposterior
APC	Adenomatous polyposis coli
AR	Androgen receptor
BCIP	5-bromo-4-chloro-3-indolyl phosphate, p-toluidine salt
bHLH	Basic helix-loop-helix
C. elegans	*Caenorhabditis elegans*
cdc2	Cyclin-dependent protein kinase 2
CK1α	Casein kinase 1α
CK2	Casein kinase II
cm	Centimeter
CNS	Central nervous system
CtBP	C-terminal binding protein
DEPC	Diethylpyrocarbonate
*d*Gro	*Drosophila* Groucho
DMF	Dimethylformamide
DNA	Deoxyribonucleic acid
DV	Dorsoventral
Dvl	Dishevelled
E(Spl)	Enhancer of split
EDTA	Ethylenediaminetetraacetic acid
eh	Engrailed homology
ES cells	Embryonic stem cells
EtBr	Ethidiumbromide
GBS	Groucho binding sequence
grg	Groucho-related gene
Gro	Groucho
Gro/Tle	Groucho/Transducine-like Enhancers of Split
GSK3-β	Glycogen synthase kinase 3β
H3	Histone 3
HCl	Hydrogen chloride
HDAC	Histone deacetylases
hdl	Headless

HDRP	HDAC-related protein
HIPK2	Homeodomain-interacting protein kinase 2
HMG	High mobility group
HMGB	High mobility group binding protein
hrs	Hours
HSE	Heat shock elements
ICD	Intracellular domain
IPTG	Isopropyl β-D-1-thiogalactopyranoside
JNK	c-jun N-terminal kinase
KCl	Potassium chloride
kDa	Kilo Dalton
KH_2PO_4	Potassium dihydrogen phosphate
kHz	Kilo Hertz
Lef	Lymphoid enhancer factor
LiCl	Lithium chloride
LR	Left-right
LRP	Lipoprotein receptor-related protein
M	Molar
MAPK	Mitogen-activated protein kinase
Mb	Megabases
mg	Milligram
$MgCl_2$	Magnesium chloride
$MgSO_4$	Magnesium sulfate
MHB	Mid-hindbrain boundary
min	Minutes
ml	Milliliter
µl	Microliter
µm	Micrometer
µM	Micromolar
Na_2HPO_4	Disodium hydrogen phosphate
NaCl	Sodium chloride
$NaHCO_3$	Sodium bicarbonate
NaOH	Sodium hydroxide
NBT	Nitro blue tetrazolium
ng	Nanogram
N^{ICD}	Notch intaracellular domain
NLS	Nuclear localization signal
PARP-1	Poly(ADP-ribose) polymerase1
PCR	Polymerase chain reaction

PEG 6000	Polyethylene glycol
PEI	Polyethyleneimine
pePNA	Phosphonic ester side chain modified PNA
PFA	Paraformaldehyde
pmol	Picomol
PNA	Peptide nucleic acids
RNA	Ribonucleic acid
RTK	Receptor tyrosine kinase
SDS	Sodium Dodecyl Sulfate
SFRP	Secreted Frizzled Related Protein
Su(H)	Suppressor of Hairless
Tcf	
Tle	Transducine-like Enhancers of Split
TrCP	b-Transducin repeat containing protein
U	Units
V	Volt
WRE	Wnt response elements
ZI	Zona interna
ZP	Zona pellucida
めだか	me-da-ka
目	Eye
高	Big
°C	Degrees Celsius

1 INTRODUCTION

1.1 MEDAKA (*ORYZIAS LATIPES*)

Medaka is a rather small fish indigenous to India and the coastal regions of Southern China, Korea and Vietnam as far east as Japan. It is known by several names and the most common among them are medaka, killifish and ricefish. However, in Japan the most widespread name is medaka deriving from its physical appearance. The name is either depicted in syllabic alphabet めだか (me-da-ka) or in traditional writing 目高, where the ideogram 目 stands for "eye" and 高 meaning „big" and translated as "tiny fish with large eyes". The other two names characterize its habitat. A killifish is any oviparous ray-finned fish found in fresh or brackish water. On the other hand, the name ricefish describes its preferred natural habitat, the rice paddies of Southeast Asia.

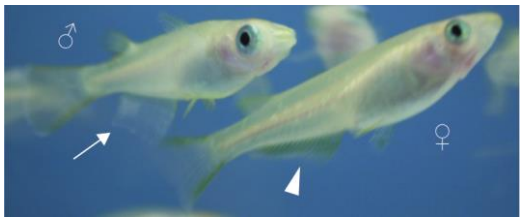

Figure 1| *Medaka fish.* Male (left) and female (right) medaka can be distinguished due to distinct differences in their anal fins. The male anal fin is parallelogram shaped (white arrow), whereas the female fin resembles a triangle (white arrowhead).

In the Edo period, in the seventeenth century, domestic breeding of medaka became very popular in Japan. During this time several natural color mutants were isolated. In 1850, Temminck and Schlegel were the first to describe medaka scientifically. They published its taxonomical characteristics under the name *Poecilia latipes* in Siebold's Fauna Japonica (reviewed by Wittbrodt *et al.*, 2002). Nearly sixty years later, in 1906, Jordan and Snyder renamed it into *Oryzias latipes* (Jordan *et al.*, 1906), a name based on the Latin word for rice (*Oryza sativa*). Since then, medaka became a very popular model organism in biological research. It was the first vertebrate in which crossing over between X and Y chromosomes was shown (Aida, 1921). Subsequently, scientists focused on pigmentation and sex determination: Y-linked inheritance was shown for the first time in any species (Aida, 1921), hormone induced sex-reversal in vertebrates was demonstrated (Yamamoto, T., 1958, 1975) and the first non-mammalian male-determining gene, *DMY*, was identified (Matsuda *et al.*, 2002; Nanda *et al.*, 2002).

1.1.1 MEDAKA BIOLOGY

Adult medaka (**Figure 1** and **Figure 2**) are approximately three cm long and males and females are easily distinguishable by the shape and size of the dorsal and anal fins (Yamamoto, T., 1975). The dorsal fin of male fish (**Figure 2A,C**) is usually longer than that of females (**Figure 2B,D**). It has a jagged edge with a cleft at the posterior margin (**Figure**

2A,C). The female anal fin has a triangle shape (**Figure 1** and **Figure 2B**), whereas the male fin is larger and parallelogram-shaped (**Figure 1** and **Figure 2A**). During mating, the female lays a cluster of up to 30 eggs per day, which are attached with filaments between the anal and pelvic fins (**Figure 2D**). Both fertilization and embryonic development occurs externally. The embryos are enclosed by a tough egg envelope, the chorion (**Figure 3**), which protects them from environmental hazards during development. The medaka chorion will be discussed later in chapter 1.1.3 (page 3). Depending on the temperature, the embryos hatch seven to ten days after fertilization and grow to sexual maturity within three months.

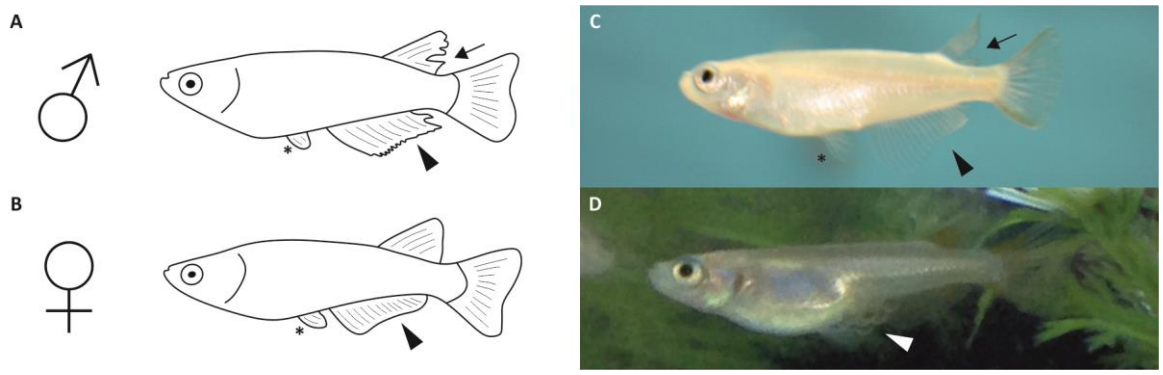

Figure 2| *Morphological differences between male and female medaka.* (A,B) Schematic drawing of medaka, (C,D) pictures of alive medaka. (A,C) Male medaka have a cleft in the posterior side of their dorsal fins (black arrow). (B,D) Female medaka have triangle-shaped anal fins. Egg clusters (white arrowhead) are attached to the belly between the anal (black arrowhead) and pelvic fins (asterisk). Adult fish are depicted in lateral view with anterior to the left.

1.1.2 MEDAKA AS A MODEL FISH

As mentioned before, medaka research has a long history in Japan. However, outside the Far East, another teleost fish, the zebrafish (*Danio rerio*), is far better known and favored as a vertebrate model. Only in the last decades medaka reached a certain degree of population among biologists, especially as a test system for environmental research and carcinogenesis studies (Ishikawa, T. *et al.*, 1975; Ishikawa, T. *et al.*, 1984; Hawkins *et al.*, 1985; Masahito *et al.*, 1989).

Even if medaka and zebrafish share many biological features, such as a short generation time, extra-uterine development and transparent embryos (**Figure 3**), medaka has, nevertheless, some advantages. First, compared to zebrafish, medaka are very hardy and highly resistant to fish diseases. Even if indigenous to a subtropical climate with seasonal temperature fluctuations between 16-22°C, it easily adapts to changes from 10-40°C. Embryos can even be kept at temperatures as low as 4°C for some time to slow down development, a feature that facilitates microinjection and transplantation studies as well as staging of developing embryos and the isolation of temperature-sensitive mutants. Furthermore, medaka tolerates a wide range of salinities because it is amphidromous, meaning that at it can be found in both fresh- and saltwater. Second, in addition to over 80 wild type strains, there a highly polymorphic inbred strains available as well as induced and spontaneous mutants (reviewed by Wittbrodt *et al.*, 2002; Naruse

et al., 2004). Finally, the medaka genome is relatively small. With a total length of 700.4 megabases (Mb) (Kasahara *et al.*, 2007) it has less than half the size of the zebrafish genome, which makes medaka even more attractive for genome analysis.

1.1.3 CHORION

In medaka, like in most animals, the embryo and the yolk are surrounded by an egg envelope (**Figure 3**). As there is no general terminology for this envelope, many different names, such as vitelline envelope, vitelline membrane, zona radiate and zona pellucida (ZP), have been used in literature. To avoid confusion, hereafter the term "chorion" will be used. The overall function of the chorion of animal eggs is to attract and activate spermatozoa and to block polyspermy. Once fertilized it protects the embryo against environmental (physical, chemical and biological) influences (Villalobos *et al.*, 2000).

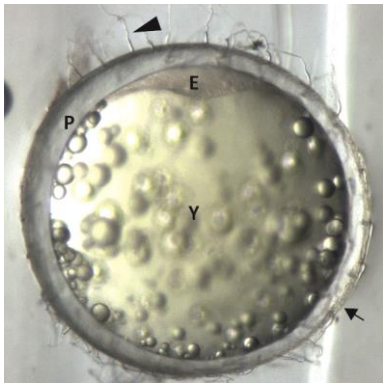

Figure 3| *Medaka embryos are surrounded by a chorion.* The embryo (E) and the yolk (Y) are surrounded by a transparent envelope, the chorion (black arrow), which is covered with attaching filaments (black arrowhead). (P), Perivitellin space. Embryo ate the 1-cell stage is depicted in lateral view, animal pole to the top.

The unfertilized medaka chorion consists of two layers. The thin outer layer is approximately 0.3 µm thick and it consists of a dense lamina and a fibrous coat. It is covered with attaching filaments and villi and the surface shows a honeycomb-like pattern. The inner layer is composed of twelve dense lamellae separated by eleven gaps with less density. Thus, the inner layer is much thicker, approximately 15 µm in a fertilized embryo, than the outer membrane (Yamamoto, M. *et al.*, 1975). It consists of two major Zona Interna (ZI) subunit glycoproteins, ZI-1,2 (74-76 kDa) and ZI-3 (49 kDa), both deriving from precursor proteins, called choriogenin (Yamagami, Kenjiro, 1972, 1973; Hamazaki *et al.*, 1987; Murata *et al.*, 1991; Murata *et al.*, 1993). The spawning female synthesizes the different choriogenins in the liver and transports them then via the blood stream to the ovary (Murata *et al.*, 1991; Murata *et al.*, 1993). Heterogenous ZI-1,2 derives from the precursors choriogenin H (Murata *et al.*, 1997) and choriogenin H minor (Sugiyama, H. *et al.*, 1998), while choriogenin L is the precursor of homogenous ZI-3 (Murata *et al.*, 1995). In addition to ZI-1,2 and ZI-3, a third protein (150 kDa) was reported to be present in the unfertilized chorion, however, this protein disappears once the egg is fertilized (Masuda *et al.*, 1991; Iwamatsu *et al.*, 1995).

The chorion has a single small pore, the micropyle, through which the sperm can enter and attach to the eggs plasma membrane. Cortical alveoli in the cytoplasm fuse with the plasma membrane, thereby releasing their content. This exocytosis seems to be induced by an increase of cytoplasmatic calcium and occurs in a wave-like manner, from the animal to the vegetal pole (Nakano, 1956; Ridgway *et al.*, 1977). In the same wave-like manner, the chorion contracts, except for the innermost layer which first swells before gradually contracting. As a consequence, the fragile chorion turns into a rigid structure, thereby becoming thinner which results in a gap between the embryo/yolk and the chorion, the perivitellin space (**Figure 3**) (Nakano, 1956). During chorion hardening ε-(γ-glutamyl) lysine isopeptide bonds form between the subunit proteins ZI-1,2 and ZI-3, mainly in the inner layer (Hagenmaier *et al.*, 1976; Ha *et al.*, 1997a). This crosslink is catalyzed by transglutaminase (Ha *et al.*, 1997b, 1998). Several other factors have been reported to support chorion hardening in fish embryos: oxidation of sulfhydryl groups in chorion proteins (Nakano, 1956; Ohtsuka, Eiji, 1960), mucopolysaccharides (Nakano, 1956), and environmental factors such as pH (Iwamatsu, 1984).

Once the medaka embryo has finished embryonic development it hatches from the chorion. According to classical Iwamatsu staging this occurs at stage 39 or after nine days, if bred at standard conditions (Iwamatsu, 2004). Hatching is a two-step process: first the inner layer of the chorion is digested by hatching enzyme and then the outer membrane is ruptured by excessive movement of the tail. The embryo produces the hatching enzyme *de novo* in hatching glands which are located in the pharyngeal wall (Yamagami, Kenjiro, 1981; Inohaya *et al.*, 1995). It consists of two metalloproteases, HCE (high choriolytic enzyme) (Yasumasu *et al.*, 1989b) and LCE (low choriolytic enzyme) (Yasumasu *et al.*, 1989a), which act together in choriolysis (Yasumasu *et al.*, 1988). HCE swells the inner layer of the chorion due to partial hydrolysis (Yasumasu *et al.*, 1989c) and LCE solubilizes it (Yasumasu *et al.*, 1989a). The outer layer remains undigested but is broken down mechanically by movement of the tail. Recently, Yasumasu *et al.* proposed a model for the structural change of the chorion during water hardening and choriolysis: during chorion hardening ε-(γ-glutamyl) lysine isopeptide bonds are formed between the N-termini of ZI-1,2 and ZI-3 which loop out from the ZP domain filaments. HCE cleaves specific sequences in these crosslinks, mainly in ZI-1,2, thereby loosening the tight interaction of the filaments which results in swelling of the inner layer of the chorion. Through this swelling LCE gains access to its preferred cleavage site which is located in the middle of the ZP domain (Yasumasu *et al.*, 2010).

1.1.4 MEDAKA IN TOXICITY TESTING

Besides for the study of developmental processes, small aquarium fish, such as medaka, are also very popular in toxicity testing. Toxicity test are important to evaluate the adverse effects of any chemical or biological substance on organisms and the ecosystem and mainly performed by animal experiments. Following massive criticism, testing of cosmetic and personal care products has been reduced over the last years. However, numerous chemicals, such as new pharmaceutical products and food additives, remain where animal tests are still necessary (reviewed by Lilienblum *et al.*, 2008). Programs like the OECD HPV (Organization for Economic Co-operation and Development High

Production Volume) or the European Union REACH (Registration, Evaluation, Authorization and Restriction of Chemicals) Initiative were initiated, regulating these tests and the chemical industry globally (reviewed by Braunbeck *et al.*, 2005; Scialli, 2008). Such regulations are important particularly with regard to ecotoxicology and environmental toxicology. In various countries the aquatic environment is used as a sink for waste disposal and pesticides and chemicals may travel long distances cross country borders (reviewed by Schwarzenbach *et al.*, 2006). However, these new regulations require extensive tests for most chemicals which increase the number of animal experiments even further.

Historically, acute and chronic fish toxicity testing plays an important role in ecotoxicology and aquatic toxicology as an economical alternative to the established animal systems. However, in conventional tests the endpoints are death or moribundity, which led to the controversial question whether fish are a replacement for mammals and birds because they may experience the same levels of pain and distress as other animals (Embry *et al.*, 2010). In the European Union, Directive 86/609/EEC regulates the use of animals in scientific experiments. Member states should reduce the number of animals to a minimum and avoid unnecessary pain, suffering and distress. An animal is characterized as any free-living, non-human vertebrate, including larvae. Excluded are foetal or embryonic forms (Council, 1986). Therefore, acute and chronic fish toxicity tests are more and more replaced by alternative methods such as the fish embryo toxicity (FET) test (Embry *et al.*, 2010; Strahle *et al.*, 2012). Newly fertilized eggs are exposed to a chemical for 48 hours and as endpoints coagulation of the embryos, aberrations of somite development and non-detachment of the tail from the yolk as well as lack of heartbeat are recorded (Lammer *et al.*, 2009). Furthermore, compared to conventional fish tests, FET allows the detection of substances which induce strong and minor toxicity (Nagel, R., 2002; Braunbeck *et al.*, 2005). It seems to be even more sensitive than in vitro tests performed with the permanent rainbow trout cell line RTG-2 (Lange *et al.*, 1995). Most FET tests have been conducted with zebrafish but inter-species comparison with fathead minnow and medaka showed comparable results and applicability for other species (Braunbeck *et al.*, 2005).

Economic husbandry, high fecundity, and the extra-uterine development of transparent embryos make fish an ideal organism for FET and their application in high throughput protocols (Yang *et al.*, 2009). Compared to zebrafish, one advantage of medaka is their relatively long embryonic development, which provides extended time for testing.

1.2 GROUCHO/TLE CO-REPRESSORS

The *groucho* (*gro*) gene family and related family members encode transcriptional co-repressors which are expressed ubiquitously and play an important role in developmental and some pathological processes (reviewed by Buscarlet *et al.*, 2007). It was first identified in a *Drosophila melanogaster* loss-of-function mutant and named after its phenotype: mutant flies display numerous patches of extra bristles above the eyes, resembling somewhat the bushy eyebrows of Groucho Marx (Lindsley *et al.*, 1968). Since then, several homologs in different organisms were identified with a somehow complicated nomenclature. In human and teleost fish usually the term *Transducin-Like*

Enhancer of split (*TLE*) is used. It derives on one hand from a structural similarity to the β subunit of transducin, a heterotrimeric G protein, and on the other hand from its adjacency to the *Enhancer of split* [E(Spl)] complex (Hartley *et al.*, 1988). More detailed characterization revealed that Gro proteins play a role in transcriptional repression and that they are not related to β-transducin, except for their structural similarities. However, homologs in mouse and rats are termed g*roucho-related-gene* (*Grg*) (Schmidt *et al.*, 1993; Mallo *et al.*, 1995) and *unc-37* is used for *Caenorhabditis elegans* (*C. elegans*) (Pflugrad *et al.*, 1997). To avoid further confusion, here after the term Gro/TLE will be used if the entire protein family is addressed and Tle if specifically referred to medaka.

1.2.1 STRUCTURE

Despite a different nomenclature and variable number, the primary protein structure of Gro/TLE family members is highly conserved throughout species. In general it consists of five domains, which are named based on their evolutionary conservation: Q, GP, CcN, SP, and WD-repeat domain. The amino-terminal and the carboxy-terminal end are remarkably conserved, whereas the central regions are less conserved (**Figure 4**).

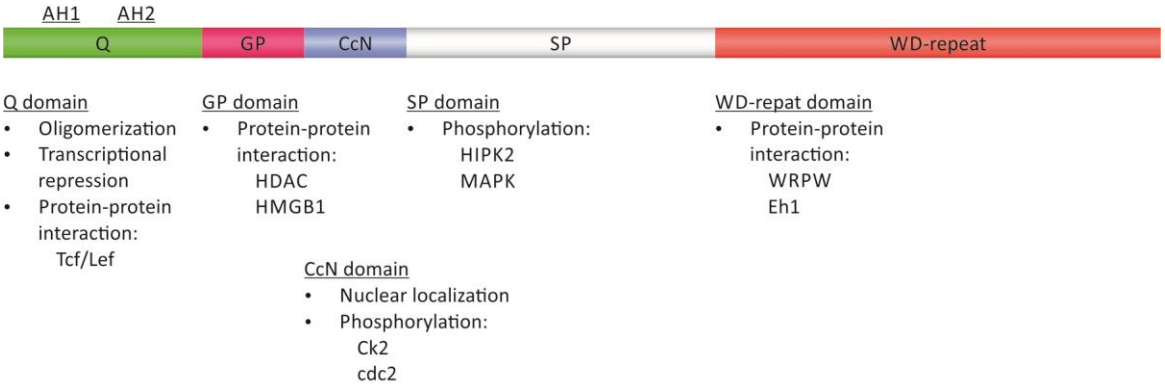

Figure 4| *The structure of Gro/TLE proteins.* Gro/TLE proteins consist of five conserved domains. The amino-terminal Q domain (green) contains two predicted amphipathic α-helices (AH1 and AH2). It mainly mediates Oligomerization, transcriptional repression and protein-protein interactions. The three central domains, the GP domain (pink), the CcN domain (blue) and the SP domain (grey), are less conserved. They are relevant for chromatin interaction, phosphorylation and nuclear transport. The highly conserved carboxy-terminal WD-repeat domain (red) folds into a seven bladed β-propeller. Its central pore binds proteins with WRPW-related motifs and eh1 motifs.

WD-Repeat Domain

The carboxy-terminal tryptophan/aspartic (WD) acid tandem repeat WD-repeat domain (also referred to as WDR or WD40 domain) is the most conserved of all five regions. They were first described in the β-subunit of heterotrimeric GTP-binding proteins (hereafter referred to as G proteins) (Fong *et al.*, 1986). Each unit has a region of variable length and a conserved core which is confined by glycine-histidin (GH) on one end and WD on

the other: $\{X_{6-94} - [GH - X_{23-41} - WD]\}^{N4-8}$ (Neer *et al.*, 1994). Neer *et al.* performed intensive database research and identified 27 regulatory proteins (no enzymes) containing at least four WD repeat units with an average length of 34 to 46 amino acids from one WD to the next. The maximum length of the core unit (GH - WD) ranged from 23 to 41 amino acids, however, 82% of the repeating units enclosed 27 ± 2 amino acids. Although the distance between the single core units (from WD to the next GH) showed to be more variable (6-94 amino acids), the majority (61%) was 11 ± 2 residues long (Neer *et al.*, 1994).

Based on the model of heteromeric G proteins, the WD-repeat domain was described to form a toroidal structure consisting of seven blades (also referred to as β propeller), each made up of a β sheet with four antiparallel strands (**Figure 5**) (Wall et al., 1995; Lambright et al., 1996; Sondek et al., 1996). Together they build a flat ring around a water-solvated central pore (**Figure 5**). The inner three β sheets have a relatively invariant structure, while the sheets facing the outside of the ring, which are connecting adjacent blades, are more variable in structure and length (reviewed by Chen *et al.*, 1998; Hamm, 1998). The core β propeller of human TLE1 is very similar to that of G proteins (Pickles *et al.*, 2002). However, analysis of the crystal structure revealed differences in the preceding segments. In G proteins, the N-terminal segment of Gβ subunit forms six turns of α helix. Together with the N-terminal segment of the Gγ subunit a coiled coil structure is generated which leads into the β propeller's seventh blade. In the WD repeat domain of human TLE1, on the other hand, a dimer interface is generated between blade 5 and the β ribbon of a β hairpin formed by the adjacent proline riche SP domain (**Figure 5**) (Pickles et al., 2002). In murine Grg1 the equivalent sequence was identified as high mobility group (HMG) box protein HMGB1 binding site (Dintilhac *et al.*, 2002).

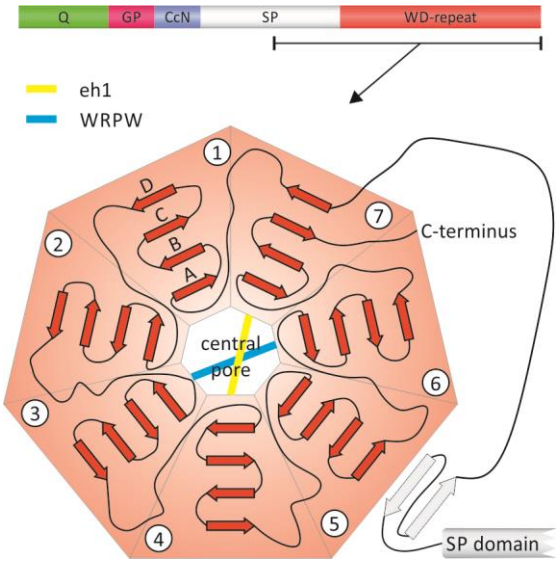

Figure 5| *Schematic presentation of the Gro/TLE WD-repeat domain.* The caboxy-termainal WD-repeat domain (red) of Gro/TLE proteins forms a toroidal structure consisting of seven blades (also referred to as β propeller), each made up of a β sheet with four antiparallel strands (red arrows). A dimer interface is generated between blade 5 and the β ribbon of a β hairpin formed by the adjacent proline riche SP domain (grey arrows). Proteins with WRPW-related (blue) and eh1 (yellow) binding motifs interact with the WD-repeat domain within the central pore. Abbreviations: eh1, engrailed homology; C-terminus, carboxy-terminal end.

The importance of the WD repeat domain was emphasized by the fact that missense mutations in the associated genes often occur within one of the WD units. A distinct point mutation in *Drosophila gro*, for example, resulted in a loss of function mutant

(Paroush *et al.*, 1994) and several UNC-37 mutants were identified in *C. elegans* (Pflugrad *et al.*, 1997). Still, the WD repeat domain of UNC-37 was functionally interchangeable with human TLE1, suggesting that both its structure and function are conserved throughout the Gro/TLE family (Pflugrad *et al.*, 1997).

Structural comparison with other non-WD repeat containing proteins revealed additional proteins which form β propellers. However, despite an almost identical propeller folding, these proteins had no apparent sequence similarity with WD repeat proteins. Nevertheless, this indicates that WD repeat domain containing proteins, including Gro/TLEs, may belong to a larger β propeller family (reviewed by Neer *et al.*, 1996).

Most of the DNA-bound repressors recruit Gro/TLEs through the WD-repeat domain. The majority of them belong to two protein groups, based on their Gro/TLE-interacting motif. The first group binds via WRPW (tryptophan-arginine-proline-tryptophan) or WRPY (tryptophan-arginine-proline-tyrosine) tetrapeptides (Paroush *et al.*, 1994; Fisher *et al.*, 1996; Grbavec *et al.*, 1996; Aronson *et al.*, 1997) and the second via the Engrailed homology-1 (eh1) domain (Jimenez et al., 1997) (**Figure 5**). Despite their differences in sequence and conformation, both peptide motifs share overlapping interaction sites within the central pore of the β propeller (Jennings *et al.*, 2006). The WRPW motif is found in members of the basic helix-loop-helix (bHLH) transcription factor family, including *Drosophila* Hairy and Enhancer of split E(spl) as well as mammalian Hes proteins (Paroush *et al.*, 1994; Fisher *et al.*, 1996; Grbavec *et al.*, 1996). Variations of this Gro/TLE recognition sequence were identified in proteins of the Runt family (WRPY) (Aronson *et al.*, 1997), Huckebein (FRPW) (Goldstein *et al.*, 1999) and Brinker (FKPY) (Hasson *et al.*, 2001; Zhang, H. *et al.*, 2001). While Hairy-like proteins seem to act exclusively as repressors, Runt proteins show both transcriptional activation and repression activity (Aronson *et al.*, 1997). A similar Gro/TLE-dependent and independent mechanism was also observed in Engrailed proteins (de Celis *et al.*, 1995; Smith *et al.*, 1996; Jimenez *et al.*, 1997). Engrailed belongs to a group of proteins that contain the second short peptide motif, the eh1 domain, which directly interacts with the WD-repeat domain of Gro/TLEs (Smith *et al.*, 1996; Jimenez *et al.*, 1997; Tolkunova *et al.*, 1998; Jennings *et al.*, 2006). The eh1 motif (FxIxxIL) is relatively variable and recognized by Gro/TLEs in a large number of proteins, for example, Goosecoid (Chen *et al.*, 2000; Courey *et al.*, 2001; Gasperowicz *et al.*, 2005), Pax2/5/8 (Eberhard *et al.*, 2000; Gasperowicz *et al.*, 2005), Nkx (Choi *et al.*, 1999), Six3/6 (Zhu *et al.*, 2002; Gasperowicz *et al.*, 2005), Hesx1 (Dasen *et al.*, 2001; Carvalho *et al.*, 2010), Otx2 (Heimbucher *et al.*, 2007) and Gbx2 (Heimbucher *et al.*, 2007). Additionally, an eh1 motif resembling sequence was identified in Tcf/Lef proteins (Arce *et al.*, 2009). Although the eh1 sequence binds primarily within the pore of the WD-repeat domain, also weak interaction of Tcf/Lef (Brantjes *et al.*, 2001; Daniels *et al.*, 2005), Bf1 (Yao *et al.*, 2001) and Six3 (Zhu *et al.*, 2002) with the Q domain was observed.

Q Domain

The glutamine rich amino-terminal Q domain interacts weakly with several proteins that are crucial during embryonic development, such as Tcf/Lef1 (Brantjes *et al.*, 2001; Daniels *et al.*, 2005), Pax5 (Eberhard *et al.*, 2000), Nk3 (Choi *et al.*, 1999), Hes1 and Bf1 (Yao *et al.*, 2001). However, its main function is to mediate homo- and hetero-

dimerization (Pinto *et al.*, 1996) and tetramerization (Chen *et al.*, 1998) of Gro/TLE proteins through two tandem leucine-zipper-like motifs (**Figure 6**). These motifs are predicted to form a pair of amphipathic α-helices (AH1 and AH2), leading to coiled-coil structures (Miyasaka *et al.*, 1993; Pinto *et al.*, 1996; Chen *et al.*, 1998; Ren *et al.*, 1999; Song *et al.*, 2004). Song *et al.* located the leucine-zipper-like motifs from amino acid residues 24 to 52 (AH1) and 73 to 100 (AH2) in *Drosophila* Groucho (*d*Gro). Oligomerization is required for Gro/TLE-mediated transcriptional repression and seems to be dependent on these α-helices. Site-directed single proline substitutions in AH1 (L38P) and AH2 (L87P) disrupted tetramerization and thereby transcriptional repression in vitro (Chen *et al.*, 1998) and in vivo (Song *et al.*, 2004). While single point mutations only reduced the repression ability of *d*Gro, it was entirely abolished in double mutants (Song *et al.*, 2004).

Also, a genetic screen in *Drosophila* identified two mutated alleles within the Q domain (Jennings *et al.*, 2008b). gro^{MB5} contains a small in-frame deletion which affects the first 4 amino acids of AH1. Jennings *et al.* observed reduced dimerization ability of the Q domain; however, oligomerization was not completely abolished. In the second mutation, gro^{MB12}, the guanine in the ATG start codon was substituted by adenine (ATG → ATA). This led to an N-terminal truncation of the Q domain and to a complete loss of the AH1 α-helix. *In vitro* tests showed that oligomerization was abolished entirely. Nevertheless, gro^{MB12} mutant embryos still show residual repressive activity. This indicates that *d*Gro proteins have the ability of acting oligomerization-independently (Jennings *et al.*, 2008b).

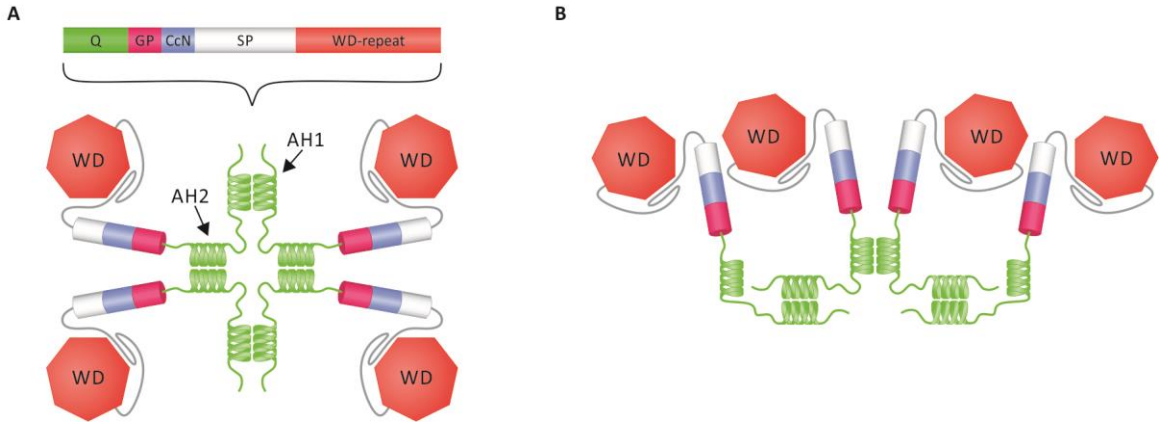

Figure 6| *Gro/TLE tetramerization.* Speculative model for Gro/TLE oligomerization modified from Chen *et al.* Gro/TLE proteins bind to each other via their coiled-coil alpha helical motifs (AH1 and AH2) within the Q domain (green). (A,B) Gro/TLE tetramere, built out of four Gro/TLE proteins. (A) closed, (B) open tetramere.

Besides the primarily found tetramers, Gro/TLEs were also shown to build higher order oligomers (Song *et al.*, 2004). Song *et al.* suggested them to be heterogeneous polymers with a variable number of subunits which might play an important role in long range repression.

Non-Conserved Region

The less conserved internal domains are not so well understood as the large domains on each end of the protein. However, the glycine/proline-rich GP domain (**Figure 4**) seems to be involved in recruiting and binding of Gro/TLE to histone deacetylases (HDACs (Chen *et al.*, 1998; Chen *et al.*, 1999; Choi *et al.*, 1999; Brantjes *et al.*, 2001) and HMGB1 (Dintilhac *et al.*, 2002).

The CcN domain (**Figure 4**) contains a nuclear localization signal (NLS), which is defined by a cluster of four positively charged residues, separated by phosphorylation sites for protein kinase CK2 (formerly referred to as casein kinase II) and cyclin-dependent protein kinase cdc2 (Stifani *et al.*, 1992). Whether this domain is the only region responsible for nuclear localization is unclear. Truncated forms of Gro/TLE proteins, which contain only the Q and GP domain, are mainly found in the cytoplasm (Cavallo *et al.*, 1998; Roose *et al.*, 1998). However, Aes proteins, which naturally lack all regions except the Q and GP domain, are only found in the nucleus (Schmidt *et al.*, 1993; Mallo *et al.*, 1995).

The serine/proline-rich SP domain (**Figure 4**) is phosphorylated by both homeodomain-interacting protein kinase 2 (HIPK2) and mitogen-activated protein kinase (MAPK), which negatively regulate Gro/Tle-mediated transcriptional repression (Choi *et al.*, 2005; Cinnamon *et al.*, 2008a).

For a long time, the three central domains were considered to be dispensable for Gro/TLE function, due to the fact that lethal point mutations were mapped mainly to the WD-repeat domain and also a few to the Q domain but none to the non-conserved region (Jennings *et al.*, 2006; Jennings *et al.*, 2008b). However, internal deletion experiments suggest the opposite. Both the GP and the CcN domain are required for viability and the SP domain seems to restrain Gro/TLE from unlimited repression (Turki-Judeh *et al.*, 2012). Turki-Judeh and Courey also suggest that the central domains are a region of disordered structure, which could explain their high tolerance of point mutations. This could provide a flexible hub to bind to a multitude of different proteins with lower affinity than the Q and WD-repeat domain and which can be easily reversed (reviewed by Dunker *et al.*, 2005).

1.2.2 AES

In addition to the long pentadomain Gro/TLE proteins, a short truncated form, consisting only of the Q and the GP domain, was identified (Mallo et al., 1993; Miyasaka et al., 1993; Schmidt et al., 1993) (**Figure 7**). Consistent with the nomenclature for full-length murine Gro/TLEs, Grg1-4, it was named Grg5 in mouse (Mallo *et al.*, 1993), however, in humans the name Amino-terminal Enhancer of Split (Aes) is commonly used (Miyasaka *et al.*, 1993). To avoid any confusion, here after the term Aes/Grg5 will be used if the entire protein group is addressed and Aes if specifically referred to medaka.

Figure 7| ***The structure of Aes/Grg5 proteins.*** Compared to full length Gro/TLE proteins, Aes/Grg5 consists only of the amino-terminal Q domain (green) and the GP domain (pink).

Additionally to Aes/Grg5, other truncated forms of Gro/TLE family members exist which result from alternative splicing of the respective genes (Mallo *et al.*, 1993; Leon *et al.*, 1997; Lepourcelet *et al.*, 2002; Milili *et al.*, 2002). Aes/Grg5, however, is not alternatively spliced from full-length Gro/TLEs but is a distinct family member (Mallo *et al.*, 1993; Miyasaka *et al.*, 1993; Mallo *et al.*, 1995; Bajoghli, 2007). Therefore, the term "truncated form", which was used earlier in this section, is probably misused if referred to Aes/Grg5. Phylogenetic analysis suggested that the Aes/Grg5 subgroup evolved from tandem duplication of the *Grg2/TLE2* gene (Bajoghli, 2007). While the Q domain remained conserved during this duplication event, mutations in the main coding sequence of the GP domain occurred (Bajoghli, 2007). For example, unlike Gro/TLEs, Aes/Grg5 does not interact with HDACs (Yu *et al.*, 2001; Zhang, X. *et al.*, 2008). However, Acre *et al.* showed more recently, that Aes/Grg5 might recruit HDAC for transcription repression, at least if bound to Lef1 (Arce *et al.*, 2009).

But then, how do Aes/Grg5 proteins interact? Aes/Grg5 proteins lack the carboxy-terminal end of full-length Gro/TLEs, meaning that they cannot bind to transcription factors that interact exclusively with the SP and WD-repeat domain (Eberhard *et al.*, 2000; McLarren *et al.*, 2001). On the other hand, the conserved Q domain allows oligomerization with Gro/TLEs and interaction with non-WD-repeat domain-dependent transcription factors (Pinto *et al.*, 1996; Chen *et al.*, 1998; Choi *et al.*, 1999; Eberhard *et al.*, 2000; Brantjes *et al.*, 2001; Yao *et al.*, 2001; Lopez-Rios *et al.*, 2003). By this means, Aes/Grg5 can tether either its full-length ancestors or their respective interaction partners in a dominant negative way (**Figure 9B**). In either way, the co-repressing function of Gro/TLEs is lost, meaning that Aes/Grg5 interacts as their antagonist. However, Gro/TLE co-repression is not generally blocked by Aes/Grg5. For example, it interacts neither with Pax5 (Eberhard *et al.*, 2000) nor with Hes1 (McLarren *et al.*, 2001). Furthermore, Aes/Grg5 proteins can themselves also exhibit repressing activity, as shown for NF-κB (Tetsuka *et al.*, 2000) and androgen receptor (AR)-mediated transcription (Yu *et al.*, 2001; Zhang, Y. *et al.*, 2010). Interestingly, while human AES repressed AR activity, both TLE2 and TLE3 failed to do (Zhang, Y. *et al.*, 2010). Zhang *et al.* showed that the Q domain of Aes/Grg5 contains three regulatory sub-domains. Residues 1 to129 are required for AR interaction and inhibition. This AR inhibitory domain is able to bind intramolecularly to residues 156 to 176, thereby inhibiting intermolecular dimerization between Aes/Grg5 proteins, which is prevented by a short third so-called positive regulatory domain, located from amino acid 190 to 193 (Zhang, Y. *et al.*, 2010). Additionally, Aes/Grg5 interacts as well with non-transcription factors such as HDAC-related protein (HDRP) (Zhang, X. *et al.*, 2008) and the soluble intracellular domain (ICD) of LRP6 (Beagle *et al.*, 2010b).

Due to the fact that Aes/Grg5 proteins only consist of the very first two amino-terminal domains, they lack the NLS which is found within the CcN domain of full-length Gro/TLEs (Stifani *et al.*, 1992). Nevertheless, it is found in both the cytoplasm and the

nucleus, depending on the respective cell type (Mallo *et al.*, 1995; Cavallo *et al.*, 1998; Roose *et al.*, 1998; Jan *et al.*, 2004; Zhang, X. *et al.*, 2008). It seems that subcellular distribution is influenced by certain Tcfs as well as Gro/TLEs (Mallo *et al.*, 1995; Chen *et al.*, 2000; Brantjes *et al.*, 2001).

1.2.3 Mechanisms of Gro/TLE-Mediated Repression

Even if the structure of Gro/TLE proteins is well-established and many of its binding partners were identified, the actual mechanism of interrupting transcription is not known. In general, they are considered to mediate long-range transcriptional repression due to their preferential interaction with long-range repressors such as Dorsal and Hairy in *Drosophila* (Barolo *et al.*, 1997; Zhang, H. *et al.*, 1999). Nevertheless, binding to some short-range repressors (e.g., Knirps and Sloppy-paired 1) indicate that Gro/TLEs might use several mechanisms to repress transcription (Andrioli *et al.*, 2004; Payankaulam *et al.*, 2009). Therefore, different models have been proposed over the last years, depending on their particular interaction partner and the respective domains involved:

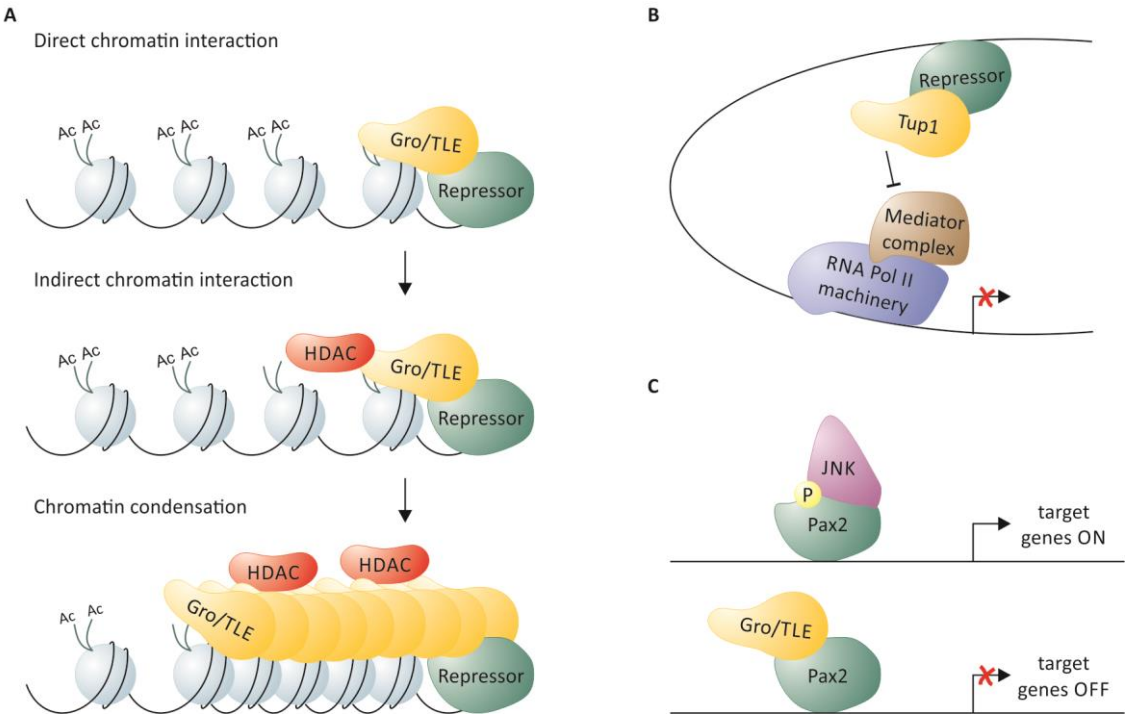

Figure 8| ***Mechanisms of Gro/TLE-mediated repression.*** (A) Direct interaction of Gro/TLE with the amino-terminal tails of histones. Binding of HDAC catalyzes histone deacetylation, thereby facilitating chromatin interaction in an indirect manner, which leads to chromatin condensation and reduced accessibility to the transcriptional machinery. (B) Direct interaction of Tup1 (Gro/TLE-related protein in yeast) with the transcriptional core machinery. (C) Turning of activators into repressors. Gro/TLE binds to Pax2, thereby preventing its phosphorylation.

One way of Gro/TLE-mediated repression may result from direct and indirect changes in chromatin structure (**Figure 8A**). In direct interactions, Gro/TLEs bind to the amino-

terminal tails of the four core histones, with the highest affinity to histone H3 (Palaparti *et al.*, 1997; Flores-Saaib *et al.*, 2000). However, it is not entirely clear which domains of the Gro/TLE proteins are involved in this interaction. While in *Drosophila* Gro the amino-terminal region was necessary and sufficient for histone interaction (Flores-Saaib *et al.*, 2000), in murine Grg3 the WD-repeat domain seemed to be more important (Sekiya *et al.*, 2007). Sekiya *et al.* further showed that this interaction causes condensed chromatin structures. Chromatin binding seems to stabilize Grg3 tetramers and enables transcription factor recruitment. Together this causes a compact, nuclease resistant chromatin structure that spreads over a distance of 3 to 4 nucleosomes (Sekiya *et al.*, 2007). In a second (indirect) chromatin interaction, Gro/TLE proteins bind to the class I histone deacetylase Rpd3/HDAC1 via their GP domain (Chen *et al.*, 1999; Choi *et al.*, 1999; Brantjes *et al.*, 2001). The functional relevance of this interaction on *Drosophila* embryonic lethality and development was shown in several experiments (Chen *et al.*, 1999; Mannervik *et al.*, 1999; Winkler *et al.*, 2010). Winkler *et al.*, for example, analyzed wing-patterning defects upon *gro* misexpression. Histone deacetylase inhibitors (TSA and HC-toxin) inhibited the observed wing phenotypes and these effects were even enhanced when *rpd3* expression levels were reduced. They also showed that co-localization of Gro and Rpd3 at the chromatin leads to specific deacetylation of the lysine residues H3K9, H3K14, H4K5, H4K8, and H4K12 of histones H3 and H4 (Winkler *et al.*, 2010). Indeed, the interaction of Gro with the amino-terminal tail of histones is significantly enhanced in hypoacetylated histones (Flores-Saaib et al., 2000) (**Figure 8B**). Taken together, this proposes a repression model in which Gro/TLE tetramers bind to transcription factors and histones. Subsequent interaction with Rpd3/HDAC1 catalyzes histone deacetylation and enables binding of additional Gro/TLEs, which in turn leads to a compact chromatin structure (**Figure 8A**) with reduced accessibility to the transcriptional machinery (reviewed by Chen *et al.*, 2000; Buscarlet *et al.*, 2007; Jennings *et al.*, 2008a).

Another way to repress transcription may result from direct interaction of Gro/TLE with the core machinery (**Figure 8B**). It was shown in yeast that the Gro-related co-repressor in yeast, Tup1, interacts with the Mediator complex that transfers information from regulatory proteins to the basal RNA polymerase II machinery (Kuchin *et al.*, 1998; Gromoller *et al.*, 2000; Papamichos-Chronakis *et al.*, 2000; Malik *et al.*, 2010). A similar function was observed in *C. elegans* Unc-37 (Zhang, H. *et al.*, 2002).

In addition, Gro/TLE's co-repressing ability can turn certain transcriptional activators into repressors (**Figure 8C**). A frequently mentioned example for this is the paired domain protein Pax2. In an activated state, the activation domain of Pax2 is phosphorylated by c-jun N-terminal kinase (JNK) (Cai *et al.*, 2003). Gro/TLE binding inhibits this phosphorylation and thereby antagonizes Pax2-mediated transactivation (Cai *et al.*, 2003).

1.2.4 The Regulation of Gro/TLE-Mediated Repression

The different mechanisms of Gro/TLE-mediated transcriptional repression show that this is a rather complex process. Its ubiquitous expression and the important role in development and pathological pathways suggest a tight regulation.

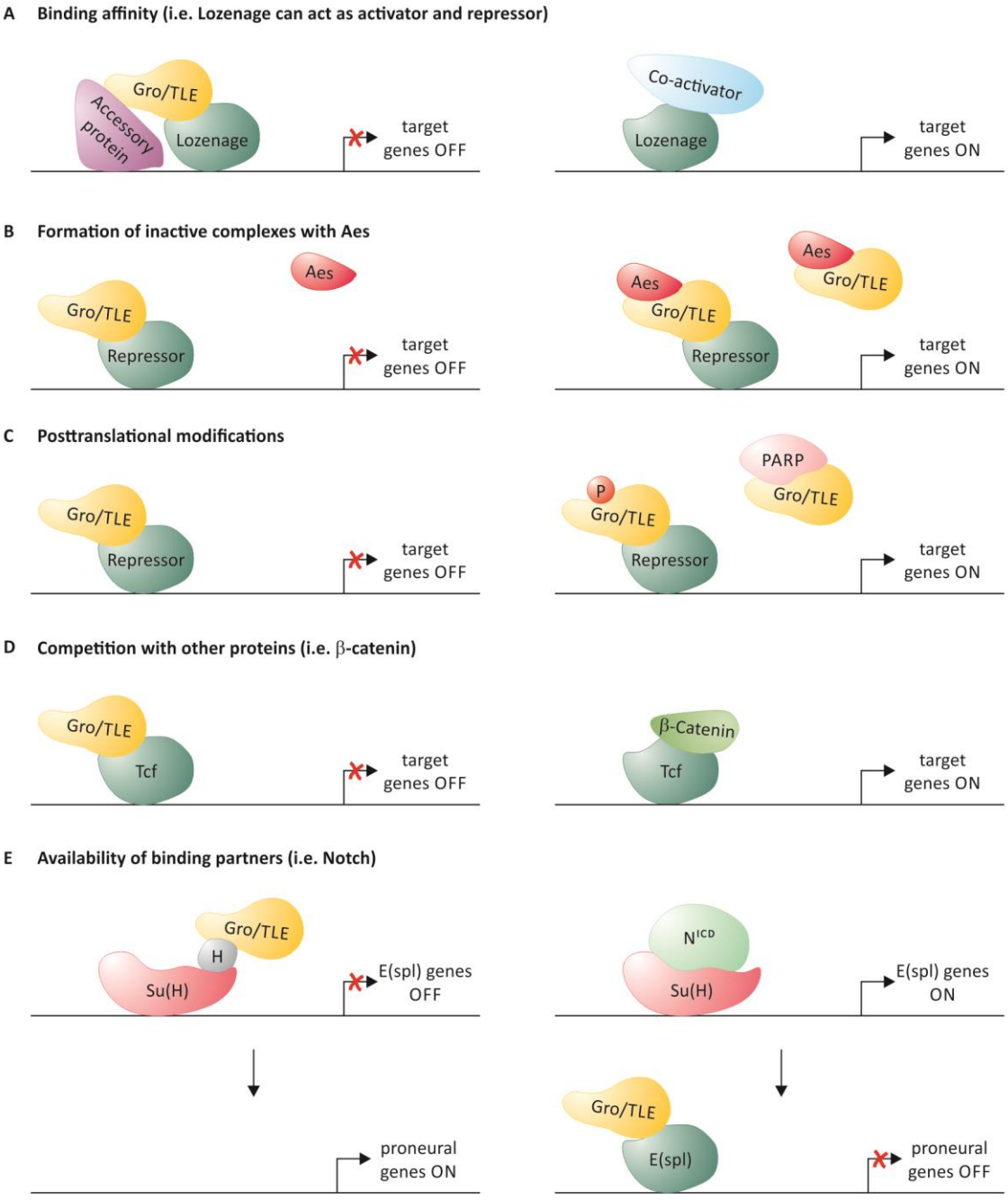

Figure 9| ***The regulation of Gro/TLE-mediated repression.*** (A) Regulation by binding affinity. Proteins, such as Lozenage, have both repressing and activating potential. If bound to Gro/TLE and additional auxiliary protein they act as repressors. Interaction with co-activators turns them into activators. (B) Oligomerization of Gro/TLE proteins with their antagonist Aes leads to a loss their co-repressing activity. Aes can inhibit the co-repressing function either directly at the transcription factor or by tethering away Gro/TLE from its interaction partner. (C) Posttranslational modifications can change the co-repressing activity of Gro/TLE. Phosphorylation and sumoylation lead to a down-regulation of Gro/TLE, whereas poly(ADP-ribosy)lation by PARP1 results in dissociation of Gro/TLE from its interaction partners. (D) Competition with co-activators. In the Wnt/β-catenin signaling pathway, Wnt stabilizes β-catenin, which leads to a displacement of Gro/TLE at their mutual interaction partner Tcf/Lef. (E) The availability of interaction partners influences the activity of Gro/TLE. Activation of Notch signaling leads to the expression of *E(spl)* genes. Interaction of Gro/TLE with E(spl) represses the expression of proneural genes. If Notch signaling is turned off, Gro/TLE binds to Hairy, an interaction that inhibits the expression of E(spl) genes which enables the expression of proneural genes. Abbreviations: P, phosphorylation; PARP1, poly(ADP-ribose) polymerase1; H, Hairy; Su(H), Suppressor of Hairless; N^{ICD}, Notch intra cellular domain, E(spl), Enhancer of split.

One way of regulating Gro/TLE-mediated depends on the binding affinity of the interaction motif (**Figure 9A**). As described in a previous section, most of the DNA-bound repressors recruit Gro/TLE through the WD-repeat domain via two distinct motifs, the WRPW tetrapeptide or the eh1 domain (Paroush *et al.*, 1994; Fisher *et al.*, 1996; Grbavec *et al.*, 1996; Aronson *et al.*, 1997; Jimenez *et al.*, 1997). Crystal structure analysis revealed that the four amino acids of WRPW meet the WD-repeat domain in a strong hydrophobic interaction. Slight alterations in the motif, like a replacement of the carboxy-terminal tryptophan with tyrosine, results in the loss of a hydrogen bond and thereby weakens the affinity of this WRPY motif (Jennings *et al.*, 2006). Lozenage, a member of the Runt protein family, for example, contains such a motif and acts as an activator or a repressor, depending on additional accessory proteins. However, if the WRPY motif is replaced by WRPW, Lozenage turns into a strong repressor and together with Gro/TLE it is able to repress transcription independently (Canon *et al.*, 2003).

Besides the WD-repeat domain the Q domain also takes place in regulating Gro/TLE's co-repressor function. Oligomerization of full-length Gro/TLE with short Aes/Grg5 proteins seems to inhibit their co-repressing activity in a dominant negative manner either directly at the transcription factor or by tethering Gro/TLE away from its binding partner (Pinto *et al.*, 1996; Chen *et al.*, 1998; Choi *et al.*, 1999; Eberhard *et al.*, 2000; Brantjes *et al.*, 2001; Yao *et al.*, 2001) (**Figure 9B**). A more detailed description of Aes/Grg5 and its function was already presented in chapter 1.2.2 Aes (page 10).

As mentioned before, the internal CcN and SP domains are targets of phosphorylation by several kinases. The CcN domain contains phosphorylation sites for CK2 and cdc2 (Stifani *et al.*, 1992). Phosphorylation by these kinases leads to a down-regulation of Gro/TLE function (Nuthall *et al.*, 2002; Nuthall *et al.*, 2004). For example, phosphorylation is up regulated during neuronal and chondrocyte differentiation (Husain *et al.*, 1996; Yao *et al.*, 1998; Nuthall *et al.*, 2002). Such a hyperphosphorylated state was observed after interaction of Gro/TLE1 and Hes1 (Nuthall *et al.*, 2002). Immediately after translation CK2 phosphorylates Gro/TLE1 at S239 which is critical for cofactor-activated phosphorylation that Gro/TLE1 undergoes as a result of Hes1 binding (Nuthall *et al.*, 2004). In the SP domain, phosphorylation by MAPK in response to the receptor tyrosine kinase (RTK)/Ras/MAPK pathway (**Figure 9C**) or by HIPK2, mediate decreased Gro/TLE activity (Choi *et al.*, 2005; Cinnamon *et al.*, 2008a). Experiments in *Drosophila* showed that Degringolade targets Gro and thereby antagonizes its function, suggesting that Gro/TLE is sumolyated (Abed *et al.*, 2011). Finally, Gro/TLE is also poly(ADP-ribosy)lated by poly(ADP-ribose) polymerase1 (PARP-1), which leads to its dissociation from Hes1 (Ju *et al.*, 2004).

In addition to the RTK/Ras/MAPK pathway, Gro/TLE plays also a role in Notch and Wnt/Wingless signaling, as well as in the decapentaplegic (Dpp)/BMP/TGF-β pathway (reviewed by Buscarlet *et al.*, 2007). While in Wnt signaling Gro/TLE co-repression is regulated by a competition with β-catenin about their mutual interaction partner Tcf/Lef (**Figure 9D**) (Daniels *et al.*, 2005), in Notch signaling its regulation depends on the availability of interaction partners (**Figure 9E**) (Barolo *et al.*, 2002; Nagel, A. C. *et al.*, 2005). In the absence of Notch, *Drosophila* Gro forms a large protein complex together with Hairless, Suppressor of Hairless [Su(H)] and C-terminal binding protein (CtBP) (Morel *et al.*, 2001; Barolo *et al.*, 2002; Nagel, A. C. *et al.*, 2005). This complex represses the expression of *E(Spl)* genes, which on the other hand enables the transcription of proneural genes. Upon Notch activation, the intracellular domain (N^{ICD}) breakes away and

translocates to the nucleus where it binds to Su(H) and Mastermind (MAM) which allows the expression of Notch target genes, such as E(Spl) (Guruharsha *et al.*, 2012). Gro then interacts with E(Spl), thereby repressing the transcription of proneural genes (Paroush *et al.*, 1994).

1.2.5 The Role of Gro/TLEs in Development

The role of Gro/TLEs in both invertebrate and vertebrate development has been studied and reviewed intensively (Chen *et al.*, 1998; Fisher *et al.*, 1998; Parkhurst, 1998; Courey *et al.*, 2001; Gasperowicz *et al.*, 2005; Buscarlet *et al.*, 2007). This chapter summarizes its most important functions.

One of the major events in embryonic development is the formation of the three body axes: anteroposterior (AP), dorsoventral (DV) and left-right (LR) (reviewed by Schier *et al.*, 2005; Petersen *et al.*, 2009); and Gro/TLEs seem to play a role in establishing each of them (reviewed by Buscarlet *et al.*, 2007). For example, Gro/TLE4 negatively regulates Wnt signaling by interaction with Hex proteins via the eh1-domain (Swingler *et al.*, 2004; Zamparini *et al.*, 2006). Using the same motif they also bind to both Otx2 and Gbx2 in medaka mid-hindbrain boundary (MHB) development. However, while Gro/TLE is required for Otx2 repression by Gbx2, this seems not to be the case *vice versa* (Heimbucher *et al.*, 2007). Further analysis of Tle4 in medaka showed its effects on cardiac asymmetry. Misexpression of either *tle4* or the truncated version *aes* at the 1-cell stage resulted in reversed heart looping phenotypes, accompanied by a randomized expression of marker genes such as *BMP4*, *lefty* and *spaw*. However, induction of *tle4* and *aes* during gastrulation revealed their contrary effects on Kupffer's vesicle formation (Bajoghli *et al.*, 2007). Analysis of DV patterning in *Drosophila* showed that correct expression of dorsal genes strongly depends on the formation of a repressor complex which involves Groucho (reviewed by Fisher *et al.*, 1998; Chen *et al.*, 2000; Courey *et al.*, 2001). In DV boundary formation of the wing imaginal disc another complex is formed between Groucho, Hairless and CtBP which turns Su(H) into a transcriptional repressor in the absence of Notch signaling (Barolo *et al.*, 2002).

The interaction of Hes proteins with the WD-repeat domain of Gro/TLEs plays an important role in various developmental processes. Hes1, for example, represses the activity of MyoD, thereby inhibiting myogenesis (Sasai *et al.*, 1992), and Hes6, on the other hand, promotes myoblast differentiation (Gao *et al.*, 2001). However, Hes proteins are primarily known for their essential role in the development of the central nervous system. Especially the interaction between mammalian Hes1 and Grg1/TLE1 was studied intensively. Together they repress postmitotic neuronal differentiation in the forebrain of the developing embryo (Sasai *et al.*, 1992; Ishibashi *et al.*, 1994; Ishibashi *et al.*, 1995; Ohtsuka, T. *et al.*, 1999; Yao *et al.*, 2000). Like Grg1/TLE1, the other three vertebrate Gro/TLEs are also present in the central nervous system and seem to influence brain development. TLE2 takes part in postmitotic neuron maturation and survival (Grbavec *et al.*, 1998), whereas *tle3* and *tle4* are expressed in the external and internal layers of the cortical plate in cortical neurons and differentiating/differentiated neurons as well as neural progenitors (Dehni *et al.*, 1995; Koop *et al.*, 1996; Yao *et al.*,

1998), respectively. Additionally, Grg4 was shown to interact with Lmx1b to repress *fgf8* expression in the isthmus (Sugiyama, S. *et al.*, 2000; Matsunaga *et al.*, 2002).

Hes proteins are also key players during somitogenesis. Somites are formed by periodical segmentation of the anterior presomitic mesoderm. During this process, Notch synchronizes the expression of *Hes* genes and their homologs (reviewed by Kageyama *et al.*, 2007). The fact that *Gro/TLEs* are expressed during somitogenesis implicates that they might interact with Hes-related proteins (Koop *et al.*, 1996). Also, Gro/TLEs were shown to interact with zebrafish Ripply1 (via the WD-repeat domain), which is important for intersomitic boundary formation (Kawamura *et al.*, 2005).

Besides Hes proteins, Runt related transcription factors also interact with the Gro/TLE WD-repeat domain via a WRPY motif (Aronson *et al.*, 1997). Runx3, which is down regulated by Gro/TLE (Castilla *et al.*, 1996; Javed *et al.*, 2000; Guo *et al.*, 2002; Inoue *et al.*, 2002; Levanon *et al.*, 2002; Li, Q. L. *et al.*, 2002), plays an important role in neurogenesis (Levanon *et al.*, 1998; Inoue *et al.*, 2002). Runx2, on the other hand, is co-expressed with Gro/TLEs during osteogenesis where it is required for cell differentiation (Ducy *et al.*, 1997; Komori *et al.*, 1997; Otto *et al.*, 1997; Inada *et al.*, 1999; Kim, I. S. *et al.*, 1999). For example, they inhibit Runx2-dependent induction of osteocalcin (Javed *et al.*, 2000). Hes1, on the other hand, which binds to both Runx2 (McLarren *et al.*, 2000) and Gro/TLE (Grbavec *et al.*, 1996) is able to antagonize this interaction by competing for the same binding region (McLarren *et al.*, 2000). The third Runt domain protein, Runx1, interacts with human TLE1, thereby inhibiting the transactivation of hematopoetic lineage-specific genes (Imai *et al.*, 1998; Levanon *et al.*, 1998). However, additional Gro/TLEs play additional roles during hematopoiesis. TLE1 but also TLE2 and AES, for example, bind to PRDI-Blimp1 during B-cell development (Ren *et al.*, 1999) and Grg4 seems to mediate the repressive function of Pax5 in B-cell lineage commitment (Nutt *et al.*, 1999; Eberhard *et al.*, 2000).

Besides the above mentioned developmental processes, Gro/TLEs also play a role in the formation of the eyes, the neural tube, the pituitary gland, the placenta and the intestines (reviewed by Gasperowicz *et al.*, 2005).

1.2.6 The Role of Gro/TLEs in Diseases

Due to its interaction with a vast number of transcription factors and other proteins (reviewed by Gasperowicz *et al.*, 2005) and its involvement as downstream partner in several major signaling pathways (reviewed by Buscarlet *et al.*, 2007; Cinnamon *et al.*, 2008b) it is not surprising that Gro/TLEs show altered expression levels in a number of different tumors. In many cases this is correlated with deregulated members of the Notch signaling pathway as found in grade I astrocytomas, several kinds of meningiomas, pituitary adenomas as well as in cervical and colonic carcinomas (reviewed by Buscarlet *et al.*, 2007). On the other hand, decreased expression of the tumor suppressor-gene *p53* was associated with a deregulation in Gro-TLE/Pax5-mediated repression in human astrocytomas (Stuart *et al.*, 1995). Whether tumors are caused by these correlations or if they are the consequence is not known. Nevertheless, that Gro/TLE possesses *in vivo* oncogenic capabilities was shown in adult mice. Misexpression of Grg1 induced lung

adenocarcinomas, which is consistent with the observation that in 20% of human lung adenocarcinomas TLE1 levels are elevated (Allen *et al.*, 2006).

As described in the previous chapter, human TLE1 is closely connected to hematopoiesis. Therefore, it is not surprising that TLE1 plays an essential role in several hematologic malignancies (Fraga *et al.*, 2008). Fraga *et al.* found hypermethylated CpG islands around TLE1 transcription start sites in acute myeloid leukemia, non-Hodgkin's lymphoma and chronic myeloid leukemia. Furthermore, elevated levels of TLE1 are associated with lymphomas (Shipp *et al.*, 2002). Jan *et al.* speculated that TLE1 might protect lymphoma cells that lost their cell attachment from apoptosis. However, they also showed that *TLE1* overexpression inhibits the formation of a complex formed between Bit1 and AES which mediates this kind of apoptosis (Jan *et al.*, 2004).

1.2.7 TLE AND AES IN MEDAKA

Whereas *D. melanogaster* and *C. elegans* each only contain a single Gro protein (Lindsley *et al.*, 1968), the Gro/TLE family consists of four proteins in mammals, termed TLE 1-4 in humans (Stifani *et al.*, 1992) and Grg 1-4 in mice (Mallo *et al.*, 1993; Koop *et al.*, 1996; Leon *et al.*, 1997). Six Tle proteins are found in medaka, where genome duplication events during evolution resulted in two proteins for Tle2 (Tle2a and Tle2b) and Tle3 (Tle3a and Tle3b), respectively (Lopez-Rios *et al.*, 2003; Aghaallaei *et al.*, 2005). In the last decade their expression pattern and some of their roles in medaka embryonic development were analyzed (Lopez-Rios *et al.*, 2003; Aghaallaei *et al.*, 2005; Bajoghli *et al.*, 2005; Bajoghli *et al.*, 2007; Heimbucher *et al.*, 2007):

At early neurula, *tle1* is expressed in the most anterior part of the embryo. From there it spreads into the anterior brain and the bulging optic vesicles where it largely overlaps with the expression of *six3* and *six6* (Lopez-Rios *et al.*, 2003). Lopez-Rios *et al.* showed that tle1 overexpression results in an enlargement of the optic vesicles, accompanied by an expanded expression of eye marker genes, and bulging of the midbrain. At later stages, expression of *tle1* is still found in the optic cups, parts of the diencephalon and in the hindbrain (Lopez-Rios *et al.*, 2003), where it is particularly strong in the cells surround the otic vesicle (Aghaallaei *et al.*, 2005).

Aghaallaei *et al.* identified the two genes medaka paralogs for Gro/TLE2, *tle2a* and *tle2b,* which overlap only partially in their expression. While *tle2b* is already expressed in the embryonic body at late gastrulation, *tle2a* is first detected at stage 20 in the tail bud. During later stages tle2b can also be observed in the tail bud, however, its expression there decreases over time and becomes more noticeable in the anterior part of the embryo (from the diencephalon to the MHB region) the optic cups and the lens placode. In contrast, the expression of *tle2a* in the tail bud increases at later stages. However, the anterior expression is mainly observed the MHB and the diencephalon. Both genes are the only full-length medaka *Gro/TLEs* expressed substantially in the otic vesicles. The early expression of *tle2b* is already observed in the presumptive otic region, continuing in the preplacodal otic region and remaining in the medial region of the otic vesicle. *tle2a* on the other hand, is first seen at stage 26 in the ventral epithelium of the otic vesicle. Additionally, *tle2b* is expressed in the pectoral fin buds (Aghaallaei *et al.*, 2005).

The early expression of *tle3a* and *tle3b* is relatively similar. They are first observed in the embryonic body and become then restricted to the CNS in the mid-hindbrain region (Lopez-Rios *et al.*, 2003; Aghaallaei *et al.*, 2005). While *tle3b* expression is most noticeable in the midbrain, especially at the MHB (Aghaallaei *et al.*, 2005), *tle3a* spreads into the forebrain and the lens later on in development (Lopez-Rios *et al.*, 2003). Even if initial weak expression of *tle3b* is observed in the developing eye, it is subsequently lost in later stages (Aghaallaei *et al.*, 2005). Like *tle2b*, *tle3b* expression is also observed in the pectoral fin buds (Aghaallaei *et al.*, 2005).

Similar to *tle2a*, the onset of *tle4* expression is relatively late. At first it overlaps with the stronger expression pattern of *six3* in the neural retina and the optic stalk. Later on, it is restricted to the ventral diencephalon and the optic chiasm (Lopez-Rios *et al.*, 2003). In contrast to *Xenopus Gro/TLE4* which is expressed in the otic vesicles, medaka *tle4* is not (Aghaallaei *et al.*, 2005). Nevertheless, misexpression experiments at early gastrula stage resulted in their enlargement and the formation of ectopic vesicles. Additionally, in rare cases enlarged lenses or loss of eyes were observed (Bajoghli *et al.*, 2005).

Co-injection *aes* rescued the above described phenotype of *tle4* and misexpression of *aes* alone during early gastrulation reduced the size of the otic vesicles about half (Bajoghli *et al.*, 2005). However, like *tle2a* and *tle2b*, *aes* is expressed in the otic vesicles (Aghaallaei *et al.*, 2005). Furthermore, Bajoghli *at al.* observed size reduction in the eyes (leading to a complete absence of the eyes in some cases) and the midbrain. Similar eye phenotypes for *aes* misexpression were initially described by López-Ríos *et al.* They also showed that *ae*s overexpression could counteract *six3* and *six6* gain of function phenotypes (Lopez-Rios *et al.*, 2003). Bajoghli *et al.* also showed that both the eye and the ear phenotype are time dependent due to the fact that complete loss of structures was usually observed in early inductions (Bajoghli *et al.*, 2005). Additionally, excess Aes could result in partial axis duplication and an altered orientation of the heart tube (Bajoghli *et al.*, 2005; Bajoghli *et al.*, 2007). Other visceral organs, such as the spleen, the gallbladder and the gut were also misplaced upon *tle4* or *aes* induction (Bajoghli *et al.*, 2007). In addition, the antagonistic effect of both genes was observed in the formation of the Kupffer's vesicle. While excess Aes led to a strong size reduction, Tle4 caused the opposite effect (Bajoghli *et al.*, 2007).

1.3 TCF TRANSCRIPTION FACTORS

T-cell factor (Tcf) and lymphoid enhancer factor (Lef) proteins are members of the HMG box-containing superfamily of transcription factors (van de Wetering *et al.*, 1991). They are the main partner for β-catenin and the most distal players in Wnt signaling (Behrens *et al.*, 1996; Arce *et al.*, 2006). Therefore, they play an important role during embryogenesis in establishing the body plan (Brannon *et al.*, 1997; Merrill *et al.*, 2004), and in specifying cell fate and regulating cell proliferation (van Genderen *et al.*, 1994; Merrill *et al.*, 2001).

Despite its myriad of different functions, the Tcf/Lef family is rather small. Transcriptional activation and repression is regulated by a single *Tcf* gene in non-vertebrates (*pangolin* for *Drosophila* (Brunner *et al.*, 1997) and *POP-1* for the

Ceanorhabditis ortholog (Lin, R. *et al.*, 1995)), whereas vertebrates possess four, more specialized and partly redundant, homologs: Tcf1 (Tcf7) (van de Wetering *et al.*, 1991), Lef1 (Tcf7L3 or Tcf-1α) (Waterman *et al.*, 1991), Tcf3 (Tcf7L1) (Castrop *et al.*, 1992), and Tcf4 (Tcf7L2) (Castrop *et al.*, 1992). However, alternative splicing and promoters give rise to multiple isoforms which explain the differences in DNA-binding affinity and repression/activation potentials of the single Tcf/Lef proteins (reviewed by Mao *et al.*, 2011). Although Tcf3 is in general reported as a unique protein, recently alternative exon cassettes that regulate stem cell pluripotency and differentiation were found in mouse (Salomonis *et al.*, 2010) and in zebrafish two different Tcf3 isoforms were identified (Kim, C. H. *et al.*, 2000; Dorsky *et al.*, 2003).

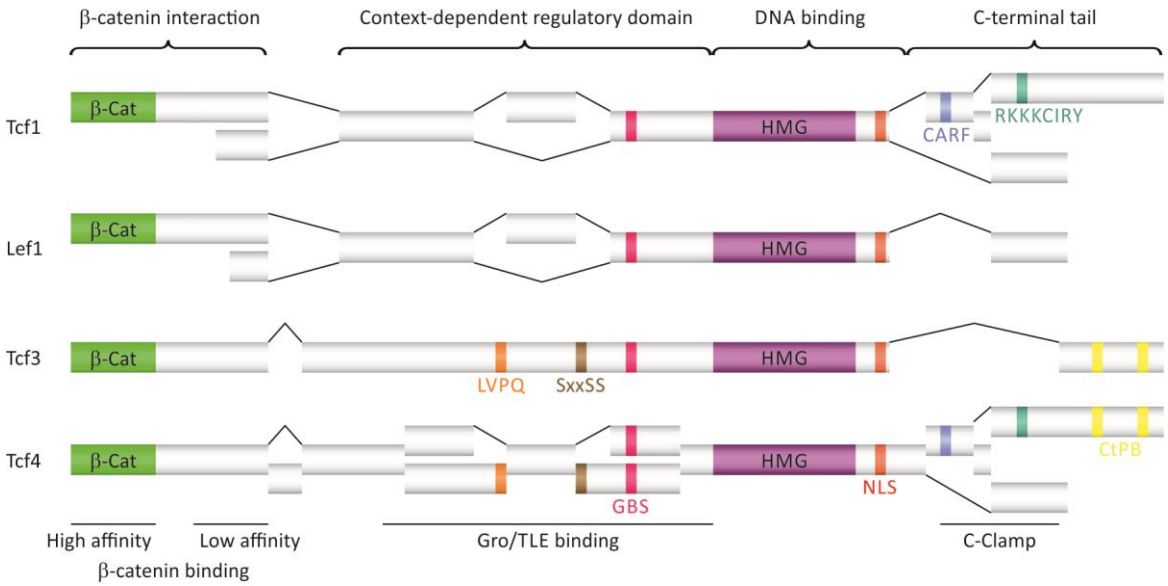

Figure 10| ***Schematic structure of human Tcf/Lef proteins and their splice variants.*** All Tcf/Lef proteins contain the conserved β-catenin binding domain (green), GBS (pink) and HMG domain (puple). Short Tcf1 and Lef1 splice variants have an alternative amino-terminal start, lacking the β-catenin binding domain (green). A carboxy-terminal CtBP binding domain (yellow) is present in Tcf3 and the long Tcf4 isoforms. Short LVPQ (orange) and SxxSS (brown) motifs are found in Tcf3 and Tcf4. The long splice variants of Tcf1 and Tcf4 contain DNA stabilizing C-Clamps with CARF (blue) and RKKKCIRY (light green) motifs. Abbreviations: β-cat, β-catenin; HMG, high mobility group; CtBP, C-terminal binding protein; NLS, Nuclear localization signal; GBS, Groucho binding sequence; C-Clamp, cysteine clamp.

In principle Tcf/Lef proteins contain an amino-terminal β-catenin binding domain, followed by the Gro/TLE binding domain, the HMG domain and a carboxy-terminal end. However, alternative splicing in Tcf1 and Lef1 results in short forms that lack the amino-terminal β-catenin domain or parts of the Gro/TLE binding domain (reviewed by Mao *et al.*, 2011) (**Figure 10**). Nervertheless, all four Tcf/Lef proteins, as well as their *Drosophila* and *C. elegans* orthologs, contain a groucho binding sequence (GBS), FS/TxxxI/L/V, which is similar to the eh1 motif (Arce *et al.*, 2009). The HGM domain contains two conserved sequences. On one side the HGM box which recognizes specific sequences in the minor groove of the DNA. These so called Wnt response elements (WRE) contain a core element (YCTTTGWW with Y representing either G or C and W representing either A or T) (van Beest *et al.*, 2000). Binding of Tcf/Lef to WREs causes a bend of the DNA up to 130° away from the protein (Giese *et al.*, 1992). The second sequence of the HGM domain is an NLS which is separated from the HMG box by a nine residue linker sequence (**Figure 10**). Bending of the DNA places this region underneath the major groove where it

interacts with the phosphate backbone and enhances the binding affinity of Tcf/Lef (Love *et al.*, 1995). The carboxy-terminus is the most divergent region of Tcf/Lef proteins. In long proteins Tcf3 and Tcf4 isoform a CtBP binding domain is located at the most carboxy-terminal end (**Figure 10**) (reviewed by Mao *et al.*, 2011). Experiments in *Xenopus* showed that removal of this region was sufficient to turn Tcf3 from a repressor into a strong transcriptional activator (Gradl *et al.*, 2002). Tcf1, on the other hand contains instead a cysteine clamp (c-clamp) which is also found in Tcf4 in addition to the CtBP domain (**Figure 10**) (reviewed by Mao *et al.*, 2011). C-clamps bind to GC-rich sequences adjacent to the WRE which stabilizes the Tcf/Lef-DNA complex (Atcha *et al.*, 2007).

1.3.1 Tcf3

Tcf/Lef proteins show differences in function due to the large number of isoforms. While Tcf1 and Tcf4 play a role in both activation and repression, Lef1 shows primarily activator abilities (Kengaku *et al.*, 1998). Tcf3, on the other hand, seems to function exclusively as a repressor (Houston *et al.*, 2002). For example, *Tcf3* knockout experiments in mice resulted in gastrulation defects that resemble ectopic *Wnt* expression, followed by anterior-posterior axis duplication, abundant neuroectodermal cells and defective neural patterning at later stages (Merrill *et al.*, 2004). Furthermore, Tcf3 seems to be a negative regulator of pluripotency. Under standard conditions embryonic stem (ES) cells remain in a balanced state between pluripotency and differentiation, due to high levels of Tcf3 and only low Wnt pathway activation. If either *Tcf3* is knocked down or *Wnt* overexpressed, the balance will tip towards pluripotency because the ES cells do not undergo efficient differentiation anymore (Pereira *et al.*, 2006; Cole *et al.*, 2008).

In zebrafish two Tcf3 isoforms were identified, *headless* (*hdl*)/*ztcf3* (Kim, C. H. *et al.*, 2000) and *ztcf3b* (Dorsky *et al.*, 2003), both acting as repressors. Whereas *hdl* is broadly expressed in the epiblast during shield stage, *tcf3b* shows only weak expression. In late gastrula, both genes are expressed in the rostral neuroectoderm. The expression then spreads throughout the brain. However, the expression pattern of *tcf3b* is interrupted at the MHB (Dorsky *et al.*, 2003). In zebrafish *hdl* mutants forebrain development is disturbed, while the expression of characteristic MHB genes is expanded (Kim, C. H. *et al.*, 2000). Both *tcf3b* overexpression and Wnt signalling are able to rescue this phenotype. Zebrafish embryos with a knock down of the *hdl* gene developed an eye-less phenotype, whereas knock down of *tcf3b* resulted in smaller heads but with otherwise normal brain patterning. Knock down of *tcf3b* in *hdl* mutants, however, led to further caudalization (Dorsky *et al.*, 2003). In contrast to zebrafish, the medaka genome contains only a single *tcf3* gene (Wang, D. *et al.*, 2011). However, except for the sequence, little is known about medaka *tcf3*.

1.3.2 The Wnt/β-Catenin Pathway, Tcf/Lef and Gro/TLE

Tcf/Lef proteins are the most downstream components of the Wnt/β-catenin pathway. *Wnt* genes encode secretory glycoproteins that are crucial for many developmental and homeostatic processes in animals (reviewed by Logan *et al.*, 2004). The name “Wnt”

derives from a combination of two genes. In 1982, Nusse *et al.* identified an oncogene in mouse mammary tumors, which they called *Int1* (Nusse *et al.*, 1982; van Ooyen *et al.*, 1984). The second gene is the *Drosophila* homologe *wingless* (*wg*), which controls segment polarity during larval development (Sharma *et al.*, 1976; Baker, 1987). Due to their similarity in sequence, both names were combined and *Int1* was renamed to *Wnt1* (Rijsewijk *et al.*, 1987). Since then, conserved members of the Wnt family were identified in all metazoan animals. In mammals, for example, 19 Wnt genes are known (reviewed by MacDonald *et al.*, 2009).

Currently, three different Wnt signaling pathways are known: the canonical Wnt/β-catenin pathway, the non-canonical or planar cell polarity pathway (PCP), and the Wnt/Ca^{2+} pathway (reviewed by Croce *et al.*, 2008). Out of these three, the first pathway is the best known and the one where β-catenin and Tcf are major downstream components (**Figure 11**) (Behrens *et al.*, 1996; Arce *et al.*, 2006).

In the absence of Wnt ligand (**Figure 11**), cytosolic β-catenin is constantly phosphorylated by a so called degradation complex, which is composed of the scaffolding protein Axin, the tumor suppressor *adenomatous polyposis coli* gene product (APC), Casein kinase 1α (CK1α), and Glycogen synthase kinase 3β (GSK3-β) (Aberle *et al.*, 1997; Behrens *et al.*, 1998; Kishida *et al.*, 1998; Liu *et al.*, 2002; Kimelman *et al.*, 2006). This phosphorylation creates binding sites for the E3 ubiqitine ligase F-box/WD repeat-containing protein β-TrCP (β-Transducin repeat containing protein), which in turn leads to ubiquination and proteosomal degradation of β-catenin (reviewed by Cadigan *et al.*, 2009; MacDonald *et al.*, 2009; Kim, W. *et al.*, 2013; Stamos *et al.*, 2013). The role of APC in this complex has been enigmatic and several functions have been suggested. It protects β-catenin from dephosphorylation, which in turn enhances β-catenin phosphorylation and degradation (Su *et al.*, 2008). On the other hand, APC and Axin use the same binding interface, which led to the conclusion, that APC removes phosphorylated β-catenin from Axin, thereby making Axin available for another round of β-catenin phosphorylation (Xing *et al.*, 2003). Additionally, APC promotes Axin degradation, which could be a mechanism to buffer β-catenin fluctuations at varying APC levels (Takacs *et al.*, 2008). APC facilitates β-catenin nuclear export (reviewed by Henderson *et al.*, 2002) and acts as chromatin-associated suppressor for β-catenin target genes (Sierra *et al.*, 2006).

As long as β-catenin is degraded, the Q-domain of Gro/TLE proteins bind to the central domain of Tcf/Lef (Roose *et al.*, 1998; Brantjes *et al.*, 2001; Daniels *et al.*, 2005; Arce *et al.*, 2009). Two interaction domains were identified within the Gro/TLE binding domain. The short GBS (**Figure 10**), and a second region within the highly conserved HGM box. Whether this interaction is mediated by a single Gro/TLE tetramer or results from higher order complexes is yet not known (Arce et al., 2009). Once the Wnt/ β-catenin pathway is activated (**Figure 11B**), β-catenin is no longer phosphorylated and free to translocate to the nucleus (reviewed by Cadigan *et al.*, 2009; MacDonald *et al.*, 2009; Kim, W. *et al.*, 2013; Stamos *et al.*, 2013). There it binds to the amino-terminal β-catenin domain of Tcf/Lef. In principle, the β-catenin and the Gro/TLE binding domains are not located in close vicinity. Nevertheless it seems that both proteins compete for an overlapping binding domain in the central region of Lef1 (Daniels *et al.*, 2005) and cannot be present on the chromatin simultaneously (Sierra *et al.*, 2006).

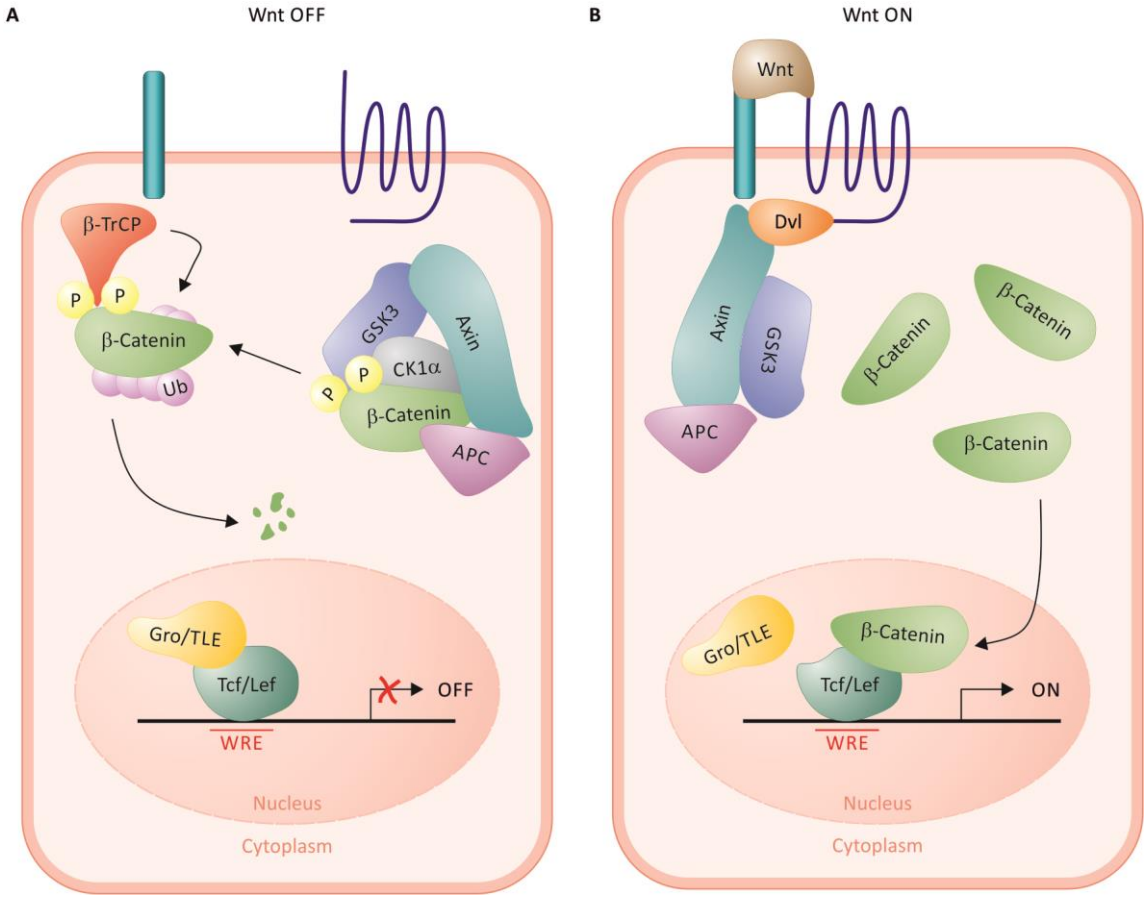

Figure 11| ***The canonical Wnt/β-catenin signaling pathway.*** (A) In the absence of Wnt, β-catenin is phosphorylated by the degradation complex (Axin, GSK3, CK1α, APC). Phosphorylated β-catenin interacts with β-TrCP, leading to its ubiquitination and proteosomal degration. This enables binding of Gro/TLE to Tcf/Lef and the repression of *Wnt* target gene expression. (B) Activation of the Wnt signaling pathway protects β-catenin from degradation. It translocates to the nucleus where it displaces Gro/TLE from Tcf/Lef. Abbreviations: APC, adenomatous polyposis coli; CK1α, Casein kinase 1α (CK1α); Dvl, Dishevelled; GSK3, Glycogen synthase kinase 3β; LRP, lipoprotein receptor-related protein; β-TrCP, β-Transducin repeat containing protein; WRE, Wnt response elements.

2 MATERIALS AND METHODS

2.1 MATERIALS

2.1.1 LABORATORY EQUIPMENT

Equipment	**Company**
VacuSafe pump	Integra
AlphaImager ®	Cell Biosciences
Centrifuge	Eppendorf
Cooling centrifuge	Eppendorf
Electrode	WTW
Glass pipettes 10 + 5 ml	Roth
Heating block	Eppendorf
Laminar Flow Hood danLAF VFB 1206 GS	Heraeus
Horizontal needle puller	Sutter Instruments
Incubator 27°C	MEMMERT
Incubator 37°C	Sanyo
Injector	Eppendorf
Inkubator 17°C	Binder
Luminoskan Ascent ®	Thermo Scientific
Magnetic stirrer	VWR
Neubauer counting chamber	Roth
pH meter	Hanna
Pipetten	Labmate
Pistill	Roth
Quarz cuvette	Hellma
Shaker	VWR
Waterbath	Grant

Table 1| ***List of consumables and companies they were purchased from.***

2.1.2 CONSUMABLES

Consumable	**Company**
1.5 ml tubes	Sarstedt
1.5 ml tubes with screw caps	Sarstedt
1-20 µl filter tips	Greiner
1-20 µl tips	Greiner

Consumable	Company
2 ml tubes	Sarstedt
200 - 1000 µl filter tips	Greiner
200-1000 µl tips	Greiner
20-200 µl filter tips	Greiner
20-200 µl tips	Sarstedt
6-well plates	PAA
96-well plates	PAA
Borosilicate glass capillaries	Clark Electromedical Instruments
Cell culture flask 75 cm2	PAA
CO_2	Air Liquid
Culture dishes 10 cm	Greiner
Culture dishes 3.5 cm	Greiner
Falcons 15 ml	Sarstedt
Falcons 50 ml	Sarstedt
Filtropur S 0.2 µM	Sarstedt
Gene Pulser® disposable Cuvettes, 0.4 cm gap width	BioRad
Glasware	Schott
Gloves, nitril	Hygiene Products
Inoculating loops	Roth
Microloader	Eppendorf
Pasteur pipettes, glass 240 cm	Roth
Pasteur pipettes, plastic 3 ml small tip	Sarstedt
Pasteur pipettes, plastic 3ml	Roth
PCR caps, 8-strips	Sarstedt
PCR tubes, 8-strips	Sarstedt
Syringes 3 ml	Roth
Tweezers	Roth

Table 2| ***List of consumables and companies they were purchased from.***

2.1.3 CHEMICALS AND REAGENTS

Reagent	Name	Company
Agar-agar		Roth
Agarose		Biozym
BCIP	5-bromo-4-chloro-3-indolyl phosphate, p-toluidine salt	Fermentas
Boric acid		Roth
Bromphenol blue		Sigma
Coelenterazine		Synchen OHG
DCTA	Titreplex IV	Merck
DEPC	Diethylpyrocarbonate	Roth
DMEM high		PAA

Reagent	Name	Company
glucose		
DMF	N,N-Dimethylformamide	Roth
EDTA	Ethylenediaminetetraacetic acid	Roth
EtBr	Ethidiumbromide	Roth
Ethanol		Roth
Ficoll		Sigma
FITC Dextran		Sigma
Formamide		Roth
Glycerin 86%		Roth
Glycin		Roth
HCl	Hydrogen chloride	Roth
Heparin		Sigma
HEPES		Roth
IPTG	Isopropyl β-D-1-thiogalactopyranoside	Fermentas
KCl	Potassium chloride	Roth
KH_2PO_4	Potassium dihydrogen phosphate	Roth
LiCl	Lithium chloride	Sigma
Luciferin		Synchen OHG
Methanol		Roth
$MgCl_2$	Magnesium chloride	Roth
$MgSO_4$	Magnesium sulfate	Roth
Na_2HPO_4	Disodium hydrogen phosphate	Roth
NaCl	Sodium chloride	Roth
$NaHCO_3$	Sodium bicarbonate	Roth
NaOH	Sodium hydroxide	Roth
NBT	Nitro blue tetrazolium	Fermentas
PEG 6000	Polyethylene glycol	Roth
PEI	Polyethyleneimine	Sigma
Pepton		Roth
PFA	Paraformaldehyde	Roth
RNA (torula yeast)		Sigma
SDS		Roth
sheep serum		Sigma
Tris		Roth
Trypsin		PAA
TurboFect		Fermentas
Tween20		Roth
X-gal	5-bromo-4-chloro-indolyl-β-D-galactopyranoside	Fermentas
Yeast exctract		Roth

Table 3| ***List of chemicals and companies they were purchased from.***

2.1.4 *Buffers and Solutions*

Buffers and solutions that are not otherwise mentioned in the chapter "Methods" and used in several methods and various concentrations.

10x PBS: 1.37 M NaCl; 27 mM KCl; 43 mM Na_2HPO_4; 14 mM KH_2PO_4; pH 7.4

PTW: PBS dilution + 0.1% tween20

20x SSC: 3 M NaCl; 0.3 M trisodium citrate; pH 7

SSCT: SSC dilution + 0.1% tween20

10x ERM: 170 mM NaCl; 4mM KCl; 270 mM $CaCl_2 \times 2H_2O$; 65 mM $MgSO_4 \times 7H_2O$; pH 7.0

10x Yamamoto's: 1.28 M NaCl; 27 mM KCl; 14 mM $CaCl_2$; 2.4 mM $NaHCO_3$; pH 7.3

NBT: 50 mg/ml in 100% DMF

BCIP: 75 mg/ml in 70% DMF/DEPC-H_2O

16% PFA: 16% PFA in 1x PTW; pH 7.5

LB agar: for 500 ml: 7.5 g agar-agar

2.1.5 *Enzymes*

Enzyme	Company
Proteinase K	Fermentas
T4 DNA ligase	Fermentas
T7 polymerase	Fermentas
T3 polymerase	Fermentas
SP6 polymerase	Fermentas
Phusion polymerase	Finnzymes
Taq polymerase	Apogene
RNase inhibitor	Fermentas
DNase I	Fermentas
I-Sce I Meganuclease	New England Biolabs
FastAP Thermosensitive Alkaline Phosphastase	Fermentas
Restriction enzymes	Fermentas

Table 4| ***List of enzymes.***

2.1.6 *ANTIBIOTICS*

Penicillin/Streptomycin (PAA)

Ampicillin (Roth)

2.1.7 *OLIGONUCLEOTIDES*

Name	**Sequence 5'-3'**
Morpholinos:	
Tcf3	GCATGTTTGCACACCAGTCGATCAG
Tle1	CGCGTCTTGTCCTGAAACCCCGCTA
Tle 2b	GGCAGTGCGTCCTCGTGGCTCTTTC
Tle 3b	CGGCCTTGTGGATACATGTCTCGTC
PCR primers:	
Tcf3 Fw	CGGATCCATGGCTCAACTGAACGGAGGC
Tcf3 Rev	CGAAGACGGCTGGACATGGATGCATTCA
WRPW Fw	CGCGTGACTCCGTGTGGAGGCCGTGGTA
WRPW Rev	AGCTTACCACGGCCTCCACACGGAGTCA
Gbx1 Fw	TTAGAAAATACAGCCACAA
Gbx1 Rev	TCACTGTAAAAAGTACCTG
Sequencing primers:	
SP6	GGATTTAGGTGACACTATAG
T7	TAATACGACTCACTATAGGG
pMC	TCCATTCGGGTGTTCTT

Table 5| ***Oligonucleotides and their sequences.***

2.1.8 *PLASMIDS*

For cell culture experiments pMC (Fink *et al.*, 2006) and pKC (polylinker modification of pKW) (Adams *et al.*, 1992) were used (both vectors contain cytomegalovirus promoters). DNA constructs for microinjection were under the control of a bi-directional heat-inducible promoter (Bajoghli *et al.*, 2004). pLucF24ZF; luciferase reporter under the control of a Fos minimal promoter and 24 zinc finger binding sites. The resulting vectors were analysed by restriction enzyme digestion. Insert orientation was verified by sequencing.

Plasmid	Vector	Insert
pLucF24ZF	pLucF	24 zinc-finger binding sites
pKC Aes	pKC	Medaka Aes
pMC hSix3(85-203)mZFb6	pMC	Human Six3 domain myc-linked to a zinc-finger; base (acid-base interaction)
pMC Tle1VP16	pMC	Medaka Tle1; herpes simplex virus VP16 domain
pMC Grg4VP16	pMC	Mouse Grg4; herpes simplex virus VP16 domain
pMC amVP16	pMC	Herpes simplex virus VP16 domain; myc-linked acid (acid-base interaction)
pSGH3 Tle1	pSGH3	Medaka Tle1
pSGH3 Tle1 R534A	pSGH3	Mutated medaka Tle1
pSGH3 WRPW	pSGH3	WRPW motif
pSGH3 Aes ATG	pSGH3	Mouse Aes
pSGH3 Tle 4	pSGH3	Mouse Tle4
pSGH3 Tle 4 Q	pSGH3	Mouse Tle4 Q domain
pSGH3 Tle Q2	pSGH3	2x Q domain
pSGH3 Tle Q3	pSGH3	3x Q domain
pSGH3 Tle Q4	pSGH3	4x Q domain
pSGH3 Tle 4 D494C	pSGH3	C-terminally truncated Mouse Tle4
pSGH3 Tle 4 WD40	pSGH3	Mouse Tle4 WD40 repeat domain
pSGH3 Tcf3	pSGH3	*Xenopus* Tcf3
pSGH3 Tcf3 ΔGro	pSGH3	*Xenopus* Tcf3 lacking the groucho binding domain
pSGH3 Tcf3 (1-434)	pSGH3	*Xenopus* Tcf3 lacking the CtBP domain
pSGH3 Tcf3 (1-434) ΔGro	pSGH3	*Xenopus* Tcf3 lacking the CtBP domain and the groucho binding domain

Table 6| ***Vectors and inserts.***

	Plasmid/Vector	Origin
	pGEM® T Easy	Promega
	pMC	(Fink *et al.*, 2006)
	pKC	(Adams *et al.*, 1992)
1)	pLucF24ZF	Sub-clone: pLucF 12ZF and pLucF 12ZF
1)	pKC Aes	Sub-clone: pKW2TGrg5
1)	pMC hSix3(85-203)mZFb6	Sub-clone: pGemT hSix3(85-203)
1)	pMC Tle1VP16	Sub-clone: pMC ZFVP16 and pMC maFK
1)	pMC Grg4VP16	Sub-clone: pMC Grg4 and pMC ZFVP16
1)	pMC amVP16	Sub-clone: pMC VP16 and pGemT Tle1
	pSGH3	Modified from (Bajoghli *et al.*, 2004)
2)	pSGH3 Tle1	Sub-clone (Aghaallaei *et al.*, 2005)
2)	pSGH3 Tle1 R534A	Sub-clone provided by Stefano Stifani
2)	pSGH3 WRPW	PCR amplified, medaka embryonic cDNA
2)	pSGH3 Aes ATG	Sub-clone (Aghaallaei *et al.*, 2005)

	Plasmid/Vector	Origin
	pSGH3 Tle 4	Sub-clone (Bajoghli *et al.*, 2005)
2)	pSGH3 Tle 4 Q	Sub-clone (Heimbucher *et al.*, 2007)
2)	pSGH3 Tle Q2	Sub-clone: pMC (Qg)2maFK
2)	pSGH3 Tle Q3	Sub-clone: pMC (Qg)3maFK
2)	pSGH3 Tle Q4	Sub-clone: pMC (Qg)4maFK
2)	pSGH3 Tle 4 D494C	Sub-clone (Heimbucher *et al.*, 2007)
2)	pSGH3 Tle 4 WD40	Sub-clone (Heimbucher *et al.*, 2007)
2)	pSGH3 Tcf3	Sub-clone: pHA XTcf3
2)	pSGH3 Tcf3 ΔGro	Sub-clone: pHA XTcf3
2)	pSGH3 Tcf3 (1-434)	Sub-clone: pHA XTcf3
2)	pSGH3 Tcf3 (1-434) ΔGro	Sub-clone: pHA XTcf3
3)	pGemT OlTcf3C	PCR amplified, medaka embryonic cDNA
3)	pGemT Gbx1	PCR amplified, medaka embryonic cDNA
3)	pOL Pax6	Partial medaka Pax6 cDNA provided by Felix Loosli and Jochen Wittbrodt
3)	pOl Pax2-20	Medaka Pax2 cDNA provided by Reinhard Koester and Jochen Wittbrodt
3)	pOl goosecoid	Medaka goosecoid cDNA provided by Keiji Inohaya and Jochen Wittbrodt
3)	pOl Rx2	Medaka Rx2 cDNA provided by Jochen Wittbrodt
3)	pCG OlBf1	Partial medaka Bf1 cDNA provided by Clemens Grabher and Jochen Wittbrodt
3)	pOl Wnt1	Medaka Wnt1 cDNA provided by Mathias Carl and Jochen Wittbrodt
3)	pOl Six3	Medaka Six3 cDNA provided by Jochen Wittbrodt
3)	pOl Otx2	Medaka Otx2 cDNA provided by Felix Loosli and Jochen Wittbrodt

Table 7| *Plasmids and their origin.* 1) used for cell culture experiments; 2) used for microinjection, 3) used for *in situ* hybridization. All plasmids are commonly used in the laboratory. PCR amplified vectors were prepared with the indicated primers.

2.1.9 Cell Lines

For all cell culture experiments, the human epithelial cervix adenocarcinoma cell line (HeLa), ATCC name: CCL-2, was used. Cells were grown in DMEM high glucose medium supplemented with 10% FCS and 1x penicillin/streptomycin (100 U/ml) in a humidified atmosphere and the standard conditions of 37°C and 5% CO_2. The cells were propagated twice a week with an average sub-culturing rate of 1/10. For cell detachment, 1x trypsin was used.

2.1.11 MEDAKA STOCKS

Wild type medaka from the Cab strain and the transgenic lines were kept under an artificial 14/10 hours day/night light cycle. For optimal egg-laying efficiencies, the fish were fed 3x per day (2x with commercially available fish flakes and 1x with newly hatched brine shrimp). Male and female fish (1 male and 3 females) were only separated when embryos at the 1-cell stage were needed.

2.1.12 SOFTWARE

Name	Company/Developer
AxioVision	Carl Zeiss Microscopy
CorelDraw Graphics Suite X6	Corel
EndNote X5	Thomson Reuters
ImageJ	Wayne Rasband (NIH)
Microsoft Office 2010	Microsoft
VectorNTI Advance10	Invitrogen

Table 8| ***Software and its origin/developer.***

2.2 METHODS

2.2.1 DNA AND RNA METHODS

Polymerase chain reaction (PCR)

For a PCR from plasmid DNA or medaka cDNA the following components were mixed in a PCR tube and kept on ice until amplification:

10	ng	DNA
25	pmol	forward primer
25	pmol	reverse primer
1	µl	dNTPs (10 mM)
0.5-1	U	Phusion polymerase
10	µl	5x HF buffer

ad 50 µl with autoclaved dH_2O

PCR reactions were performed in standard PCR cyclers with heated lids. The number of cycles varied depending on the template. For plasmid DNA 25 cycles were used, for medaka cDNA usually a higher number of cycles were required.

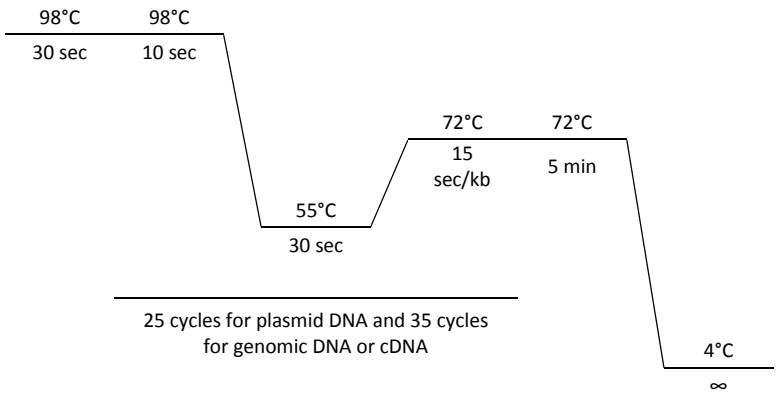

Figure 12| ***Standard PCR program using Phusion polymerase.***

DNA/RNA gel electrophoresis

DNA and RNA were visualized by agarose gel electrophoresis. For separation of the fragments agarose gels (Biozym LE Agarose, Biozym), with different percentages (0.5%, 1%, or 2%) of agarose depending on the size of the fragment, were prepared in SB running buffer (2 M NaOH; 7.3 M boric acid). To visualize DNA or RNA under ultraviolet light, 0.01% ethidium bromide was added to the gel prior casting. The samples were mixed with 5x loading buffer (20% Ficoll 400; 0.1 M EDTA; 1% SDS; 0.1% bromphenol blue; pH 8.0) (final concentration is 1x), loaded into the wells, and the gels were run at 120 V in 1x SB running buffer. As size standards the O'Gene Ruler 100 bp ladder (Fermentas) mixed with λ BstEII (Fermentas) was used for DNA separation and the Ribo Ruler High Range Ladder 200 to 6,000 bases (Fermentas) for RNA separation.

DNA gel purification

To extract and purify DNA fragments from 1% agarose gels, the Invisorb® Spin DNA Extraction Kit (Invitek) was used. All centrifugation steps were carried out in a bench-top centrifuge. After every spinning step the centrifuge was discarded, except after elution.

DNA fragments were excised from the gel with a clean scalpel and 500 µl Gel Solubilizer S were added. To enhance dissolving, the gel pieces were incubated at 50°C for 10 minutes while shaking and additionally mixed several times. Before adding the samples to the spin columns, 250 µl Binding Enhancer were added. The columns were centrifuged for 1 minute at 10,000 rpm and washed twice with 500 µl Wash Buffer, using the same spinning conditions. To remove all traces of ethanol from the Washing Buffer, an additional centrifugation step was carried out at maximum speed (~ 13,400 rpm) for 4 minutes. For elution, the spin columns were placed into a sterile 1.5 ml tube, 10 µl H_2O, pre-warmed to 70°C, were added and the samples were spun for 1 minute at maximum speed. Another 10 µl H_2O were added and centrifugation was repeated. The purified DNA was kept at -20°C until further use.

Calf intestinal phosphatase (CIP) dephosphorylation

CIP dephosphorylation was used for plasmid DNA after restriction enzyme digest to prevent recirculating of the cut ends during the ligation step.

The linearized plasmid DNA was incubated for 10 minutes at 37°C with 1 µl FastAP Thermosensitive Alkaline Phosphastase. The reaction was stopped by adding 1µl 0.5 M EDTA and 20 minutes incubation at 80°C. To purify the DNA, 100 µl Binding Enhancer were added and the samples were applied to the spin columns of the Invisorb® Spin DNA Extraction Kit (Invitek). Further purification was performed as described in the chapter "DNA gel purification" and reviewed on an agarose gel.

A-tailing

For further cloning into a pGEM® T-Easy (Promega) vector a 3'-terminal A-overhang was amplified:

6	µl	purified DNA
1	µl	Buffer (-$MgSO_4$)
2	µl	dATP (0.1 µM)
0.5	µl	$MgSO_4$
0.5	µl	Taq polymerase

ad 10 µl with autoclaved dH_2O

The 3'-terminal A-overhang was amplified in a standard PCR cycler with heated lid for 20 minutes at 72°C.

Ligation

Ligation with pGEM® T-Easy was performed according to the Promega Technical Manual "pGEM®-T and pGEM®-T Easy Vector Systems" using a modified reaction mix:

x	µl	Insert (3:1 insert:vector molar ratio)
50	ng	pGEM® T-Easy vector
1	µl	T4 DNA Ligase
1	µl	T4 DNA Ligase buffer

ad 10 µl with autoclaved dH_2O

Ligation was performed at room temperature overnight. If a shorter incubation time was necessary, the ligase had to be inactivated for 20 minutes at 65°C.

Transformation

To 100 µl TOP10F' cells (Invitrogen), thawed on ice, the whole ligation reaction was added and gently mixed by tapping the tube. The cell were incubated on ice for 10 minutes, heat-shocked for 90 sec at 42°C and immediately chilled on ice for 2 minutes. 1 ml LB broth (1% bacto trypton, 0.5% yeast extract, 0.5% NaCl, 1 ml 5 M NaOH) was added and the tubes were incubated at 37°C for 30 minutes while shaking. Subsequently, the cells

were centrifuged for 4 minutes at 5,000 rpm and the supernatant was discarded. The pellet was resuspended with the remaining supernatant and spread on a pre-warmed LB-Ampicillin agar plate which was then incubated over night at 37°C.

For blue/white screening 10 µl IPTG (1 M) and 10 µl X-gal (20 mg/ml DMF) were added prior plating.

Mini-preparation of plasmid DNA

For a standard mini-preparation 2 ml of LB Broth containing 0.1% ampicillin were inoculated with a single colony of transformed bacteria. The culture was incubated overnight at 37°C with vigorous shaking. All centrifugation steps were carried out in a bench-top centrifuge.

The culture was transferred to a 2 ml tube and centrifuged for 2 minutes at 6,000 rpm. The bacterial pellet was resuspended in 100 µl buffer P1 (50 mM Tris, 10 mM EDTA, 100 µg/ml RNase A) and lysis was performed for 5 minutes with 200 µl lysis buffer P2 (0.2 M NaOH, 1 % SDS). To pellet cell debris, 200 µl neutralization buffer P3 (3 M KAc, 11.5 % Glacial acetic acid) were added and the mix was centrifuged for 20 minutes at full speed. The supernatant was transferred to a new 2 ml tube and the DNA was precipitated in 0.5 ml 24% PEG for 15 minutes at 37°C with shaking and centrifuged for 15 minutes at 4°C with max. speed. Washing was performed in 500 µl 70% ethanol, followed by a 5 minutes centrifugation step at full speed. The air-dried pellet was resuspended in 20 µl dH_2O and the DNA was controlled by agarose gel electrophoresis.

Midi-preparation of plasmid DNA

For a standard midi-preparation 75 ml of LB broth containing 0.1% ampicillin were inoculated with a single colony of transformed bacteria or 10 µl of mini-preparation culture. The culture was incubated overnight at 37°C with vigorous shaking. For DNA extraction 50 ml of the bacterial culture were centrifuged 6 minutes at 4,000 g and processed using the JETSTAR 2.0 Midi Kit (Genomed). All steps were carried out according to the manufacturers' protocol except for cell lysis and washing steps, where only half of the recommended volume was used. The concentration of the DNA was quantified by OD_{260} measurement and the DNA quality was controlled with a restriction enzyme digest and agarose gel electrophoresis.

RNA probe synthesis for *in situ* hybridization

For the in vitro transcription plasmid DNA was linearized with an enzyme that generates a 5' overhang for 2 hours at 37°C:

10-15	µg	Plasmid DNA
10	µl	Enzyme buffer
5	µl	Enzyme

ad 100 µl with DEPC-H_2O

To clean up the digestion mix, the Invisorb® Spin DNA Extraction Kit (Invitek) was used as described before except for the amount of Binding Enhancer used, 400 µl in this case, and elution was carried out with DEPC-H_2O. The linearized DNA was controlled and quantified with agarose gel electrophoresis.

Depending on the construct orientation in the plasmid, T3, T7 or SP6 polymerase were used for the *in vitro* transcription.

In vitro transcription reaction mix:

1	µg	Linearized DNA
4	µl	5x transcription buffer
8	µl	rNTP-Dig-mix
0.1	µl	RNAse inhibitor
1	µl	RNA polymerase
ad 20 µl with DEPC-H_2O		

rNTP-Dig-mix for 1 reaction:

2	µl	10 mM rATP
2	µl	10 mM rCTP
2	µl	10 mM rGTP
1.3	µl	10 mM rUTP
0.7	µl	Dig-rUTP
8	µl	

In vitro transcription was performed for 2 hours at 37°C. Remaining DNA was removed by adding 2 µl DNAse I and another 15 minutes incubation at 37°C and DNAse activity was stopped with 1 µl 0.5 M EDTA pH 8. The RNA was precipitated with 2.5 µl 4 M LiCl and 75 µl ethanol for 30 minutes at -80°C and centrifuged 30 minutes at 4°C and 14,000 rpm. The pellet was washed with 100 µl 70% ethanol/DEPC-H_2O and centrifugation was repeated. The resulting pellet was resuspended in 20 µl DEPC-H_2O and controlled and quantified with agarose gel electrophoresis.

2.2.2 Protein Methods

Antibody pre-adsorbtion for *in situ* hybridization

For antibody pre-adsorbtion, wild type embryos shortly prior hatching were fixed as described before. Dechorionation is not necessary in this case. Approximately 200 µl embryos were stored at -20°C for at least 24 hours.

The embryos were rehydrated by washing them 3x 5 minutes in 1x PTW and then homogenized with a pestle and the volume was adjusted to 200 µl with 1x PTW. 2 µl Anti-Digoxigenin-AP Fab fragments (Roche) (final antibody dilution 1:100) were added and the solution was incubated over night at 4°C on a shaker.

The pre-adsorbed antibody was spun for 10 minutes at 4°C and 14,000 rpm and the supernatant was sterile filtered using a Filtropur S 0.2 (Sarstedt) filter. The embryonic debris was resuspended in 1x PTW and spun with the same conditions as described before and filtered again. The two antibody solutions were combined and the volume was adjusted to 4 ml with 1x PTW (final dilution 1:2,000). Stored at 4°C the pre-adsorbed antibody was stable for 3-4 months.

Dual luciferase assay

For luciferase measurement, the cells in each well of the 96-well plate were first washed with 40 µl 1x PBS and then lysed in 25 µl lysis buffer (0.1 M Tris pH 7.5; 1% Triton X) for 10 minutes and vigorous shaking. Firefly and *Gaussia* luciferase were detected using the Luminoskan Ascent® (Thermo Scientific) luminometer.

Firefly luciferase substrate solution for one 96-well plate:

50	µl	10 mM Luciferin
62.5	µl	0.2 M ATP
31.25	µl	1 M Tris pH 7.5
46.88	µl	1 M $MgCl_2$
4.8	ml	dH_2O

Gaussia luciferase substrate solution for one 96-well plate:

3.125	µl	Coelentherazine
25	µl	0.5 M EDTA
31.25	µl	1 M Tris pH 7.5
4.9	ml	dH_2O

2.2.3 Cell Culture Methods

Coating

96-well plates were coated with 50µl PEI (2.5 µg/ml; pH 7.4 adjusted with 5 mM HEPES) per well. The plates were incubated for at least 30 minutes at 37°C and subsequently washed with 50 µl 1x PBS per well. The plates were kept at 4°C for at least 15 minutes or until further use, but not longer than one week.

Transfection

For transfection, 0.3 x 10^4 cells per well were seeded in 100 µl DMEM high glucose medium supplemented with 10% FCS and 1x Penicillin/Streptomycin in polyethylenimine coated 96-well plate and incubated for 24 hours. DNA mixes (see below), containing approximately 90 ng of DNA per well, were incubated with 0.14 µl TurboFect Transfection Reagent per well for 30 minutes at room temperature. 40 µl of transfection mix were added to each well and the plate was incubated for 2 hours at standard conditions. To stop the reaction, 100 µl DMEM high glucose medium containing supplements were added to the cells. Luciferase was measured after 24 hours incubation at standard conditions.

		Control	Tle4 vs. Aes	Tle1 vs. Aes
Reporter	70 ng	pLucF 24ZF		
Internal control	2 ng	pMCGlucS		
Bait	20 ng	pMC hSix3 (85-203)mZFb6		
Pray	20 ng	pMC am VP16	pMC Grg4 VP16	pMC Tle1 VP16
Repressor	0-20 ng	pKC Aes		

Table 9| ***Transfection mix for 2-hybrid transfection.***

2.2.4 FISH METHODS

Fixation and dechorionation of medaka embryos

Medaka embryos were fixed in 4% paraformaldehyde (PFA) in 2x PTW at 4°C overnight or at least 4 hours at RT on a shaker. Instead of 2x PTW, 1x PTW can be used for fixation. This avoids deformation of the yolk but makes chorion removal more difficult.

For dechorionation, the embryos were transferred into a larger plate containing 1x PTW and the chorion was removed with tweezers. Dechorionated embryos were washed 4x 5 minutes with 1x PTW and 1x 5 minutes at RT on a shaker. The methanol was replaced and the embryos were stored at -20°C at least over night or until further use. Longer storage than overnight is recommended, thus methanol treatment enhances probe penetration.

Microinjection of medaka embryos

Medaka embryos were collected 30 minutes. after mating and kept in pre-cooled 1x ERM, to slow down development. For injection the eggs were cleaned and separated, and placed into an injection dish containing 1.5% agarose and pre-cooled 1x Yamamoto. Injection was performed using a microinjector and borosilicate glass capillaries.

The glass capillaries were prepared with a horizontal needle puller (Sutter Instruments) in two heating steps using the following settings: pressure 800, heat 560, pull 50, velocity 80, time 200.

Injection mix for transient expression or transgenic lines:

5-80	ng	Plasmid DNA
1	µl	10x meganuclease buffer
1	µl	10x Yamamoto
1	µl	I-SceI

ad 20 µl with H_2O

Injection mix for knockdown experiments:

0.5 µl	10x Yamamoto
x µl	morpholino

ad 5 µl with H_2O

Whole mount *in situ* hybridization in medaka

Unless otherwise mentioned all steps of the *in situ* hybridization were performed on a shaker at RT using fixed and dechorionated embryos.

Prior to Proteinase K treatment, the embryos were re-hydrated for 5 minutes each in 75% MeOH/1x PTW, 50% MeOH/1x PTW, 25% MeOH/1x PTW and 2x 5 minutes with 1x PTW. Digestion with Proteinase K, 10 µg/ml in 1x PTW, was performed depending on the developmental stage of the embryos.

Stage	**Proteinase K digestion time**
1-13	1-2 min
14-16	3-4 min
17-20	5 min
21-24	7 min
25-30	10-15 min
>30	>15 min

Table 10| ***Time of Proteinase K digestion.***

To avoid unwanted damage of the fragile embryos, the digestion step is not performed on the shaker. Digestion was stopped by rinsing 2x in 2mg/ml Glycine/1x PTW. The embryos were re-fixed for 20 minutes in 4% PFA/2x PTW and washed 5x 5minutes in 1x PTW.

For hybridization, all subsequent steps were performed in a water bath pre-heated to 65°C. The embryos were transferred to 2 ml tubes and pre-hybridized for at least 1 hour. The probe was diluted in the hybridization-mix (10-20 ng/150 µl) and denatured for 10 minutes at 80°C. After pre-hybridization the embryos were incubated overnight in the probe/hybridization-mix.

All post-hybridization washes were performed using pre-heated washing solutions in the 65°C water bath. The embryos were washed 2x 30 minutes in 50% Formamide/2x SSCT, 1x 15 minutes in 2x SSCT and 2x 30 minutes in 0.2x SSCT.

Prior antibody incubation the embryos were blocked for 1 hour in 5% sheep serum/1x PTW. The embryos were incubated in 200 µl pre-adsorbed antibody for 1.5 hours and the washed 6x 10 minutes in 1x PTW. The last washing step was performed overnight at 4°C.

For the staining reaction the embryos were equilibrated 2x 5 minutes in SB staining buffer (100 mM Tris pH 9.5; 100 mM NaCl; 50 mM $MgCl_2$; 0.1% tween20) and then

incubated in the NBT/BCIP/SB staining solution (337.5 µg/ml NBT; 175 µg/ml BCIP in SB staining buffer) until stained. As this reaction is light sensitive, staining was performed in the dark and without shaking. To stop the reaction, the embryos were washed 3x 5 minutes in 1xPTW, fixed in 4% PFA/2x PTW and washed again 3x 5 minutes in 1x PTW. To remove excess staining, the embryos were de-stained in MeOH until the yolk was transparent. De-staining was stopped by adding 1x PTW and the MeOH was removed by 2x 5 minutes washing in 1x PTW. 86% Glycerol was used for documentation under a light microscope and storage at 4°C.

Heat shock

Heat induction was performed in a standard PCR cycler tube, filled with 100 µl 1x ERM. To ensure fast and equal heat distribution, only one embryo was used per tube. The tubes were placed into a PCR cycler and pre-incubated for 30 minutes at 27°C. The actual heat treatment was performed for 10 minutes at 43.5°C, followed by a recovery phase of 30 minutes at 27°C. For Gfp selection (earliest 4 hours after induction), the embryos were placed into the furrows of an agarose coated plate.

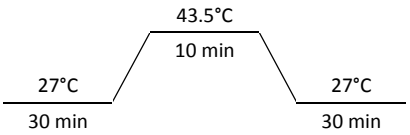

Figure 13| ***PCR cycler program for standard heat treatment.***

Diffusion and electroporation

Four embryos at 40% epiboly were incubated with 100 µl 0.4 M lithium chloride (LiCl) for 10 minutes at 27°C. To remove excess LiCl, the embryos were then washed 3x with 1x ERM. For embryos that were further used for electroporation the diffusion was performed in cuvettes, followed by immediate electroporation using the standard settings: pulse frequency 330 Hz; voltage 15 V; burst time 100 ms; 1 burst. Subsequent washing steps were performed as described before.

3 RESULTS

Part I

3.1 ANALYSIS OF GRO/TLE IN MEDAKA EMBRYONIC DEVELOPMENT

The structure and function of Gro/TLE proteins has been studied intensively in many organisms during the last years. Whereas the genomes of *Drosophila* and *C. elegans* contain only a single *Grouch*o gene, four full length *TLE* genes were identified in chicken and mammals (reviewed by Li, S. S., 2000), and six homologes were found in the genome of teleost fish (Aghaallaei *et al.*, 2005). Aghaallaei *et al.* showed that in medaka the two additional genes resulted from duplications of *tle2* and *tle3*. Expression pattern analysis revealed a considerable overlap especially in the CNS and sensory organs (Aghaallaei *et al.*, 2005). In gain of function experiments with *tle1* mRNA the embryos showed enlargement of the optic vesicles. This was often accompanied by bulging of the midbrain (Lopez-Rios *et al.*, 2003). Misexpression of an inducible *tle4* construct led to enlarged otic vesicles and in rare cases to anophthalmia (Bajoghli *et al.*, 2005). Injection of the truncated family member *aes*, on the other hand, resulted in the opposite phenotype: reduced size of both the eyes (Lopez-Rios *et al.*, 2003) and the otic vesicles (Bajoghli *et al.*, 2005). Moreover, co-injection with *Aes* and *Tle1* or *Tle4* could rescue the phenotypes (Lopez-Rios *et al.*, 2003; Bajoghli *et al.*, 2005). To learn more about the function of Gro/TLEs during medaka embryonic development we decided to analyze Gro/TLE loss of function phenotypes.

3.1.1 LOSS OF FUNCTION THROUGH A DOMINANT-NEGATIVE APPROACH

In an initial attempt to interrupt Gro/TLE function, we started with a dominant-negative approach (**Figure 14**) using the HSE-inducible misexpression system (Bajoghli *et al.*, 2004). The principle idea was, to misexpress truncated forms of Gro/TLE proteins (**Figure 14B**), single domains (**Figure 14A,D**), mutated forms (**Figure 14C**) and interaction motifs (**Figure 14E**) that hinder Gro/TLE-mediated repression. Excess of these truncated or mutated proteins would then either displace the endogenous Gro/TLEs in the tetramers, thereby forming heterotetramers with reduced repressing ability (**Figure 14A-C,E**), or tether away its interaction partners (**Figure 14D**).

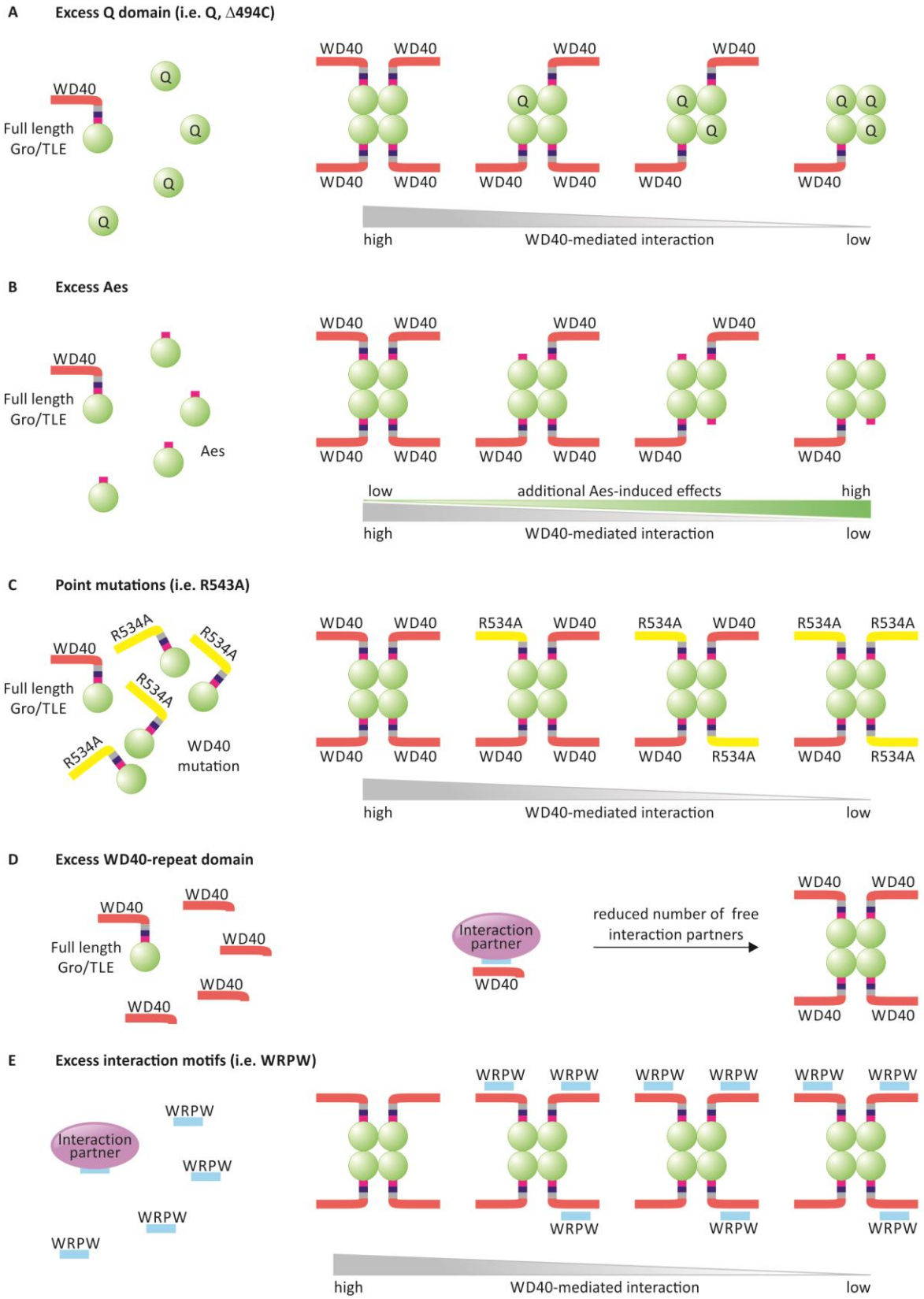

Figure 14| *Gro/TLE loss of function through a dominant-negative approach.* Schematic presentation of a successive loss of function of Gro/TLE tetramers by an excess of proteins/domains (A-D) and interaction motifs (E). An excess of the Q domain (green) (A) or Aes (B) expression leads to loss of WD40-repeat domains (red) within the tetramer. This reduces the number of potential binding sites of Gro/TLE interaction partners and thereby Gro/TLE-mediated repression. However, Aes might induce phenotypes on its own (B). (C)

Heterotetramers with full length Gro/TLE proteins harboring a mutation within the WD-repeat domain (yellow). (D) Excess of WD40-repeat domains tethers potential Gro/TLE interaction partners (purple) away from the tetramers. (E) Excess WRPW motifs (light blue) block the WD40-repeat domains, thereby hindering Gro/TLE interaction partners from binding. The Gro/TLE non-conserved domains GP (pink), CcN (dark blue) and SP (grey) are indicated between the Q domain (green) and the WD40-repeat domain (red) in full length Gro/TLE proteins.

To prevent protein-protein interaction, removal of the domain primarily responsible for this, the WD40-repeat domain, seems to be an obvious approach (**Figure 14A**). For this, C-terminally truncated Gro/TLE proteins (**Figure 15**), such as the Q domain (as described in **Figure 14A**), or the naturally occurring truncated Aes/Grg5 can be used. Indeed, it was shown that misexpression of *aes* in medaka blocked the repressive function of Tle proteins in the otic vesicles (Bajoghli *et al.*, 2005) and eye development (Lopez-Rios *et al.*, 2003). These truncated proteins are incorporated into Gro/TLE tetramers, thereby preventing binding to interaction partners. On the other hand, an excess of small peptides with the sequence of typical interaction motifs, such as WRPW (**Figure 15**), would block Gro/TLE's protein-protein interaction sites, displacing endogenous interaction partners (**Figure 14D**). *Vice versa*, an excess of the WD40-repeat domain (**Figure 15**) would bind to Gro/TLE's interaction partners leaving only low numbers of unbound proteins for full length Gro/TLE (**Figure 14C**).

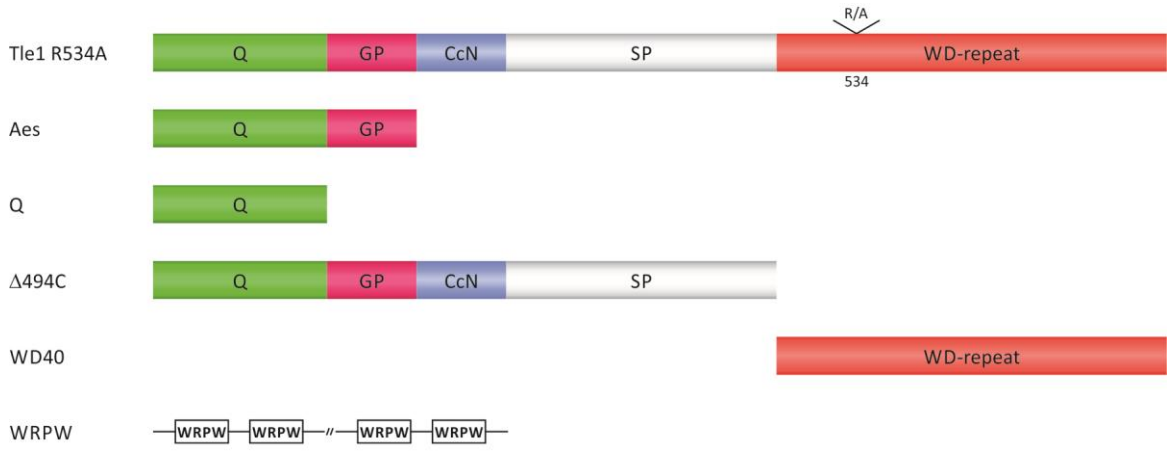

Figure 15| *Schematic protein structure of Gro/TLE deletion mutants.* For Tle1 R534A, arginine at position 534 was changed to alanine. Aes represents the full-length Aes protein. Truncation of Tle4 at the C-terminus resulted in either the Q-domain (Q) or a Tle4 lacking the WD40 repeat domain (Δ494C). Truncation at the N-terminus of Tle4, on the other hand, resulted in the WD40 repeat domain alone. WRPW represents the WRPW peptide motif that binds to the WD40 repeat domain of Gro/TLEs. All constructs were cloned into a heat-inducible plasmid vector.

In a first attempt to disrupt Tle function, we used a point mutation within the WD40-repeat domain of the C-terminal end of Tle1 (kindly provided by Stefano Stifani) (**Figure 14B** and **Figure 15**) (Buscarlet *et al.*, 2008). In *Drosophila*, several missense mutations within the WD40-repeat domain were identified, which resulted in cuticle phenotypes (Delidakis *et al.*, 1991; Jennings *et al.*, 2006). One of these mutants affects arginine at position 483 (R483) which contributes to the binding of WRPW peptides and the eh1 motif of the interaction partners (Jennings *et al.*, 2006; Buscarlet *et al.*, 2008). In the Gro^{MB41} mutant (R483H) this binding is interrupted by a substitution of arginine to

histidine at position 483, which results in excessive neural tissue formation and reduced cuticles (Jennings *et al.*, 2006). We used a Tle1 and introduced an arginine to alanine mutation at position 534 (**Figure 15**). This R534A substitution corresponds to the R483H change in *Drosophila* (Jennings *et al.*, 2006).

For our experiments we used the mutated form *tle1(R534A)* under the control of a bi-directional heat-inducible promoter with *gfp* being expressed as a control simultaneously (Bajoghli *et al.*, 2004). The embryos were co-injected with HSE-inducible *tle1(R534A)* and meganuclease at the 1-cell stage and heat induction was performed at early gastrula. Phenotype evaluation at stage 30-32 revealed that 30% of the embryos developed enlarged eyes and 15% had a bulging midbrain (**Table 11**). However, in control embryos misexpressing wild type *tle1* the number of large eye phenotypes was with 32% comparable to the mutated form, as was the number of embryos with a bulging midbrain (15%) (**Table 11**). Comparable results for *tle1* misexpression were also observed by López-Ríos *et al.* They connected the observed phenotype with Six3 and showed that Six3 not only binds to the Q domain of Tle1 but also weakly to the WD40 repeat domain (Lopez-Rios *et al.*, 2003) through an eh1-like motif in the Six-domain (Zhu *et al.*, 2002).

	control	dominant negative	empty vector
Embryos	27	73	107
Dead	5	12	4
Mortality	19%	16%	4%
Enlarged eyes	7	18	0
Bulging midbrain	4	9	0
unspecific phenotypes	1	2	4
Eye phenotypes in surviving	32%	30%	0%

Table 11| *Dominant-negative effects of Tle1 containing C-terminal amino acid substitutions.* Embryos at the 1-cell stage were co-injected with meganuclease and 80 ng/µl of tle1(R534A) under the control of a heat-inducible promoter (HSE:Tle1R534A) (Bajoghli et al., 2004). Heat induction was performed at early gastrulation (43.5°C, 10 minutes) and the phenotypes of Gfp positive embryos were observed at stage 30-32. As a control HSE:Tle1 was used. As an injection control the embryos were injected with the empty vector but otherwise treated the same.

Since the single point mutation in the WD40-repeat domain was not effective we decided to block the WD40-repeat domains of endogenous TLEs by an excess of WRPW peptides (**Figure 15** and **Table 12**). Induction at early gastrula, however, resulted in no phenotypes at all and compared to the group of control embryos only a slight increase in mortality was observed (**Table 12**). Also the *vice versa* approach, excess expression of the WD40 repeat domain (**Figure 15**) to hinder proteins with a WRPW or an eh1 motif from binding endogenous TLEs, resulted in no significant number of morphological phenotypes (**Table 12**). Only one out of 29 embryos had slightly smaller eyes than heat-induced control embryos injected with the empty vector or the wild type control.

We then decided to concentrate on the N-terminal end of TLE proteins. We chose Tle4 as a suitable candidate due to the fact that it is expressed in the eye at late stages (Aghaallaei *et al.*, 2005). From full length Tle4 we created three truncated forms (**Figure 15** and **Table 13**): "Q" contains only the N-terminal Q-domain; in "Δ494C" the WD40 repeat

domain was removed; and in "WD40" only the C-terminal part of Tle4 remained. The results of the "WD40" truncated form of Tle4 were described in the previous section. Additionally to the *tle4* mutations, we misexpressed *aes* (**Figure 15** and **Table 13**), which is the naturally truncated form of Gro/TLE proteins. Interaction via the Q domain seems to repress the function of full length Gro/TLE proteins in a dominant negative manner (Pinto *et al.*, 1996; Brantjes *et al.*, 2001; Lopez-Rios *et al.*, 2003; Swingler *et al.*, 2004; Bajoghli *et al.*, 2005; Allen *et al.*, 2006; Bajoghli, 2007; Bajoghli *et al.*, 2007; Zhang, X. *et al.*, 2008). The phenotypes observed for Aes and Q misexpression are shown in **Figure 16** and were categorized according to the severity of the observed eye phenotype into weak and strong. Embryos with a weak phenotype developed slightly smaller eyes pointing toward the midline (**Figure 16B,F,J**), whereas embryos with a strong phenotype showed cyclopic eyes (**Figure 16D,H,L**). At first, we also introduced a class of moderate phenotypes. Here, additionally to the weak phenotype, the lenses were shifted anteriorly and beginning cyclopia anterior to the forebrain could be observed (**Figure 16C,G,K**). However, to simplify the overview of the different phenotypes, weak and moderate phenotypes were combined into a single group of weak phenotypes and cyclopic embryos constitute the strong phenotype group (**Table 13**).

	WRPW	WD40	empty vector
Embryos	113	29	107
Dead	13	1	4
Mortality	12%	3%	4%
Small eyes	0	1	0
unspecific phenotypes	4	1	4
Eye phenotypes in surviving	0%	4%	0%

Table 12| *Misexpression of the WRPW motif and the WD40-repeat domain have no effect on medaka embryonic development.* Embryos at the 1-cell stage were co-injected with meganuclease and 80 ng/µl of DNA under the control of a heat-inducible promoter (Bajoghli *et al.*, 2004). Heat induction was performed at early gastrulation (43.5°C, 10 minutes) and the phenotypes of Gfp positive embryos were observed at stage 30-32. Control embryos were injected with the empty vector but otherwise treated the same.

Initial transient injection experiments (co-injection of 80 ng/µl DNA with meganuclease, heat induction at mid-gastrula) showed that both Aes and the C-terminally truncated forms of Tle4 (Q and Δ494C) developed the same eye phenotypes as described in **Figure 16**. We therefore created three heat-inducible transgenic lines. In the F1 generation (**Table 13**), Q showed the best results with 34% overall phenotypes. However, only 5% of the embryos developed a strong phenotype. In Aes embryos, on the other hand, a total of 24% developed a phenotype, equally distributed between weak (12%) and strong (11%), whereas Δ494C only had weak phenotypes, which corresponded to **Figure 16B,F,J**. Observation of these transgenic lines over several generations, however, showed a change in the ability to induce phenotypes. The morphological phenotype stayed the same as described in **Figure 16**, but in the F5 generation of the Q transgenic line only 4% of the Gfp positive embryos developed a weak phenotype, whereas the number of eye phenotypes in the F5 generation of Aes transgenic embryos increased to almost 90% (**Table 13**). Unfortunately, the Δ494C transgenic line had lost the ability to induce phenotypes after the second generation and was therefore not included into further experiments.

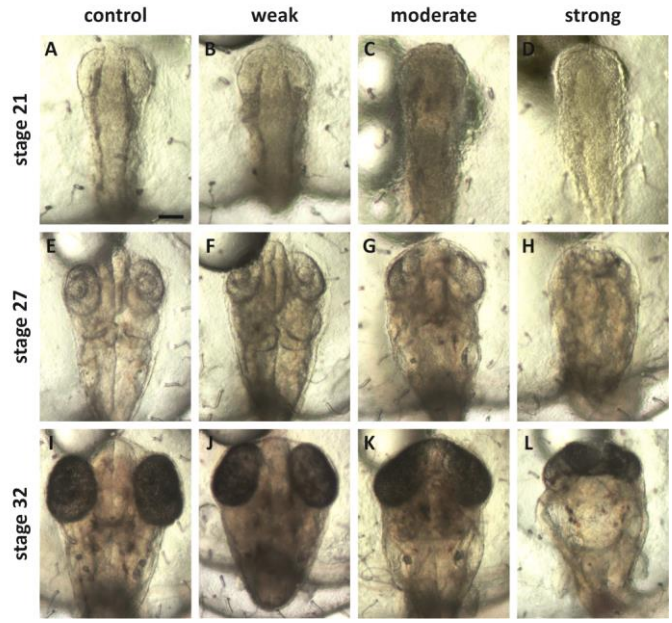

Figure 16| *Overview of Aes/Q misexpression phenotypes.* F2 generation embryos of the Aes and Q transgenic lines were heat induced at mid-gastrulation (43.5°C, 10 minutes). Gfp positive embryos were categorized in the indicated groups according to their eye development. (B,F,J) weak phenotype, smaller eyes tilted towards the midline; (C,G,K) moderate phenotype, upwards shift of the lens and beginning cyclopia anterior of the forebrain; (D,H,L) strong phenotype, cyclopic eyes. Control embryos (A,E,I) were normal wild type embryos heat-induced as described above. Dorsal view of all embryos at the indicated stages, anterior to the top. Scale bar 100 µm.

	Aes F1	Aes F5	Q F1	Q F5	Δ494C
GFP positive	97	73	79	50	96
Weak	12	21	23	2	25
Strong	11	43	4	0	0
Eye phenotypes	24%	88%	34%	4%	26%

Table 13| *Medaka heat-inducible transgenic lines.* Embryos were co-injected with meganuclease and either full-length Aes, the Q domain of Tle4, or a truncated form of Tle4 that misses the C-terminus (Δ494C). For the generation of transgenic lines 10 ng/µl DNA were used, transient injections were performed with 80 ng/µl. The embryos were heat induced at mid-gastrula (43.5°C, 10 minutes) and the phenotypes of Gfp positive embryos were evaluated at stage 30-32.

A single Q-Domain Represses Gro/TLE Function

Formation of the Gro/TLE tetramers depends on protein-protein interaction between the Q domains. To enrich complexes with a reduced number of full length proteins we tested multimerized versions of the Q domain. Here the Q domains are separated by a long flexible linker. Due to the presence of more than on Q domain the proteins have a strong tendency to form intramolecular interactions. A version containing 4 Q domains therefore will form complete complexes with almost no tendency to include other molecules. Contrary to this 3 Q domain proteins and 2 Q domain proteins should strongly bind one or two additional Q-domains, respectively. We performed co-injections with heat-inducible single or multimerized Q domains (40 ng/µl DNA) (**Figure 17**): Expression was induced at mid-gastrula and the embryos were Gfp-selected 24 hours later. The Q-monomer showed with 26% the highest rate of eye phenotypes. Misexpression of Q-tetramers resulted in 10% less phenotypes, although the ratio of strong phenotypes (8%) was twice as high. With a phenotype rate of 6% and 13%, Q-dimers and Q-trimers were considerably lower. Surprisingly, the Q tetramer, which should not participate in complexes with wild type proteins, showed similar numbers of phenotypes (16%). This

suggests that a considerable part of the phenotypes are caused by Q domain-mediated interactions which are also blocked by Q tetramers.

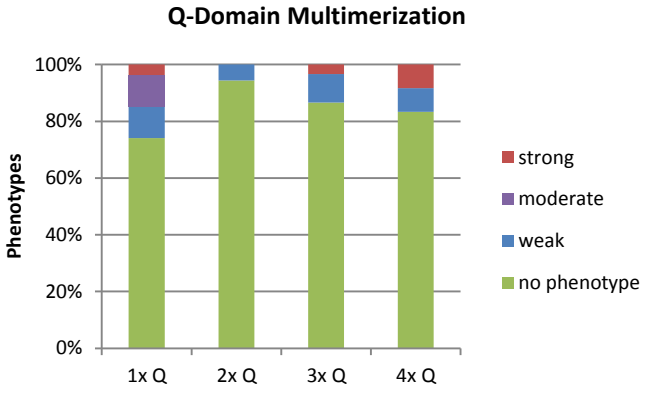

Figure 17| *Q-domain multimerization.* Embryos at the 1-cell stage were co-injected with 40 ng/µl heat-inducible vectors containing 1, 2, 3, or 4 Q-domains (gfp:HSE:Tle4Q1; gfp:HSE:Tle4Q2; gfp:HSE:Tle4Q3; gfp:HSE:Tle4Q4) and meganuclease. The embryos were Gfp-selected 24 hours after injection and phenotypes were categorized after eye pigmentation (stage 30). Embryos with a weak (blue) phenotype developed smaller eyes tilted towards the midline and moderate (purple) phenotypes showed a weak phenotype with beginning cyclopia. Embryos with cyclopic eyes were categorized as strong (red). Total number (*N*) of heat-induced embryos: 1xQ, *N*=38, 2xQ, *N*=278, 3xQ, *N*=36, 4xQ, *N*=25.

Aes Mediates the Repression of Tle1 and Tle4

The interaction of Six3 with Gro/TLEs and Aes has been studied intensively (Zhu *et al.*, 2002; Lopez-Rios *et al.*, 2003). Nevertheless, we wanted to test the ability of Aes to compete with a natural interaction partner of Gro/TLE proteins performing mammalian two-hybrid experiments in HeLa cells. **Figure 18** depicts the basic experimental setup: We used a luciferase reporter under the control of a Fos minimal promoter and 24 zinc finger binding sites (pLucF24ZF). To ensure an optimal Six3-Gro/TLE interaction, the six domain of human Six3 (pMC hSix3(85-203)mZFb6) served as a bait for Tle1 (pMC Tle1VP16) and Tle4 (pMC Grg4VP16). A zinc finger protein fusion (Pomerantz *et al.*, 1995) enabled binding of the six domain to the luc-reporter. The prey, represented by Tle1 or Tle4, was fused to the transcriptional activation domain of the herpes simplex virus protein VP16. In the absence of Aes (pKC Aes), either Tle1 or Tle4 bind to the six domain, which brings VP16 in close proximity to the Fos minimal promoter (**Figure 18B**). On the other hand, the addition of Aes blocks the Six3-Tle-interaction in two possible ways. It can either directly inhibit Gro/TLE complexes by binding to Six3 (**Figure 18D**) (Lopez-Rios *et al.*, 2003) or tether them away from Six3 (**Figure 18C**). In both cases Gro/TLE's binding affinity to Six3 is reduced (**Figure 18B**).

As a reference we used a vector that contained the VP16 transcriptional activation domain linked to an artificial leucine zipper domain (O'Shea *et al.*, 1993) (**Figure 18A**). The counterpart for this leucine zipper was fused to Six3. Furthermore, we used secreted *Gaussia* luciferase as transfection control. The measured luciferase values of the reference were normalized to the transfection control and set to 100%. Addition of Aes did not influence the reference; only at very high concentrations the relative luciferase levels were reduced to almost 70% (**Figure 19; blue bars**). Both Tle1 (**Figure 19; red bars**) and Tle4 (**Figure 19; green bars**) reached 100% binding efficiency in the absence of Aes. However, co-transfection of only 2 ng of Aes expression construct already decreased the luciferase levels of Tle4 and Tle1 to 58% and 45%, respectively.

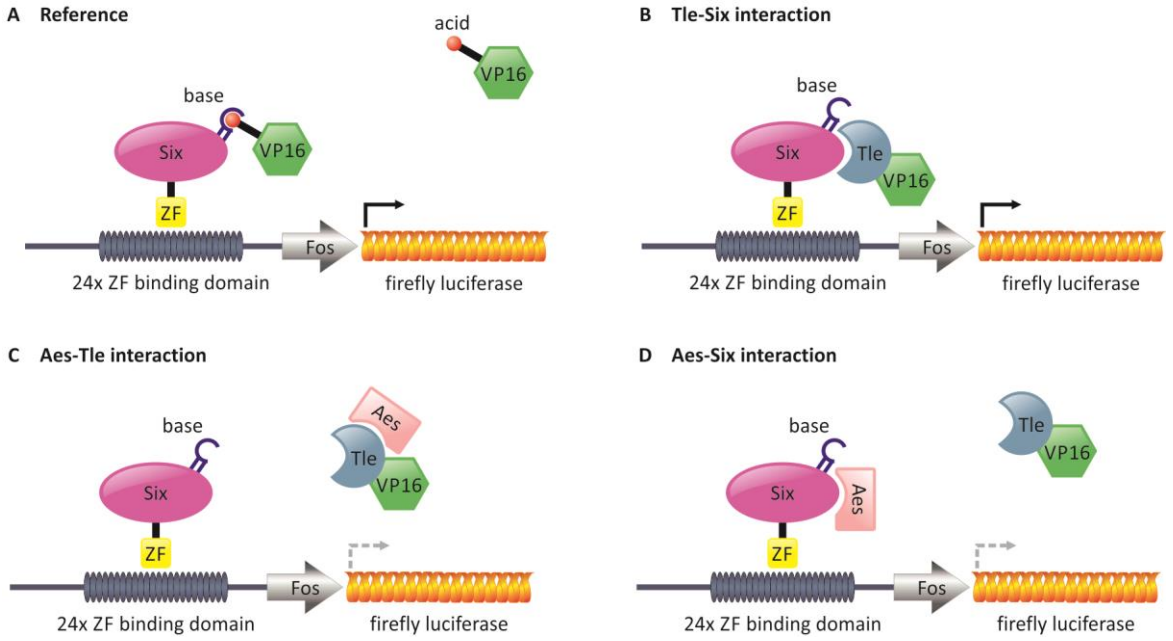

Figure 18| ***Schematic picture of the mammalian two-hybrid setup.*** (A-D) A firefly luciferase reporter (orange helix) under the control of a minimal Fos promoter (grey arrow). Six (purple) binds to 24 zinc-finger binding sites (dark grey) on the reporter via a myc-linked (black line) zinc-finger (yellow box). (B) Luciferase expression: Gro/TLE (blue) binds to Six, thereby bringing a fused transcriptional activation domain of VP16 (green hexagon) in proximity of the Fos promoter. (A) The reference contains of the VP16 domain and a myc-linked acid (red circle). Binding of the acid to a base (blue cup) connected to Six activates luciferase expression via the same principle as described for Gro/TLE. (C,D) Decreased luciferase expression: (C) Aes interaction with Gro/TLE tethers Gro/TLE away from Six; (D) Aes (pink) directly binds to Six (Lopez-Rios *et al.*, 2003), thereby blocking an interaction of Gro/TLE with Six.

Higher amounts of Aes further inhibited the binding of Gro/TLE to the Six domain and reduced the relative luciferase levels of Tle4 to 35% and 18%. The effect on Tle1 was even more significant. With 18% and 9% it reached half the activity of Tle4. Even if a decrease of the reference was observed at high levels of Aes, the values (68% relative luciferase activity) were still considerably higher than those of Tle1 and Tle4. Nevertheless, at these high protein concentrations, the cells were in general already affected, which might explain the lower activity compared to assays in which lower amounts of Aes were used.

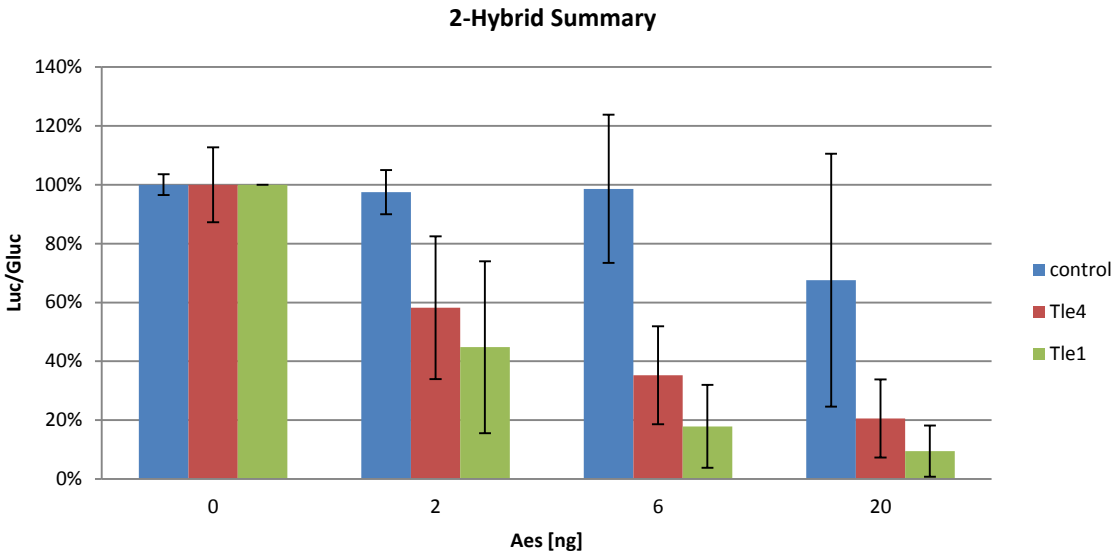

Figure 19| ***Two-hybrid analysis of Tle1 and Tle4 with Aes.*** Tle proteins (20 ng of either pMC Grg4 VP16 or pMC Tle1 VP16) were co-transfected with the six-domain of human Six3 (20 ng of pMC hSix3 (85-203)mZFb6) and full length Aes (pKC Aes at the indicated concentrations) into HeLa cells. The expression level of the luciferase reporter (70 ng of pLucF24ZF) was reduced for the interaction of both Tle1 (green) and Tle4 (red) with Aes compared to the control (20 ng of pMC am VP16; blue). Luciferase levels were normalized to the control and the internal Gaussia luciferase reference (2 ng of pMC GlucS). Both Tle1 and Tle4 are repressed by Aes, whereas the control is unaffected.

Characterization of the Aes/Q Phenotype

After having characterized the morphologic phenotype of our inducible transgenic medaka lines, we further analyzed the effects of the Aes/Q-mediated loss of function of Gro/TLE in whole mount *in situ* hybridization experiments (**Figure 20**). To be able to roughly distinguish between weak and strong phenotypes, we selected embryos at stage 21, a stage were eye development had already begun. First, we used a probe against *Retinal homeobox 2* (*rx2*) (**Figure 20A-C**), a retina marker, to ensure that the categorization in weak and strong matched to the phenotype groups described in **Figure 16**. In embryos with a weak phenotype (**Figure 20B**) the eyes were smaller compared to the wild type control (**Figure 20A**) and tilted towards the midline. In strong phenotypes, an additional faint stripe of *rx2* expression, that connects the two optic vesicles, can be observed in the forebrain (**Figure 20C**). These results are in good agreement with the morphologic phenotype observed in older embryos (**Figure 16J-L**). Due to the fact that the connection of the cyclopic eye was observed in the most anterior part of the telencephalon (**Figure 16K and Figure 20C**), we then wanted to analyze if forebrain development was also affected. Indeed, the expression of *Brain factor 1* (*bf1*) was reduced in both weak (**Figure 20E**) and strong (**Figure 20F**) phenotypes. Furthermore, the expression surrounding the otic vesicles was shifted anteriorly (**Figure 20E,F**), resulting from a 2/3 reduction of the midbrain, as indicated by *wnt1* expression (**Figure 20H,I**). Instead of a defined expression at the midline (**Figure 20G**), here an indistinct expression pattern throughout the midbrain was observed (**Figure 20H,I**).

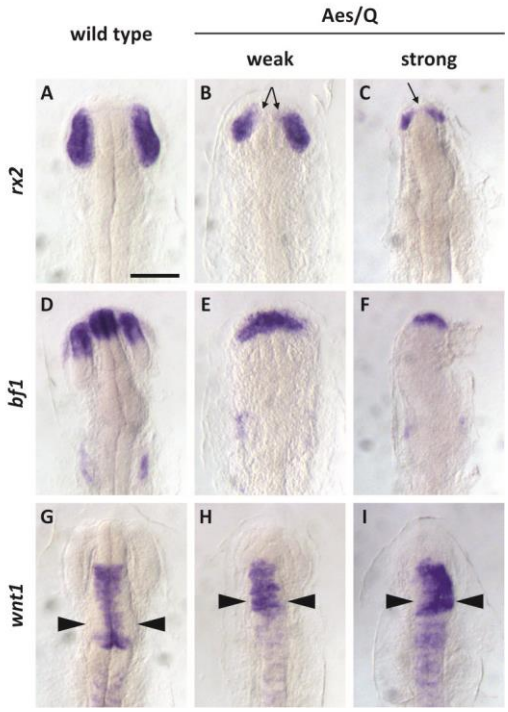

Figure 20| ***Genotypic characterization of the Aes/Q-induced Gro/TLE loss of function phenotype.*** Whole mount *in situ* hybridization of aes transgenic embryos (B,C,E,F,H,I) and wild type controls (A,D,G) using digoxigenin-labeled RNA probes against rx2 (A-C), bf1 (D-F) and wnt1 (G-H). The F1 generation was heat-induced (10 min, 43.5°C) at stage 15/16. Phenotypes were categorized according to their eye phenotype into: (B,E,H) weak, smaller eyes tilted towards the midline; (C,F,I) strong), cyclopic eye. Fixation was performed at stage 21. (B,C) rx2 expression indicates a reduction in eye size, the eye are tilted at the anterior end towards the midline (B, double arrow) or fused to a cyclopic eye in strong phenotypes (C, arrow). (E,F) bf1 expression is reduced. (H,I) wnt1 expression indicates a reduction in midbrain size and shows an indistinct expression pattern throughout the midbrain (arrowheads). (A,D,G) Control embryos were heat-treated wild type embryos. Embryos are shown in dorsal view, anterior to the top. Scale bar 100 µm.

As mentioned before, the Q transgenic line lost its ability to develop reasonable numbers of phenotypes at later generations. However, we wanted to eliminate the possibility of injection-based phenotypes. Whole mount *in situ* hybridization experiments performed with transiently injected embryos overexpressing the Q domain (**Table 14**) were consistent with the experiments shown in **Figure 20**. The overall number of phenotypes ranged from 29% (*rx2*) and 38% (*bf1*) to slightly elevated 50% for *wnt1* (**Table 14**). Strong phenotypes were rarely observed which is again in good agreement with the phenotypes observed in older embryos of the transgenic line (**Table 13**). For the *aes* transgenic line, the observed phenotypes (**Table 14**) were in the range of 44% (*rx2*) to 50% (for both *bf1* and *wnt1*) and thereby slightly lower than in older embryos (**Table 13**). However, determination of the exact phenotype, especially in weak mutations, is rather imprecise at these early stages, which could explain the variations of the statistics in **Table 13** and **Table 14**.

	Aes			Q		
	bf1	*rx2*	*wnt1*	*bf1*	*rx2*	*wnt1*
Embryos	38	36	28	16	17	18
Weak phenotype	13	9	12	6	3	9
Strong Phenotype	6	7	2	0	2	0
Total eye phenotypes	50%	44%	50%	38%	29%	50%

Table 14| ***Statistical overview of marker gene expression in Aes/Q-induced Gro/TLE loss of function phenotypes.*** Embryos of the Aes overexpressing transgenic line (F5 generation) and embryos transiently overexpressing the Q domain (co-injection of meganuclease and 40 ng/µl gfp:HSE:Q) were heat induced at stage 15-16. Gfp positive embryos were selected for whole mount *in situ* hybridization experiments using the indicated RNA probes. Embryos at stage 21 were categorized into weak and strong phenotypes according to their eye development. Embryos of the respective groups showed the genotypic phenotypes indicated in **Figure 20**.

3.1.2 KNOCK DOWN WITH ANTISENSE MORPHOLINO OLIGONUCLEOTIDES

The previous section showed that misexpression of *aes* and the Q-domain can both induce a phenotype in medaka embryos. Indeed, the expression of the Q-domain alone resulted in a considerable number of embryos with phenotypes, however, the amount of strong phenotypes increased with *aes* misexpression (**Table 13**). From the experiments performed so far, we could not exclude the fact that the observed phenotypes might result from a gain of function phenotype of *aes* instead of a Gro/TLE loss of function strategy. We therefore replaced this dominant-negative approach by an actual loss of function by knock down. For this, we designed antisense morpholino oligonucleotides directed against *Tle1*, *Tle2b*, and *Tle3b*. Due to the fact that our transgenic lines were induced during mid-gastrulation we selected genes that are expressed at the same stage. *Tle1* (Lopez-Rios *et al.*, 2003), as well as *Tle2b* and *Tle3b* (Aghaallaei *et al.*, 2005) roughly fulfill this requirement.

According to the established protocols (Summerton, J. *et al.*, 1997), a 25 base target sequence at the 5' untranslated region (UTR) of an mRNA is optimal to specifically inhibit translation. We first used the National Center for Biotechnology Information (NCBI) server to obtain coding sequences for all three genes. However, this database search revealed only partial coding sequences: a 1965 bp long fragment for Tle1 (GenBank accession number AY158892) (Lopez-Rios *et al.*, 2003), a 939 bp long fragment for Tle2b (GenBank accession number EF201813) (Aghaallaei *et al.*, 2005), and a 787 bp long fragment for Tle3b (GenBank accession number EF201814) (Aghaallaei *et al.*, 2005). Comparison with the medaka genome, using the basic local alignment search tool (BLAST) at the Ensembl Genome Browser (Birney *et al.*, 2004a), identified three genes: *Tle1* on chromosome 9 (GeneID ENSORLG00000005051), *Tle2b* on chromosome 4 (GeneID ENSORLG00000016856), and *Tle3b* on chromosome 3 (GeneID ENSORLG00000001969). In order to obtain high quality N-terminal sequences, we performed a Genewise search (Birney *et al.*, 2004b) against the identified regions of the medaka genome. Based on phylogenetic analysis (Bajoghli, 2007), amino acid sequences of human Tle1 (GenBank accession number NM_2205007), Tle2 (GenBank accession number NM_003260), and Tle3 (GenBank accession number NM_005078) served as a reference. Clustal analysis (Sievers *et al.*, 2011) of the obtained sequences showed high sequence homology in the first 76 amino acids of Tle1 and the first 297 amino acids of Tle3b. However, the correct N-terminus of Tle2b remained unclear. We therefore used the first known exon to perform an expressed sequence tag (EST) search. The sequence of EST clone TC132252 in the EST library of "The Computational Biology and Functional Genomics Laboratory" at the Dana-Faber Cancer Institute and Harvard School of Public Health (Quackenbush *et al.*, 2001) showed a 100% match with the query sequence. The putative eleven missing N-terminal amino acids MFPQNRPPAPL could be deduced from the upstream sequences and they fit very well to the sequence of zebrafish Tle2 (Strausberg *et al.*, 2002). Using the Tle2 EST sequence together with the Genewise search sequences, specific 25 bases morpholino target sequences were designed from the amended sequences for Tle1 (Appendix I, page 103), Tle2b (Appendix I, page 103), and Tle3b (Appendix I, page 104) mRNA, as indicated in **Figure 21**. Additional end modifications were not included in the design; instead, FITC-Dextran was used as a co-injected control.

Tle1 mRNA: 5'- cccucgcuagcgggguuucaggacaagacgcguuugcagucuccccggagauaacaAUGUUUCCCCAG -3'

Tle2b mRNA: 5'- gaaagagccacgaggacgcacugccagacccccuccuccuccccgguaacaAUGUUUCCCCAGAACC -3'

Tle3b mRNA: 5'- cccccgugugaaagacgagacAUGUAUCCACAAGGCCGGCAUCCG -3'

Figure 21| ***Gro/TLE antisense morpholino oligonucleotide design.*** Medaka mRNA sequences for Tle1, Tle2b and Tle3b; including the partial 5' UTR (red) and the partial amino acid coding region (black). The AUG translational start site is underlined. Morpholino Sequences (yellow box) were designed according to established protocols (Summerton, J. *et al.*, 1997).

Embryos at the 1-cell stage were co-injected with either single *Tle* antisense morpholino oligonucleotides (**Figure 21**) or combinations of morpholinos and 1 µg/ml of FITC Dextran. Tests with several different concentrations showed that the embryos tolerated concentrations up to 1 mM before they showed unspecific phenotypes. Best results were obtained with a concentration of 600 µM and a minimum of 300 µM was necessary to induce phenotypes. We therefore used 600 µM to test the individual morpholinos and 300 µM per morpholino for injections of morpholino combinations (**Table 15**). The most prominent phenotypes of all three morpholino oligonucleotides affected eye development, similar to the Aes/Q injected embryos. They (**Table 15**) were therefore categorized into weak and strong phenotypes according to the same criteria as described for Aes/Q-mediated loss of function. Comparable to **Figure 16**, embryos with a weak phenotype developed smaller eyes, slightly shifted towards the midline (**Figure 22C,D,I,J**), whereas strong phenotypes showed cyclopic eyes (**Figure 22B,G,H**). In rare cases, the embryos lost their eyes entirely (**Figure 22E**). However, whereas the Aes/Q-mediated phenotypes strongly resembled a *six3* inactivation phenotype (Carl *et al.*, 2002; Dorn *et al.*, 2012), the *tle* knock down phenotypes looked different. Instead of tilting to the midline at the most anterior part of the eye (**Figure 16J**), here it seems that the inner edges of the eyes moved together (**Figure 22C,D,I,J**). Therefore, cyclopic eye connections appear in the middle of the eyes, underneath the forebrain, (**Figure 22B,G,H**) and not anterior of it (**Figure 16K,L**). Both weak and strong phenotypes were observed in all morpholino oligonucleotide injected embryos, independent of single or combinatorial injections. However, the overall phenotype rate was higher in double knock downs (**Table 15**).

The overall phenotype rate was with 16% observed phenotypes in the surviving FITC Dextran positive embryos the highest in *tle2b* inactivated embryos (**Table 15 and Figure 22C**), followed by 12% for *tle3b* (**Table 15 and Figure 22D**) and 10% for *tle1* (**Table 15 and Figure 22B**). Also in the number of strong phenotypes, *tle2*b morpholino oligonucleotide injected embryos showed the best results. Of all phenotypes recorded, 2/3 developed strong phenotypes (with almost half of them being eye-less), compared to 1/3 in *tle1* inactivated embryos and only 18% in *tle3b*. In double morpholino injection experiments, combining either *tle1* and *tle2b* or *tle1* and *tle3b*, the number of phenotypes roughly added up to 27% and 21%, respectively, whereas with 15% it remained the same for the combination of *tle2b* with *tle3b*. The latter even failed to induce strong phenotypes. Addition of *tle1* morpholino oligonucleotide only elevated this number to 17%, however, 50% of the embryos developed cyclopic eyes.

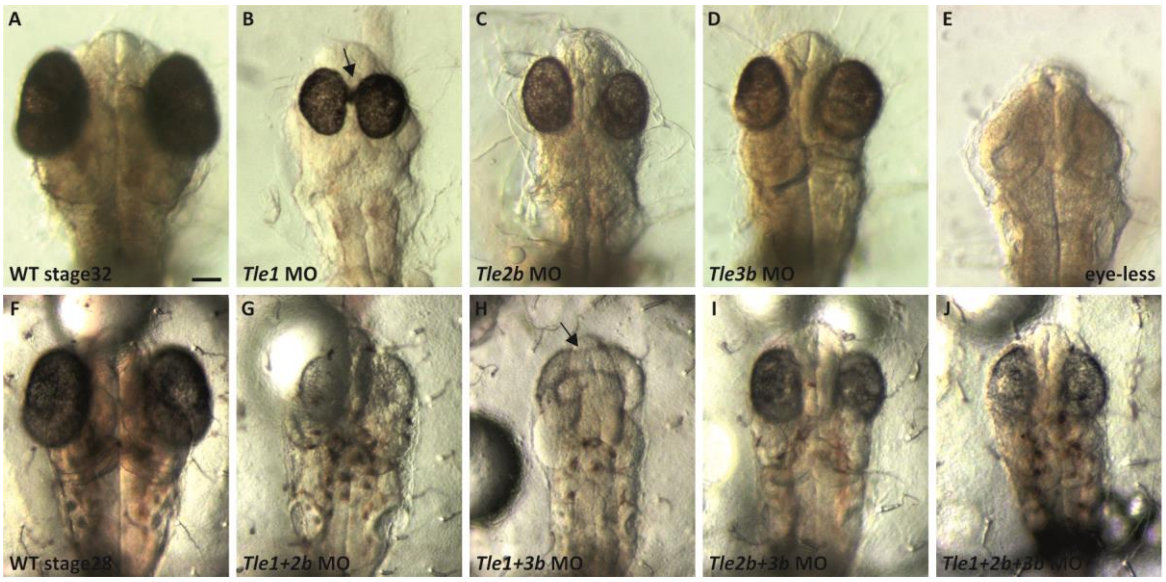

Figure 22| ***Gro/TLE antisense morpholino-induced loss of function phenotypes.*** Embryos at the 1-cell stage were co-injected with morpholino oligonucleotides and 1 µg/ml FITC Dextran. Injections were performed using either a single morpholino directed against *tle1* (B), *tle2b* (C,E), and *tle3b* (D), or combinations directed against *tle1+2b* (G), *tle1+3b* (H), *tle2b+3b* (I), and *tle1+2b+3b* (J). Single morpholino oligonucleotides were injected at a concentration of 600 µM (B-E) and combinatorial injections (G-J) were performed using 300 µM per morpholino. Phenotypes of FITC Dextran positive embryos were observed after the beginning of eye pigmentation at stage 32 (A-E) and stage 28 (F-J). Wild type control embryos were injected with 1x Yamamoto's and FITC Dextran. All embryos are shown in dorsal view with anterior at the top. Compared to the wild type controls (A,F), morpholino injected embryos developed smaller eyes that were shifted towards the midline (C,D,I,J) or cyclopic eyes (B,G,H). In rare cases the eyes were lost entirely (E). Scale bar 100 µm. Abbreviations: MO, morpholino oligonucleotide; st, stage; WT wild type.

Concentration	**600 µM**			**300 µM for each morpholino**			
Morpholino	***tle1***	***tle2b***	***tle3b***	***tle1+2b***	***tle1+3b***	***tle2b+3b***	***tle1+2b+3b***
Embryos	95	267	117	55	115	45	58
Dead	11	30	6	11	16	5	4
Mortality	12%	11%	5%	20%	14%	11%	7%
Weak	6	23	11	7	17	6	6
Strong	2	16	2	5	4	0	3
Eye-less[*)]	0	7	1	3	3	0	0
Eye phenotypes in surviving embryos	10%	16%	12%	27%	21%	15%	17%

[*)] included in the group "strong" phenotype

Table 15| ***Statistical overview of the Gro/TLE antisense morpholino-induced loss of function phenotypes.*** Embryos at the 1-cell stage were co-injected with 1 µg/ml FITC Dextran and either 600 µM (for a single morpholino) or 300 µM (for combinatorial injections) morpholino oligonucleotides. Phenotypes of FITC-positive embryos were categorized at stage 28-32 into weak and strong phenotypes. Weak phenotypes developed smaller eyes that were shifted towards the midline, whereas strong phenotypes showed cyclopic eyes. Eye-less phenotypes were included into the group of strong phenotypes.

Expression of the retinal marker *rx2* was reduced in weak embryos (**Figure 23B**) and lost entirely in eye-less embryos (**Figure 23C**). Similar results were observed in embryos hybridized with *six3* (**Figure 23K,L**). However, here residual expression in the strong embryos (**Figure 23L**) indicated that the eyes were not lost completely. Additionally, *pax6* (**Figure 23E,F**) expression confirmed the above seen eye phenotypes. In embryos developing a weak phenotype, the size of the eyes were again reduced and the expression domain of *pax6* was expanded into the anterior forebrain (**Figure 23E, arrow**). Whether the embryo with a strong phenotype (**Figure 23F**) was eye-less as in **Figure 23C** or had rudimentary eyes (compare **Figure 23L**) was not evident, due to the fact that *pax6* is expressed in both the eyes and the forebrain (**Figure 23D,E**). However, a clear size reduction of the midbrain could be observed in both the weak and, even severer, in the strong phenotypes (**Figure 23E,F; bars**).

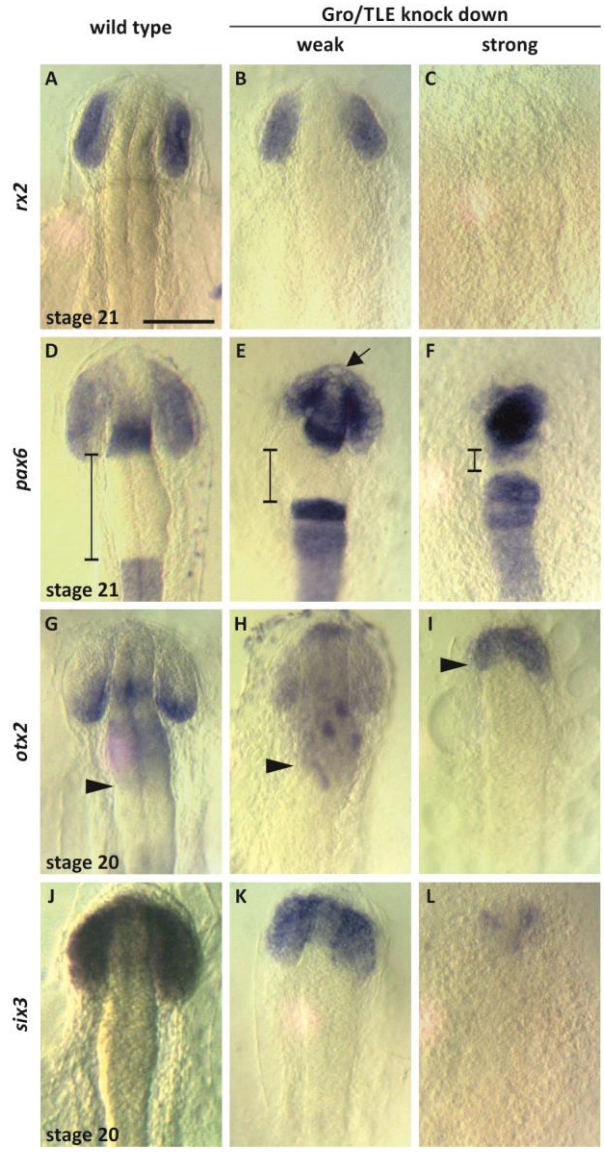

Figure 23| *Whole mount in situ hybridization experiments with Gro/TLE knock down embryos.* Medaka embryos at the 1-cell stage were co-injected with the indicated antisense morpholino oligonucleotides (600 µM) and FITC Dextran. FITC positive embryos at the indicated stages were selected for hybridization experiments using digoxigenin-labeled RNA probes against *rx2* (A-C), *pax6* (D-F), *otx2* (G-I), and *six3* (J-L), and categorized into weak and strong, according to their morphologic appearance: (B,E,H,K) weak, smaller eyes; (C,F,I,L) strong, very small eye or eye-less. Embryos are shown in dorsal view, anterior to the top. (B,C) In strong phenotypes eye markers are expressed very weak (L) or lost entirely (C). Expression of *otx2* (G-I) shows an anterior shift of the mid hindbrain boundary in injected embryos (black arrowhead). *Pax6* expression indicates a size reduction of the midbrain (E,F; bars) and an enlarged expression domain at the anterior forebrain (E, arrow). (A,D,G,J) Wild type control; (B,H,L) *tle2b* MO; (C,E,F,I,K) *tle3b* MO. Scale bar 100 µm. Abbreviations: MO, morpholino oligonucleotide.

The embryos were staged according to the age of the wild type control (**Figure 23A,D,G,J**). Morpholino oligonucleotide injected embryos developed somewhat slower. At the time of fixation, most of the knock down embryos showed the same number of somites as the

control embryos, however, the anterior development seemed slightly retarded. Therefore, we concluded that the strong staining of the anterior rhombomere region in **Figure 23E** is an artifact, due to the fact that wild type embryos at stage 20 show the same expression pattern. We further analyzed this anterior shift of the fore- and midbrain using *otx2* as a marker (**Figure 23G,H,I**). In medaka development, the neural plate is divided into an anterior *otx*-expressing domain and a posterior *gbx*-expressing domain (Heimbucher *et al.*, 2007). Both domains are separated by the MHB and its spatial position depends on the mutual interaction between these two genes (Millet *et al.*, 1999; Tour *et al.*, 2002). Embryos with a weak phenotype showed a mild upwards shift of the posterior end of the *otx2*-expressing domain (**Figure 23H; arrowhead**), whereas in embryos developing a strong phenotype, *otx2* expression was only found in the very anterior part of the embryo (**Figure 23I; arrowhead**), indicating a drastic anterior shift.

In principle, both the morphologic and the gene expression phenotypes of the different morpholino oligonucleotides were comparable amongst each other. However, the frequency with which they occurred differed, as already described in **Table 15**. Furthermore, the number of embryos with gene expression phenotypes (**Table 16**) differed from the number of morphologic phenotypes (**Table 15**). We explained this deviation due to the fact that morphologic phenotypes were categorized at older stages and older embryos, predominantly those with a weak phenotype, often recover into a normal state. With 11% and 10% phenotypes in *rx2* and *pax6* hybridization experiments (**Table 16**), respectively, *tle1* morpholino oligonucleotide injected embryos showed comparable phenotypes as described in **Table 15**. However, both *otx2* and *six3* showed normal expression patterns in all embryos. On the other hand, embryos injected with morpholino oligonucleotides against *tle2b* and *tle3b* developed comparable numbers of phenotypes (**Table 16**). With 33% and 25% the percentage of phenotypes were even exactly the same for *otx2* and *six3* expression, whereas in *pax6* expression the numbers varied from 42% in *tle2b* inactivated embryos and 46% for *tle3b* loss of function. With 22% and 40% the biggest difference was observed in *rx2* expression. Here *tle3b* morpholino oligonucleotide injected embryos showed nearly twice the number of phenotypes compared to *tle2b* injected embryos (**Table 16**).

Probe	*Otx2*			*Rx2*			*Pax6*			*Six3*		
Morpholino	***tle1***	***tle2b***	***tle3b***	***tle1***	***tle2b***	***tle3b***	***tle1***	***tle2b***	***tle3b***	***tle1***	***tle2b***	***tle3b***
Embryos	8	18	15	9	9	15	10	12	13	7	16	12
Weak phenotype	0	2	3	0	1	4	0	4	3	0	2	3
Strong phenotype	0	4	2	1	1	2	1	1	3	0	2	0
Total eye phenotypes	0%	33%	33%	11%	22%	40%	10%	42%	46%	0%	25%	25%

Table 16| *Statistical overview of whole mount in situ hybridization experiments with Gro/TLE morpholino oligonucleotide injected embryos.* Embryos at the 1-cell stage were co-injected with 600µM antisense morpholino oligonucleotides and FITC-Dextran. FITC-positive embryos at stage 20-21 were selected for hybridization experiments using digoxigenin-labeled RNA probes against *otx2*, *rx2*, *pax6*, and *six3*. Phenotypes were categorized into weak and strong, according to the morphologic eye phenotype.

A more detailed analysis of the Gro/TLE knock-down phenotype was performed on embryos at late gastrulation. To carefully investigate the anterior shift, observed in **Figure 23**, whole mount *in situ* hybridization experiments were performed using probes against *pax2* and *goosecoid* (**Figure 24A-D**). In 15%-33% of the embryos (**Table 17**), a significant anterior shift of the MHB was observed for *Pax2* expression (**Figure 24B**). As an additional marker, we used *goosecoid*, which is mainly expressed in the anterior embryonic body of the wild type control group (**Figure 24C**). In hyper-dorsalized zebrafish embryos, due to lithium induction, *goosecoid* expression was stronger and expanded posteriorly (Stachel *et al.*, 1993). Lithium induction activates the Wnt pathway (Kao *et al.*, 1998) and similar effects were shown for medaka *Wnt1* overexpression experiments (Bajoghli *et al.*, 2009). Interestingly, we observed quite the opposite phenotype in *Gro/TLE* inactivated embryos. In 22%-38% of the injected embryos, *Goosecoid* expression was weaker and shortened to approximately half of its original size (**Figure 24D**). Together with the results for *otx2* (**Figure 24H,I**) and *pax2* (**Figure 24B**) this indicates an anteriorization of *Gro/TLE* morpholino oligonucleotide-induced loss of function.

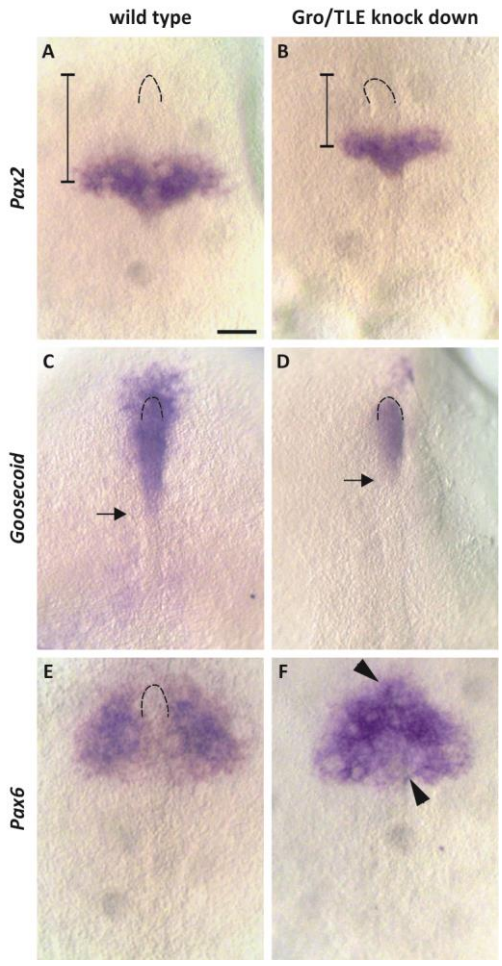

Figure 24| *Analysis of the Gro/TLE knock-down phenotype at late gastrula.* Embryos at the 1-cell stage were co-injected with antisense morpholino oligonucleotides (600 µm) and FITC Dextran. Whole mount *in situ* hybridization experiments were performed with digoxigenin-labeled RNA probes against *pax2* (A,B), *goosecoid* (C,D), and *pax6* (E,F). Embryos at stage 16 are shown in dorsal view with anterior to the top. The broken line indicates the anterior end of the embryo. *Pax2* (A,B) expression reveals an anterior shift of the mid hindbrain boundary (B, bar). In late gastrula, *goosecoid* is expressed in the prechordal plate and the anterior embryonic body of the control embryos (C). *Gro/TLE* knock-down causes an anterior shift of the expression domain (D), indicated by the arrow. In wild type embryos *pax6* (C) is expressed in two separate expression domains on both sides of the embryonic body. *Gro/TLE* knock-down shows an expansion of *pax6* expression (D, arrowheads), thereby closing this gap. (A,C,E) Wild type control; (B) *tle2b* MO; (D,F) *tle3b* MO. Scale bar 100 µm. Abbreviations: MO, morpholino oligonucleotide.

Expression of *pax6* in older stages showed enlargement of the anterior expression domain (**Figure 23E,F**). To get more insight, we analyzed the expression of *pax6* in younger stages. At late gastrulation, *pax6* is expressed in two distinct domains, lateral of the prospective

head region (**Figure 24E**). However, in morpholino oligonucleotide injected embryos the expression domain was fused at both the most anterior top as well as at the posterior end. Taken together, instead of two distinct domains, a triangle-shaped expression domain was formed (**Figure 24F**) in 20% to 44% of all morpholino oligonucleotide injected embryos (**Table 17**). Comparable results were also observed in embryos injected with different combinations of morpholino oligonucleotides (**Table 17**).

Morpholino	*tle1*		*tle2b*		*tle3b*		*tle1+2b*		*tle1+3b*		*tle2b+3b*		*tle1+2b+3b*	
	N	PT	*N*	PT	*N*	PT	*N*	PT	*N*	PT	*N*	PT	*N*	PT
pax2	26	4	12	4	9	3	21	6	17	4	12	2	8	2
goosecoid	13	5	8	2	3	1	3	1	9	2	20	6	9	2
pax6	10	3	9	4	15	5	10	4	7	3	10	2	9	3

Table 17| *Statistical overview of the Gro/TLE kock-down phenotype at late gastrula.* Whole mount *in situ* hybridization experiments were performed on *Gro/TLE* inactivated embryos using the indicated RNA probes. Anterior shifts of the expression domains were observed for *pax2* and *goosecoid*. The two lateral expression domains of *pax6* were fused into a single domain. Abbreviations: *N*, total number of embryos; PT, phenotype.

Part II

3.2 Characterization of Medaka Tcf3

So far we showed that loss of function of Gro/TLE, caused either by a dominant-negative approach or by morpholino knock down, resulted in cyclopic eyes or an eye-less phenotype in very severe cases (**Figure 22E**). Comparison of these observed morphological phenotypes with phenotypes caused by loss of function of Gro/TLE interaction partners revealed a strong resemblance to those seen for *six3* knock down in medaka (Carl *et al.*, 2002). Additionally to anophthalmia, knock down of *six3* also resulted in deletion of the forebrain (Carl *et al.*, 2002), a phenotype that we could confirm in recent studies, where we tested modified peptide nucleic acids (PNAs) (Dorn *et al.*, 2012). However, Tcf3 is another interaction partner that has a strong connection to anterior-posterior development (Roose *et al.*, 1998; Merrill *et al.*, 2004; Arce *et al.*, 2009). Members of the Tcf/LEF transcription factor family are the most downstream interaction partners of the Wnt signaling pathway. In the absence of Wnt signaling, Tcf/LEFs interact with Gro/TLE proteins through a groucho binding site (Arce *et al.*, 2009) and together they repress Wnt target gene expression (Cavallo *et al.*, 1998; Levanon *et al.*, 1998; Roose *et al.*, 1998). Experiments in zebrafish have shown, that knock down of the *hdl* gene resulted in an eye-less phenotype (Dorsky *et al.*, 2003), similar to the one that we observed for *Gro/TLE* loss of function. In contrast to zebrafish, the medaka genome contains only a single *tcf3* gene (Wang, D. *et al.*, 2011). However, except for the sequence, little is known about medaka *tcf3*. We, therefore, decided to analyze its expression and function in early embryonic development. Based on the observations of Dorsky *et al.*, we further hypothesized that our Gro/TLE inactivation phenotype caused by antisense morpholino oligonucleotides (**Figure 22**) might be connected to *tcf3* loss of function.

3.2.1 Isolation and Expression of the Medaka Tcf3 Gene

As a starting point we used the published sequence of the medaka *tcf3* gene (GenBank accession number HQ705658), which is located on chromosome 9 and encodes for a 1728 bp long mRNA (Wang, D. *et al.*, 2011), and the two known zebrafish sequences for the *hdl* gene (GenBank accession number BC053135) (Artinger *et al.*, 1999) and *tcf3b* (GenBank accession number AY221031) (Dorsky *et al.*, 2003). Clustal analysis (Sievers *et al.*, 2011) of the amino acid sequences (**Figure 25**) of the medaka Tcf3 protein and the two zebrafish orthologs showed 65% and 69% sequence identity for Tcf3b and Hdl, respectively. Highest similarities were found in the conserved domains (**Figure 25; colored boxes**), whereas the most divergent regions were observed shortly before the C-terminal end.

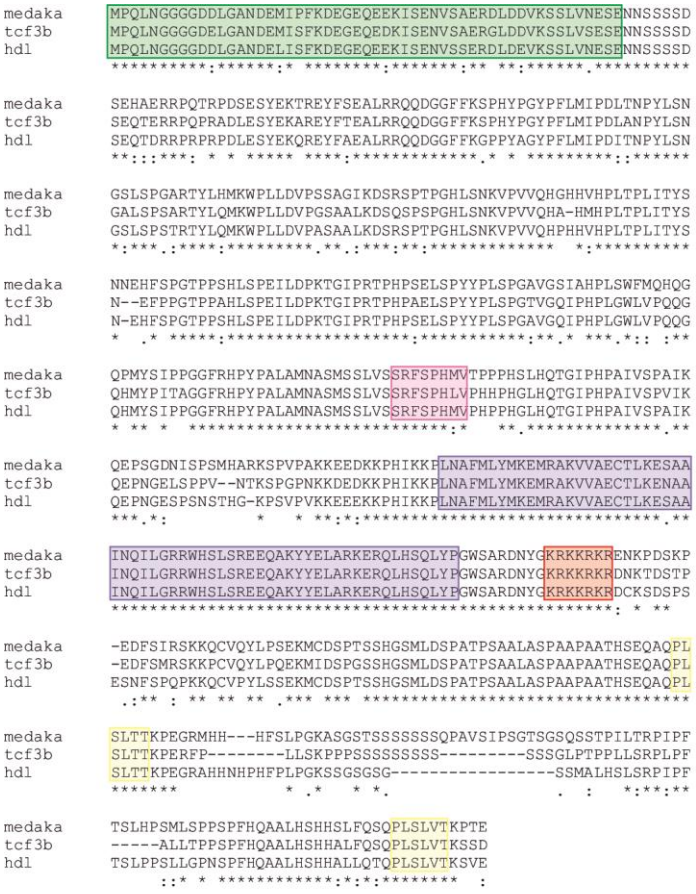

Figure 25| ***Clustal alignment of medaka and zebrafish Tcf3 protein sequences.*** The amino acid sequences of medaka and zebrafish (tcf3b and hdl) show high similarity, being most divergent near the C-terminus. (asterisk) identical amino acids in all sequences; (colon) highly conserved amino acids; (dot) different but very similar amino acids; gaps indicates dissimilar amino acids or gaps. Green box, β-catenin binding domain; pink box, groucho binding sequence; purple box, high mobility group; red box, nuclear localization sequence, yellow boxes CtBP interaction domain.

To analyze the expression pattern of *tcf3*, we performed whole mount *in situ* hybridization experiments using a digoxigenin-labeled RNA probe against the 5' end of *tcf3*. The sequence for the RNA probe was PCR amplified from medaka embryonic cDNA and cloned into a pGem®-T Easy (Promega) vector.

During gastrulation, *tcf3* is broadly expressed throughout the embryonic shield (**Figure 26A**) at 40% epiboly, followed by an anterior shift towards the prospective head region (**Figure 26C**) and into the embryonic body (**Figure 26B,C**) at late gastrula. The expression becomes further restricted to the head region during neurula (**Figure 26D,D'**) from where it slowly expands posteriorly (**Figure 26E-I'**). As soon as the three different parts of the brain can be distinguished, *tcf3* expression is segmented into distinctive stripes (**Figure 26E**). However, the expression is still enhanced in the telencephalic region and the midbrain, whereas only a faint stripe can be observed in the hindbrain. Comparable to zebrafish *tcf3b*, a gap of expression is clearly visible in the MHB (**Figure 26E-G**) (Dorsky *et al.*, 2003). Furthermore, weak expression was also detected in the eyes and the otic placodes (**Figure 26E**). During somitogenesis, *tcf3* expression extends further caudally (**Figure 26F'-I'**), where it is then found in the pectoral fins and the somites in late stages (**Figure 26I,I'**). Taken together, the expression of medaka *tcf3* overlaps with both the expression domains described for the zebrafish orthologs *tcf3b* and *hdl* (Dorsky *et al.*, 2003).

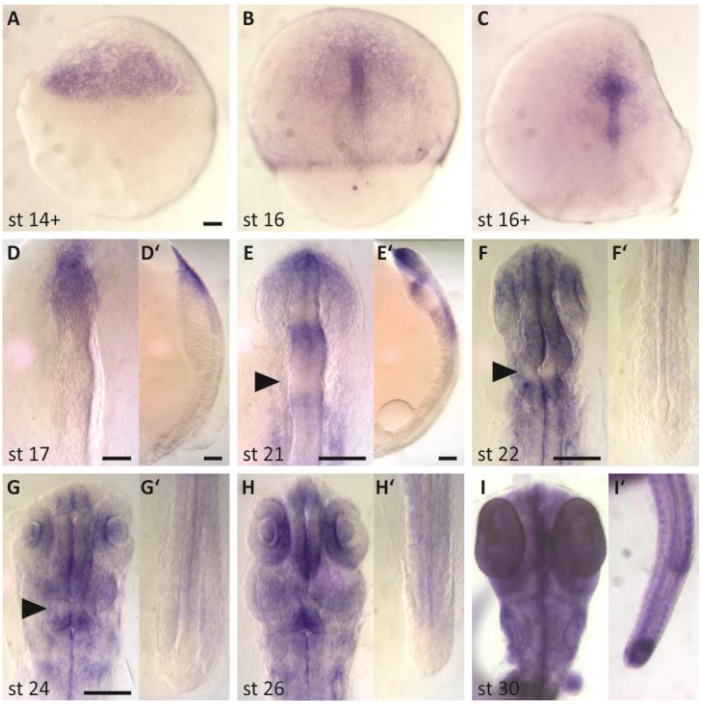

Figure 26| *Expression pattern of tcf3 during medaka embryonic development.* Whole mount *in situ* hybridization experiments were performed in wild type embryos at the indicated stages, using a digoxigenin-labeled RNA probe against *tcf3*. Embryos are shown in dorsal view, anterior at the top. (F-I) Flat mounts; (F'-I') tail view. During gastrulation (A-C) *Tcf3* is expressed throughout the epiblast and the embryonic body (C-D). In neurula the expression becomes restricted to the head (D,D') from where it spreads caudal and divides into a forebrain, midbrain, and hindbrain section (E;E'). Black arrow head indicates a gap in expression at the mid-hindbrain boundary (F-H) which is slowly closed at stage 26 (H). In later stages, expression is observed throughout the entire body (G-I'). Scale bars 100 µm. Abbreviations: st, stage.

3.2.2 Morpholino Knock Down of the Medaka Tcf3 Gene

After having identified the expression pattern of *tcf3* and monitored it during many stages of early medaka development, we next wanted to investigate its function. For this, we used antisense morpholino oligonucleotides directed against *tcf3*. They were designed from the predicted sequence of *tcf3* (TCF7L1, transcription factor 7-like 1, GeneID ENSORLG00000011813) and its 5' UTR in the Ensembl Genome Browser (Birney *et al.*, 2004a) according to the established protocols (Summerton, J. *et al.*, 1997). To specifically inhibit mRNA translation a 25 bases target sequence, which overlaps the AUG translational start site at the 5' end, was selected as antisense morpholino sequence (**Figure 27**). Additional end modifications were not included in the design; instead, FITC-Dextran was used as an injection control.

Tcf3 mRNA: 5'- auuuuuggucuuguugagcugaucgacuggugugcaaacAUGCCUCAACUGAACGGAGGCGGCGGGG -3'

Figure 27| *Tcf3 antisense morpholino oligonucleotide design.* Medaka Tcf3 mRNA sequence; including the partial 5' UTR (red) and the partial amino acid coding region (black). The AUG translational start site is underlined. Morpholino Sequences (yellow box) were designed according to the guidelines of the Gene-Tools homepage (Sievers *et al.*, 2011).

Wild type embryos at the 1-cell stage were co-injected with *tcf3* antisense morpholino and 1 µg/ml FITC-Dextran (**Figure 28**). Embryos, which contained an evenly distributed fluorescent signal throughout the entire body, were observed under the microscope. During young stages, until neurulation, no significant changes in development were observed between the injected and the control embryos (**Figure 28A-D**). Only after the

beginning eye development, phenotypic alterations became visible (**Figure 28 columns weak – strong**).

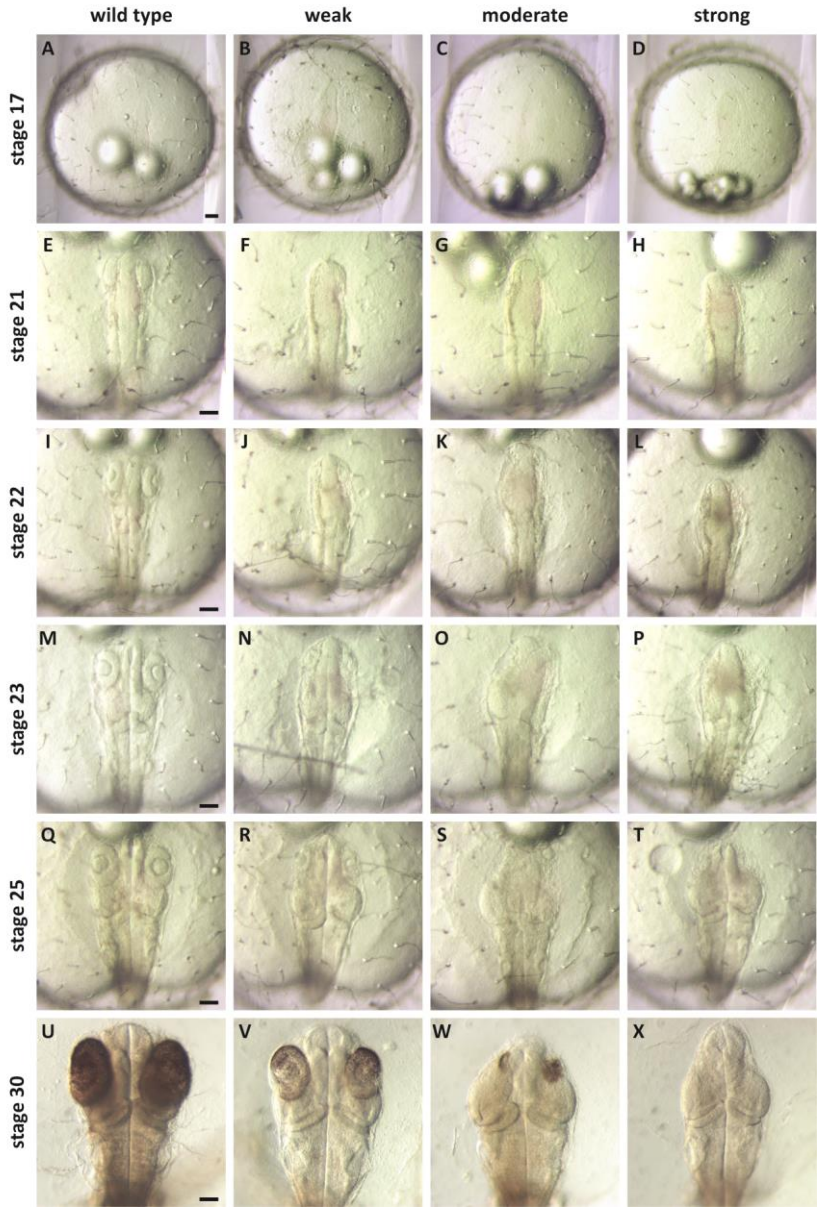

Figure 28| ***Overview of tcf3 loss of function phenotypes during early medaka development.*** Embryos at the 1-cell stage were co-injected with 300 µM *tcf3* morpholino and 1 µg/ml FITC-Dextran (columns weak – strong). Control embryos (A,E,I,M,Q,U) were co-injected with 1x Yamamoto's and FITC-Dextran. Pictures of embryos with a fluorescent signal were taken at several developmental stages, which were defined according to the control embryo: (A-D) stage 17; (E-H) stage 21; (I-L) stage 22; (M-P) stage 23; (Q-T) stage 25; (U-X) stage 30. Embryos are shown in dorsal view, anterior to the top. Classification was performed after the onset of eye pigmentation, according to the size of the eye: weak, slightly reduced size; moderate, severe size reduction; strong, anophthalmia. Scale bar 100 µm.

The phenotype concentrated on the eye region, leaving the trunk and tail unharmed. However, a distinct classification into groups was still not possible. We therefore followed the development of the embryos over several stages until the eyes of the control embryos were clearly pigmented (**Figure 28U**) and three main groups of phenotypes (weak,

moderate, and strong) were distinguishable (**Figure 28V-X and Figure 29**). Embryos, which developed a weak phenotype (**Figure 28V**), had slightly smaller eyes than the control group, whereas in embryos with a moderate phenotype (**Figure 28W**) the size reduction was severe. As a strong phenotype (**Figure 28X**), we classified eye-less embryos that looked otherwise normal and resembled the extreme anophthalmic phenotypes observed in *tle* loss of function experiments (**Figure 22**). Interestingly, compared to zebrafish morpholino injections, the strong phenotype resembles more the phenotype seen for morpholinos against *hdl* than for morpholinos against *tcf3b*. This is in contrast to the observed expression pattern of the whole mount *in situ* experiments in wild type (**Figure 26**), where the expression overlaps more with zebrafish *tcf3b* in earlier stages (Dorsky *et al.*, 2003).

Best results were obtained using a morpholino concentration of 300 µM. In 64% of the embryos we observed eye phenotypes with more than half of them being eye-less. The rest was divided into moderate and weak phenotypes with 17% and 12%, respectively. However, at lower concentrations the phenotype rate decreased to less than 30% with 9% developing a moderate phenotype and only 3% being anophthalmic (**Figure 29**).

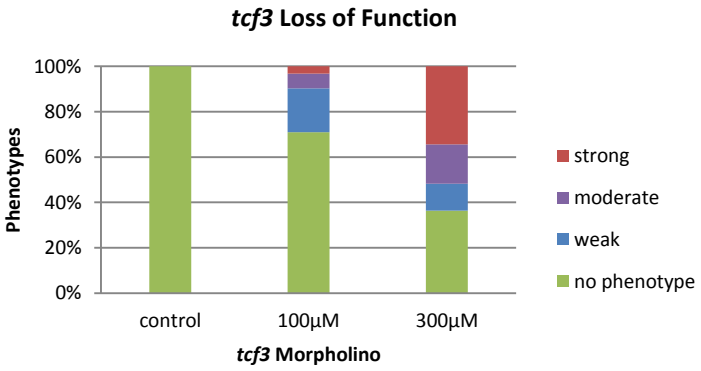

Figure 29| *Tcf3 antisense morpholino induced phenotypes.* Embryos at the 1-cell stage were co-injected with different concentrations (100 µM and 300 µM) of *tcf3* morpholino and 1 µg/ml FITC-Dextran. Control embryos were co-injected with buffer (1x Yamamoto's) and FITC Dextran. Embryos, containing a positive fluorescent signal, were categorized according to their phenotypes: green, normal development; blue, weak phenotype (smaller eyes); purple, moderate phenotype (very small eyes); red, strong phenotype (anophthalmia). Number (*N*) of surviving embryos: control, *N*=119, 100 µM, *N*=32, 300 µM, *N*=204.

In **Figure 30A-C** the *tcf3* loss of function phenotype is depicted in more detail. The extreme size reduction of the eyes is indicated by black dotted lines, which represent the average outlines of normal wild type eyes in comparable stages (**Figure 30A-D**). Comparison to the eye-less phenotype of *tle* inactivated embryos (**Figure 30D**) showed a remarkable resemblance of these two loss of function phenotypes. However, the phenotype of Aes/Q-induced embryos (**Figure 30E**) does not fit into this picture. **Figure 30E** shows an embryo with an almost eye-less phenotype. Instead of a severe size reduction, lateral of the forebrain, the eyes shifted anteriorly and towards the midline, thereby overlaying the forebrain. Cyclopia is indicated by the streak of pigmented retinal epithelium (**Figure 30E, arrowhead**).

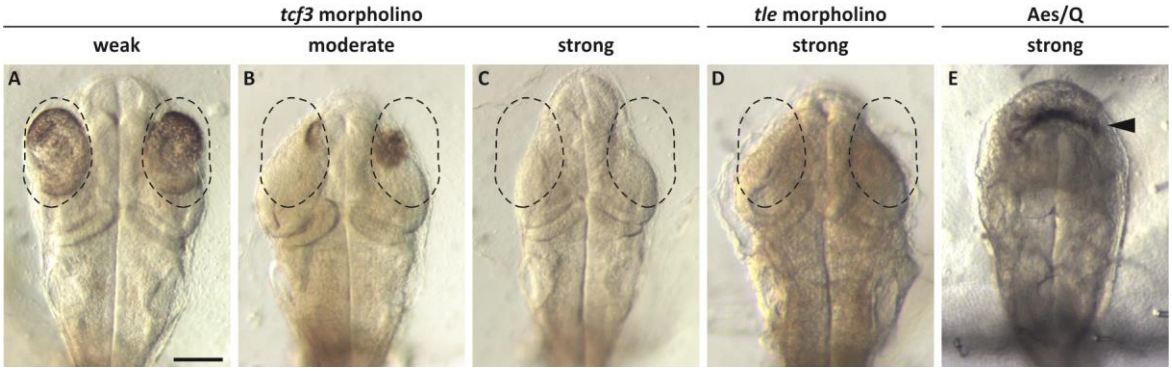

Figure 30| *Comparison of tcf3 loss of function with Gro/TLE morpholino and Aes/Q-induced phenotypes.* Antisense morpholino oligonucleotides against either *tcf3* (A-C; 300µM) or *tle2b* (D; 600µM) were co-injected with FITC Dextran. (E) Aes/Q embryos of theF2 generation were heat-induced at stage 15. Embryos are shown in dorsal view with anterior to the top. (A-C) stage 28, (D,E) stage 30. (A-D) dotted line indicates the position of the eyes in a wild type embryo. (E, arrowhead) pigmented retinal epithelium of the remaining cyclopic eye. Scale bar 100 µm.

Next we analyzed the phenotype with whole mount *in situ* hybridization using digoxigenin-labeled RNA probes against *pax2*, *pax6*, and *gbx1*. Dorsky *et al.* tested the zebrafish equivalents in *hdl* inactivated embryos and *hdl/tcf3* double knockdowns. In zebrafish, *hdl* mutants showed a decrease in *pax6* expression in the presumptive head region and *pax2.1* expression was expanded rostrally. The expression of *gbx1* remained unchanged. However, if both *hdl* and *tcf3b* were inactivated, *gbx1* also expanded anteriorly, thereby encircling the expression domain of *pax2.1*. Furthermore, the anterior expression of *pax6* was completely lost (Dorsky *et al.*, 2003). In medaka, only a single *tcf3* gene was found (Wang, D. *et al.*, 2011). However, its expression (**Figure 26**) overlaps that of both *hdl* and *tcf3b* (Dorsky *et al.*, 2003). Furthermore, the observed loss of function phenotypes (**Figure 28**), resemble those of *hdl* inactivated zebrafish embryos (Dorsky *et al.*, 2003). We used similar probes as described by Dorsky *et al.* for our *in situ* hybridization experiments, to see if the zebrafish results are also true for medaka embryonic development. Indeed, the expression domains of all three genes were shifted anteriorly (**Figure 31A-D**) compared to the wild type control (**Figure 31E-H**). The caudal borders of this shift are indicated with white lines in **Figure 31H**. Embryos that showed expression patterns comparable to those of the zebrafish embryos injected with *hdl* antisense morpholino oligonucleotides (Dorsky *et al.*, 2003) were categorized as weak (**Table 18**) and those comparable to the *hdl/tcf3b* combinatorial knockdown of Dorsky *et al.* as strong (**Table 18**). In 48% of the embryos (**Table 18**) the expression domain of *pax6* was smaller (**Figure 31E,H**). Instead of two separate domains on either side of the prospective head (**Figure 31A,D**), only a single cap-like structure was observed at the most anterior part of the head (**Figure 31E,H**). However, we failed to see a complete loss of anterior *pax6* expression (**Table 18**). Also 56% of the embryos, hybridized with the MHB marker *pax2*, showed the same upwards shift (**Table 18**). Additionally, the expression of *pax2* was expanded anteriorly, thereby overlapping with *pax6* (**Figure 31F,H**), which was again in good agreement with the expression in zebrafish *hdl* loss of function embryos (Dorsky *et al.*, 2003). However, only 14% were categorized as strong (**Table 18**), resembling more an intermediate state between the two injection variants described by Dorsky *et al.* and none developed the severe horseshoe-like phenotypes. In 37% of the embryos an altered expression of *gbx1* was observed (**Table 18**). Again, the expression domain was shifted anteriorly (**Figure 31G,H**). Additionally to the upward shift of the entire expression domain,

the lateral edges of less severely caudalized embryos pointed anteriorly and in more severe phenotypes, the expression expanded into an arc-like shape, thereby overlapping the expression domains of both *pax6* and *pax2* (**Figure 31G,H**).

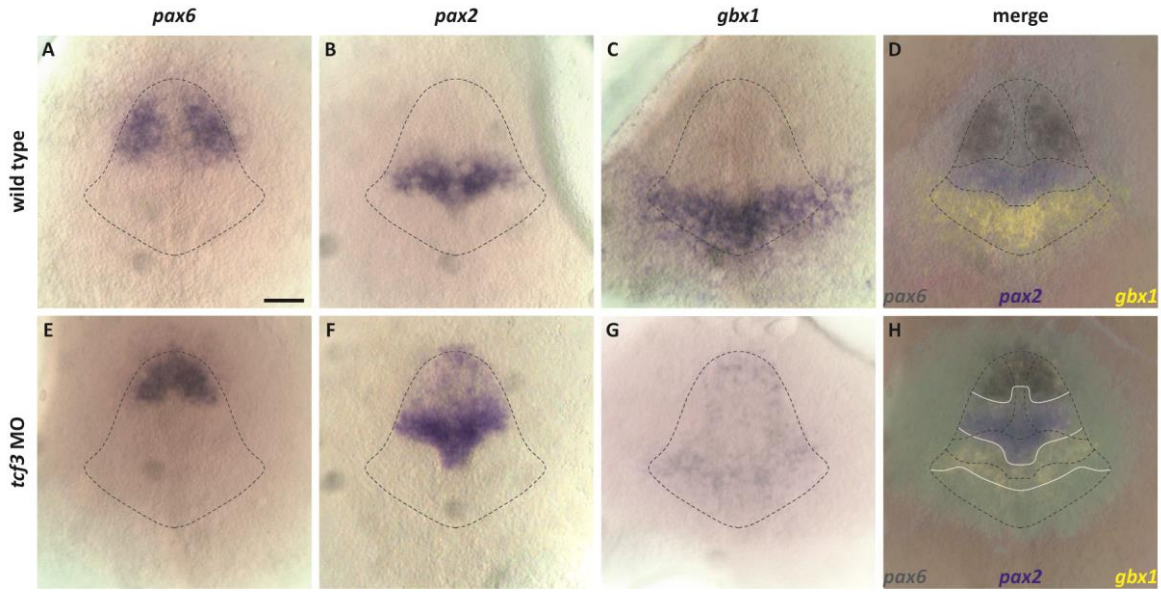

Figure 31| *Genotypic analysis of the tcf3 loss of function phenotype.* Embryos at the 1-cell stage were co-injected with 300 µM antisense morpholino oligonucleotides against *tcf3* and 1 µg/ml FITC Dextran (E-G). Control embryos (A-C) were co-injected with 1x Yamamoto's and FITC Dextran. FITC-positive embryos were selected at stage 16. Whole mount *in situ* hybridization experiments were performed using digoxigenin-labeled RNA probes against *pax6* (A,E), *pax2* (B,F), and *gbx1* (C,G). (D), Figures A-C were merged, the outlines of the wild type expression of all three genes is indicated by broken lines; *pax2* (yellow) served as background; the colors of *pax6* (brown) and *gbx1* (yellow) were altered using the transparency tool of CorelDRAW (intensity for *pax6* and inversion for *gbx1*). (H), pictures (E-G) were treated the same way as described for (A-C) in (D); the altered caudal borders of the expression are indicated with white lines. All embryos are shown in dorsal view with anterior to the top. *Tcf3* inactivation (E-G) caused an anterior shift in the expression domains of all three genes (A-C). Expression of *gbx1* (G) and *pax2* (F) expands anterior and overlaps with *pax6* expression (E). Scale bar 100 µM.

	pax6	***pax2***	***gbx1***
Embryos	61	36	43
Weak phenotype	29	15	0
Strong Phenotype	0	5	16
Total phenotypes	48%	56%	37%

Table 18| *Statistical overview of the genotypic analysis of tcf3 loss of function.* Whole mount *in situ* hybridization experiments were performed on *tcf3* inactivated embryos. Stage 16 embryos were hybridized with the indicated RNA probes. Phenotypes were categorized according to the expression pattern shifts similar to zebrafish embryos (Dorsky *et al.*, 2003): weak, zebrafish *hdl* mutant; strong, *hdl* mutant injected with *tcf3* morpholino oligonucleotide. Abbreviations: hdl, headless.

3.2.3 MEDAKA TCF3 GAIN OF FUNCTION

So far we analyzed *tcf3* loss of function phenotypes and their consequences. We then focused on our initial hypothesis, the connection between *Gro/TLE* genes and *tcf3* (**Figure 22**). For this, wild type embryos at the 1-cell stage were injected with full length *tcf3* (**Figure 32; Tcf3**) under the control of the heat-inducible HSE-promoter, which allowed stage-dependent ectopic gene expression (Bajoghli *et al.*, 2004). Stage 14 embryos were heat-induced for 10 minutes at 43.5°C and Gfp-selected 24 hours later. Phenotypes were categorized at stage 30, when the onset of eye pigmentation allowed distinct differentiation between normal development and weak alterations. Initially we expected that misexpression of Tcf3 would not result in an eye phenotype. However, **Table 19** shows that gain of function of full length Tcf3 resulted in 31% of the embryos showing smaller eyes, comparable to the weak phenotype of the *tcf3* morpholino injections. Neither elevated DNA concentrations nor variations of the heat-induction time did change this result.

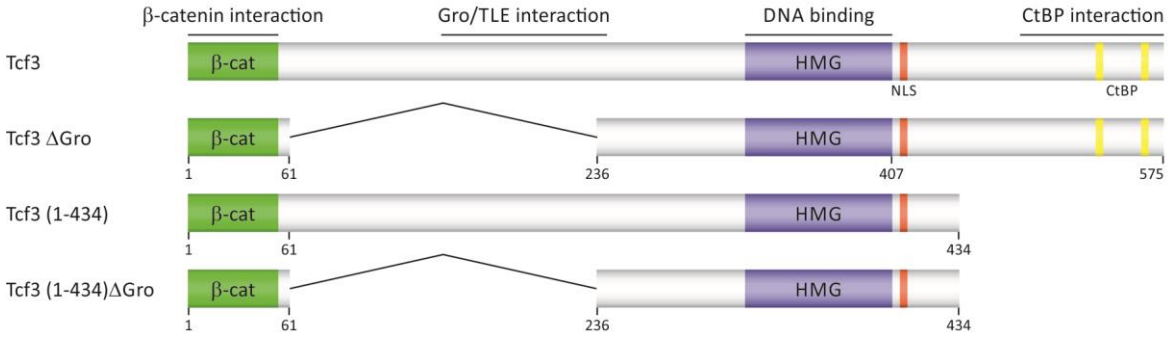

Figure 32| ***Schematic protein structure of Tcf3 and Tcf3 mutants.*** Green, β-catenin binding domain; purple, high mobility group (HMG) domain; red, nuclear localization sequence (NLS); yellow, CtBP-binding domain. The black triangle indicates the deletion of the Gro/TLE interaction domain.

We next concentrated on functional domains of Tcf3 that mediate transcriptional repression. Misexpression experiments in *Xenopus* showed that the C-terminus of Tcf3 mediates repression upon interaction with CtBP (Brannon *et al.*, 1999). To test whether an interaction with CtBP is responsible for the observed eye phenotypes we designed a truncated Tcf3 version (**Figure 32; Tcf3(1-434)**). With 49% the number of embryos developing smaller eyes was even higher in the truncated form without the CtBP-binding domain (**Table 19**). In addition to the C-terminus, the N-terminal region of Tcf/Lef proteins was also assigned with a repressing function. Experiments in *Xenopus* embryos showed that *siamois* is repressed by the N-terminal half of Tcf3 (Brannon *et al.*, 1997) and that this repression is mediated by interaction with Gro/TLE (Roose *et al.*, 1998). To specifically asses Tcf3-Gro/TLE-mediated repression, we then generated deletion versions for both full length Tcf3 and the C-terminally truncated Tcf3. These deletion spanned from amino acids 62 to 236 (**Figure 32; Tcf3ΔGro and Tcf3 (1-434) ΔGro**), including the Gro/TLE interaction domain but retaining the N-terminal β-catenin domain and the central HMG domain (Arce *et al.*, 2009). Loss of the GBS slightly decreased the number of eye phenotypes to 27% (**Table 19**), which indicates a strong effect of Gro/TLE corepressors on Tcf3, in particular during eye development.

	Tcf3	Tcf3 ΔGro	Tcf3(1-434)	Tcf3(1-434) ΔGro
Embryos	27	23	85	66
Dead	1	1	16	14
Mortality	4%	4%	19%	21%
weak	2	4	9	5
moderate	4	1	7	4
strong	2	1	18	5
Ectopic otic vesicles *)	0	7	0	14
Small eye phenotype in surviving embryos	31%	27%	49%	27%

*) The development of ectopic otic vesicles can overlap with the eye phenotype.

Table 19| *Gain of function phenotypes of the medaka tcf3 gene.* Embryos at the 1-cell stage were co-injected with 40 ng/µl heat-inducible DNA construct (gfp:HSE:Tcf3; gfp:HSE:Tcf3ΔGro; gfp:HSE:Tcf3(1-434)*;* gfp:HSE*:*Tcf3(1-434)ΔGro) and meganuclease. Heat treatment was applied at stage 14. Phenotypes of gfp-positive embryos were categorized at stage 30. Abbreviations: HSE, heat shock element.

Interestingly, in 31% of the embryos overexpressing Tcf3 mutants lacking the GBS, ectopic otic vesicles were observed. All of them formed in the trunk and tail region of the developing embryo, hence, posterior to the endogenous vesicles (**Figure 33B**). These results strongly resemble misexpression experiments of *sox3*. Koster *et al.* performed mRNA injections into 1-cell stage medaka embryos and observed ectopic otic vesicle formation at the dorso-lateral trunk (Koster *et al.*, 2000). The numbers in **Table 19** refer to the number of embryos that developed ectopic otic vesicles. However, as shown in **Figure 33**, several embryos developed multiple otic vesicles.

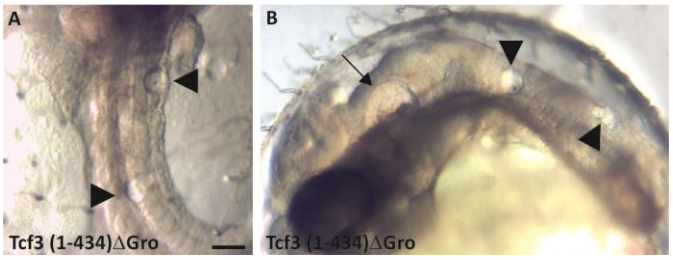

Figure 33| *Ectopic otic vesicle formation in Tcf3 mutants lacking the GBS.* Embryos at the 1-cell stage were co-injected with 40ng/µl gfp:HSE:Tcf3(434)ΔGro and meganuclease. Heat treatment was applied at stage 14 and pictures of gfp-positive embryos were taken at stage 31. (A) dorsal view with anterior at the top, (B) lateral view with anterior at the left. Arrow heads indicate ectopic otic vesicles, the arrow points to the endogenous otic vesicle. Scale bar 100 µm.

For further characterization of the gain of function phenotype, we selected the truncated mutants of Tcf3 due to their higher eye phenotype rate compared to full length Tcf3 (**Table 19**). While following the embryos during their development until final categorization, we noticed that the percentages of embryos showing phenotypes were considerably higher in younger embryos, suggesting rescue mechanisms. However, morphologic evaluation of phenotypes in stages without eye pigmentation is rather inaccurate. Using the retinal marker *rx2*, in *in situ* hybridization experiments, it was, however, possible to quantify eye development during early stages (**Figure 34**). At stage 21-22, 90% of the embryos developed eye defects, if injected with C-terminally truncated Tcf3 (**Figure 34A,C-E**). On the other hand the number of phenotypes in Tcf3ΔGro was again lower (50%) (**Figure 34A**). At these young stages, embryos were categorized as weak (**Figure 34C**) if the size of the eyes was

considerably smaller, but the intensity of the *in situ* hybridization staining was comparable to the wild type control (**Figure 34B**), whereas moderate (**Figure 34D**) and strong (**Figure 34E**) phenotypes showed a clear reduction or loss of staining, respectively.

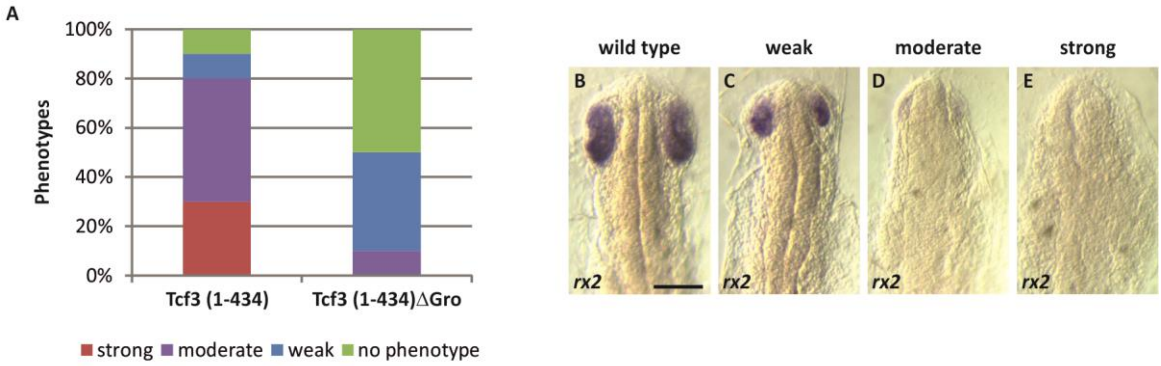

Figure 34| ***The tcf3 gain of function phenotype is enhanced in younger developmental stages.*** Embryos at the 1-cell stage were co-injected with meganuclease and either heat-inducible truncated Tcf3 (Gfp:HSE:Tcf3(1-434); 40 ng/µ) or Gro-depleted Tcf3 (Gfp:HSE:Tcf3(1-434)ΔGro; 40 ng/µl). Heat induction was performed at stage 14-15. Gfp positive embryos were selected at stage 22 for subsequent whole mount *in situ* hybridization experiments using digoxigenin-labeled RNA probes against *rx2*. (B) wild type controls were heat-induced at stage 14. (A) Statistical overview of the phenotype distribution. (B-E) whole mount *in situ* hybridization against *rx2*, embryos are shown in dorsal view, anterior at the top. Phenotypes were categorized according to their eye size and the expression intensity compared to the control: (C) weak, small eyes, normal expression intensity; (D) small eyes, weak expression; (E), missing eyes and expression. Total number (*N*) of embryos used for *in situ* hybridization experiments: Tcf3(1-434), *N*=10, Tcf3(1-434)ΔGro, *N*=10. Scale bar 100 µM.

We also directly compared the phenotypes of *tcf3* loss of function phenotypes with the gain of function phenotypes (**Figure 35**). For this, whole mount *in situ* hybridization experiments with digoxigenin-labeled RNA probes against *tcf3*, *rx2*, *bf1*, and *wnt1* were performed and compared with heat-induced wild type control embryos (**Figure 35**). Due to the observed small-eye phenotype, *rx2* expression was reduced in morpholino injected (**Figure 35F**) as well as in the *tcf3* injected embryos (**Figure 35J**). However, the latter showed a somewhat weaker expression compared to the control (**Figure 35**Figure **35B**). The observed staining for *tcf3* was comparable to the control and the morpholino injected embryos but showed a blurred outline surrounding the embryo (**Figure 35K,P**). The most distinct differences between the morpholino injected embryos and the Tcf3 mutants were observed with *bf1* (**Figure 35G,K**) and *wnt1* (**Figure 35H,L**) probes. Using morpholino oligonucleotides, the forebrain and midbrain seemed relatively unaffected (**Figure 35G,H**) compared to control embryos (**Figure 35C,D**). However, looking at the expression of *bf1*, it rather seemed that the anterior part of the eyes was missing, leaving only the posterior part as a remaining small eye (**Figure 35G**). In the *tcf3* misexpressing embryos, on the other hand, the eyes developed more anteriorly; resulting in a more line-shaped (**Figure 35K**) and not a cascaded staining. A clear difference was observed in *wnt1* expression, which was wide and blurred in the midbrain and weak in the trunk and tail region. Furthermore, the size of the midbrain was reduced in *tcf3* gain of function (**Figure 35L**).

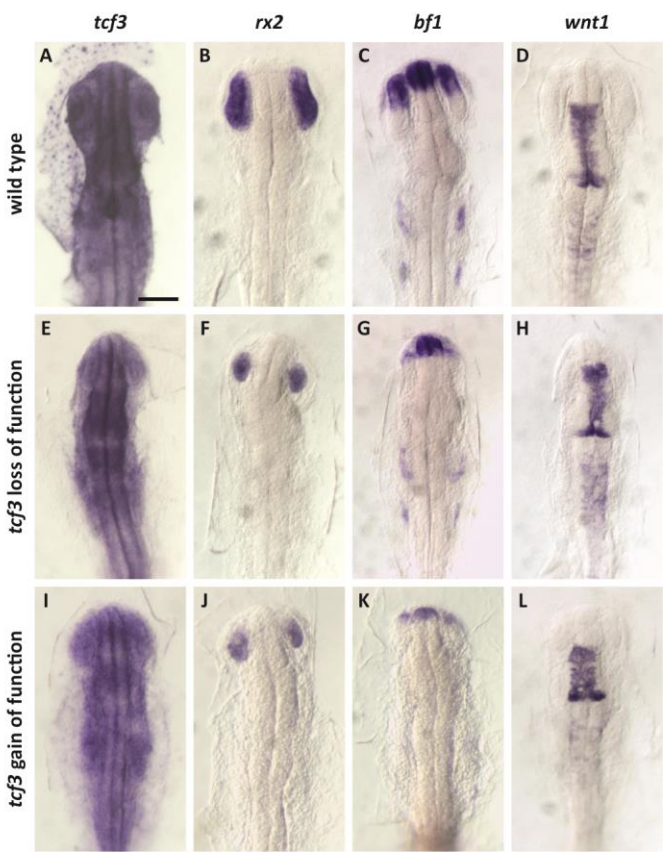

Figure 35| *Comparison of tcf3 loss of function with tcf3 gain of function phenotypes.* Embryos at the 1-cell stage were injected with either 300 µM antisense morpholino against *tcf3* (E-H) or co-injected with 40 ng/µl gfp:HSE:Tcf3(1-434) and meganuclease (I-L). Injected and wild type control embryos were heat-induced at stage 14 at 43.5°C for 10 minutes (I-L). Whole mount *in situ* hybridization experiments were performed using digoxigenin-labeled RNA probes against *tcf3* (A,E,I), *rx2* (B.F,J), *bf1* (C,G,K), and *wnt1* (D,H,L). Reduced expression of *rx2* (F,J) and *bf1* (G,K) in the eyes. Diffused *Wnt1* expression in the Tcf3 mutants (L) shows a small smaller midbrain and only weak expression in the hindbrain. *Tcf3* expression was unchanged (E,I). Scale bar 100 µm.

Part III

3.3 Electroporation of Small Molecules

In fish developmental biology, microinjection is a standard technique to introduce DNA or RNA into an embryo. However, to obtain reproducible results, good training and long experience is necessary and still the outcome may vary. One of the critical factors during microinjection is the droplet size. An injection solution has a defined concentration but the final amount of DNA/RNA inside the embryo depends on the injected volume. In gain-of-function experiments, the generation of transgenic lines eliminates this problem. However, for loss-of-function experiments (e.g. morpholino knock down), transient injections are inevitable. More than twenty years ago Japanese scientists addressed this problem and introduced electroporation as an alternative to classical microinjection to produce transgenic medaka fish (Inoue *et al.*, 1990). Finally, Hostetler *et al.* improved this technique, by using direct current-shift radio pulses, to generate large numbers of stable transgenic fish (Hostetler *et al.*, 2003).

Based on their results we wanted to use electroporation for our loss-of-function experiments. In an attempt to adapt their protocols, we used the same conditions as a starting point (modulation frequency, 35 kHz; voltage, 25 V; pulse duration, 10 ms; using 3 pulses with 1 second pulse interval) as Hostetler *et al.* to electroporate a vector which constitutively expresses *gfp* into 1-cell stage embryos (Fargas Madriles, 2011). However, no gfp expression could be detected within the embryo, even after modulating the original settings. We then used smaller FAM-labeled oligonucleotides (Friesenhengst, 2012) and again failed to detect fluorescence. Only dechorionation slightly improved the uptake of both the vector and the oligonucleotides.

We reasoned that the rigid chorion, surrounding the medaka embryo, might be a barrier for the uptake of molecules and, therefore, started analyzing its characteristics.

3.3.1 Diffusion Into Medaka Embryos

To analyze the diffusion properties of the medaka chorion we chose fluorescing substances as small and easily quantifiable tracer molecules. For this, several tracer dyes were tested: fluorescein, rhodamine B, acridine orange, acriflavine, alizarine red, fuchsine acid, and neutral red. Depending on their molecular properties, they were distributed differently within the egg (including the embryo and the yolk) and were detectable at variable concentrations. We finally selected fluorescein as a representative small molecule for most experiments.

To determine the optimal conditions for medaka embryos, we incubated the embryos with fluorescein at 27°C for variable durations and at various concentrations. Best quantifiable results were obtained after 40 minutes incubation with a concentration of 10

mg/ml and 30 minutes washing time. However, the embryos tolerated even higher concentrations (100 mg/ml) without any phenotypic alterations. To quantify the uptake of fluorescein by the embryo, we mainly used fluorescence microscopy (measurement of pixel intensities from microscopic pictures) but we also tested fluorescent spectroscopic determination (Thaler, 2010). Although the latter method is more sensitive, we preferred microscopic measurement. This allowed us to follow the same embryos during development and to qualify tissue distribution of the tracer substance, survival, and possible phenotypic alterations.

Fluorescein Reference

To be able to quantify the amount of fluorescein within the egg we prepared a reference. The volume of an average egg (embryo and yolk) was determined by measuring its diameter. This resulted in an average volume of 0.8 µl. Fluorescein droplets with variable concentrations and a volume comparable to an average egg were measured in mineral oil. However, the spherical-shape of the droplet was lost, once it touched the bottom of a plate. Therefore, cellulose sulfate beads (Ortner *et al.*, 2012) were soaked in different concentrations of fluorescein for several days and the pixel intensity of the microscopic pictures was determined (Dorn *et al.*, 2012; Jung *et al.*, 2013). Measurement of the beads resulted in an average diameter of 730 nm and consequently a volume of 0.2 µl. Concentrations between 100 µg/ml and 1 µg/ml were linear over a broad range of exposures (**Figure 36**). Taking the differences in the volume into account, a fluorescein reference was calculated from these values (**Figure 37**).

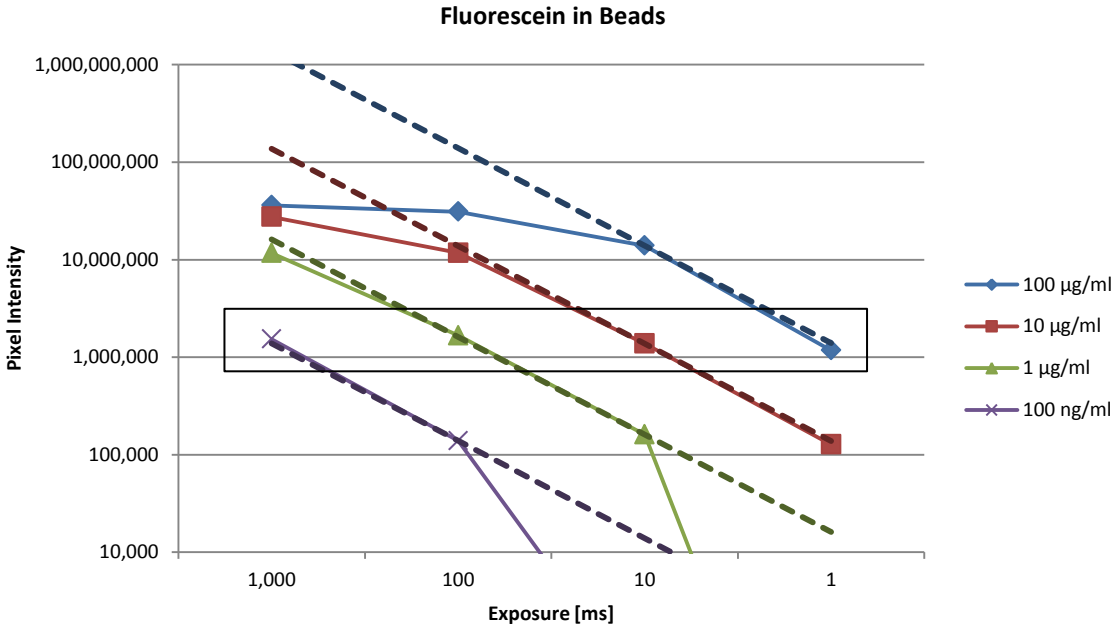

Figure 36| *Fluorescein in beads.* Microscopic pixel measurement of cellulose sulfate beads, soaked in fluorescein staining solution with different concentrations: blue, 100 mg/ml; red, 10 µg/ml; green, 1 µg/ml; purple, 100 ng/ml. Pixel intensities were quantified for several exposure times, using ImageJ (Schneider *et al.*), and a linear range (black box) with a pixel intensity around 1,000,000 was determined.

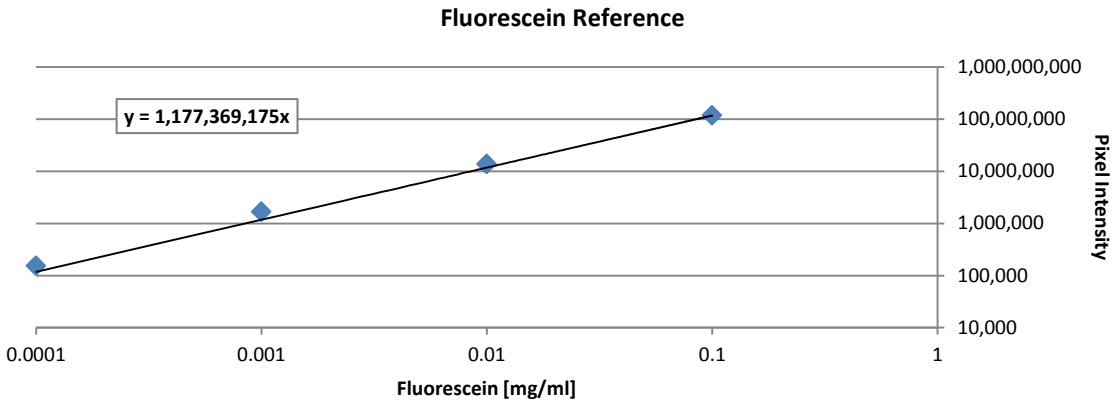

Figure 37| ***Fluorescein reference.*** To quantify the amount of fluorescein within the embryos, a reference was calculated from the pixel intensities measured in the cellulose sulfate beads in **Figure 36**.

Fluorescein Uptake and Distribution in Medaka Embryos

Initial experiments, using a concentration of 10 mg/ml fluorescein, showed that if incubated at the 1-cell stage, fluorescein was internalized by the zygote (Appendix (Jung *et al.*, 2013) Figure 1A). Extensive washing with ERM over several days removed the excess fluorescence and only a weak signal remained in the liver/gallbladder (Appendix (Jung *et al.*, 2013) Additional File 1A). Also during blastula (Appendix (Jung *et al.*, 2013) Figure 1B) and in later stages of development (Appendix (Jung *et al.*, 2013) Figure 1C), fluorescein was preferably localized within the embryo. Only shortly before hatching, the signal was enriched in the liver and the gallbladder (Appendix (Jung *et al.*, 2013) Figure 1D). This distribution made fluorescein a well suited model for small substances diffusing into the embryo.

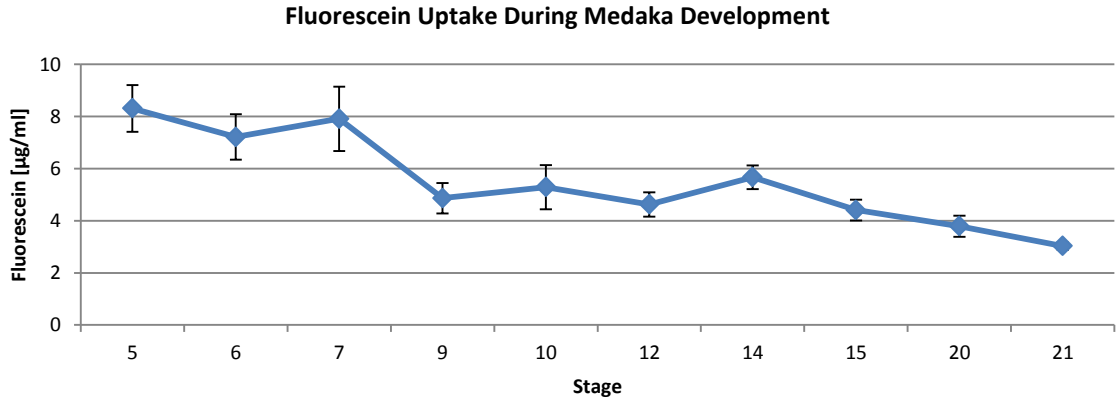

Figure 38| ***Fluorescein uptake during early medaka development.*** Embryos at several stages were incubated with 10 mg/ml fluorescein for 40 minutes at 27°C. Pictures were taken after 30 minutes washing and fluorescence intensities were measured. Fluorescein uptake into fertilized embryos is slightly reduced.

Measurements of the fluorescence intensity showed a slight decrease in the uptake of fluorescein during early embryonic development (**Figure 38**). However, following fluorescein uptake during most developmental stages, the pixel intensities remained relatively constant, except from the 4-cell stage to early morula and shortly before hatching, where the signal slightly increased (Appendix (Jung *et al.*, 2013) Figure 1E).

Diffusion Kinetics

As described in the previous section, the embryos were incubated with a concentration of 10 mg/ml. However, after 40 minutes of in-diffusion and 30 minutes washing time only 3-9 µg/ml of fluorescein were detected within the embryo (Appendix (Jung *et al.*, 2013) Figure 1E) which represents less than 0.1% of the supernatant. We therefore decided to investigate the diffusion kinetics through the chorion. Due to a quantification limit of approximately 100 µg/ml (**Figure 36**) and an external concentration that exceeds this value, we could not analyze the kinetics of in-diffusion and therefore concentrated on the out-diffusion.

To remove excess material on the surface of the chorion, several fast washing steps, including a 3- fold exchange of ERM within the first 5 minutes, were introduced directly after incubation and first reproducible results were obtained after 7 minutes washing time. Further survey points after 10, 20, 30, 60, 90, and 120 minutes identified two phases. The first phase describes a fast decrease of the signal within 30 minutes of washing, whereas during the second phase this process is considerably slower (Appendix (Jung *et al.*, 2013) Figure 2A). The calculated diffusion half-times for fluorescein resulted in 4 minutes for the first phase and 2.4 hours for the second phase.

Diffusion Barriers within the Medaka Egg

Initially we considered the rigid chorion surrounding the medaka embryo and yolk as the main diffusion barrier. However, this bi-phasic out-diffusion made us reconsider and question which structures of the egg are responsible for the observed kinetics. Additionally to the outer acellular chorion, the embryo and yolk are covered by extra-embryonic membrane systems, another potential barrier. In order to distinguish these possibilities, we manipulated the eggs to create two different experimental models (Appendix (Jung *et al.*, 2013) Figure 2B). To mimic chorion diffusion, dead embryos were used. Since the chorion still had to be intact in these embryos, they were prepared by applying high voltage pulses (60 V, 0.5 A, 35 kHz, 60 ms, 3 pulses with 200 ms interval). Upon this treatment, the embryo, the yolk, and all membranes shrink to a ball-like structure that remains within the chorion barrier but is relatively small compared to the volume of the chorion. To mimic the extra-embryonic membrane systems, the embryos were dechorionated using natural hatching enzyme.

Quite unexpectedly, dead embryos showed strong fluorescence after 40 minutes of incubation (Appendix (Jung *et al.*, 2013) Figure 2C' and (Hug, in preparation)), indicating that the chorion is easily passed by fluorescein and hence not the limiting barrier. Quantification of the signal (Appendix (Jung *et al.*, 2013) Figure 2E and (Hug, in preparation)) revealed that fluorescein is taken up relatively fast during the first 40 minutes. It then reaches a saturated phase with approximately 90% of the supernatants

concentration. On the other hand, dechorionated embryos showed only weak fluorescence (Appendix (Jung *et al.*, 2013) Figure 2D and (Hug, in preparation)) and the concentration of internalized fluorescein was at basal levels, comparable to intact eggs(Appendix (Jung *et al.*, 2013) Figure 2E and (Hug, in preparation)). Some of the dechorionated embryos had spike levels of pixel intensities. Microscopic controls, however, showed that these embryos were not stained uniformly but rather showed patches of fluorescence. Closer inspection revealed lesions in the membranes of such embryos (**Figure 39**). Disruption of theses membranes is a common side effect observed in dechorionated embryos and they were excluded from evaluation.

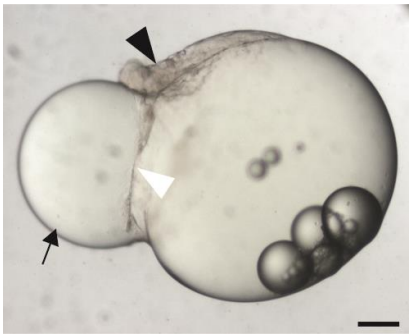

Figure 39| *Disrupted membrane systems of a dechorionated embryo.* Lateral view of a dechorionated embryo at stage 17, anterior at the left. Black arrow head indicates the embryo. White arrow head indicates the disrupted membrane system surrounding the embryo and yolk. The black arrow points to the yolk bulging from the covering membrane systems. Scale bars 250 µm.

We therefore concluded that not the chorion of medaka eggs is the diffusion barrier for small molecules but the membrane systems surrounding the embryo and the yolk. This would predict that small molecules diffuse relatively fast through the chorion of intact eggs into the perivitelline space where they are stopped at the inner membranes. Based on this hypothesis, we tested the in-diffusion into the perivitelline space. For this, intact eggs at the 2-cell stage were shortly exposed (10 minutes) to low concentrations of fluorescein (100 µg/ml), which should be sufficient to reach high fluorescence with still quantifiable pixel intensities inside the perivitelline space but not the embryo. Indeed, the expected distribution of fluorescein was observed after a few washing steps (3-fold medium exchange in 2 minutes) (Appendix (Jung *et al.*, 2013) Figure 2F"). We also assumed that if the incubation time would be prolonged (40 minutes), as in the experiments shown previously (Appendix (Jung *et al.*, 2013) Figure 1), fluorescein would not only be enriched in the perivitelline space but have further diffused into the embryo. Hence, after short washing (3-fold medium exchange in 2 minutes), fluorescence could be detected both in the perivitelline space and the embryo (Appendix (Jung *et al.*, 2013) Figure 2G"). On the other hand, after additional washing steps fluorescein in the perivitelline space rapidly disappeared, due to fast out-diffusion through the chorion, and only remained within the embryo (Appendix (Jung *et al.*, 2013) Figure 2H"). As a second small molecule methylene blue was tested using the same procedure. It rapidly accumulated within the perivitelline space (Appendix (Jung *et al.*, 2013) Additional File 2) but did not diffuse further into the embryo or yolk and comparable to fluorescein it was quickly removed from the perivitelline space.

Triton X-100 Affects the Membrane Behavior

One possible attempt to overcome the diffusion barriers is microinjection. For early stages this is a well-established method. However, during later stages the injection mix needs to be applied into larger internal cavities, for example the neural tube. In zebrafish, yolk-injections are often performed to accomplish uniform distribution. Indeed, in medaka yolk-injected fluorescein was distributed evenly throughout the yolk after 30 minutes (Appendix (Jung *et al.*, 2013) Additional File 3). However, detection of fluorescent signal within the embryo was only possible after 4 hours and in very low concentrations. Moreover, medaka embryos have a very sticky yolk which leads to rapid clogging of the injection needle and hence to low reproducibility.

In an initial attempt to overcome the diffusion barriers, we incubated the embryos with de-ionized water, due to the fact that chorion permeability is decreased in the presence of cations (Cameron *et al.*, 1984). The idea of using de-ionized water resulted from a time when we were not yet aware of the membrane system as actual barrier and still assumed that the chorion is the main barrier for diffusion. To be able to clearly see changes in diffusion, we chose 3-days old embryos which have previously shown the lowest uptake of fluorescein (Appendix (Jung *et al.*, 2013) Figure 1C). Intact eggs were pre-incubated with de-ionized water for 0 (no treatment), 3, and 24 hours. The embryos tolerated both incubation times very well (100% survival for both pre-incubations), without developing phenotypes. Measurement of pixel intensities was performed after 30, 60, and 24 hours. Compared to the untreated control (0 hours pre-incubation), 3 hours pre-incubation resulted in an almost 3-fold increase of fluorescence within the egg after 30 minutes of washing (**Figure 40, red bar**). Prolonged washing showed a slow decrease of the internalized signal which reaches almost basal levels after 24 hours. However, pre-incubation for 24 hours resulted only in a small increase of fluorescence (**Figure 40, green bar**).

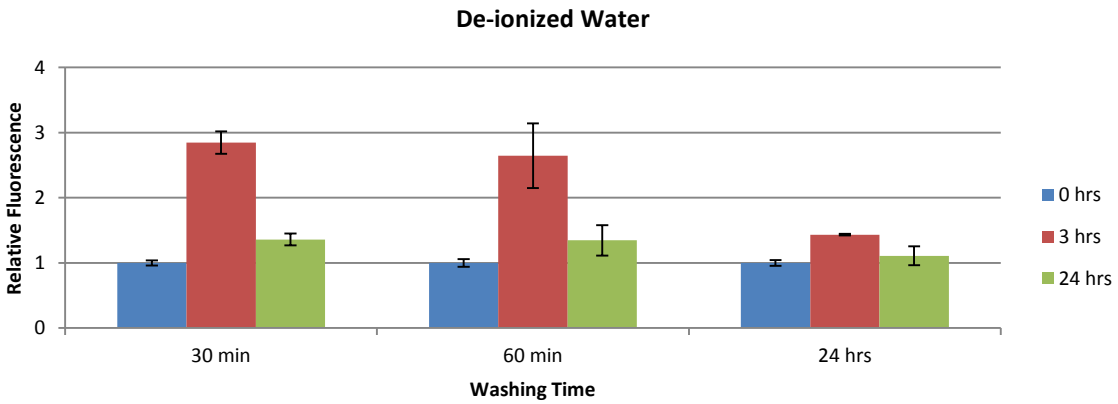

Figure 40| ***Fluorescein uptake into medaka embryos after pre-incubation with de-ionized water.*** Intact 3 days old embryos were incubated with de-ionized water for 3 (red bars) and 24 (green bars) hours prior staining with fluorescein (10 mg/ml, 40 minutes, at 27°C). Fluorescence intensities were measured after 30 and 60 minutes and 24 hours washing. Control embryos (blue bars) were incubated with fluorescein but otherwise untreated. Pre-treatment with de-ionized water for 3 hours enhances the uptake of fluorescein into the embryo, whereas with 24 hours pre-incubation only a slight increase was observed. Abbreviations: hrs, hours; min, minutes.

Pre-incubation with de-ionized water clearly improved the uptake of small molecules. However, the increase in fluorescent signal was only small. To further improve diffusion into the embryo, we decided to use detergents. In contrast to SDS which is an ionic detergent and appears to be highly toxic, we chose Triton X-100, which the embryos tolerated well. Concentrations up to 0.01% showed no phenotypes. Only at higher concentrations the survival was reduced (69% for 0.03% Triton and 25% for a concentration of 0.1%). Compared to the untreated control (0% Triton), co-incubation with fluorescein and 0.01% Triton had almost no effect on the uptake (**Figure 41, red bar**). However, co-incubation with higher concentrations resulted in a 10-fold increase of fluorescence measured within the egg after 30 and 60 minutes of washing (**Figure 41, green and purple bars**). The difference was even higher after 24 hours washing time, where the signal showed a more than 100-fold increase of fluorescein concentration compared to the control.

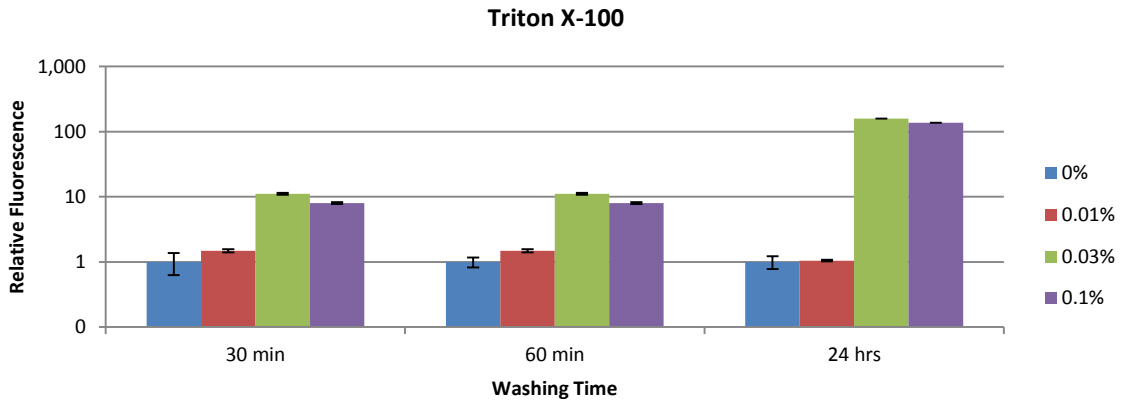

Figure 41| ***Fluorescein uptake into medaka embryos after co-incubation with Triton X-100.*** Intact 3 days old embryos were co-incubated with fluorescein (10 mg/ml) and Triton X-100 at various concentrations (0.01%, red bars; 0.03%, green bars; 0.1% purple bars) for 40 minutes at 27°C. Control embryos (blue bars) were stained normally without Triton treatment. Fluorescence intensity was measured after 30 and 60 minutes and 24 hours washing. Triton concentrations higher than 0.01% facilitated the uptake of fluorescein into the embryo. Abbreviations: hrs, hours; min, minutes.

Taken together, pre-incubation with de-ionized water increased the uptake of small molecules through the chorion. During the first 60 minutes of washing the signal was clearly higher than compared to the control (**Figure 42D,E**). However, most of the internalized fluorescein diffused out of the chorion after 24 hours of washing, remaining only fluorescence in the gallbladder/liver (**Figure 42F**). Triton X-100, on the other hand, showed a tremendous effect on the uptake of fluorescein into the embryo and yolk (**Figure 42G-H**). It seems to trap the molecules inside, even after 24 hours of washing (**Figure 42H**). Whereas, after 60 minutes of washing, fluorescein can be seen in the perivitellin space and on the chorion in control embryos (**Figure 42B**) and also in embryos pre-incubated with de-ionized water (**Figure 42E**), all of the marker molecules were inernalized into the embryo and yolk if co-incubated with Triton (**Figure 42H**) (note that different exposure times were used for the pictures of Triton-treated embryos).

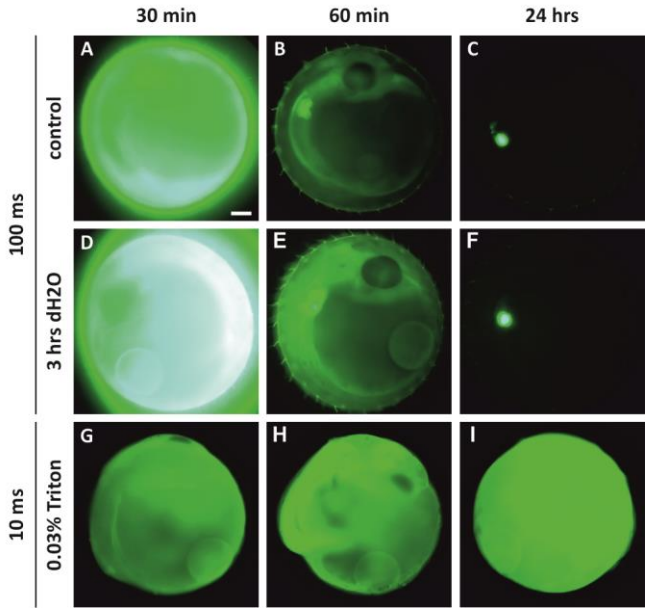

Figure 42| *Improvement of fluorescein uptake.* Embryos were either pre-incubated with de-ionized water (D-F) or co-incubated with Triton X-100 (G-I). Control embryos (A-C) were incubated in 10 mg/ml fluorescein for 40 minutes at 27°C. Normal washing steps were performed and pictures were taken after 30 and 60 minutes and after 24 hours of washing with ERM. (A-F) exposure time set to 100 ms, (G-I) due to a higher fluorescent signal the exposure time was reduced to 10 ms. Abbreviations: min, minutes; ms, milliseconds; dH_2O, de-ionized water. Scale bar 250 µM.

3.3.2 Electroporation of Small Molecules Into Medaka Embryos

As shown in the previous section, the addition of Triton X-100 strongly improved the uptake of small molecules into the embryo and yolk. However, it also affected the distribution between single compartments (**Figure 42G-H**), making the assessment of other substances and their pharmacological or toxicological properties difficult. We also showed that not the acellular chorion, but a membrane system surrounding the embryo and yolk is the main barrier for the uptake of small molecules. Therefore, we tested electroporation, a technique that is known to provide transport across cellular membranes.

Electroporation Improves the Uptake of Small Molecules into Medaka Embryos

To enhance the uptake of fluorescein into embryos at stage 17 by electroporation, we again used the settings described by Hostetler *et al.* (Hostetler *et al.*, 2003). Due to the fact that the chorion is easily passed by fluorescein and that the concentration in the perivitelline space is almost saturated after 40 minutes (Appendix (Jung *et al.*, 2013) Figure 2E and (Hug, in preparation)), we pre-incubated the eggs. We then varied the pulse duration and voltage over a wide range and finally obtained optimal conditions (a compromise between good fluorescence intensity and survival) at 15 V and 5 seconds pulse duration (Appendix (Jung *et al.*, 2013) Figure 4A and (Hug, in preparation)). Additional pulses, as used by Hostetler *et al.*, did not improve the uptake of fluorescein. Furthermore, the same conditions were applicable for both younger (Appendix (Jung *et al.*, 2013) Figure 4B' and (Hug, in preparation)) and older (Appendix (Jung *et al.*, 2013) Figure 4C' and (Hug, in preparation)) stages.

In order to verify our assumption that electroporation improves the uptake of small molecules through the rate limiting inner membrane system, we performed the same experiments with dead (diffusion through the chorion) and dechorionated (diffusion through the membrane) embryos (Appendix (Jung *et al.*, 2013) Figure 5 and (Hug, in preparation)). Indeed, electroporation improved the uptake in intact (Appendix (Jung *et al.*, 2013) Figure 5A,E and (Hug, in preparation)) and in dechorionated (Appendix (Jung *et al.*, 2013) Figure 5A,G and (Hug, in preparation)) embryos, whereas the signal in dead embryos did not change (Appendix (Jung *et al.*, 2013) Figure 5A,F and (Hug, in preparation)).

So far we used fluorescein as a representative substance for small molecules. In order to verify this method for other small molecules we selected two additional dyes (rhodamine B and acridine orange) with a different distribution than fluorescein. Electroporation resulted in an increase of both molecules compared to diffusion alone. Rhodamine B was strongly enriched in the yolk throughout all stages (Appendix (Jung *et al.*, 2013) Figure 6B-D) and was only partially removed by washing. Acridine orange, on the other hand, was taken up by the yolk and the embryo (Appendix (Jung *et al.*, 2013) Figure 6E-G). Similar to fluorescein, at later stages strong fluorescence was visible in the gallbladder/liver (Appendix (Jung *et al.*, 2013) Figure 6G).

Until now, all electroporation experiments were performed using the modified settings from Hostetler *et al.*, thereby changing the voltage, pulse duration, and number of pulses to our optimum. However, we never altered the modulation frequency of 35 kHz. To finally optimize all parameters, we next varied the frequencies from 1 to 100,000 Hz and found the highest fluorescein uptake at 330 Hz (Appendix (Jung *et al.*, 2013) Figure 6A and (Hug, in preparation)).

Lithium Induces Deficiencies in Anterior-Posterior Development

After having analyzed the diffusion properties of medaka embryos and after having established electroporation as a method to improve the uptake of fluorescent dyes into the egg, we tested a combination of these two procedures with a substance known to induce phenotypic alterations when applied during early embryonic development. For this we selected lithium chloride, a GSK-3 inhibitor that activates the Wnt signaling pathway (Kao *et al.*, 1998). Lithium induction in zebrafish induces clear dorsalization of the embryo when applied during early gastrulation (Stachel *et al.*, 1993). For our experiments we used comparable concentrations (0.4 M lithium chloride), incubation times (10 minutes), and stages (stage 14, 40% epiboly).

Diffusion alone resulted in normal development of the embryos, but with the addition of electroporation (15 V, 330 Hz, 100 ms, 1 pulse) 63% developed deficiencies in anterior-posterior development (Appendix (Jung *et al.*, 2013) Figure 7A). Almost 40% of the observed phenotypes were classified as strong. They showed severe axis truncation anterior to the midbrain, thereby lacking both eyes and forebrain (Appendix (Jung *et al.*, 2013) Figure 7D,G). Furthermore, one quarter of the embryos with a strong phenotype developed multiple ectopic otic vesicles anterior to the natural ones (Appendix (Jung *et al.*, 2013) Additional File 6). As a weak phenotype we classified 24% of the surviving embryos where only the eyes were affected (Appendix (Jung *et al.*, 2013) Figure 7C,F). Untreated control embryos that were electroporated developed normally; however,

compared to non-electroporated embryos they showed an elevated mortality rate (Appendix (Jung *et al.*, 2013) Figure 7A).

Taken together, we characterized the diffusion of small molecules into the medaka embryo and showed that the chorion is not the limiting barrier but a membrane system surrounding the embryo. We were able to overcome this second barrier using electroporation. This method allowed us to improve the uptake of small molecules into the embryo. To show the relevance of this method for developmental biology, we selected the GSK-3 inhibitor lithium as a representative substance. Embryos that were induced with lithium and subsequently electroporated, obtained the expected deficiencies in anterior-posterior development.

4 DISCUSSION

The main part of this thesis deals with the analysis of Gro/TLE loss of function and its interaction with Tcf3 during early medaka development. In addition the diffusion properties of the medaka chorion were analyzed and the uptake of small molecules into the embryo could be improved by electroporation. The discussion is therefore divided into the three main topics, corresponding to the three main parts in the Results section.

4.1 ANALYSIS OF GRO/TLE LOSS OF FUNCTION IN MEDAKA

In developmental biology the study of mutants is a standard method to analyze and understand the function of genes. However, many gene families, such as the *Gro/TLE* family, contain several members that largely overlap in sequence and thereby in function. Medaka, for example contains six *tle* genes and the proteins associated are highly conserved in both their N-terminal Q domain and the C-terminal WD40-repeat domain (Lopez-Rios *et al.*, 2003; Aghaallaei *et al.*, 2005). Especially the WD40-repeat domain, which mainly mediates protein-protein interaction, shows high sequence similarity (Fisher *et al.*, 1998; Li, S. S., 2000) and therefore often binds to the same transcription factors (Choi *et al.*, 1999; Ren *et al.*, 1999; Eberhard *et al.*, 2000). This complicates the analysis of mutants and knockdown experiments because changes in single genes will only hamper partly Gro/TLE function. We addressed this problem by different approaches. On one side we used morpholino oligonucleotides to specifically knock down early expressed *tle* genes (**Figure 22** and **Table 15**). Alternatively, we used a dominant-negative approach to obtain a more general loss of function. The principle idea was that excess of mutated Tle proteins, interaction motifs or simply truncated protein versions would displace endogenous Tle from the repressing complexes and thereby inhibit its function. Using the inducible HSE-promoter for this approach allowed stage-specific expression (Bajoghli *et al.*, 2004).

We started with an amino acid substitution within the highly conserved WD40-repeat domain of Tle1. This R534A substitution affects the interaction with both the WRPW and the Eh1 motif (Jennings *et al.*, 2006; Buscarlet *et al.*, 2008). In *Drosophila*, the corresponding MB^{41} mutation resulted in the formation of excessive neural tissue and reduced cuticles (Jennings *et al.*, 2006). However, in contrast to medaka the *Drosophila* genome contains only one *gro* gene (Lindsley *et al.*, 1968). Cell culture experiments showed that the anti-neurogenic activity of Gro/TLE1 was lost in R534A mutants. However, loss of function does not result from general misfolding of the WD40-repeat domain, since mutated proteins were able to translocate to the nucleus and interact with Tcf/Lef (Buscarlet *et al.*, 2008). Mutated Gro/TLE1 could still mediate repression via the N-terminus (Brantjes *et al.*, 2001). By disrupting the ability of WRPW and Eh1 motifs to bind to the WD40 repeat domain of Tle1, we expected specific loss of function phenotypes. In contrast, we rather observed gain of function phenotypes (**Table 11**) with enlarged eyes and a bulging midbrain (Lopez-Rios *et al.*, 2003). López-Ríos *et al.* strongly

connected the observed eye phenotype to Six3. As Tle1 and Six3 interact via the Q domain, which is intact in the R534A mutant, this could explain the observed gain of function phenotype. Therefore, we generated version without the Q domain (**Figure 15**). Contrary to our expectations, embryos misexpressing just the WRPW motif or the WD40-repeat domain developed no phenotypes (**Table 12**). We expected that an excess of WD40-repeat domain would tether away potential Gro/TLE interaction partners. The truncated Gro/TLE version containing only the WD40-repeat domain lacks the NLS, which is located within the CcN domain of full length Gro/TLE proteins (Stifani *et al.*, 1992). One reason for the failure might therefore be a wrong localization within the cell. Small WRPW peptides, on the other hand, could block the interaction with other proteins and translocate to the nucleus by binding to the WD40-repeat domain of endogenous Gro/TLE. However, the lack of phenotypes leaves room for speculations. One possibility would be that the interaction is not strong enough and the WRPW peptides are replaced by full length proteins. On the other hand, similar experiments in *Xenopus* caused abnormal brain development and eye defects (Tsuji *et al.*, 2005).

The previous paragraph suggests that interference with the WD40-repeat domain is not enough to disrupt Gro/TLE-mediated repression in medaka. We therefore concentrated on Aes/Grg5 (**Figure 15**), a naturally occurring truncated family member of full length Gro/TLE proteins that consists of only the Q and the GP domain (Mallo *et al.*, 1993; Miyasaka *et al.*, 1993; Schmidt *et al.*, 1993). The conserved Q domain allows Aes/Grg5 to oligomerize with other full length Gro/TLE proteins and interaction with non-WD-repeat domain-dependent transcription factors (Pinto *et al.*, 1996; Chen *et al.*, 1998; Choi *et al.*, 1999; Eberhard *et al.*, 2000; Brantjes *et al.*, 2001; Yao *et al.*, 2001; Lopez-Rios *et al.*, 2003). The GP domain, however, is functionally different from full length Gro/TLE proteins because it does not interact with HDACs (Yu *et al.*, 2001; Bajoghli *et al.*, 2007; Zhang, X. *et al.*, 2008; Arce *et al.*, 2009). It is suggested that by this interaction Aes/Grg5 turns Gro/TLE oligomers into non-functional complexes [(Pinto *et al.*, 1996; Palaparti *et al.*, 1997; Chen *et al.*, 1998; Choi *et al.*, 1999; Brantjes *et al.*, 2001) and reviewed by Beagle *et al.*, 2010a]. Indeed, ectopic expression of *aes* in medaka resulted in considerably smaller eyes and otic vesicles and reduced expression of the optic and otic marker genes, suggesting a block of Tle1 and Tle4 activity (Lopez-Rios *et al.*, 2003; Bajoghli *et al.*, 2005). We therefore selected Aes as a candidate to generally block the function of all six medaka Tle proteins simultaneously. In mammalian two-hybrid experiments we confirmed that Aes is capable of mediating the repression of both Tle1 and Tle4 (**Figure 19**). To eliminate the possibility of injection-based phenotypes in our *in vivo* experiments, we generated heat-inducible transgenic lines and concentrated primarily on the most prominent phenotype, the reduction in eye size (**Figure 16** and **Table 13**).

However, Aes exhibits additional repressing function on its own (Tetsuka *et al.*, 2000; Yu *et al.*, 2001; Zhang, Y. *et al.*, 2010). We therefore compared the Aes-induced phenotypes with C-terminally truncated versions of full length Gro/TLE proteins (**Figure 15**). Indeed, the observed phenotypes were comparable to those of the Aes transgenic line (**Figure 16** and **Table 13**). Closer inspection revealed that the Q domain is mainly responsible for the observed eye phenotypes (**Figure 17**). We selected Tle4 for the truncations which has been reported to interact with Six3 during eye development (Zhu *et al.*, 2002). Also, the morphological phenotypes were already visible at early stages, before the onset of *tle4* expression (**Figure 16**) which is relatively late in medaka (Lopez-Rios *et al.*, 2003; Bajoghli *et al.*, 2005). *In situ* hybridization experiments using *rx2* confirmed these early effects

(**Figure 20A-C**). Additional experiments showed a severe reduction in size of both the forebrain and the midbrain, as indicated by the expression patterns of *bf1* and *wnt1* (**Figure 20D-I**). Similar results have been reported for *bf1* in WRPW-induced Gro/TLE loss of function in *Xenopus* (Tsuji *et al.*, 2005). On the other hand, compared to the wild type control, the expression of *wnt1* seems diffuse and slightly stronger in the Aes/Q-induced Gro/TLE loss of function embryos (**Figure 20G-I**). Ectopic *wnt1* expression during early medaka development also causes anterior truncations (Appendix: (Bajoghli *et al.*, 2009)) which can be interpreted by a dose-dependent AP gradient (Kiecker *et al.*, 2001). Interestingly, ectopic expression of *wnt8* repressed the expression of *bf1* and high doses of the Wnt inhibitor Dickkopf had the opposite effect in *Xenopus* (Kiecker *et al.*, 2001). Anterior truncations have also been observed for *tcf3* loss of function in zebrafish, which is the most distal player in the Wnt/β-catenin signaling pathway (Behrens *et al.*, 1996; Kim, C. H. *et al.*, 2000; Dorsky *et al.*, 2003; Arce *et al.*, 2006). In addition, a rostral expansion of the MHB was observed in *hdl* mutants (Kim, C. H. *et al.*, 2000). A possible explanation could be that upon Aes/Q-induced Gro/TLE loss of function Tcf/Lef no longer acts as a repressor but instead switches to an activator, thereby promoting the expression of Wnt target genes.

We assumed that this dominant negative approach of Aes/Q-mediated loss of function targeted most or all Gro/TLE proteins expressed at the time. Therefore, the observed phenotypes may very well result from a combination of distinct effects. To be able to address individual *Gro/TLE* genes we applied morpholino oligonucleotides against *tle1*, *tle2b*, and *tle3b*. All three genes are expressed early in medaka development (Lopez-Rios *et al.*, 2003; Aghaallaei *et al.*, 2005), which is in agreement with the Aes/Q induction time. Careful comparison between the distinct *tle* genes revealed that the anterior expression pattern of *tle1* mainly overlaps with that of *six3* throughout the entire development. At stage 20 strong expression is detected in the fore- and midbrain, as well as in the optic vesicles and the MHB (Lopez-Rios *et al.*, 2003). *Tle2b* is first detected in the embryonic body during gastrulation. It then spreads into the optic vesicles, the midbrain and the MHB (Aghaallaei *et al.*, 2005). *Tle3b* is also detected in the embryonic body during late gastrulation (Aghaallaei *et al.*, 2005). However, compared to the two previous *tle* genes, at stage 21 it shows clearly defined stripes of expression in the midbrain, the MHB and the prospective neural retina (Lopez-Rios *et al.*, 2003; Aghaallaei *et al.*, 2005). We ignored the expression patterns posterior of the MHB because the phenotypes of the Aes/Q misexpression experiments were restricted to the anterior region. We therefore ruled out *tle2a* as a suitable candidate which is first expressed in the tailbud. Only at later stages anterior expression is detectable (Aghaallaei *et al.*, 2005). The late onset of *tle4* expression was discussed earlier in this chapter. Even if *tle3a* is expressed at early stages, the expression starts in the midbrain from where its spreads posteriorly (Lopez-Rios *et al.*, 2003).

The morphologic phenotype of the individual *tle* genes but also of the combinatorial knock downs was comparable. Differences occurred mainly in frequency and severity (**Figure 22** and **Table 15**). At first glance the phenotypes resembled those of the dominant negative experiments. We observed a clear reduction in eye size, cyclopic eyes as well as eye-less embryos (**Figure 22**). Closer inspection, however, showed differences. In Aes/Q-mediated loss of function the eyes tilted towards the midline at the anterior top where they fused to a cyclopic eye (**Figure 16**). In the knock down experiments, on the other hand, they fused ventrally of the forebrain at their anterior and posterior end, whereas the size reduction started anteriorly (**Figure 22**). Similar phenotypes were reported for

zebrafish *silberblick* mutants (Heisenberg *et al.*, 1997). The zebrafish *silberblick* locus encodes Wnt11 which mediates correct convergent extension movements during gastrulation (Heisenberg *et al.*, 1997; Heisenberg *et al.*, 2000). Cyclopia is caused by an impaired extension of the axial mesoderm and the overlying ventral CNS (Heisenberg *et al.*, 1997). Indeed, staging of the morpholino oligonucleotide injected embryos during gastrulation and neurulation turned out a rather challenging task. We considered the observed phenotype as an injection side effect.

However, regional specification of the anterior neural plate is in general strongly regulated by Wnt signaling. The canonical and non-canonical pathways are necessary to establish the forebrain and the eyes and they are regulated by different Wnt antagonists, such as Secreted Frizzled Related Proteins (SFRPs) (Esteve *et al.*, 2006). One member of the family, *sfrp1*, is broadly expressed throughout the anterior neural plate. Knock down of *sfrp1* in medaka embryos disrupted anterior neural plate patterning, followed by an abnormal morphology of the forebrain and a severe size reduction of the optic vesicles (Esteve *et al.*, 2004). Expression analysis of *goosecoid*, a marker that demarcates the anterior axial mesoderm (Schulte-Merker *et al.*, 1994), showed a shorter but wider domain (Esteve *et al.*, 2004). Interestingly, a reduction in eye size was also observed in Gro/TLE knock down phenotypes (**Figure 22**) and the expression domain of *goosecoid* was shortened (**Figure 24D**). The impaired extension of the axial mesoderm agrees with the phenotypes observed in *silberblick* mutants (Heisenberg *et al.*, 1997). Esteve *et al.* also noticed differences in length of the axial mesoderm which was not associated with an increase in apoptotic cell death. However, the expression of *wnt11* was unaffected by *sfrp1* knock down. Furthermore, they observed a strong decrease in the expression of optic markers, which is comparable to our results for *rx2* and *six3* and agrees with the reduction in eye size. In *sfrp1* loss of function embryos the telencephalic domain of *pax6* expression was expanded at the expenses of the eye domains (Esteve *et al.*, 2004). This clearly differed from our results. Although it seemed that the telencephalic domain is expanded as well, this might very well result from a cyclopic eye (**Figure 23D-F**). Also both the forebrain and especially the midbrain were clearly reduced in size (**Figure 23D-I**) which was not observed for the *sfrp1* knockdown (Esteve *et al.*, 2004). Furthermore, the expression patterns of *otx2* and *pax2* revealed a clear loss of anterior neural domains and an anterior shift of the MHB (**Figure 23G-I**). In contrast, Esteve *et al.* observed a possible anterior expansion of *otx2* but the position of the posterior expression did not change (Esteve *et al.*, 2004).

Taken together, the results show that the Q domain is mainly responsible for the observed eye phenotypes (**Figure 17**) and both Six3 and Tcf/Lef interact with it (Brantjes *et al.*, 2001; Zhu *et al.*, 2002; Lopez-Rios *et al.*, 2003; Daniels *et al.*, 2005). In our experiments we observed a morphologic phenotype that resembles *six3* loss of function (Carl *et al.*, 2002 and (Appendix: Dorn *et al.*, 2012). This is in good agreement with the findings that both Aes and Tle4 interact with Six3 (Zhu *et al.*, 2002; Lopez-Rios *et al.*, 2003). On the other hand, gene expression analysis showed a clear decrease in *bf1* and a possible increase in *wnt1* expression (**Figure 20D-I**) which may indicate a shift of the AP Wnt gradient.

The morphological phenotypes of actual medaka *tle* loss of function resemble that of zebrafish *silberblick* mutants. However, impaired extension of the axial mesoderm is also associated with *sfpr1* knock down. Indeed, we observed similar expression of marker genes in *Gro/TLE* loss of function in most cases (**Figure 23** and **Figure 24**). In *Xenopus*,

SFRP1 was shown to both bind and antagonize Wnt1 and Wnt8 but not Wnt11 (Leyns *et al.*, 1997; Lin, K. *et al.*, 1997; Wang, S. *et al.*, 1997a; Wang, S. *et al.*, 1997b). A loss of *sfrp1* function would therefore explain an expanded posterior neural fate. Also, the activity of the β-catenin-Tcf/Lef complex was associated with SFRP1 induction (Caldwell *et al.*, 2006). It therefore will be interesting to investigate if SFRP1 is connected to Gro/TLE in further experiments, as Gro/TLE proteins compete with β-catenin about Tcf/Lef binding (Daniels *et al.*, 2005).

4.2 Characterization and Analysis of Medaka Tcf3

The second part of this thesis developed primarily from the previous topic. Tcf3 is the most downstream interaction partner of Gro/TLEs in the Wnt/β-catenin signaling pathway (Brantjes *et al.*, 2001; Daniels *et al.*, 2005; Arce *et al.*, 2009). Knock down experiments in zebrafish showed eye phenotypes that had remarkable resemblance to those of *tle* knock down in medaka (Dorsky *et al.*, 2003). We therefore performed *tcf3* knock down experiments in medaka using both common morpholino oligonucleotides and novel pePNAs (Appendix, Paper Manuscript). In pePNAs phosphonic ester side chains are linked to an otherwise unmodified backbone which improves their properties considerably (Appendix: (Dorn *et al.*, 2012)). We tested both translational and splice pePNAs against medaka *tcf3* with further modified side chains (Appendix, Paper Manuscript). However, besides the sequence, little is known about medaka *tcf3* (Wang, D. *et al.*, 2011). An analysis of its morphologic and genotypic phenotype was therefore necessary.

In a database search, Wang *et al.* identified *tcf3* as one of seven pluripotency genes in the medaka genome. They showed that medaka has only a single *tcf3* gene, which is a homologe of the mammalian *tcf3/tcf7l1* gene. In phylogenetic analysis, Tcf3 clusters with the two known zebrafish proteins (Wang, D. *et al.*, 2011). Both the expression pattern and the loss of function phenotypes of *hdl* and *tcf3b*, the two zebrafish orthologs, have been studied extensively (Kim, C. H. *et al.*, 2000; Dorsky *et al.*, 2003) and we used their findings to compare them with medaka.

We used the sequence of Wang *et al.* to generate an *in situ* hybridization probe and monitored its expression pattern through several developmental stages (**Figure 26**). Comparison with the two zebrafish orthologs *hdl* and *tcf3b* (Dorsky *et al.*, 2003) showed an overlapping expression first in the embryonic shield and later on in the brain (**Figure 26**). This suggests that a single medaka *tcf3* gene undertakes the function of both *hdl* and *tcf3b*. Knock down experiments resulted in embryos with reduced eye size or complete loss of eyes (**Figure 28**). Resemblance with the zebrafish morphants seemed to be dose-dependent (**Figure 29**). We categorized embryos with smaller eyes as weak or moderate, which compares to the zebrafish *tcf3b* knockdown. Embryos with *hdl* loss of function were eye-less and resembled our strong phenotype (Dorsky *et al.*, 2003). Finally, we ensured the *tcf3* loss of function phenotype by analyzing marker gene expression in *tcf3* knock down medaka embryos (**Figure 31**) and comparing it to the results in zebrafish (Dorsky *et al.*, 2003).

Interestingly, as observed for *tle* loss of function (**Figure 24**), the expression domain of *pax6* was connected at the anterior top and there seemed to be more expression in the telecephalic region. Also the MHB was shifted anterior, which was indicated by the expression pattern of *pax2* and *gbx1* (**Figure 31B-D** and **Figure 31F-H**). In addition to the anterior shift, both pax2 and gbx1 showed an anterior expansion into the presumptive forebrain region (**Figure 31F-H**). Similar expression patterns for *gbx1* and *pax2* were observed in zebrafish embryos misexpressing either *wnt8* or *gbx1* respectively (Rhinn *et al.*, 2009) and for *nemo-like kinase* (*nlk*) gain of function (Thorpe *et al.*, 2004). Like in *hdl* knock down, *nlk* gain of function embryos have small or missing eyes and display forebrain defects. It seems that downregulation of Hdl increases Nlk levels, which in turn may negatively regulate the repression of posterior neural genes (Thorpe *et al.*, 2004). Under the influence of Wnt8, Nlk phosphorylates Tcf proteins of a Tcf/β-catenin complex and thereby inhibits their DNA-binding ability (Ishitani *et al.*, 1999; Thorpe *et al.*, 2004). Interestingly, *hdl/tcf3b* double morphants have elevated levels of Lef1. In contrast to Tcf3, Lef1 seems to have predominantly an activating function (Kengaku *et al.*, 1998; Merrill *et al.*, 2001). Dorsky *et al.* therefore suggested that *tcf* genes negatively regulate *lef1* expression (Dorsky *et al.*, 2003). Thorpe *et al.* complemented this theory by proposing a model where *nlk* is required for normal *lef1* expression and subsequent ventro-lateral mesoderm formation (Thorpe *et al.*, 2004). Interestingly, changes in Nkl levels had severe effects on the *silberblick* mutant. These changes were associated with a *wnt8* ORF2 (open reading frame) interaction of Nlk and non-canonical Wnt signaling. However, loss of function of *wnt8* ORF2 and a double knock down of *wnt11* and *nlk* enhanced the *silberblick* phenotype (Thorpe *et al.*, 2004).

To complete our analysis of medaka *tcf3*, we also performed gain of function experiments (**Figure 34**). Interestingly, the morphological phenotypes seemed to match those of loss of function experiments (**Figure 28**) and were greatly enhanced by loss of the GBS (**Figure 34**). However, gene expression analysis showed that the small eye phenotype in *tcf3* gain of function resembled more that of Aes/Q-induced loss of function phenotypes. The eyes seemed to shrink starting at the posterior end (**Figure 35I-L**), whereas the situation was vice versa in morpholino injected embryos (**Figure 35F-H**). Differences were also seen in the expression of *bf1*, which seemed to be normal in *tcf3* loss of function but was reduced in gain of function (**Figure 35G,K**) and in Aes/Q experiments (**Figure 20E,F**). Again, it will be interesting to see in further experiments if this correlates with an increase in posterior markers additionally to *wnt1* (**Figure 35L**). Interestingly, knock down of *tcf3* had no effect on the expression of *wnt1* in older embryos (**Figure 35H**), although the MHB was clearly shifted anteriorly during gastrulation (**Figure 31**).

Interestingly, several embryos misexpressing Tcf3 developed ectopic vesicles in the hindbrain and tail (**Figure 33**). However, multiple otic vesicles were only observed if Tcf3-Tle interaction was inhibited and seemed to be independent of CtBP binding. At first, this result seems to be in good agreement with our previous results. Given that Tcf3 has predominantly a repressing function and knockout experiments resulted in phenotypes that resembled ectopic *wnt* expression (Houston *et al.*, 2002; Merrill *et al.*, 2004), this would correlate with the observed anterior shift of the MHB and the possible increase in *wnt1* expression in *tcf3* inactivation and loss of Tcf3-Gro/TLE interaction ability, respectively (**Figure 20G-I, Figure 23D-I, Figure 24A-D, Figure 31, 22L**). Furthermore, in medaka the formation of ectopic vesicles has been shown in *wnt1* misexpression experiments (Appendix: (Bajoghli *et al.*, 2009)) and upon lithium induction (Appendix: (Jung *et al.*, 2013)). Additionally, both in zebrafish and medaka the induction of otic vesicles requires

a tight regulation of Pax8/2, Foxi1 and Dlx3/4 by Fgf and Bmp signaling (Aghaallaei *et al.*, 2007; Hans *et al.*, 2007). However, all these factors induce otic vesicles at the upper margin of the anterior neural plate, whereas our results show ectopic formation in the trunk (**Figure 33**), similar to those reported for *sox3* misexpression (Koster *et al.*, 2000). It will be interesting to analyze the connection between Tcf3, Gro/TLE and the different signaling pathways during otic development.

Taken together, in contrast to zebrafish, the medaka genome harbors only a single *tcf3* gene (Wang, D. *et al.*, 2011) that combines the function of both zebrafish orthologs. Interestingly, both knock down as well as gain of function experiments result in similar phenotypes which strongly resemble that of *Gro/TLE* loss of function (**Figure 30A-D**). In contrast, the Aes/Q-induced loss of function phenotype is slightly different (**Figure 30E**). It therefore seems to play an important role if Gro/TLE proteins are still present in the cell, only inhibited in their function or binding ability, or if they are not translated.

4.3 Electroporation Improves The Uptake of Small Molecules Into Medaka Embryos

The third part of this thesis originally started as a small side project but then developed into a complex subject. As a starting point, we wanted to introduce electroporation of nucleic acids as an alternative to microinjection for our laboratory on the basis of already established protocols (Hostetler *et al.*, 2003). Electroporation has a long history in the generation of transgenic fish (Inoue *et al.*, 1990; Hostetler *et al.*, 2003) and was recently improved by the technique of nanosecond pulsed electric fields (Tominaga *et al.*, 2010). In medaka developmental biology, however, microinjection is the standard technique to apply small molecules, such as DNA and RNA, into embryos. Reproducible experimental conditions are essential because phenotypes can only be qualified and statistically evaluated if the morphologic alterations are distinct and not caused by injection side effects. Generation of transgenic lines is one possibility to bypass this problem. Especially our heat-inducible HSE promoter allows misexpression of genes in a time-dependent manner (Bajoghli *et al.*, 2004). However, the generation of transgenic lines is time consuming before reasonable amounts of embryos can be used. Furthermore, as of today it is only applicable for gain of function experiments. In fish, the standard technique for loss of function experiments is the transient injection of morpholino oligonucleotides or PNAs. Both are synthetic antisense oligonucleotides that specifically bind complementary regions on a target mRNA (Nielsen *et al.*, 1991; Summerton, J., 1999; Summerton, James, 2003) and we recently tested modified PNAs against *six3* (Appendix: (Jung *et al.*, 2013)) and *tcf3* (Appendix, Paper Manuscript) in medaka embryonic development. However, in any case the amount of injected DNA, RNA or inhibitor molecule is important for the outcome of the experiments. Hence, reproducible results strongly depend on the amount of injected volume. Therefore, microinjection requires good training and long experience to acquire good skills and even then the outcome may vary. Taken together, electroporation would allow large scale transient experiments with defined conditions that could be performed by less experienced scientists and independent of the embryos developmental stage.

Already more than 20 years ago, electroporation was introduced as an alternative method to classical microinjection in medaka (Inoue *et al.*, 1990). Hostetler *et al.* adapted this approach and used a commercially available device that produced direct current-shifted radio frequency pulses. In our initial experiments we used a comparable electroporation device (Appendix: (Jung *et al.*, 2013), Methods) and the same settings and buffers for our experiments (Hostetler *et al.*, 2003). However, we failed to reproduce their results with both DNA (Fargas Madriles, 2011) and small FAM-labeled oligonucleotides (MW 6,000) (Friesenhengst, 2012). Due to the fact that only dechorionation improved the uptake, we reasoned that the chorion might be the main barrier that hinders the uptake into the embryo (Fargas Madriles, 2011). We therefore concentrated on the analysis of its characteristics.

Little is known about the diffusion properties of the rigid chorion and the membrane systems covering the embryo and the yolk. Nonetheless, fish embryos are getting more and more important as a model organism in common animal toxicology tests and the FET is discussed as an alternative to experiments with adult animals (Strahle *et al.*, 2012). Recently several ecotoxicological studies were performed on fish embryos that qualified the adverse effects of small molecules (e.g. pesticides, platinum) (Oxendine *et al.*, 2006; Osterauer *et al.*, 2008; Osterauer *et al.*, 2009; Scheil *et al.*, 2009; Modra *et al.*, 2011). Our experiments focused on the chorion's diffusion properties in the first place. We therefore selected mainly fluorescing substances (fluorescein, rhodamine B, acridine orange) but also added lithium chloride which is known to have severe adverse effects on zebrafish embryonic development (Stachel *et al.*, 1993). Fluorescing molecules allowed us to follow each embryo individually and to observe changes over time by simply using a fluorescence microscope. Also, repeated quantification of the signal intensities was possible and the internal distribution and metabolism (e.g. accumulation of fluorescein and acredine orange in the liver/gallbladder (Appendix (Jung *et al.*, 2013) Figure 1D, 6G) of the molecules could be examined. Depending on the physicochemical nature of the fluorescing substances and the developmental stage of the embryos, their distribution between the embryo and the yolk varied (Appendix (Jung *et al.*, 2013) Figure 1A-D, 6B-G). In toxicity testing, changes in the specific distribution between the different compartments, as seen after the incubation with detergents (**Figure 40**, **Figure 41**, **Figure 42**), is highly important to assess the pharmacokinetic properties of drugs.

We selected small molecules that cover a wide spectrum of different characteristics: from ionic lithium chloride to non-charged acridine orange. Microscopic analysis suggested differences in their hydrophobic properties, indicated by varying distributions within the egg. Rhodamine B, for example, was strongly enriched in the yolk (Appendix (Jung *et al.*, 2013) Figure 6B-D), whereas fluorescein was mainly detected in the embryo (Appendix (Jung *et al.*, 2013) Figure 1A-D). Nevertheless, they all share low diffusion rates into medaka embryos. Our fist hypothesis that the chorion is a diffusion barrier which protects the embryo from chemicals in their environment was strongly supported by suggestions from literature. Villalobos *et al.* tested the effects of an herbicide strongly associated with fish deaths in agricultural drains. They showed that toxicity was stage specific and that the chorion played a role in protecting the embryo (Villalobos *et al.*, 2000). The observed stage specificity was also in agreement with the changes in chorion hardness during early embryonic development. Upon sperm entry, a calcium wave moves along the surface and the chorion matures into a rigid structure (Gilkey *et al.*, 1978). Maximum rigidity is reached approximately six hours after fertilization (Yamagami, K. *et al.*, 1992). We therefore expected a dramatic drop of diffusion, and thereby fluorescein

uptake into the egg, after chorion hardening and an increase shortly before hatching. Although we could see a mild decrease in diffusion after six hours, the reduction was not as severe as expected (**Figure 38** and Appendix (Jung *et al.*, 2013) Figure 1). Observation throughout the entire embryonic development showed only small fluctuations in diffusion properties (Appendix (Jung *et al.*, 2013) Figure 1).

Changes in environmental factors have been reported to have an influence on chorion permeability. For example, calcium ions (Masuda *et al.*, 1991; Masuda *et al.*, 1992) and changes in the pH value (Iwamatsu, 1984) seem to affect the chorion permeability. However, incubation of the embryos with calcium-free medium right after fertilization (Iwamatsu *et al.*, 1995) had no effect on the uptake of small molecules (Friesenhengst, 2012). Neither had changing of pH values (Friesenhengst, 2012) or incubation in distilled water (**Figure 40** and **Figure 42D-F**). We therefore concluded that conditions affecting the chorion hardening process had no influence on the diffusion rates into the embryo and next tried dechorionation. However, dechorionation of living embryos is rather tricky and relatively time consuming. First hatching enzyme has to be purified from numerous embryos and then the chorion has to be digested in a couple of steps, which makes diffusion experiments at younger stages impossible. Moreover, dechorionated embryos are very fragile and susceptible to various bacterial and fungal infections. This makes pre-preparations, longer incubation times, changing between plates and cuvettes, and repeated washing steps a challenging task that needs long experience and steady hands. Anyway, dechorionation did not enhance the uptake of small molecules into the egg except for some experiments (Appendix (Jung *et al.*, 2013) Figure 2D-D',E), which most probably resulted from lesions in the membrane system surrounding the embryo (**Figure 39**). Instead we observed a rapid diffusion through the chorion into dead embryos where the embryo, including the surrounding membranes, shrinks to a small ball within the chorion (Appendix (Jung *et al.*, 2013) Figure 2C-C',E). It therefore rather seems that not the outer chorion but inner membrane systems surrounding the embryo and the yolk are the main diffusion barrier in medaka eggs. The first cell lineages of the embryo contain the pluripotent deep layer blastomeres (DEL), which produce the future embryo proper. The second domain is composed of a syncytium of multiple nuclei, called the yolk syncytial layer (YSL). The envelope layer (EVL) is the third domain. It is a thin cell layer which covers the DEL and will eventually form the periderm. Both the second and the third domain are extra-embryonic. According to our results, the EVL/periderm would be a candidate to block the diffusion into the embryo (Kimmel *et al.*, 1990). This theory was supported by the observation that the chorion allows both a fast in-diffusion, where the fluorescing molecules accumulated in the perivitelline space (Appendix (Jung *et al.*, 2013) Figure 2F-F"), and a fast out-diffusion (Appendix (Jung *et al.*, 2013) Figure 2G-H"). In contrast, in-diffusion of fluorescent signals from the perivitelline space into the embryo needed extensive time compared to the accumulation within the perivitelline space, but once achieved it stayed considerably longer (Appendix (Jung *et al.*, 2013) Figure 2F-H"). Hence, these results propose that diffusion into medaka embryos is a bi-phasic process; a fast step through the chorion and second slow step through embryonic membrane systems.

Assuming that the main diffusion barrier is not the acellular chorion but a membrane system, it should be possible to enhance the eggs permeability by adding detergents (reviewed by le Maire *et al.*, 2000). Indeed, addition of Triton X-100 considerably improved the uptake of fluorescein into the embryo (**Figure 41** and **Figure 42G-I**). However, this severely affected the embryo's membrane systems and thereby the internal

distribution between compartments (**Figure 42G-I**). Also injections directly into the yolk, a technique often used in zebrafish, turned out to be ineffective. Although fluorescein was evenly distributed in the yolk within 30 minutes, it took almost 4 hours until a relatively weak fluorescing signal became detectable in the embryo (Appendix (Jung *et al.*, 2013) Additional File 3). Furthermore, the rather sticky yolk of medaka embryos leads to rapid clogging of the injection needle which again reduces reproducibility.

Another possibility to transiently enhance the permeability of membranes is electroporation (Neumann, Eberhard *et al.*, 1972; Turnbull *et al.*, 1973; Neumann, E. *et al.*, 1982). We used current shifted radio frequency pulses (Hostetler *et al.*, 2003) and optimized the conditions for our medaka fish which derive from the Cab strain (Ishikawa, Yuji, 2000). Indeed, this method worked effectively for small molecules (Appendix (Jung *et al.*, 2013) Figure 5, (Hug, in preparation) and Figure 7), however, we failed to transfer DNA (Fargas Madriles, 2011). To increases the sensitivity of this assay, we used DNA expression constructs that contain both gfp and luciferase (Fargas Madriles, 2011). Closer inspection showed that not even FAM-labeled oligonucleotides (MW 6,000) could pass the chorion (Friesenhengst, 2012), which suggests a size exclusion of the chorion's pores in that range. Only after dechotionation we could detect fluorescent signals within the embryo. However, dechorionated embryos are very fragile and their survival is very low during electroporation, which makes this method inapplicable for routine experiments. Alternatively, the DNA could be injected first into the perivitelline space and subsequent electroporation would enable the transfer into the embryo. This is again time consuming and for younger stages direct injection into the zygote represents a simple and well established method.

Taken together, these results show that diffusion into the medaka embryo is a bi-phasic process (Appendix (Jung *et al.*, 2013) Figure 2A). Substances are enriched in the perivitelline space within a few minutes, followed by a slow diffusion step into the embryo that takes several hours. Electroporation can overcome this barrier and enhance the uptake of small molecules. Our observation of the bi-phasic diffusion process could have consequences for the future use of FET. They implicate that extended exposure to test substances is necessary to be able to evaluate the adverse effects on medaka embryonic development. Therefore, pharmacological and toxicologic effects will not be detectable in the first few hours of development without enhanced transfer. As an example that electroporation can enhance the uptake of chemicals we selected lithium chloride. The effects of lithium on embryonic development have been shown in several organisms. It inhibits GSK-3β, a key component of the Wnt signaling pathway (Klein *et al.*, 1996; Stambolic *et al.*, 1996) and upon exposure during gastrulation, embryos develop severe anterior truncations (reviewed by Kao *et al.*, 1998). Diffusion and subsequent electroporation of lithium induced similar deficiencies in AP development of medaka embryos and comparable phenotypes as observed for ectopic *wnt1* expression (Appendix (Bajoghli *et al.*, 2009) Figure 6B-D).

5 REFERENCES

ABED, M., BARRY, K. C., KENYAGIN, D., KOLTUN, B., PHIPPEN, T. M., DELROW, J. J., PARKHURST, S. M. and ORIAN, A. (2011). "Degringolade, a SUMO-targeted ubiquitin ligase, inhibits Hairy/Groucho-mediated repression." Embo J 30(7): 1289-1301.

ABERLE, H., BAUER, A., STAPPERT, J., KISPERT, A. and KEMLER, R. (1997). "beta-catenin is a target for the ubiquitin-proteasome pathway." Embo J 16(13): 3797-3804.

ADAMS, B., DORFLER, P., AGUZZI, A., KOZMIK, Z., URBANEK, P., MAURER-FOGY, I. and BUSSLINGER, M. (1992). "Pax-5 encodes the transcription factor BSAP and is expressed in B lymphocytes, the developing CNS, and adult testis." Genes Dev 6(9): 1589-1607.

AGHAALLAEI, N., BAJOGHLI, B. and CZERNY, T. (2007). "Distinct roles of Fgf8, Foxi1, Dlx3b and Pax8/2 during otic vesicle induction and maintenance in medaka." Dev Biol 307(2): 408-420.

AGHAALLAEI, N., BAJOGHLI, B., WALTER, I. and CZERNY, T. (2005). "Duplicated members of the Groucho/Tle gene family in fish." Dev Dyn 234(1): 143-150.

AIDA, T. (1921). "On the Inheritance of Color in a Fresh-Water Fish, APLOCHEILUS LATIPES Temmick and Schlegel, with Special Reference to Sex-Linked Inheritance." Genetics 6(6): 554-573.

ALLEN, T., VAN TUYL, M., IYENGAR, P., JOTHY, S., POST, M., TSAO, M. S. and LOBE, C. G. (2006). "Grg1 acts as a lung-specific oncogene in a transgenic mouse model." Cancer Res 66(3): 1294-1301.

ANDRIOLI, L. P., OBERSTEIN, A. L., CORADO, M. S., YU, D. and SMALL, S. (2004). "Groucho-dependent repression by sloppy-paired 1 differentially positions anterior pair-rule stripes in the Drosophila embryo." Dev Biol 276(2): 541-551.

ARCE, L., PATE, K. T. and WATERMAN, M. L. (2009). "Groucho binds two conserved regions of LEF-1 for HDAC-dependent repression." BMC Cancer 9: 159.

ARCE, L., YOKOYAMA, N. N. and WATERMAN, M. L. (2006). "Diversity of LEF/TCF action in development and disease." Oncogene 25(57): 7492-7504.

ARONSON, B. D., FISHER, A. L., BLECHMAN, K., CAUDY, M. and GERGEN, J. P. (1997). "Groucho-dependent and -independent repression activities of Runt domain proteins." Mol Cell Biol 17(9): 5581-5587.

ARTINGER, K. B., CHITNIS, A. B., MERCOLA, M. and DRIEVER, W. (1999). "Zebrafish narrowminded suggests a genetic link between formation of neural crest and primary sensory neurons." Development 126(18): 3969-3979.

ATCHA, F. A., SYED, A., WU, B., HOVERTER, N. P., YOKOYAMA, N. N., TING, J. H., MUNGUIA, J. E., MANGALAM, H. J., MARSH, J. L. and WATERMAN, M. L. (2007). "A unique DNA binding domain converts T-cell factors into strong Wnt effectors." Mol Cell Biol 27(23): 8352-8363.

BAJOGHLI, B. (2007). "Evolution of the Groucho/Tle gene family: gene organization and duplication events." Dev Genes Evol 217(8): 613-618.

BAJOGHLI, B., AGHAALLAEI, N. and CZERNY, T. (2005). "Groucho corepressor proteins regulate otic vesicle outgrowth." Dev Dyn 233(3): 760-771.

BAJOGHLI, B., AGHAALLAEI, N., HEIMBUCHER, T. and CZERNY, T. (2004). "An artificial promoter construct for heat-inducible misexpression during fish embryogenesis." Dev Biol 271(2): 416-430.

BAJOGHLI, B., AGHAALLAEI, N., JUNG, G. and CZERNY, T. (2009). "Induction of otic structures by canonical Wnt signalling in medaka." Dev Genes Evol 219(8): 391-398.

BAJOGHLI, B., AGHAALLAEI, N., SOROLDONI, D. and CZERNY, T. (2007). "The roles of Groucho/Tle in left-right asymmetry and Kupffer's vesicle organogenesis." Dev Biol 303(1): 347-361.

BAKER, N. E. (1987). "Molecular cloning of sequences from wingless, a segment polarity gene in Drosophila: the spatial distribution of a transcript in embryos." Embo J 6(6): 1765-1773.

BAROLO, S. and LEVINE, M. (1997). "hairy mediates dominant repression in the Drosophila embryo." Embo J 16(10): 2883-2891.

BAROLO, S., STONE, T., BANG, A. G. and POSAKONY, J. W. (2002). "Default repression and Notch signaling: Hairless acts as an adaptor to recruit the corepressors Groucho and dCtBP to Suppressor of Hairless." Genes Dev 16(15): 1964-1976.

BEAGLE, B. and JOHNSON, G. V. (2010a). "AES/GRG5: more than just a dominant-negative TLE/GRG family member." Dev Dyn 239(11): 2795-2805.

BEAGLE, B. and JOHNSON, G. V. (2010b). "Differential modulation of TCF/LEF-1 activity by the soluble LRP6-ICD." PLoS One 5(7): e11821.

BEHRENS, J., JERCHOW, B. A., WURTELE, M., GRIMM, J., ASBRAND, C., WIRTZ, R., KUHL, M., WEDLICH, D. and BIRCHMEIER, W. (1998). "Functional interaction of an axin homolog, conductin, with beta-catenin, APC, and GSK3beta." Science 280(5363): 596-599.

BEHRENS, J., VON KRIES, J. P., KUHL, M., BRUHN, L., WEDLICH, D., GROSSCHEDL, R. and BIRCHMEIER, W. (1996). "Functional interaction of beta-catenin with the transcription factor LEF-1." Nature 382(6592): 638-642.

BIRNEY, E., ANDREWS, T. D., BEVAN, P., CACCAMO, M., CHEN, Y., CLARKE, L., COATES, G., CUFF, J., CURWEN, V., CUTTS, T., DOWN, T., EYRAS, E., FERNANDEZ-SUAREZ, X. M., GANE, P., GIBBINS, B., GILBERT, J., HAMMOND, M., HOTZ, H. R., IYER, V., JEKOSCH, K., KAHARI, A., KASPRZYK, A., KEEFE, D., KEENAN, S., LEHVASLAIHO, H., MCVICKER, G., MELSOPP, C., MEIDL, P., MONGIN, E., PETTETT, R., POTTER, S., PROCTOR, G., RAE, M., SEARLE, S., SLATER, G., SMEDLEY, D., SMITH, J., SPOONER, W., STABENAU, A., STALKER, J., STOREY, R., URETA-VIDAL, A., WOODWARK, K. C., CAMERON, G., DURBIN, R., COX, A., HUBBARD, T. and CLAMP, M. (2004a). "An overview of Ensembl." Genome Res 14(5): 925-928.

BIRNEY, E., CLAMP, M. and DURBIN, R. (2004b). "GeneWise and Genomewise." Genome Res 14(5): 988-995.

BRANNON, M., BROWN, J. D., BATES, R., KIMELMAN, D. and MOON, R. T. (1999). "XCtBP is a XTcf-3 co-repressor with roles throughout Xenopus development." Development 126(14): 3159-3170.

BRANNON, M., GOMPERTS, M., SUMOY, L., MOON, R. T. and KIMELMAN, D. (1997). "A beta-catenin/XTcf-3 complex binds to the siamois promoter to regulate dorsal axis specification in Xenopus." Genes Dev 11(18): 2359-2370.

BRANTJES, H., ROOSE, J., VAN DE WETERING, M. and CLEVERS, H. (2001). "All Tcf HMG box transcription factors interact with Groucho-related co-repressors." Nucleic Acids Res 29(7): 1410-1419.

BRAUNBECK, T., BOETTCHER, M., HOLLERT, H., KOSMEHL, T., LAMMER, E., LEIST, E., RUDOLF, M. and SEITZ, N. (2005). "Towards an alternative for the acute fish LC(50) test in chemical assessment: the fish embryo toxicity test goes multi-species -- an update." ALTEX 22(2): 87-102.

BRUNNER, E., PETER, O., SCHWEIZER, L. and BASLER, K. (1997). "pangolin encodes a Lef-1 homologue that acts downstream of Armadillo to transduce the Wingless signal in Drosophila." Nature 385(6619): 829-833.

BUSCARLET, M., PERIN, A., LAING, A., BRICKMAN, J. M. and STIFANI, S. (2008). "Inhibition of cortical neuron differentiation by Groucho/TLE1 requires interaction with WRPW, but not Eh1, repressor peptides." J Biol Chem 283(36): 24881-24888.

BUSCARLET, M. and STIFANI, S. (2007). "The 'Marx' of Groucho on development and disease." Trends Cell Biol 17(7): 353-361.

CADIGAN, K. M. and PEIFER, M. (2009). "Wnt signaling from development to disease: insights from model systems." Cold Spring Harb Perspect Biol 1(2): a002881.

CAI, Y., BROPHY, P. D., LEVITAN, I., STIFANI, S. and DRESSLER, G. R. (2003). "Groucho suppresses Pax2 transactivation by inhibition of JNK-mediated phosphorylation." Embo J 22(20): 5522-5529.

CALDWELL, G. M., JONES, C. E., TANIERE, P., WARRACK, R., SOON, Y., MATTHEWS, G. M. and MORTON, D. G. (2006). "The Wnt antagonist sFRP1 is downregulated in premalignant large bowel adenomas." Br J Cancer 94(6): 922-927.

CAMERON, I. L. and HUNTER, K. E. (1984). "Regulation of the permeability of the medaka fish embryo chorion by exogeneous sodium and calcium ions." Journal of Experimental Zoology 231(3): 447-454.

CANON, J. and BANERJEE, U. (2003). "In vivo analysis of a developmental circuit for direct transcriptional activation and repression in the same cell by a Runx protein." Genes Dev 17(7): 838-843.

CARL, M., LOOSLI, F. and WITTBRODT, J. (2002). "Six3 inactivation reveals its essential role for the formation and patterning of the vertebrate eye." Development 129(17): 4057-4063.

CARVALHO, L. R., BRINKMEIER, M. L., CASTINETTI, F., ELLSWORTH, B. S. and CAMPER, S. A. (2010). "Corepressors TLE1 and TLE3 interact with HESX1 and PROP1." Mol Endocrinol 24(4): 754-765.

CASTILLA, L. H., WIJMENGA, C., WANG, Q., STACY, T., SPECK, N. A., ECKHAUS, M., MARIN-PADILLA, M., COLLINS, F. S., WYNSHAW-BORIS, A. and LIU, P. P. (1996). "Failure of embryonic hematopoiesis and lethal hemorrhages in mouse embryos heterozygous for a knocked-in leukemia gene CBFB-MYH11." Cell 87(4): 687-696.

CASTROP, J., VAN NORREN, K. and CLEVERS, H. (1992). "A gene family of HMG-box transcription factors with homology to TCF-1." Nucleic Acids Res 20(3): 611.

CAVALLO, R. A., COX, R. T., MOLINE, M. M., ROOSE, J., POLEVOY, G. A., CLEVERS, H., PEIFER, M. and BEJSOVEC, A. (1998). "Drosophila Tcf and Groucho interact to repress Wingless signalling activity." Nature 395(6702): 604-608.

CHEN, G. and COUREY, A. J. (2000). "Groucho/TLE family proteins and transcriptional repression." Gene 249(1-2): 1-16.

CHEN, G., FERNANDEZ, J., MISCHE, S. and COUREY, A. J. (1999). "A functional interaction between the histone deacetylase Rpd3 and the corepressor groucho in Drosophila development." Genes Dev 13(17): 2218-2230.

CHEN, G., NGUYEN, P. H. and COUREY, A. J. (1998). "A role for Groucho tetramerization in transcriptional repression." Mol Cell Biol 18(12): 7259-7268.

CHOI, C. Y., KIM, Y. H., KIM, Y. O., PARK, S. J., KIM, E. A., RIEMENSCHNEIDER, W., GAJEWSKI, K., SCHULZ, R. A. and KIM, Y. (2005). "Phosphorylation by the DHIPK2 protein kinase modulates the corepressor activity of Groucho." J Biol Chem 280(22): 21427-21436.

CHOI, C. Y., KIM, Y. H., KWON, H. J. and KIM, Y. (1999). "The homeodomain protein NK-3 recruits Groucho and a histone deacetylase complex to repress transcription." J Biol Chem 274(47): 33194-33197.

CINNAMON, E., HELMAN, A., BEN-HAROUSH SCHYR, R., ORIAN, A., JIMENEZ, G. and PAROUSH, Z. (2008a). "Multiple RTK pathways downregulate Groucho-mediated repression in Drosophila embryogenesis." Development 135(5): 829-837.

CINNAMON, E. and PAROUSH, Z. (2008b). "Context-dependent regulation of Groucho/TLE-mediated repression." Curr Opin Genet Dev 18(5): 435-440.

COLE, M. F., JOHNSTONE, S. E., NEWMAN, J. J., KAGEY, M. H. and YOUNG, R. A. (2008). "Tcf3 is an integral component of the core regulatory circuitry of embryonic stem cells." Genes Dev 22(6): 746-755.

COUNCIL, EU, (1986). Council Directive 86/609/EEC of 24 November 1986 on the approximation of laws, regulations and administrative provisions of the Member States regarding the protection of animals used for experimental and other scientific purposes. E. UNION. Official Journal L 358 , 18/12/1986. 31986L0609: 28.

COUREY, A. J. and JIA, S. (2001). "Transcriptional repression: the long and the short of it." Genes Dev 15(21): 2786-2796.

CROCE, J. C. and MCCLAY, D. R. (2008). "Evolution of the Wnt pathways." Methods Mol Biol 469: 3-18.

DANIELS, D. L. and WEIS, W. I. (2005). "Beta-catenin directly displaces Groucho/TLE repressors from Tcf/Lef in Wnt-mediated transcription activation." Nat Struct Mol Biol 12(4): 364-371.

DASEN, J. S., MARTINEZ BARBERA, J. P., HERMAN, T. S., CONNELL, S. O., OLSON, L., JU, B., TOLLKUHN, J., BAEK, S. H., ROSE, D. W. and ROSENFELD, M. G. (2001). "Temporal regulation of a paired-like homeodomain repressor/TLE corepressor complex and a related activator is required for pituitary organogenesis." Genes Dev 15(23): 3193-3207.

DE CELIS, J. F. and RUIZ-GOMEZ, M. (1995). "groucho and hedgehog regulate engrailed expression in the anterior compartment of the Drosophila wing." Development 121(10): 3467-3476.

DEHNI, G., LIU, Y., HUSAIN, J. and STIFANI, S. (1995). "TLE expression correlates with mouse embryonic segmentation, neurogenesis, and epithelial determination." Mech Dev 53(3): 369-381.

DELIDAKIS, C., PREISS, A., HARTLEY, D. A. and ARTAVANIS-TSAKONAS, S. (1991). "Two genetically and molecularly distinct functions involved in early neurogenesis reside within the Enhancer of split locus of Drosophila melanogaster." Genetics 129(3): 803-823.

DINTILHAC, A. and BERNUES, J. (2002). "HMGB1 interacts with many apparently unrelated proteins by recognizing short amino acid sequences." J Biol Chem 277(9): 7021-7028.

DORN, S., AGHAALLAEI, N., JUNG, G., BAJOGHLI, B., WERNER, B., BOCK, H., LINDHORST, T. and CZERNY, T. (2012). "Side chain modified peptide nucleic acids (PNA) for knock-down of six3 in medaka embryos." BMC Biotechnol 12: 50.

DORSKY, R. I., ITOH, M., MOON, R. T. and CHITNIS, A. (2003). "Two tcf3 genes cooperate to pattern the zebrafish brain." Development 130(9): 1937-1947.

DUCY, P., ZHANG, R., GEOFFROY, V., RIDALL, A. L. and KARSENTY, G. (1997). "Osf2/Cbfa1: a transcriptional activator of osteoblast differentiation." Cell 89(5): 747-754.

DUNKER, A. K., CORTESE, M. S., ROMERO, P., IAKOUCHEVA, L. M. and UVERSKY, V. N. (2005). "Flexible nets. The roles of intrinsic disorder in protein interaction networks." FEBS J 272(20): 5129-5148.

EBERHARD, D., JIMENEZ, G., HEAVEY, B. and BUSSLINGER, M. (2000). "Transcriptional repression by Pax5 (BSAP) through interaction with corepressors of the Groucho family." Embo J 19(10): 2292-2303.

EMBRY, M. R., BELANGER, S. E., BRAUNBECK, T. A., GALAY-BURGOS, M., HALDER, M., HINTON, D. E., LEONARD, M. A., LILLICRAP, A., NORBERG-KING, T. and WHALE, G. (2010). "The fish embryo toxicity test as an animal alternative method in hazard and risk assessment and scientific research." Aquat Toxicol 97(2): 79-87.

ESTEVE, P. and BOVOLENTA, P. (2006). "Secreted inducers in vertebrate eye development: more functions for old morphogens." Curr Opin Neurobiol 16(1): 13-19.

ESTEVE, P., LOPEZ-RIOS, J. and BOVOLENTA, P. (2004). "SFRP1 is required for the proper establishment of the eye field in the medaka fish." Mech Dev 121(7-8): 687-701.

FARGAS MADRILES, L. (2011). Gene transfer by electroporation into fish embryos. Bachelor Bachelor.

FINK, M., FLEKNA, G., LUDWIG, A., HEIMBUCHER, T. and CZERNY, T. (2006). "Improved translation efficiency of injected mRNA during early embryonic development." Dev Dyn 235(12): 3370-3378.

FISHER, A. L. and CAUDY, M. (1998). "Groucho proteins: transcriptional corepressors for specific subsets of DNA-binding transcription factors in vertebrates and invertebrates." Genes Dev 12(13): 1931-1940.

FISHER, A. L., OHSAKO, S. and CAUDY, M. (1996). "The WRPW motif of the hairy-related basic helix-loop-helix repressor proteins acts as a 4-amino-acid transcription repression and protein-protein interaction domain." Mol Cell Biol 16(6): 2670-2677.

FLORES-SAAIB, R. D. and COUREY, A. J. (2000). "Analysis of Groucho-histone interactions suggests mechanistic similarities between Groucho- and Tup1-mediated repression." Nucleic Acids Res 28(21): 4189-4196.

FONG, H. K., HURLEY, J. B., HOPKINS, R. S., MIAKE-LYE, R., JOHNSON, M. S., DOOLITTLE, R. F. and SIMON, M. I. (1986). "Repetitive segmental structure of the transducin beta subunit: homology with the CDC4 gene and identification of related mRNAs." Proc Natl Acad Sci U S A 83(7): 2162-2166.

FRAGA, M. F., BERDASCO, M., BALLESTAR, E., ROPERO, S., LOPEZ-NIEVA, P., LOPEZ-SERRA, L., MARTIN-SUBERO, J. I., CALASANZ, M. J., LOPEZ DE SILANES, I., SETIEN, F., CASADO, S., FERNANDEZ, A. F., SIEBERT, R., STIFANI, S. and ESTELLER, M. (2008). "Epigenetic inactivation of the Groucho homologue gene TLE1 in hematologic malignancies." Cancer Res 68(11): 4116-4122.

FRIESENHENGST, A. (2012). Electroporation of Medaka Embryos. BSc Bachelor, FH Campus Wien.

GAO, X., CHANDRA, T., GRATTON, M. O., QUELO, I., PRUD'HOMME, J., STIFANI, S. and ST-ARNAUD, R. (2001). "HES6 acts as a transcriptional repressor in myoblasts and can induce the myogenic differentiation program." J Cell Biol 154(6): 1161-1171.

GASPEROWICZ, M. and OTTO, F. (2005). "Mammalian Groucho homologs: redundancy or specificity?" J Cell Biochem 95(4): 670-687.

GIESE, K., COX, J. and GROSSCHEDL, R. (1992). "The HMG domain of lymphoid enhancer factor 1 bends DNA and facilitates assembly of functional nucleoprotein structures." Cell 69(1): 185-195.

GILKEY, J. C., JAFFE, L. F., RIDGWAY, E. B. and REYNOLDS, G. T. (1978). "A free calcium wave traverses the activating egg of the medaka, Oryzias latipes." The Journal of Cell Biology 76(2): 448-466.

GOLDSTEIN, R. E., JIMENEZ, G., COOK, O., GUR, D. and PAROUSH, Z. (1999). "Huckebein repressor activity in Drosophila terminal patterning is mediated by Groucho." Development 126(17): 3747-3755.

GRADL, D., KONIG, A. and WEDLICH, D. (2002). "Functional diversity of Xenopus lymphoid enhancer factor/T-cell factor transcription factors relies on combinations of activating and repressing elements." J Biol Chem 277(16): 14159-14171.

GRBAVEC, D., LO, R., LIU, Y. and STIFANI, S. (1998). "Transducin-like Enhancer of split 2, a mammalian homologue of Drosophila Groucho, acts as a transcriptional repressor, interacts with Hairy/Enhancer of split proteins, and is expressed during neuronal development." Eur J Biochem 258(2): 339-349.

GRBAVEC, D. and STIFANI, S. (1996). "Molecular interaction between TLE1 and the carboxyl-terminal domain of HES-1 containing the WRPW motif." Biochem Biophys Res Commun 223(3): 701-705.

GROMOLLER, A. and LEHMING, N. (2000). "Srb7p is a physical and physiological target of Tup1p." Embo J 19(24): 6845-6852.

GUO, W. H., WENG, L. Q., ITO, K., CHEN, L. F., NAKANISHI, H., TATEMATSU, M. and ITO, Y. (2002). "Inhibition of growth of mouse gastric cancer cells by Runx3, a novel tumor suppressor." Oncogene 21(54): 8351-8355.

GURUHARSHA, K. G., KANKEL, M. W. and ARTAVANIS-TSAKONAS, S. (2012). "The Notch signalling system: recent insights into the complexity of a conserved pathway." Nat Rev Genet 13(9): 654-666.

HA, C.-R. and IUCHI, I. (1997a). "Extraction and Partial Characterization of Egg Envelope (Chorion) Transglutaminase of Rainbow Trout, Oncorhynchus mykiss: Properties for Efficient Chorion Hardening." Comparative Biochemistry and Physiology Part B: Biochemistry and Molecular Biology 118(2): 293-301.

HA, C.-R. and IUCHI, I. (1997b). "Purification and partial characterization of 76 kDa transglutaminase in the egg envelope (chorion) of rainbow trout, Oncorhynchus mykiss." J Biochem 122(5): 947-954.

HA, C.-R. and IUCHI, I. (1998). "Enzyme responsible for egg envelope (chorion) hardening in fish: purification and partial characterization of two transglutaminases associated with their substrate, unfertilized egg chorion, of the rainbow trout, Oncorhynchus mykiss." J Biochem 124(5): 917-926.

HAGENMAIER, H. E., SCHMITZ, I. and FOHLES, J. (1976). "[On the occurence of isopeptide bonds in the chorion of the rainbow trout (Salmo gairdneri Rich.) (author's transl)]." Hoppe Seylers Z Physiol Chem 357(10): 1435-1438.

HAMAZAKI, T. S., IUCHI, I. and YAMAGAMI, K. (1987). "Isolation and partial characterization of a “spawning female-specific substance” in the teleost, Oryzias latipes." Journal of Experimental Zoology 242(3): 343-349.

HAMM, H. E. (1998). "The many faces of G protein signaling." J Biol Chem 273(2): 669-672.

HANS, S., CHRISTISON, J., LIU, D. and WESTERFIELD, M. (2007). "Fgf-dependent otic induction requires competence provided by Foxi1 and Dlx3b." BMC Dev Biol 7: 5.

HARTLEY, D. A., PREISS, A. and ARTAVANIS-TSAKONAS, S. (1988). "A deduced gene product from the Drosophila neurogenic locus, enhancer of split, shows homology to mammalian G-protein beta subunit." Cell 55(5): 785-795.

HASSON, P., MULLER, B., BASLER, K. and PAROUSH, Z. (2001). "Brinker requires two corepressors for maximal and versatile repression in Dpp signalling." Embo J 20(20): 5725-5736.

HAWKINS, W. E., OVERSTREET, R. M., FOURNIE, J. W. and WALKER, W. W. (1985). "Development of aquarium fish models for environmental carcinogenesis: tumor induction in seven species." J Appl Toxicol 5(4): 261-264.

HEIMBUCHER, T., MURKO, C., BAJOGHLI, B., AGHAALLAEI, N., HUBER, A., STEBEGG, R., EBERHARD, D., FINK, M., SIMEONE, A. and CZERNY, T. (2007). "Gbx2 and Otx2 interact with the WD40 domain of Groucho/Tle corepressors." Mol Cell Biol 27(1): 340-351.

HEISENBERG, C. P. and NUSSLEIN-VOLHARD, C. (1997). "The function of silberblick in the positioning of the eye anlage in the zebrafish embryo." Dev Biol 184(1): 85-94.

HEISENBERG, C. P., TADA, M., RAUCH, G. J., SAUDE, L., CONCHA, M. L., GEISLER, R., STEMPLE, D. L., SMITH, J. C. and WILSON, S. W. (2000). "Silberblick/Wnt11 mediates convergent extension movements during zebrafish gastrulation." Nature 405(6782): 76-81.

HENDERSON, B. R. and FAGOTTO, F. (2002). "The ins and outs of APC and beta-catenin nuclear transport." EMBO Rep 3(9): 834-839.

HOSTETLER, H. A., PECK, S. L. and MUIR, W. M. (2003). "High efficiency production of germ-line transgenic Japanese medaka (Oryzias latipes) by electroporation with direct current-shifted radio frequency pulses." Transgenic Res 12(4): 413-424.

HOUSTON, D. W., KOFRON, M., RESNIK, E., LANGLAND, R., DESTREE, O., WYLIE, C. and HEASMAN, J. (2002). "Repression of organizer genes in dorsal and ventral Xenopus cells mediated by maternal XTcf3." Development 129(17): 4015-4025.

HUG, M. (in preparation). --- in preparation ---. MSc Master, Universität für Bodenkultur Wien.

HUSAIN, J., LO, R., GRBAVEC, D. and STIFANI, S. (1996). "Affinity for the nuclear compartment and expression during cell differentiation implicate phosphorylated Groucho/TLE1 forms of higher molecular mass in nuclear functions." Biochem J 317 (Pt 2): 523-531.

IMAI, Y., KUROKAWA, M., TANAKA, K., FRIEDMAN, A. D., OGAWA, S., MITANI, K., YAZAKI, Y. and HIRAI, H. (1998). "TLE, the human homolog of groucho, interacts with AML1 and acts as a repressor of AML1-induced transactivation." Biochem Biophys Res Commun 252(3): 582-589.

INADA, M., YASUI, T., NOMURA, S., MIYAKE, S., DEGUCHI, K., HIMENO, M., SATO, M., YAMAGIWA, H., KIMURA, T., YASUI, N., OCHI, T., ENDO, N., KITAMURA, Y., KISHIMOTO, T. and KOMORI, T. (1999). "Maturational disturbance of chondrocytes in Cbfa1-deficient mice." Dev Dyn 214(4): 279-290.

INOHAYA, K., YASUMASU, S., ISHIMARU, M., OHYAMA, A., IUCHI, I. and YAMAGAMI, K. (1995). "Temporal and Spatial Patterns of Gene Expression for the Hatching Enzyme in the Teleost Embryo, Oryzias latipes." Dev Biol 171(2): 374-385.

INOUE, K., OZAKI, S., SHIGA, T., ITO, K., MASUDA, T., OKADO, N., ISEDA, T., KAWAGUCHI, S., OGAWA, M., BAE, S. C., YAMASHITA, N., ITOHARA, S., KUDO, N. and ITO, Y. (2002). "Runx3 controls the axonal projection of proprioceptive dorsal root ganglion neurons." Nat Neurosci 5(10): 946-954.

INOUE, K., YAMASHITA, S., HATA, J., KABENO, S., ASADA, S., NAGAHISA, E. and FUJITA, T. (1990). "Electroporation as a new technique for producing transgenic fish." Cell Differ Dev 29(2): 123-128.

ISHIBASHI, M., ANG, S. L., SHIOTA, K., NAKANISHI, S., KAGEYAMA, R. and GUILLEMOT, F. (1995). "Targeted disruption of mammalian hairy and Enhancer of split homolog-1 (HES-1) leads to up-regulation of neural helix-loop-helix factors, premature neurogenesis, and severe neural tube defects." Genes Dev 9(24): 3136-3148.

ISHIBASHI, M., MORIYOSHI, K., SASAI, Y., SHIOTA, K., NAKANISHI, S. and KAGEYAMA, R. (1994). "Persistent expression of helix-loop-helix factor HES-1 prevents mammalian neural differentiation in the central nervous system." Embo J 13(8): 1799-1805.

ISHIKAWA, T., MASAHITO, P. and TAKAYAMA, S. (1984). "Usefulness of the medaka, Oryzias latipes, as a test animal: DNA repair processes in medaka exposed to carcinogens." Natl Cancer Inst Monogr 65: 35-43.

ISHIKAWA, T., SHIMAMINE, T. and TAKAYAMA, S. (1975). "Histologic and electron microscopy observations on diethylnitrosamine-induced hepatomas in small aquarium fish (Oryzias latipes)." J Natl Cancer Inst 55(4): 909-916.

ISHIKAWA, Y. (2000). "Medakafish as a model system for vertebrate developmental genetics." BioEssays 22(5): 487-495.

ISHITANI, T., NINOMIYA-TSUJI, J., NAGAI, S., NISHITA, M., MENEGHINI, M., BARKER, N., WATERMAN, M., BOWERMAN, B., CLEVERS, H., SHIBUYA, H. and MATSUMOTO, K. (1999). "The TAK1-NLK-MAPK-related pathway antagonizes signalling between beta-catenin and transcription factor TCF." Nature 399(6738): 798-802.

IWAMATSU, T. (1984). "Effects of pH on the Fertilization Response of the Medaka Egg." Development, Growth & Differentiation 26(6): 533-544.

IWAMATSU, T. (2004). "Stages of normal development in the medaka Oryzias latipes." Mech Dev 121(7-8): 605-618.

IWAMATSU, T., SHIBATA, Y. and KANIE, T. (1995). "Changes in chorion proteins induced by the exudate released from the egg cortex at the time of fertilization in the teleost, Oryzias latipes." Development, Growth & Differentiation 37(6): 747-759.

JAN, Y., MATTER, M., PAI, J. T., CHEN, Y. L., PILCH, J., KOMATSU, M., ONG, E., FUKUDA, M. and RUOSLAHTI, E. (2004). "A mitochondrial protein, Bit1, mediates apoptosis regulated by integrins and Groucho/TLE corepressors." Cell 116(5): 751-762.

JAVED, A., GUO, B., HIEBERT, S., CHOI, J. Y., GREEN, J., ZHAO, S. C., OSBORNE, M. A., STIFANI, S., STEIN, J. L., LIAN, J. B., VAN WIJNEN, A. J. and STEIN, G. S. (2000). "Groucho/TLE/R-esp proteins associate with the nuclear matrix and repress RUNX (CBF(alpha)/AML/PEBP2(alpha)) dependent activation of tissue-specific gene transcription." J Cell Sci 113 (Pt 12): 2221-2231.

JENNINGS, B. H. and ISH-HOROWICZ, D. (2008a). "The Groucho/TLE/Grg family of transcriptional co-repressors." Genome Biol 9(1): 205.

JENNINGS, B. H., PICKLES, L. M., WAINWRIGHT, S. M., ROE, S. M., PEARL, L. H. and ISH-HOROWICZ, D. (2006). "Molecular recognition of transcriptional repressor motifs by the WD domain of the Groucho/TLE corepressor." Mol Cell 22(5): 645-655.

JENNINGS, B. H., WAINWRIGHT, S. M. and ISH-HOROWICZ, D. (2008b). "Differential in vivo requirements for oligomerization during Groucho-mediated repression." EMBO Rep 9(1): 76-83.

JIMENEZ, G., PAROUSH, Z. and ISH-HOROWICZ, D. (1997). "Groucho acts as a corepressor for a subset of negative regulators, including Hairy and Engrailed." Genes Dev 11(22): 3072-3082.

JORDAN, D. S. and SNYDER, J. O. (1906). "A review of the Poeciliidae or killifishes of Japan." Proceedings of the United States National Museum 31: 287-290.

JU, B. G., SOLUM, D., SONG, E. J., LEE, K. J., ROSE, D. W., GLASS, C. K. and ROSENFELD, M. G. (2004). "Activating the PARP-1 sensor component of the groucho/ TLE1 corepressor complex mediates a CaMKinase IIdelta-dependent neurogenic gene activation pathway." Cell 119(6): 815-829.

JUNG, G., HUG, M., HALTER, C., FRIESENHENGST, A., WALZER, J. and CZERNY, T. (2013). "Diffusion of small molecules into medaka embryos improved by electroporation." BMC Biotechnol 13: 53.

KAGEYAMA, R., OHTSUKA, T. and KOBAYASHI, T. (2007). "The Hes gene family: repressors and oscillators that orchestrate embryogenesis." Development 134(7): 1243-1251.

KAO, K. R. and ELINSON, R. P. (1998). "The legacy of lithium effects on development." Biol Cell 90(8): 585-589.

KASAHARA, M., NARUSE, K., SASAKI, S., NAKATANI, Y., QU, W., AHSAN, B., YAMADA, T., NAGAYASU, Y., DOI, K., KASAI, Y., JINDO, T., KOBAYASHI, D., SHIMADA, A., TOYODA, A., KUROKI, Y., FUJIYAMA, A., SASAKI, T., SHIMIZU, A., ASAKAWA, S., SHIMIZU, N., HASHIMOTO, S., YANG, J., LEE, Y., MATSUSHIMA, K., SUGANO, S., SAKAIZUMI, M., NARITA, T., OHISHI, K., HAGA, S., OHTA, F., NOMOTO, H., NOGATA, K., MORISHITA, T., ENDO, T., SHIN, I. T., TAKEDA, H., MORISHITA, S. and KOHARA, Y. (2007). "The medaka draft genome and insights into vertebrate genome evolution." Nature 447(7145): 714-719.

KAWAMURA, A., KOSHIDA, S., HIJIKATA, H., OHBAYASHI, A., KONDOH, H. and TAKADA, S. (2005). "Groucho-associated transcriptional repressor ripply1 is required for proper transition from the presomitic mesoderm to somites." Dev Cell 9(6): 735-744.

KENGAKU, M., CAPDEVILA, J., RODRIGUEZ-ESTEBAN, C., DE LA PENA, J., JOHNSON, R. L., IZPISUA BELMONTE, J. C. and TABIN, C. J. (1998). "Distinct WNT pathways regulating AER formation and dorsoventral polarity in the chick limb bud." Science 280(5367): 1274-1277.

KIECKER, C. and NIEHRS, C. (2001). "A morphogen gradient of Wnt/beta-catenin signalling regulates anteroposterior neural patterning in Xenopus." Development 128(21): 4189-4201.

KIM, C. H., ODA, T., ITOH, M., JIANG, D., ARTINGER, K. B., CHANDRASEKHARAPPA, S. C., DRIEVER, W. and CHITNIS, A. B. (2000). "Repressor activity of Headless/Tcf3 is essential for vertebrate head formation." Nature 407(6806): 913-916.

KIM, I. S., OTTO, F., ZABEL, B. and MUNDLOS, S. (1999). "Regulation of chondrocyte differentiation by Cbfa1." Mech Dev 80(2): 159-170.

KIM, W., KIM, M. and JHO, E. H. (2013). "Wnt/beta-catenin signalling: from plasma membrane to nucleus." Biochem J 450(1): 9-21.

KIMELMAN, D. and XU, W. (2006). "beta-catenin destruction complex: insights and questions from a structural perspective." Oncogene 25(57): 7482-7491.

KIMMEL, C. B., WARGA, R. M. and SCHILLING, T. F. (1990). "Origin and organization of the zebrafish fate map." Development 108(4): 581-594.

KISHIDA, S., YAMAMOTO, H., IKEDA, S., KISHIDA, M., SAKAMOTO, I., KOYAMA, S. and KIKUCHI, A. (1998). "Axin, a negative regulator of the wnt signaling pathway, directly interacts with adenomatous polyposis coli and regulates the stabilization of beta-catenin." J Biol Chem 273(18): 10823-10826.

KLEIN, P. S. and MELTON, D. A. (1996). "A molecular mechanism for the effect of lithium on development." Proc Natl Acad Sci U S A 93(16): 8455-8459.

KOMORI, T., YAGI, H., NOMURA, S., YAMAGUCHI, A., SASAKI, K., DEGUCHI, K., SHIMIZU, Y., BRONSON, R. T., GAO, Y. H., INADA, M., SATO, M., OKAMOTO, R., KITAMURA, Y., YOSHIKI, S. and KISHIMOTO, T. (1997). "Targeted disruption of Cbfa1 results in a complete lack of bone formation owing to maturational arrest of osteoblasts." Cell 89(5): 755-764.

KOOP, K. E., MACDONALD, L. M. and LOBE, C. G. (1996). "Transcripts of Grg4, a murine groucho-related gene, are detected in adjacent tissues to other murine neurogenic gene homologues during embryonic development." Mech Dev 59(1): 73-87.

KOSTER, R. W., KUHNLEIN, R. P. and WITTBRODT, J. (2000). "Ectopic Sox3 activity elicits sensory placode formation." Mech Dev 95(1-2): 175-187.

KUCHIN, S. and CARLSON, M. (1998). "Functional relationships of Srb10-Srb11 kinase, carboxy-terminal domain kinase CTDK-I, and transcriptional corepressor Ssn6-Tup1." Mol Cell Biol 18(3): 1163-1171.

LAMBRIGHT, D. G., SONDEK, J., BOHM, A., SKIBA, N. P., HAMM, H. E. and SIGLER, P. B. (1996). "The 2.0 A crystal structure of a heterotrimeric G protein." Nature 379(6563): 311-319.

LAMMER, E., CARR, G. J., WENDLER, K., RAWLINGS, J. M., BELANGER, S. E. and BRAUNBECK, T. (2009). "Is the fish embryo toxicity test (FET) with the zebrafish (Danio rerio) a potential alternative for the fish acute toxicity test?" Comp Biochem Physiol C Toxicol Pharmacol 149(2): 196-209.

LANGE, M., GEBAUER, W., MARKL, J. and NAGEL, R. (1995). "Comparison of testing acute toxicity on embryo of zebrafish, Brachydanio rerio and RTG-2 cytotoxicity as possible alternatives to the acute fish test." Chemosphere 30(11): 2087-2102.

LE MAIRE, M., CHAMPEIL, P. and MOLLER, J. V. (2000). "Interaction of membrane proteins and lipids with solubilizing detergents." Biochim Biophys Acta 1508(1-2): 86-111.

LEON, C. and LOBE, C. G. (1997). "Grg3, a murine Groucho-related gene, is expressed in the developing nervous system and in mesenchyme-induced epithelial structures." Dev Dyn 208(1): 11-24.

LEPOURCELET, M. and SHIVDASANI, R. A. (2002). "Characterization of a novel mammalian Groucho isoform and its role in transcriptional regulation." J Biol Chem 277(49): 47732-47740.

LEVANON, D., BETTOUN, D., HARRIS-CERRUTI, C., WOOLF, E., NEGREANU, V., EILAM, R., BERNSTEIN, Y., GOLDENBERG, D., XIAO, C., FLIEGAUF, M., KREMER, E., OTTO, F., BRENNER, O., LEV-TOV, A. and GRONER, Y. (2002). "The Runx3 transcription factor regulates development and survival of TrkC dorsal root ganglia neurons." Embo J 21(13): 3454-3463.

LEVANON, D., GOLDSTEIN, R. E., BERNSTEIN, Y., TANG, H., GOLDENBERG, D., STIFANI, S., PAROUSH, Z. and GRONER, Y. (1998). "Transcriptional repression by AML1 and LEF-1 is mediated by the TLE/Groucho corepressors." Proc Natl Acad Sci U S A 95(20): 11590-11595.

LEYNS, L., BOUWMEESTER, T., KIM, S. H., PICCOLO, S. and DE ROBERTIS, E. M. (1997). "Frzb-1 is a secreted antagonist of Wnt signaling expressed in the Spemann organizer." Cell 88(6): 747-756.

LI, Q. L., ITO, K., SAKAKURA, C., FUKAMACHI, H., INOUE, K., CHI, X. Z., LEE, K. Y., NOMURA, S., LEE, C. W., HAN, S. B., KIM, H. M., KIM, W. J., YAMAMOTO, H., YAMASHITA, N., YANO, T., IKEDA, T., ITOHARA, S., INAZAWA, J., ABE, T., HAGIWARA, A., YAMAGISHI, H., OOE, A., KANEDA, A., SUGIMURA, T., USHIJIMA, T., BAE, S. C. and ITO, Y. (2002). "Causal relationship between the loss of RUNX3 expression and gastric cancer." Cell 109(1): 113-124.

LI, S. S. (2000). "Structure and function of the Groucho gene family and encoded transcriptional corepressor proteins from human, mouse, rat, Xenopus, Drosophila and nematode." Proc Natl Sci Counc Repub China B 24(2): 47-55.

LILIENBLUM, W., DEKANT, W., FOTH, H., GEBEL, T., HENGSTLER, J. G., KAHL, R., KRAMER, P. J., SCHWEINFURTH, H. and WOLLIN, K. M. (2008). "Alternative methods to safety studies in experimental animals: role in the risk assessment of chemicals under the new European Chemicals Legislation (REACH)." Arch Toxicol 82(4): 211-236.

LIN, K., WANG, S., JULIUS, M. A., KITAJEWSKI, J., MOOS, M., JR. and LUYTEN, F. P. (1997). "The cysteine-rich frizzled domain of Frzb-1 is required and sufficient for modulation of Wnt signaling." Proc Natl Acad Sci U S A 94(21): 11196-11200.

LIN, R., THOMPSON, S. and PRIESS, J. R. (1995). "pop-1 encodes an HMG box protein required for the specification of a mesoderm precursor in early C. elegans embryos." Cell 83(4): 599-609.

LINDSLEY, D. L. and GRELL, E. H. (1968). Genetic variations of Drosophila melanogaster.

LIU, C., LI, Y., SEMENOV, M., HAN, C., BAEG, G. H., TAN, Y., ZHANG, Z., LIN, X. and HE, X. (2002). "Control of beta-catenin phosphorylation/degradation by a dual-kinase mechanism." Cell 108(6): 837-847.

LOGAN, C. Y. and NUSSE, R. (2004). "The Wnt signaling pathway in development and disease." Annu Rev Cell Dev Biol 20: 781-810.

LOPEZ-RIOS, J., TESSMAR, K., LOOSLI, F., WITTBRODT, J. and BOVOLENTA, P. (2003). "Six3 and Six6 activity is modulated by members of the groucho family." Development 130(1): 185-195.

LOVE, J. J., LI, X., CASE, D. A., GIESE, K., GROSSCHEDL, R. and WRIGHT, P. E. (1995). "Structural basis for DNA bending by the architectural transcription factor LEF-1." Nature 376(6543): 791-795.

MACDONALD, B. T., TAMAI, K. and HE, X. (2009). "Wnt/beta-catenin signaling: components, mechanisms, and diseases." Dev Cell 17(1): 9-26.

MALIK, S. and ROEDER, R. G. (2010). "The metazoan Mediator co-activator complex as an integrative hub for transcriptional regulation." Nat Rev Genet 11(11): 761-772.

MALLO, M., FRANCO DEL AMO, F. and GRIDLEY, T. (1993). "Cloning and developmental expression of Grg, a mouse gene related to the groucho transcript of the Drosophila Enhancer of split complex." Mech Dev 42(1-2): 67-76.

MALLO, M., GENDRON-MAGUIRE, M., HARBISON, M. L. and GRIDLEY, T. (1995). "Protein characterization and targeted disruption of Grg, a mouse gene related to the groucho transcript of the Drosophila Enhancer of split complex." Dev Dyn 204(3): 338-347.

MANNERVIK, M. and LEVINE, M. (1999). "The Rpd3 histone deacetylase is required for segmentation of the Drosophila embryo." Proc Natl Acad Sci U S A 96(12): 6797-6801.

MAO, C. D. and BYERS, S. W. (2011). "Cell-context dependent TCF/LEF expression and function: alternative tales of repression, de-repression and activation potentials." Crit Rev Eukaryot Gene Expr 21(3): 207-236.

MASAHITO, P., AOKI, K., EGAMI, N., ISHIKAWA, T. and SUGANO, H. (1989). "Life-span studies on spontaneous tumor development in the medaka (Oryzias latipes)." Jpn J Cancer Res 80(11): 1058-1065.

MASUDA, K., LUCHI, I. and YAMAGAMI, K. (1991). "Analysis of Hardening of the Egg Envelope (Chorion) of the Fish, Oryzias latipes." Development, Growth & Differentiation 33(1): 75-83.

MASUDA, K., MURATA, K., IUCHI, I. and YAMAGAMI, K. (1992). "Some Properties of the Hardening Process in Chorions Isolated from Unfertilized Eggs of Medaka, Oryzias latipes." Development, Growth & Differentiation 34(5): 545-551.

MATSUDA, M., NAGAHAMA, Y., SHINOMIYA, A., SATO, T., MATSUDA, C., KOBAYASHI, T., MORREY, C. E., SHIBATA, N., ASAKAWA, S., SHIMIZU, N., HORI, H., HAMAGUCHI, S. and SAKAIZUMI, M. (2002). "DMY is a Y-specific DM-domain gene required for male development in the medaka fish." Nature 417(6888): 559-563.

MATSUNAGA, E., KATAHIRA, T. and NAKAMURA, H. (2002). "Role of Lmx1b and Wnt1 in mesencephalon and metencephalon development." Development 129(22): 5269-5277.

MCLARREN, K. W., LO, R., GRBAVEC, D., THIRUNAVUKKARASU, K., KARSENTY, G. and STIFANI, S. (2000). "The mammalian basic helix loop helix protein HES-1 binds to and modulates the transactivating function of the runt-related factor Cbfa1." J Biol Chem 275(1): 530-538.

MCLARREN, K. W., THERIAULT, F. M. and STIFANI, S. (2001). "Association with the nuclear matrix and interaction with Groucho and RUNX proteins regulate the transcription repression activity of the basic helix loop helix factor Hes1." J Biol Chem 276(2): 1578-1584.

MERRILL, B. J., GAT, U., DASGUPTA, R. and FUCHS, E. (2001). "Tcf3 and Lef1 regulate lineage differentiation of multipotent stem cells in skin." Genes Dev 15(13): 1688-1705.

MERRILL, B. J., PASOLLI, H. A., POLAK, L., RENDL, M., GARCIA-GARCIA, M. J., ANDERSON, K. V. and FUCHS, E. (2004). "Tcf3: a transcriptional regulator of axis induction in the early embryo." Development 131(2): 263-274.

MILILI, M., GAUTHIER, L., VERAN, J., MATTEI, M. G. and SCHIFF, C. (2002). "A new Groucho TLE4 protein may regulate the repressive activity of Pax5 in human B lymphocytes." Immunology 106(4): 447-455.

MILLET, S., CAMPBELL, K., EPSTEIN, D. J., LOSOS, K., HARRIS, E. and JOYNER, A. L. (1999). "A role for Gbx2 in repression of Otx2 and positioning the mid/hindbrain organizer." Nature 401(6749): 161-164.

MIYASAKA, H., CHOUDHURY, B. K., HOU, E. W. and LI, S. S. (1993). "Molecular cloning and expression of mouse and human cDNA encoding AES and ESG proteins with strong similarity to Drosophila enhancer of split groucho protein." Eur J Biochem 216(1): 343-352.

MODRA, H., VRSKOVA, D., MACOVA, S., KOHOUTKOVA, J., HAJSLOVA, J., HALUZOVA, I. and SVOBODOVA, Z. (2011). "Comparison of diazinon toxicity to embryos of Xenopus laevis and Danio rerio; degradation of diazinon in water." Bull Environ Contam Toxicol 86(6): 601-604.

MOREL, V., LECOURTOIS, M., MASSIANI, O., MAIER, D., PREISS, A. and SCHWEISGUTH, F. (2001). "Transcriptional repression by suppressor of hairless involves the binding of a hairless-dCtBP complex in Drosophila." Curr Biol 11(10): 789-792.

MURATA, K., HAMAZAKI, T. S., IUCHI, I. and YAMAGAMI, K. (1991). "Spawning Female-Specific Egg Envelope Glycoprotein-Like Substances in Oryzias latipes." Development, Growth & Differentiation 33(6): 553-562.

MURATA, K., IUCHI, I. and YAMAGAMI, K. (1993). "Isolation of H-SF substances, the high-molecular-weight precursors of egg envelope proteins, from the ascites accumulated in the oestrogen-treated fish, Oryzias latipes." Zygote 1(4): 315-324.

MURATA, K., SASAKI, T., YASUMASU, S., IUCHI, I., ENAMI, J., YASUMASU, I. and YAMAGAMI, K. (1995). "Cloning of cDNAs for the precursor protein of a low-molecular-weight subunit of the inner layer of the egg envelope (chorion) of the fish Oryzias latipes." Dev Biol 167(1): 9-17.

MURATA, K., SUGIYAMA, H., YASUMASU, S., IUCHI, I., YASUMASU, I. and YAMAGAMI, K. (1997). "Cloning of cDNA and estrogen-induced hepatic gene expression for choriogenin H, a precursor protein of the fish egg envelope (chorion)." Proc Natl Acad Sci U S A 94(5): 2050-2055.

NAGEL, A. C., KREJCI, A., TENIN, G., BRAVO-PATINO, A., BRAY, S., MAIER, D. and PREISS, A. (2005). "Hairless-mediated repression of notch target genes requires the combined activity of Groucho and CtBP corepressors." Mol Cell Biol 25(23): 10433-10441.

NAGEL, R. (2002). "DarT: The embryo test with the Zebrafish Danio rerio--a general model in ecotoxicology and toxicology." ALTEX 19 Suppl 1: 38-48.

NAKANO, E. (1956). "CHANGES IN THE EGG MEMBRANE OF THE FISH EGG DURING FERTILIZATION." Embryologia 3(1): 89-103.

NANDA, I., KONDO, M., HORNUNG, U., ASAKAWA, S., WINKLER, C., SHIMIZU, A., SHAN, Z., HAAF, T., SHIMIZU, N., SHIMA, A., SCHMID, M. and SCHARTL, M. (2002). "A duplicated copy of DMRT1 in the sex-determining region of the Y chromosome of the medaka, Oryzias latipes." Proc Natl Acad Sci U S A 99(18): 11778-11783.

NARUSE, K., HORI, H., SHIMIZU, N., KOHARA, Y. and TAKEDA, H. (2004). "Medaka genomics: a bridge between mutant phenotype and gene function." Mech Dev 121(7-8): 619-628.

NEER, E. J., SCHMIDT, C. J., NAMBUDRIPAD, R. and SMITH, T. F. (1994). "The ancient regulatory-protein family of WD-repeat proteins." Nature 371(6495): 297-300.

NEER, E. J. and SMITH, T. F. (1996). "G protein heterodimers: new structures propel new questions." Cell 84(2): 175-178.

NEUMANN, E. and ROSENHECK, K. (1972). "Permeability changes induced by electric impulses in vesicular membranes." The Journal of Membrane Biology 10(1): 279-290.

NEUMANN, E., SCHAEFER-RIDDER, M., WANG, Y. and HOFSCHNEIDER, P. H. (1982). "Gene transfer into mouse lyoma cells by electroporation in high electric fields." Embo J 1(7): 841-845.

NIELSEN, P. E., EGHOLM, M., BERG, R. H. and BUCHARDT, O. (1991). "Sequence-selective recognition of DNA by strand displacement with a thymine-substituted polyamide." Science 254(5037): 1497-1500.

NUSSE, R. and VARMUS, H. E. (1982). "Many tumors induced by the mouse mammary tumor virus contain a provirus integrated in the same region of the host genome." Cell 31(1): 99-109.

NUTHALL, H. N., HUSAIN, J., MCLARREN, K. W. and STIFANI, S. (2002). "Role for Hes1-induced phosphorylation in Groucho-mediated transcriptional repression." Mol Cell Biol 22(2): 389-399.

NUTHALL, H. N., JOACHIM, K. and STIFANI, S. (2004). "Phosphorylation of serine 239 of Groucho/TLE1 by protein kinase CK2 is important for inhibition of neuronal differentiation." Mol Cell Biol 24(19): 8395-8407.

NUTT, S. L., HEAVEY, B., ROLINK, A. G. and BUSSLINGER, M. (1999). "Commitment to the B-lymphoid lineage depends on the transcription factor Pax5." Nature 401(6753): 556-562.

O'SHEA, E. K., LUMB, K. J. and KIM, P. S. (1993). "Peptide 'Velcro': design of a heterodimeric coiled coil." Curr Biol 3(10): 658-667.

OHTSUKA, E. (1960). "On the Hardening of the Chorion of the Fish Egg after Fertilization. III. The Mechanism of Chorion Hardening in Oryzias latipes." Biological Bulletin 118(1 (Feb., 1960)): 120-128.

OHTSUKA, T., ISHIBASHI, M., GRADWOHL, G., NAKANISHI, S., GUILLEMOT, F. and KAGEYAMA, R. (1999). "Hes1 and Hes5 as notch effectors in mammalian neuronal differentiation." Embo J 18(8): 2196-2207.

ORTNER, V., KASPAR, C., HALTER, C., TOLLNER, L., MYKHAYLYK, O., WALZER, J., GUNZBURG, W. H., DANGERFIELD, J. A., HOHENADL, C. and CZERNY, T. (2012). "Magnetic field-controlled gene expression in encapsulated cells." J Control Release 158(3): 424-432.

OSTERAUER, R., HAUS, N., SURES, B. and KOHLER, H. R. (2009). "Uptake of platinum by zebrafish (Danio rerio) and ramshorn snail (Marisa cornuarietis) and resulting effects on early embryogenesis." Chemosphere 77(7): 975-982.

OSTERAUER, R. and KOHLER, H. R. (2008). "Temperature-dependent effects of the pesticides thiacloprid and diazinon on the embryonic development of zebrafish (Danio rerio)." Aquat Toxicol 86(4): 485-494.

OTTO, F., THORNELL, A. P., CROMPTON, T., DENZEL, A., GILMOUR, K. C., ROSEWELL, I. R., STAMP, G. W., BEDDINGTON, R. S., MUNDLOS, S., OLSEN, B. R., SELBY, P. B. and OWEN, M. J. (1997). "Cbfa1, a candidate gene for cleidocranial dysplasia syndrome, is essential for osteoblast differentiation and bone development." Cell 89(5): 765-771.

OXENDINE, S. L., COWDEN, J., HINTON, D. E. and PADILLA, S. (2006). "Adapting the medaka embryo assay to a high-throughput approach for developmental toxicity testing." Neurotoxicology 27(5): 840-845.

PALAPARTI, A., BARATZ, A. and STIFANI, S. (1997). "The Groucho/transducin-like enhancer of split transcriptional repressors interact with the genetically defined amino-terminal silencing domain of histone H3." J Biol Chem 272(42): 26604-26610.

PAPAMICHOS-CHRONAKIS, M., CONLAN, R. S., GOUNALAKI, N., COPF, T. and TZAMARIAS, D. (2000). "Hrs1/Med3 is a Cyc8-Tup1 corepressor target in the RNA polymerase II holoenzyme." J Biol Chem 275(12): 8397-8403.

PARKHURST, S. M. (1998). "Groucho: making its Marx as a transcriptional co-repressor." Trends Genet 14(4): 130-132.

PAROUSH, Z., FINLEY, R. L., JR., KIDD, T., WAINWRIGHT, S. M., INGHAM, P. W., BRENT, R. and ISH-HOROWICZ, D. (1994). "Groucho is required for Drosophila neurogenesis, segmentation, and sex determination and interacts directly with hairy-related bHLH proteins." Cell 79(5): 805-815.

PAYANKAULAM, S. and ARNOSTI, D. N. (2009). "Groucho corepressor functions as a cofactor for the Knirps short-range transcriptional repressor." Proc Natl Acad Sci U S A 106(41): 17314-17319.

PEREIRA, L., YI, F. and MERRILL, B. J. (2006). "Repression of Nanog gene transcription by Tcf3 limits embryonic stem cell self-renewal." Mol Cell Biol 26(20): 7479-7491.

PETERSEN, C. P. and REDDIEN, P. W. (2009). "Wnt signaling and the polarity of the primary body axis." Cell 139(6): 1056-1068.

PFLUGRAD, A., MEIR, J. Y., BARNES, T. M. and MILLER, D. M., 3RD (1997). "The Groucho-like transcription factor UNC-37 functions with the neural specificity gene unc-4 to govern motor neuron identity in C. elegans." Development 124(9): 1699-1709.

PICKLES, L. M., ROE, S. M., HEMINGWAY, E. J., STIFANI, S. and PEARL, L. H. (2002). "Crystal structure of the C-terminal WD40 repeat domain of the human Groucho/TLE1 transcriptional corepressor." Structure 10(6): 751-761.

PINTO, M. and LOBE, C. G. (1996). "Products of the grg (Groucho-related gene) family can dimerize through the amino-terminal Q domain." J Biol Chem 271(51): 33026-33031.

POMERANTZ, J. L., SHARP, P. A. and PABO, C. O. (1995). "Structure-based design of transcription factors." Science 267(5194): 93-96.

QUACKENBUSH, J., CHO, J., LEE, D., LIANG, F., HOLT, I., KARAMYCHEVA, S., PARVIZI, B., PERTEA, G., SULTANA, R. and WHITE, J. (2001). "The TIGR Gene Indices: analysis of gene transcript sequences in highly sampled eukaryotic species." Nucleic Acids Res 29(1): 159-164.

REN, B., CHEE, K. J., KIM, T. H. and MANIATIS, T. (1999). "PRDI-BF1/Blimp-1 repression is mediated by corepressors of the Groucho family of proteins." Genes Dev 13(1): 125-137.

RHINN, M., LUN, K., AHRENDT, R., GEFFARTH, M. and BRAND, M. (2009). "Zebrafish gbx1 refines the midbrain-hindbrain boundary border and mediates the Wnt8 posteriorization signal." Neural Dev 4: 12.

RIDGWAY, E. B., GILKEY, J. C. and JAFFE, L. F. (1977). "Free calcium increases explosively in activating medaka eggs." Proc Natl Acad Sci U S A 74(2): 623-627.

RIJSEWIJK, F., SCHUERMANN, M., WAGENAAR, E., PARREN, P., WEIGEL, D. and NUSSE, R. (1987). "The Drosophila homolog of the mouse mammary oncogene int-1 is identical to the segment polarity gene wingless." Cell 50(4): 649-657.

ROOSE, J., MOLENAAR, M., PETERSON, J., HURENKAMP, J., BRANTJES, H., MOERER, P., VAN DE WETERING, M., DESTREE, O. and CLEVERS, H. (1998). "The Xenopus Wnt effector XTcf-3 interacts with Groucho-related transcriptional repressors." Nature 395(6702): 608-612.

SALOMONIS, N., SCHLIEVE, C. R., PEREIRA, L., WAHLQUIST, C., COLAS, A., ZAMBON, A. C., VRANIZAN, K., SPINDLER, M. J., PICO, A. R., CLINE, M. S., CLARK, T. A., WILLIAMS, A., BLUME, J. E., SAMAL, E., MERCOLA, M., MERRILL, B. J. and CONKLIN, B. R. (2010). "Alternative splicing regulates mouse embryonic stem cell pluripotency and differentiation." Proc Natl Acad Sci U S A 107(23): 10514-10519.

SASAI, Y., KAGEYAMA, R., TAGAWA, Y., SHIGEMOTO, R. and NAKANISHI, S. (1992). "Two mammalian helix-loop-helix factors structurally related to Drosophila hairy and Enhancer of split." Genes Dev 6(12B): 2620-2634.

SCHEIL, V., KIENLE, C., OSTERAUER, R., GERHARDT, A. and KOHLER, H. R. (2009). "Effects of 3,4-dichloroaniline and diazinon on different biological organisation levels of zebrafish (Danio rerio) embryos and larvae." Ecotoxicology 18(3): 355-363.

SCHIER, A. F. and TALBOT, W. S. (2005). "Molecular genetics of axis formation in zebrafish." Annu Rev Genet 39: 561-613.

SCHMIDT, C. J. and SLADEK, T. E. (1993). "A rat homolog of the Drosophila enhancer of split (groucho) locus lacking WD-40 repeats." J Biol Chem 268(34): 25681-25686.

SCHNEIDER, C. A., RASBAND, W. S. and ELICEIRI, K. W. "NIH Image to ImageJ: 25 years of image analysis." Nat Methods 9(7): 671-675.

SCHULTE-MERKER, S., HAMMERSCHMIDT, M., BEUCHLE, D., CHO, K. W., DE ROBERTIS, E. M. and NUSSLEIN-VOLHARD, C. (1994). "Expression of zebrafish goosecoid and no tail gene products in wild-type and mutant no tail embryos." Development 120(4): 843-852.

SCHWARZENBACH, R. P., ESCHER, B. I., FENNER, K., HOFSTETTER, T. B., JOHNSON, C. A., VON GUNTEN, U. and WEHRLI, B. (2006). "The challenge of micropollutants in aquatic systems." Science 313(5790): 1072-1077.

SCIALLI, A. R. (2008). "The challenge of reproductive and developmental toxicology under REACH." Regul Toxicol Pharmacol 51(2): 244-250.

SEKIYA, T. and ZARET, K. S. (2007). "Repression by Groucho/TLE/Grg proteins: genomic site recruitment generates compacted chromatin in vitro and impairs activator binding in vivo." Mol Cell 28(2): 291-303.

SHARMA, R. P. and CHOPRA, V. L. (1976). "Effect of the Wingless (wg1) mutation on wing and haltere development in Drosophila melanogaster." Dev Biol 48(2): 461-465.

SHIPP, M. A., ROSS, K. N., TAMAYO, P., WENG, A. P., KUTOK, J. L., AGUIAR, R. C., GAASENBEEK, M., ANGELO, M., REICH, M., PINKUS, G. S., RAY, T. S., KOVAL, M. A., LAST, K. W., NORTON, A., LISTER, T. A., MESIROV, J., NEUBERG, D. S., LANDER, E. S., ASTER, J. C. and GOLUB, T. R. (2002). "Diffuse large B-cell lymphoma outcome prediction by gene-expression profiling and supervised machine learning." Nat Med 8(1): 68-74.

SIERRA, J., YOSHIDA, T., JOAZEIRO, C. A. and JONES, K. A. (2006). "The APC tumor suppressor counteracts beta-catenin activation and H3K4 methylation at Wnt target genes." Genes Dev 20(5): 586-600.

SIEVERS, F., WILM, A., DINEEN, D., GIBSON, T. J., KARPLUS, K., LI, W., LOPEZ, R., MCWILLIAM, H., REMMERT, M., SODING, J., THOMPSON, J. D. and HIGGINS, D. G. (2011). "Fast, scalable generation of high-quality protein multiple sequence alignments using Clustal Omega." Mol Syst Biol 7.

SMITH, S. T. and JAYNES, J. B. (1996). "A conserved region of engrailed, shared among all en-, gsc-, Nk1-, Nk2- and msh-class homeoproteins, mediates active transcriptional repression in vivo." Development 122(10): 3141-3150.

SONDEK, J., BOHM, A., LAMBRIGHT, D. G., HAMM, H. E. and SIGLER, P. B. (1996). "Crystal structure of a G-protein beta gamma dimer at 2.1A resolution." Nature 379(6563): 369-374.

SONG, H., HASSON, P., PAROUSH, Z. and COUREY, A. J. (2004). "Groucho oligomerization is required for repression in vivo." Mol Cell Biol 24(10): 4341-4350.

STACHEL, S. E., GRUNWALD, D. J. and MYERS, P. Z. (1993). "Lithium perturbation and goosecoid expression identify a dorsal specification pathway in the pregastrula zebrafish." Development 117(4): 1261-1274.

STAMBOLIC, V., RUEL, L. and WOODGETT, J. R. (1996). "Lithium inhibits glycogen synthase kinase-3 activity and mimics wingless signalling in intact cells." Curr Biol 6(12): 1664-1668.

STAMOS, J. L. and WEIS, W. I. (2013). "The beta-catenin destruction complex." Cold Spring Harb Perspect Biol 5(1): a007898.

STIFANI, S., BLAUMUELLER, C. M., REDHEAD, N. J., HILL, R. E. and ARTAVANIS-TSAKONAS, S. (1992). "Human homologs of a Drosophila Enhancer of split gene product define a novel family of nuclear proteins." Nat Genet 2(2): 119-127.

STRAHLE, U., SCHOLZ, S., GEISLER, R., GREINER, P., HOLLERT, H., RASTEGAR, S., SCHUMACHER, A., SELDERSLAGHS, I., WEISS, C., WITTERS, H. and BRAUNBECK, T. (2012). "Zebrafish embryos as an alternative to animal experiments--a commentary on the definition of the onset of protected life stages in animal welfare regulations." Reprod Toxicol 33(2): 128-132.

STRAUSBERG, R. L., FEINGOLD, E. A., GROUSE, L. H., DERGE, J. G., KLAUSNER, R. D., COLLINS, F. S., WAGNER, L., SHENMEN, C. M., SCHULER, G. D., ALTSCHUL, S. F., ZEEBERG, B., BUETOW, K. H., SCHAEFER, C. F., BHAT, N. K., HOPKINS, R. F., JORDAN, H., MOORE, T., MAX, S. I., WANG, J., HSIEH, F., DIATCHENKO, L., MARUSINA, K., FARMER, A. A., RUBIN, G. M., HONG, L., STAPLETON, M., SOARES, M. B., BONALDO, M. F., CASAVANT, T. L., SCHEETZ, T. E., BROWNSTEIN, M. J., USDIN, T. B., TOSHIYUKI, S., CARNINCI, P., PRANGE, C., RAHA, S. S., LOQUELLANO, N. A., PETERS, G. J., ABRAMSON, R. D., MULLAHY, S. J., BOSAK, S. A., MCEWAN, P. J., MCKERNAN, K. J., MALEK, J. A., GUNARATNE, P. H., RICHARDS, S., WORLEY, K. C., HALE, S., GARCIA, A. M., GAY, L. J., HULYK, S. W., VILLALON, D. K., MUZNY, D. M., SODERGREN, E. J., LU, X., GIBBS, R. A., FAHEY, J., HELTON, E., KETTEMAN, M., MADAN, A., RODRIGUES, S., SANCHEZ, A., WHITING, M., MADAN, A., YOUNG, A. C.,

SHEVCHENKO, Y., BOUFFARD, G. G., BLAKESLEY, R. W., TOUCHMAN, J. W., GREEN, E. D., DICKSON, M. C., RODRIGUEZ, A. C., GRIMWOOD, J., SCHMUTZ, J., MYERS, R. M., BUTTERFIELD, Y. S., KRZYWINSKI, M. I., SKALSKA, U., SMAILUS, D. E., SCHNERCH, A., SCHEIN, J. E., JONES, S. J., MARRA, M. A. and MAMMALIAN GENE COLLECTION PROGRAM, T. (2002). "Generation and initial analysis of more than 15,000 full-length human and mouse cDNA sequences." Proc Natl Acad Sci U S A 99(26): 16899-16903.

STUART, E. T., HAFFNER, R., OREN, M. and GRUSS, P. (1995). "Loss of p53 function through PAX-mediated transcriptional repression." Embo J 14(22): 5638-5645.

SU, Y., FU, C., ISHIKAWA, S., STELLA, A., KOJIMA, M., SHITOH, K., SCHREIBER, E. M., DAY, B. W. and LIU, B. (2008). "APC is essential for targeting phosphorylated beta-catenin to the SCFbeta-TrCP ubiquitin ligase." Mol Cell 32(5): 652-661.

SUGIYAMA, H., YASUMASU, S., MURATA, K., IUCHI, I. and YAMAGAMI, K. (1998). "The third egg envelope subunit in fish: cDNA cloning and analysis, and gene expression." Dev Growth Differ 40(1): 35-45.

SUGIYAMA, S., FUNAHASHI, J. and NAKAMURA, H. (2000). "Antagonizing activity of chick Grg4 against tectum-organizing activity." Dev Biol 221(1): 168-180.

SUMMERTON, J. (1999). "Morpholino antisense oligomers: the case for an RNase H-independent structural type." Biochim Biophys Acta 1489(1): 141-158.

SUMMERTON, J. (2003). "Morpholinos and PNAs compared." International Journal of Peptide Research and Therapeutics 10(3): 215-236.

SUMMERTON, J. and WELLER, D. (1997). "Morpholino antisense oligomers: design, preparation, and properties." Antisense Nucleic Acid Drug Dev 7(3): 187-195.

SWINGLER, T. E., BESS, K. L., YAO, J., STIFANI, S. and JAYARAMAN, P. S. (2004). "The proline-rich homeodomain protein recruits members of the Groucho/Transducin-like enhancer of split protein family to co-repress transcription in hematopoietic cells." J Biol Chem 279(33): 34938-34947.

TAKACS, C. M., BAIRD, J. R., HUGHES, E. G., KENT, S. S., BENCHABANE, H., PAIK, R. and AHMED, Y. (2008). "Dual positive and negative regulation of wingless signaling by adenomatous polyposis coli." Science 319(5861): 333-336.

TETSUKA, T., URANISHI, H., IMAI, H., ONO, T., SONTA, S., TAKAHASHI, N., ASAMITSU, K. and OKAMOTO, T. (2000). "Inhibition of nuclear factor-kappaB-mediated transcription by association with the amino-terminal enhancer of split, a Groucho-related protein lacking WD40 repeats." J Biol Chem 275(6): 4383-4390.

THALER, B. (2010). Diffusion into Medaka Embryos. Bachelor Bachelor, FH Campus Wien.

THORPE, C. J. and MOON, R. T. (2004). "nemo-like kinase is an essential co-activator of Wnt signaling during early zebrafish development." Development 131(12): 2899-2909.

TOLKUNOVA, E. N., FUJIOKA, M., KOBAYASHI, M., DEKA, D. and JAYNES, J. B. (1998). "Two distinct types of repression domain in engrailed: one interacts with the groucho corepressor and is preferentially active on integrated target genes." Mol Cell Biol 18(5): 2804-2814.

TOMINAGA, N., KONO, S., YAMAGUCHI, A., AKIYAMA, H. and ARIZONO, K. (2010). "A novel material incorporation technique for medaka (Oryzias latipes) eggs using nanosecond pulsed electric fields." Biosci Biotechnol Biochem 74(6): 1279-1282.

TOUR, E., PILLEMER, G., GRUENBAUM, Y. and FAINSOD, A. (2002). "Gbx2 interacts with Otx2 and patterns the anterior-posterior axis during gastrulation in Xenopus." Mech Dev 112(1-2): 141-151.

TSUJI, S. and HASHIMOTO, C. (2005). "Choice of either beta-catenin or Groucho/TLE as a co-factor for Xtcf-3 determines dorsal-ventral cell fate of diencephalon during Xenopus development." Dev Genes Evol 215(6): 275-284.

TURKI-JUDEH, W. and COUREY, A. J. (2012). "The unconserved groucho central region is essential for viability and modulates target gene specificity." PLoS One 7(2): e30610.

TURNBULL, R., NEUMANN, E. and ROSENHECK, K. (1973). "An alternate explanation for the permeability changes induced by electrical impulses in vesicular membranes." The Journal of Membrane Biology 14(1): 193-196.

VAN BEEST, M., DOOIJES, D., VAN DE WETERING, M., KJAERULFF, S., BONVIN, A., NIELSEN, O. and CLEVERS, H. (2000). "Sequence-specific high mobility group box factors recognize 10-12-base pair minor groove motifs." J Biol Chem 275(35): 27266-27273.

VAN DE WETERING, M., OOSTERWEGEL, M., DOOIJES, D. and CLEVERS, H. (1991). "Identification and cloning of TCF-1, a T lymphocyte-specific transcription factor containing a sequence-specific HMG box." Embo J 10(1): 123-132.

VAN GENDEREN, C., OKAMURA, R. M., FARINAS, I., QUO, R. G., PARSLOW, T. G., BRUHN, L. and GROSSCHEDL, R. (1994). "Development of several organs that require inductive epithelial-mesenchymal interactions is impaired in LEF-1-deficient mice." Genes Dev 8(22): 2691-2703.

VAN OOYEN, A. and NUSSE, R. (1984). "Structure and nucleotide sequence of the putative mammary oncogene int-1; proviral insertions leave the protein-encoding domain intact." Cell 39(1): 233-240.

VILLALOBOS, S. A., HAMM, J. T., TEH, S. J. and HINTON, D. E. (2000). "Thiobencarb-induced embryotoxicity in medaka (Oryzias latipes): stage-specific toxicity and the protective role of chorion." Aquat Toxicol 48(2-3): 309-326.

WALL, M. A., COLEMAN, D. E., LEE, E., INIGUEZ-LLUHI, J. A., POSNER, B. A., GILMAN, A. G. and SPRANG, S. R. (1995). "The structure of the G protein heterotrimer Gi alpha 1 beta 1 gamma 2." Cell 83(6): 1047-1058.

WANG, D., MANALI, D., WANG, T., BHAT, N., HONG, N., LI, Z., WANG, L., YAN, Y., LIU, R. and HONG, Y. (2011). "Identification of pluripotency genes in the fish medaka." Int J Biol Sci 7(4): 440-451.

WANG, S., KRINKS, M., LIN, K., LUYTEN, F. P. and MOOS, M., JR. (1997a). "Frzb, a secreted protein expressed in the Spemann organizer, binds and inhibits Wnt-8." Cell 88(6): 757-766.

WANG, S., KRINKS, M. and MOOS, M., JR. (1997b). "Frzb-1, an antagonist of Wnt-1 and Wnt-8, does not block signaling by Wnts -3A, -5A, or -11." Biochem Biophys Res Commun 236(2): 502-504.

WATERMAN, M. L., FISCHER, W. H. and JONES, K. A. (1991). "A thymus-specific member of the HMG protein family regulates the human T cell receptor C alpha enhancer." Genes Dev 5(4): 656-669.

WINKLER, C. J., PONCE, A. and COUREY, A. J. (2010). "Groucho-mediated repression may result from a histone deacetylase-dependent increase in nucleosome density." PLoS One 5(4): e10166.

WITTBRODT, J., SHIMA, A. and SCHARTL, M. (2002). "Medaka--a model organism from the far East." Nat Rev Genet 3(1): 53-64.

XING, Y., CLEMENTS, W. K., KIMELMAN, D. and XU, W. (2003). "Crystal structure of a beta-catenin/axin complex suggests a mechanism for the beta-catenin destruction complex." Genes Dev 17(22): 2753-2764.

YAMAGAMI, K. (1972). "Isolation of a choriolytic enzyme (hatching enzyme) of the teleost, Oryzias latipes." Dev Biol 29(3): 343-348.

YAMAGAMI, K. (1973). "Some enzymological properties of a hatching enzyme (chorionase) isolated from the fresh-water teleost, Oryzias latipes." Comp Biochem Physiol B 46(3): 603-616.

YAMAGAMI, K. (1981). "Mechanisms of Hatching in Fish: Secretion of Hatching Enzyme and Enzymatic Choriolysis." American Zoologist 21(2): 459-471.

YAMAGAMI, K., HAMAZAKI, T. S., YASUMASU, S., MASUDA, K. and IUCHI, I. (1992). "Molecular and cellular basis of formation, hardening, and breakdown of the egg envelope in fish." Int Rev Cytol 136: 51-92.

YAMAMOTO, M. and YAMAGAMI, K. (1975). "Electron microscopic studies on choriolysis by the hatching enzyme of the teleost, Oryzias latipes." Dev Biol 43(2): 313-321.

YAMAMOTO, T. (1958). "Artificial induction of functional sex-reversal in genotypic females of the medaka (Oryzias latipes)." J Exp Zool 137(2): 227-263.

YAMAMOTO, T. (1975). Medaka (killifish): Biology and Strains, Yugaku-sha.

YANG, L., HO, N. Y., ALSHUT, R., LEGRADI, J., WEISS, C., REISCHL, M., MIKUT, R., LIEBEL, U., MULLER, F. and STRAHLE, U. (2009). "Zebrafish embryos as models for embryotoxic and teratological effects of chemicals." Reprod Toxicol 28(2): 245-253.

YAO, J., LAI, E. and STIFANI, S. (2001). "The winged-helix protein brain factor 1 interacts with groucho and hes proteins to repress transcription." Mol Cell Biol 21(6): 1962-1972.

YAO, J., LIU, Y., HUSAIN, J., LO, R., PALAPARTI, A., HENDERSON, J. and STIFANI, S. (1998). "Combinatorial expression patterns of individual TLE proteins during cell determination and differentiation suggest non-redundant functions for mammalian homologs of Drosophila Groucho." Dev Growth Differ 40(2): 133-146.

YAO, J., LIU, Y., LO, R., TRETJAKOFF, I., PETERSON, A. and STIFANI, S. (2000). "Disrupted development of the cerebral hemispheres in transgenic mice expressing the mammalian Groucho homologue transducin-like-enhancer of split 1 in postmitotic neurons." Mech Dev 93(1-2): 105-115.

YASUMASU, S., IUCHI, I. and YAMAGAMI, K. (1988). "Medaka hatching enzyme consists of two kinds of proteases which act cooperatively." Zoological Science 5: 191-195.

YASUMASU, S., IUCHI, I. and YAMAGAMI, K. (1989a). "Isolation and some properties of low choriolytic enzyme (LCE), a component of the hatching enzyme of the teleost, Oryzias latipes." J Biochem 105(2): 212-218.

YASUMASU, S., IUCHI, I. and YAMAGAMI, K. (1989b). "Purification and partial characterization of high choriolytic enzyme (HCE), a component of the hatching enzyme of the teleost, Oryzias latipes." J Biochem 105(2): 204-211.

YASUMASU, S., KATOW, S., UMINO, Y., IUCHI, I. and YAMAGAMI, K. (1989c). "A unique proteolytic action of HCE, a constituent protease of a fish hatching enzyme: tight binding to its natural substrate, egg envelope." Biochem Biophys Res Commun 162(1): 58-63.

YASUMASU, S., KAWAGUCHI, M., OUCHI, S., SANO, K., MURATA, K., SUGIYAMA, H., AKEMA, T. and IUCHI, I. (2010). "Mechanism of egg envelope digestion by hatching enzymes, HCE and LCE in medaka, Oryzias latipes." J Biochem 148(4): 439-448.

YU, X., LI, P., ROEDER, R. G. and WANG, Z. (2001). "Inhibition of androgen receptor-mediated transcription by amino-terminal enhancer of split." Mol Cell Biol 21(14): 4614-4625.

ZAMPARINI, A. L., WATTS, T., GARDNER, C. E., TOMLINSON, S. R., JOHNSTON, G. I. and BRICKMAN, J. M. (2006). "Hex acts with beta-catenin to regulate anteroposterior patterning via a Groucho-related co-repressor and Nodal." Development 133(18): 3709-3722.

ZHANG, H. and EMMONS, S. W. (2002). "Caenorhabditis elegans unc-37/groucho interacts genetically with components of the transcriptional mediator complex." Genetics 160(2): 799-803.

ZHANG, H. and LEVINE, M. (1999). "Groucho and dCtBP mediate separate pathways of transcriptional repression in the Drosophila embryo." Proc Natl Acad Sci U S A 96(2): 535-540.

ZHANG, H., LEVINE, M. and ASHE, H. L. (2001). "Brinker is a sequence-specific transcriptional repressor in the Drosophila embryo." Genes Dev 15(3): 261-266.

ZHANG, X., CHEN, H. M., JARAMILLO, E., WANG, L. and D'MELLO, S. R. (2008). "Histone deacetylase-related protein inhibits AES-mediated neuronal cell death by direct interaction." J Neurosci Res 86(11): 2423-2431.

ZHANG, Y., GAO, S. and WANG, Z. (2010). "Structural and functional analysis of amino-terminal enhancer of split in androgen-receptor-driven transcription." Biochem J 427(3): 499-511.

ZHU, C. C., DYER, M. A., UCHIKAWA, M., KONDOH, H., LAGUTIN, O. V. and OLIVER, G. (2002). "Six3-mediated auto repression and eye development requires its interaction with members of the Groucho-related family of co-repressors." Development 129(12): 2835-2849.

APPENDIX I: TLE PROTEIN SEQUENCES

TLE1

Genewise predicted protein sequences for medaka Tle1. Input sequences were human Tle1 protein (NP_005068.2) and the medaka genome sequence from the Ensembl genome browser (9 dna:chromosome chromosome:MEDAKA1:9:9839951:9958436:1).

```
MFPQGRHPTPHQAPGQPFKFTIPESLDRIKEEFQFLQAQYHSLKLECEKLASEKTEMQRH
YVMYYEMSYGLNIEMHKQTEIAKRLNTICAQVIPFLSQEHQQQVVQAVERAKQVTMAELN
AVIGQQHLSHNHGGAPVPLTPHPAGLHPSQLGGSAGLLALSGALGAIPPHLVGKDGDKKP
HLSGPDSHPAAAELLREREPGTSNSLLPESLRNSDKRRNGPDYQNDNKKRKVDDKDSSHY
LDGYKRHNHNEKTSGKxxxxFCGCSVGSCFAAWDTSSLPRENGLDKARLLKKDPSSPAST
ASSASSSSLKSKEMAMRDKAGTPGLKSSTPTPRGDSTPGPSSTPGIRPSLSKPSSMDIPH
PPTAGLRTPLAVPGPYPGAFGMLPHAAGMNGELAGAAGAAAYAAGLHNMSPQMSAAAAAA
VAAYGRSPMVGFDPHPHMRVPGMPPSLTGIPGGKPAYSFHVAADGQMQPVPFPPDALVGP
GIPRHARQINTLNHGEVVCAVTISNPTRHVYTGGKGCVKVWDISHPGNKSPVSQLDCLNR
DNYIRSCRLLPDGRTLIVGGEASTLSIWDLATPTPRIKAELTSSAPACYALAISPDSKVC
FSCCSDGNIAVWDLHNQTLVRQFQGHTDGASCIDISNDGTKLWTGGLDNTVRSWDLREGR
QLQQHDFTSQIFSLGYCPTGEWLAVGMESSNVEVLHVTKPDKYQLHLHESCVLSLQFAYC
GKWFVSTGKDNLLNAWRTPYGASIFQSKESSSVLSCDISVDDKYIVTGSGDKKATVYEVI
Y
```

TLE2b

Genewise predicted protein sequences for medaka Tle2b. Input sequences were human Tle2 protein (NP_003251.2) and the medaka genome sequence from the Ensembl genome browser (4 dna:chromosome chromosome:MEDAKA1:4:32247497:32372245:1).

```
QMRLASGTPQSLKLTYPETLDRIKEEFQFLQTQYHSLKLECEKLATEKTEIQRHYVMYYE
MSYGLNIEMHKQTEIAKRLNVICAQLIPFLSQEVGGRTQFMCLLAQHLSQHAQGLPMGPH
PSGLPHPSLALGGGSGLLALSGALGAQLAAKDERAHLEAAAAAAAAAASAAEHHRDSLRFC
LQDPSSPHSVQSYSSRENGLDKMPPSRKEGPPQASPTSLASSSSAASPSRGKEPPQVDRN
EVFHLLSRLPLQR*FVSILLDRFSSDTEDTPLFNHLPLDLFQREKSSTPGMKPGTPMSQD
SSTPGPSGPPQFRPVPGKPGVDPLALGLRNPLAVQGAYPPGAFGLPPPGVNGDLPGAAGY
GAGLHLVSPQMNGAAAAAAAAAAGYGRSPVVSLCRSLLCVPASLFEFSPPRLLLSAYSFH
VSADGQMQPVPFPPDALLGPGIPRHARQIHTLSHGEVVCAVTISTSTRHVYTGGKGCVKV
WDISQPGSKSPMAQLDCLNRDNYIRSCKLLSDGRTLIVGGEASTLSIWDLATPTPRIKAE
LTSSAPACYALAISPDNKVCFSCCSDGNIVVWDLHNQTLVRQFQGHTDGASCIDISNDGT
KLWTGGLDNTVRCWDLREGRQLQQHDFTSQIFSLGYCPTGEWLAVGMESSNVEVLHVSKP
DKYQLHLHESCVLSLKFAYCGKWFVSTGKDNLLNAWRTPYGSSIFQSKESSSVLSCDISP
DDQFIVTGSGDKKATVYEVIY
```

Genewise predicted protein sequences for medaka Tle2b N-terminus. Input sequences were human Tle2 protein (NP_003251.2) and the medaka genome sequence from EST clone TC132252 in the EST library of "The Computational Biology and Functional Genomics Laboratory" at the Dana-Faber Cancer Institute and Harvard School of Public Health (Quackenbush *et al.*, 2001). Matching amino acids are indicated in green.

MFPQNRPPAPLQPPPGSSASVVAAAAAAAAAASGTPQSLKLTYPETLDRIKEEFQFLQTQ
YHSLKLECEKLATEKTEIQRHYVMYYEMSYGLNIEMHK

TLE3a

Genewise predicted protein sequences for medaka Tle3b. Input sequences were human Tle3 protein (NP_005069.2) and the medaka genome sequence from the Ensembl genome browser (3 dna:chromosome chromosome:MEDAKA1:3:10658143:10786884:-1).

MYPQGRHPAPHQPGQPGFKFTVAESCDRIKDEFQFLQAQYHSLKVEYDKLANEKTEMQRH
YVMYYEMSYGLNIEMHKQTEIAKRLNAILAQIMPFLSQEHQQQVAQAVERAKQVTMTELN
AIIGQQQLQAQHLSHAAHGPPVQLPPHPSGLQPPGLPPVTGAGSGLLALGALGSQAHLPV
KDEKNHHDLEHRASRVCCSRQNNSVSPSDSLRAASEKHRSSSDYGLDSKKRKVDDKDSMS
RYDSDGDKSDDLVVDVSNEDPATPRVSPAHSPPENGLDKSRVLKKDAAPNSPASVASSGS
TPSSKAKDHAHNEKSSTPSLKSNTPTPRNEVPTPGTSTTPGLRPLTMGKPPGMEALTAPA
LRTPLSYASPFAMMGPHEMNGSLTSPGVYPGLISPQMSAAAAAAYGRSPIFPFIFPQAGF
DPHPHMRAPGLPAGLTSISGGKPAYSFHVSADGQMQPVPFPPDALIGPGIPRHARQINTL
SHGEVVCAVTISNPTRHVYTGGKGCVKIWDISQPGSKSPVSQLDCLNRDNYIRSCKLLPD
GRTLIVGGEASTLTIWDLASQTPRIKAELTSSAPACYALAISPDAKVCFSCCSDGNIAVW
DLHNQTLVRQFQGHTDGASCIDISHDGTKLWTGGLDNTVRSWDLREGRQLQQHDFTSQIF
SLGYCPTGEWLAVGMESSNVEVLHHTKPDKYQLHLHESCVLSLKFAYCGKWFVSTGKDNL
LNAWRTPYGASIFQSKESSSVLSCDISADDKYIVTGSGDKKATVYEVIY

APPENDIX II: SCIENTIFIC PUBLICATIONS

MANUSCRIPT FOR A PUBLICATION IN BMC BIOTECHNOLOGY:

The function of Tcf3 in medaka embryos: efficient knock down with pePNAs

Gerlinde Jung [1, *], Sebastian Dorn [1, *], Narges Aghaallaei [2], Baubak Bajoghli [3], Elisabeth Riegel [1], Holger Bock [4], Birgit Werner [4], Thomas Lindhorst [4] and Thomas Czerny [1 #]

[1)] Department for Applied Life Sciences
University of Applied Sciences,
FH Campus Wien,
Helmut-Qualtinger-Gasse 2, A-1030 Vienna, Austria

[2)] Current address:
.....
....., 69117-Heidelberg, Germany

[3)] Current address:
Director's Research Unit,
European Molecular Biology Laboratory (EMBL)
Meyerhofstrasse 1, 69117-Heidelberg, Germany

[4)] Ugichem GmbH
Mitterweg 24, A-6020 Innsbruck, Austria

* These authors contributed equally to this work

[#] Corresponding author: Thomas Czerny
Email: thomas.czerny@fh-campuswien.ac.at
Tel: +43 1 25077 5639
Fax: +43 1 25077 5693

ABSTRACT

Background:

The application of antisense molecules, such as morpholino oligonucleotides, is an efficient way of gene inactivation in vivo. We recently introduced phosphonic ester modified peptide nucleic acids (PNA) for in vivo loss-of-function experiments in medaka embryos. Here we tested novel modifications of the PNA backbone for knock down of the medaka tcf3 gene.

Results:

Unmodified PNAs bind RNA with high affinity and specificity, however, their knock down efficiency in vivo is below that of morpholino oligonucleotides. Introduction of side chains like phosphonic esters is a possible way to improve their properties. Here we show that k-side chains further enhance the efficiency of PNAs. As a target we selected the medaka tcf3 gene. In silico analysis together with gene expression and loss-of-function experiments demonstrate that a single tcf3 gene in medaka combines the function of two genes in zebrafish (hdl and tcf3b). Inactivation of tcf3 in medaka strongly affected eye development, leading to size reduction and anophthalmia in severe cases. Additional gain-of-function experiments allowed us to analyse the co-repressor dependency of this transcription factor. For eye development we found Gro/Tle proteins to be important. Overexpression of Tcf3 variants lacking the Gro/Tle interaction domain developed considerably lower numbers of eye phenotypes. The importance of Gro/Tle proteins was further supported by different gro/tle loss-of-function experiments which all resulted in eye phenotypes. For this we used a dominant negative approach for combined inactivation of all gro/tle genes or we performed knockdown experiments with individual, early expressed, tle genes.

Conclusion:

Our results show that side chain modified PNAs reach the knock down efficiency of morpholino oligonucleotides in vivo. A single medaka tcf3 combines the function of two zebrafish tcf3 genes. In combination with Gro/Tle corepressor proteins Tcf3 acts in anterior development and is critical for eye formation.

KEY WORDS

PNA, knock down, medaka, Tcf3, Groucho, Tle

INTRODUCTION

Antisense molecules which inhibit mRNA activity through a Watson-Crick base pair mechanism have been studied for several decades. Blocker molecules, such as morpholino oligonucleotides and Peptide Nucleic Acids (PNAs), show high specificity and low toxic effects (reviewed by Summerton et al. [1]). The morpholino backbone consists of 6-membered morpholine rings connected by non-ionic phosphorodiamidate linker-units [2]. In PNAs the phosphate ribose ring of DNA is replaced with repeating N-[2-aminoethyl]-glycine (aeg) units linked by amide bonds which provides a neutral backbone

and results in stronger binding affinity of complementary PNA/DNA strands than DNA/DNA [3]. In addition, introduction of mismatches destabilizes the PNA/DNA duplex more than that of DNA/DNA. PNAs are highly stable against enzymatic degradation and changes in temperature and pH. Due to their short length (13-18 bases) the likelihood of secondary structures is reduced which results in stable and sequence specific probes [4-6]. Nevertheless, unmodified aegPNAs show low efficiency in vivo, therefore various terminal- and internal modifications have been tested. For example, addition of lysine residues improves the solubility [7]. The introduction of negative charges in mixed sequence HypNA-PNAs allowed specific down regulation of target genes in zebrafish embryos [8]. Recently pePNAs, which contain phosphonic ester (pe) side chains in an otherwise non-modified aegPNA backbone, could be applied for successful targeting of six3 in medaka embryos. In particular combined versions containing both aeg non-modified- and pe modified PNA blocks worked best. In a direct comparison morpholino oligonucleotides were active at lower concentrations, but also showed higher toxicity [9].

Tcf/Lef (T-cell factor/ lymphoid enhancer factor) proteins belong to the high mobility group (HMG) box-containing family of transcription factors [10]. They are the most distal players of the Wnt pathway and the main partner for β-catenin in gene regulation [11, 12]. In the absence of Wnt ligands, β-catenin is degraded in the cytosol and Tcf/Lef interacts with transcriptional repressors such as Gro/Tle (Groucho/Transducin-like enhancer) and CtBP (C-terminus Binding Protein), thereby repressing target gene expression. Upon Wnt stimulation, β-catenin is stabilized and translocated to the nucleus. Nuclear accumulation leads to an interaction of β-catenin with Tcf/Lef which promotes specific gene expression [11].

In non-vertebrates transcriptional activation and repression is regulated by only a single tcf gene, for example pangolin for Drosophila and POP-1 for C. elegans, whereas vertebrates have four, more specialized and partly redundant homologues [11]. While Tcf1 and Tcf4 play a role in both activation and repression, Lef1 shows primarily activator abilities [13] and Tcf3 seems to function exclusively as a repressor [14]. In mice, tcf3 knockout experiments resulted in gastrulation defects that resemble ectopic Wnt expression like duplication of the AP axis. At later stages abundant neuroectodermal cells and defective neural patterning were observed [15]. In addition, Tcf3 seems to be a regulator of pluripotency. Under standard conditions embryonic stem (ES) cells show high levels of Tcf3 and only low Wnt pathway activity, thereby remaining in a balanced state between pluripotency and differentiation. If tcf3 is knocked down or Wnt genes are overexpressed the ES cells do not undergo efficient differentiation and the balance is tipped towards pluripotency [16, 17]. In zebrafish two tcf3 genes have been reported, headless hdl/tcf3 [18] and tcf3b [19], which both act as repressors. At shield stage hdl is broadly expressed in the epiblast while tcf3b shows only weak expression, whereas in late gastrulation both genes are expressed in the rostral neuroectoderm and later on throughout the brain with a gap of expression in the mid-hindbrain boundary (MHB) [19]. In hdl mutants the forebrain is lost while the expression of genes that characterize the MHB is expanded [18]. This phenotype can be rescued by tcf3b overexpression. tcf3b knock down results in smaller heads but otherwise normal brain patterning, whereas interference with both tcf3 genes leads to strong caudalization [19].

One mechanism of Tcf3-mediated repression, results from its interaction with Gro/Tle proteins [20-22]. The latter are transcriptional co-repressors that lack direct DNA binding ability. Instead they bind to DNA bound proteins and assist in repression (reviewed by

Turki-Judeh et al. [23]). In the case of Tcf3, Gro/Tle tetramers bind to an N-terminally located groucho interaction domain [24]. This interaction is disrupted by the Gro/Tle repressor Aes [21]. Aes is a truncated form of Gro/Tle consisting only of the N-terminal Q- and GP-domains [25, 26].

Here we analysed the function of tcf3 in medaka embryos using both gain- and loss-of-function experiments. For the knock down we used pePNAs and morpholino oligos. Novel side chain modifications further improved the activity of the PNAs, resulting in knock down efficiencies directly comparable to those of morpholino oligonucleotides. Furthermore, we analysed the effect of Gro/Tle proteins on the repressive function of Tcf3 by using a dominant negative approach and antisense oligonucleotides.

MATERIALS AND METHODS

PNA and morpholino oligonucleotide synthesis

PNA monomer building blocks are commercially available. Optical pure (R-configuration according to CIP rules) Ugi-PNA monomer building blocks were synthesized according to a route reported previously [7, 27, 28]. N2-Boc-N6, N6, N6-trimethyl-(L)-lysine iodide (TML) as building block was prepared as published by Chen and Benoiton [29]. All PNAs were synthesized on a fully automated solid phase synthesizer (Multisynthec Syro) according to a protocol developed by Koch [30]. The PNAs were dissolved in nuclease free water by repeatedly shaking and vortexting. Finally they were gently sonicated for 2 minutes with repeated pulses. Subsequently the PNAs were divided into aliquots of 100 µl (2 mM final concentration) and kept at -80°C.

Morpholino oligonucleotides were designed according to the manufacturer's protocol and synthesized by Gene Tools, LLC. Morpholino sequences for the tle genes in 5'-3' direction: Tle1, CGCGTCTTGTCCTGAAACCCCGCTA; Tle2b, GGCAGTGCGTCCTCGTGGCTCTTTC; Tle3a, CGGCCTTGTGGATACATGTCTCGTC.

DNA constructs

For cell culture experiments pMC [31] and pKC (polylinker modification of pKW) [32] were used (both vectors contain cytomegalovirus promoters). DNA constructs for microinjection were under the control of a bi-directional heat-inducible HSE promoter [33] and contain the mouse Aes/Grg5 cDNA, the mouse Tle4 Q domain, or various deletion fragments of human Tcf3 (see Figure 5 for details). pLucF24ZF; luciferase reporter under the control of a Fos minimal promoter and zinc finger binding sites. pMChSix3(85-203)mZFb6; the human Six3 fragment (positions of amino acids in brackets) fused to a zinc-finger DNA binding domain [34] and the "base" leucine-zipper [35]. pMCTle1VP16 and pMCGrg4VP16; human Tle1 and mouse Tle4 were fused to the transcriptional activation domain of the herpes simplex virus protein VP16, respectively. pMCamVP16 contains the "acid" leucine-zipper fused to VP16, pKCAes the mouse Aes/Grg5 cDNA.

Microinjection into medaka embryos

Embryos of the medaka Cab strain were used for all experiments. Adult fish were maintained at 26°C with an artificial 14 hours light and 10 hours dark cycle. Stages were determined according to Iwamatsu [36]. Loss of function injections with tcf3 and tle antisense molecules were performed using concentrations between 50 and 1200 µM PNAs or morpholino oligonucleotides. DNA injections were performed at the 1-cell stage together with meganuclease. For transient injections (HSE:Tcf3 constructs) the embryos were injected with 40ng/µl and for transgenic lines (HSE:AesATG and HSE:Q) with 10 ng/µl heat inducible promoter [33], respectively. Heat induction (10 minutes at 43.5°C) was performed at stage 14 (except if otherwise indicated). After injection the embryos were incubated at normal conditions (1x ERM buffer at 27°C).

Whole-mount in situ hybridization

Whole-mount in situ hybridization using DIG-labelled RNA probes was performed as described previously [37]. Probes against tcf3 and gbx1 were PCR amplified from medaka embryonic cDNA using specific primers for tcf3 (5'-CGGATCCATGGCTCAACTGAACGGAGGC-3' and 5'-CGAAGACGGCTGGACATGGATGCATTCA-3') and gbx1 (5'-TTAGAAAATACAGCCACAA-3' and 5'-TCACTGTAAAAAGTACCTG-3').

Cell culture

HeLa cells were transfected in polyethylenimine (2.5 µg/ml) coated 96-well plates [38] using TurboFect transfection reagent according to the instructions of the manufacturer (Thermo Scientific). For luciferase reporter assays, additional transfection of 2ng Gaussia luciferase expression vector pMCGlucS served as an internal reference. Luciferase activities were measured 24 hours after transfection.

RESULTS

Isolation and expression of the medaka tcf3 gene

In zebrafish two tcf3 genes exist (tcf3a or hdl and tcf3b), which fulfil overlapping functions [19]. We screened the medaka genome [39, 40] in silico for tcf3 genes using the mouse Tcf3 amino acid sequence. In this search several members of the Tcf/Lef family appeared, but only a single tcf3 gene (corresponding GenBank accession number HQ705658 located on chromosome 9 and encoding for a 575 amino acid protein). The presence of a single tcf3 gene in medaka is also supported by a study of Wang et al. [41]. We isolated a cDNA fragment of this tcf3 gene by PCR and performed whole mount in situ hybridization with medaka embryos (Figure 1). During gastrulation, tcf3 is broadly expressed throughout the embryonic shield (Figure 1A; at 40% epiboly), followed by an anterior shift towards the prospective head region (Figure 1C) and into the embryonic body (Figure 1B,C) at late gastrula. The expression becomes restricted to the head region during neurula (Figure 1D,D'), but subsequently also appears in posterior regions of the embryo (Figure 1E-H'). When the first subdivisions of the brain can be distinguished, tcf3

expression becomes segmented into distinctive stripes (Figure 1E,E'). However, the expression is still enhanced in the telencephalic region and the midbrain, whereas only a faint stripe can be observed in the hindbrain. Comparable to the zebrafish tcf3 genes [19], a gap of expression is clearly visible in the MHB (Figure 1E-G). Furthermore, weak expression was also detected in the eyes and the otic placodes (Figure 1E). During somitogenesis, tcf3 expression further extends caudally (Figure 1F-H'), where it is then found in the pectoral fins and the somites in late stages (Figure 1H,H'). Taken together the expression of medaka tcf3 represents the sum of the expression domains described for the two zebrafish genes tcf3b and hdl [19].

Knock down of the tcf3 gene in medaka embryos with PNAs

Having established the identity of the tcf3 gene in medaka, we performed knock down experiments using both PNAs and morpholino oligonucleotides. To block translation, a 16mer mixed pePNA (Figure 2A) and a 25mer morpholino oligonucleotide sequence were designed against the medaka tcf3 mRNA directly upstream of the AUG (Figure 2B). Injection into medaka embryos at the one cell stage resulted in specific phenotypes that strongly resembled those of hdl inactivated zebrafish embryos [19]. During young stages, no significant changes in development were observed between the injected and the control embryos. Only after the beginning of eye development, phenotypic alterations became visible (Figure 3B-D). The knock down phenotype concentrated on the eye region, leaving the trunk and tail largely unaffected. Weakly affected embryos at stage 22 had slightly smaller eyes than the control group, strongly affected embryos showed dramatic reduction of eye size or lacked the eyes completely (Figure 3A-D). At stage 30 (3 days and 10 hours, 35 somites), after the onset of eye pigmentation, a clearer distinction of the extent of the eye phenotypes was possible (Figure 3F-H). We separated the embryos into three groups (weak, moderate, and strong) depending on a classification of the eye phenotypes. Weak embryos (Figure 3B,F) had slightly smaller eyes than the control group, whereas in embryos with a moderate phenotype (Figure 3C,G) the size reduction was severe. As a strong phenotype (Figure 3D,H), we classified eye-less embryos that looked otherwise normal.

Both PNAs and morpholino oligonucleotides directed against tcf3 resulted in the same phenotypes. In zebrafish the phenotypes for the two tcf3 genes differ considerably, however, in hdl/tcf3b double morphants they add up to one combined phenotype representing the complete absence of Tcf3 proteins. Medaka embryos with a strong phenotype correspond to this extreme case, whereas embryos of the weak and moderate group are in between the phenotypes for hdl and tcf3b in zebrafish.

Qualification of the eyes pigmented retinal structures allowed a simple but reliable phenotype classification. Based on these results we could compare the knock down efficiency of the different antisense molecules. We first used the Tcf3PNA mixed pePNA which contains two tri-methyl-lysine (TML) end groups. For each concentration the number of phenotypes of the different groups was determined and the total number of tcf3 knock down phenotypes among the surviving embryos was calculated (Figure 4A and Additional File1). Between 100 μM and 400 μM of Tcf3PNA the total number of phenotypes increased from 22 to 51%. At 600 μM and 900 μM the overall frequency of phenotypes (both 57%) and also the number of dead embryos (6 and 7%, respectively) did not change which indicates a low toxicity. At 1,200 μM the percentage of tcf3 specific

phenotypes increased to 86%, however also a death rate of 38% was observed suggesting beginning toxicity. As expected, these increasing numbers of phenotypes also resulted in a continuous shift from preferentially weak phenotypes at low concentrations to a high proportion of strong phenotypes at high concentrations (Additional File 1). The morpholino oligonucleotide showed phenotypes indistinguishable from the pePNAs, but differed in the efficiency. High rates of tcf3-specific phenotypes, 71% - 92%, appeared already at low concentrations, 50 and 100 μM, respectively. However, at 200 μM the mortality rate jumped to 44%, indicating toxic effects (Figure 4B and Additional File 1). At concentrations with high mortality rates, some embryos with unspecific phenotypes appeared which looked similar for both pePNAs and morpholino oligonucleotides. We previously described such unspecifically affected medaka embryos, which have smaller eyes but in addition show severe defects all over the brain [42]. Such unspecific phenotypes were not detected at non-toxic concentrations. Taken together, the morpholino oligonucleotide worked more efficiently than the pePNA at low concentrations, but also appeared to be more toxic.

We next tested the pePNAs' splice blocking efficiency. A sequence overlapping with both exon 1 and intron 1 was selected and also synthesized as a mixed PNA with a double TML end group (Tcf3spPNA; Figure 2B). PNA injection resulted in the same phenotypes as observed for the Tcf3PNA, however, with lower efficiency (Figure 4A and Additional File 1). With 49%, the highest number of embryos affected specifically was observed at a concentration of 900 μM. At 1,200 μM toxicity became dominant, similar as seen for Tcf3PNA. We reasoned that a combination of both the translational blocking and the splice blocking PNAs might result in an improved knock down efficiency. Indeed, co-injection of Tcf3PNA and Tcf3spPNA, each at a concentration of 200 μM, resulted in 50% of the embryos showing phenotypes (Figure 4A and Additional File 1), which is higher than the percentage of affected embryos for both 400 μM Tcf3PNA (39%) and 400 μM Tcf3spPNA (30%). Therefore, the combined injection of both PNAs led to a synergistic improvement, which was also observed at higher concentrations. At 900 μM (450 μM each) 74% of the embryos showed tcf3-specific phenotypes without toxic side effects (those first appeared at 1,200 μM).

We then tested K-side chains as a novel backbone modification of the PNAs (Figure 2A). A mixed 16mer PNA with the same target sequence as the Tcf3PNA was synthesized (Tcf3kPNA; Figure 2B). Injection of these new PNAs resulted in the same tcf3 specific phenotypes, but at considerably higher numbers (Figure 4B and Additional File 1). At 100 μM the Tcf3kPNA produced 76% tcf3 specific phenotypes, compared to 22% for the Tcf3PNA. Similar improvements were also seen for other concentrations. Peak levels of 92% phenotypes were observed at 400 μM. First toxic effects of these modified PNAs appeared at 600 μM. Therefore, the K-side chain modification strongly improved the antisense efficiency of PNAs. To test their specificity, an exchange of two nucleotides was tested (GT to TG in the middle of the PNA; Tcf3kPNAmut Figure 2B). This resulted in a dramatic loss of tcf3 knock down efficiency (Figure 4B and Additional File 1). At 100 μM none of the embryos showed tcf3-specific phenotypes and at 600 μM only 11% (compared to 93% for the non-mutated version). Therefore, a highly specific antisense function of the K-modified PNAs in an in vivo environment could be observed at low concentrations, directly comparable to the results for morpholino oligonucleotides.

The repeated appearance of the same phenotypes with various different antisense molecules clearly demonstrated specificity of the tcf3 knock down experiments. To

further analyse the tcf3 loss of function phenotype, we next performed whole mount in situ hybridization experiments with injected embryos using probes against pax2, pax6, and gbx1 (Figure 3I-P). Dorsky et al. analysed the expression of these genes in zebrafish upon tcf3 inactivation. hdl mutants showed a decrease in pax6 expression in the presumptive head region and pax2.1 expression was expanded rostrally, whereas the gbx1 domain remained unchanged. However, if both hdl and tcf3b were inactivated, gbx1 also expanded anteriorly, thereby encircling the expression domain of pax2.1 and the anterior expression of pax6 was completely lost [19]. Taken together, stepwise reduction of Tcf3 activity in zebrafish resulted in a progressive anterior shift of the marker genes centring around the position of the prechordal plate [43]. In medaka tcf3 morphants, the expression domains of all three genes were shifted anteriorly (Figure 3M-O) compared to the wild type control (Figure 3I-K). In 48% of the embryos (29/61) the expression domain of pax6 was smaller (Figure 3M) and instead of two separate domains on either side of the prospective head (Figure 3I), only a single cap-like structure was observed at the most anterior part of the prospective neural domain (Figure 3M). However, we failed to see a complete loss of anterior pax6 expression. 56% of the embryos (20/36) hybridized with the MHB marker pax2, also showed an anterior shift. Moreover, the pax2 expression was expanded anteriorly, thereby partially overlapping with the pax6 domain (Figure 3N), which was in good agreement with the expression in zebrafish hdl loss of function embryos [19]. In 37% of the embryos (16/43) an altered expression of gbx1 was observed. Again, the expression domain was shifted anteriorly (Figure 3O). In addition to the anterior shift of the entire expression domain, the lateral edges of less severely caudalized embryos pointed anteriorly and in more severe phenotypes, the expression expanded into an arc-like shape, thereby overlapping the expression domains of both pax6 and pax2. We also analysed the MHB marker wnt1 in tcf3 knock down embryos and found expression in a more anterior position (Figure 3B). Taken together, the expression of all marker genes clearly indicates the expected anterior shift for tcf3 inactivation.

tcf3 gain-of-function experiments

So far we had performed tcf3 loss-of-function experiments. Now we focused on the consequences of tcf3 overexpression. For this, wild type embryos at the one-cell stage were injected with full length tcf3 cDNA (Figure 5A). We used the heat-inducible HSE promoter [33], which allowed stage-dependent ectopic gene expression (HSE:Tcf3). When heat induction was performed at mid-gastrulation (stage 14/15) preferentially eye phenotypes appeared, confirming the importance of tcf3 for eye development. A closer inspection of the eye phenotypes after the onset of eye pigmentation revealed that 8% of the Gfp positive embryos were eye less. In total, 31% (8/27) showed a reduced eye size, thus resembling the phenotype of the tcf3 loss-of-function embryos. Varying DNA concentrations did not change the eye phenotypes and neither did a variation of the time of heat-induction.

We next concentrated on the functional domains of Tcf3 mediating transcriptional repression. In absence of a Wnt signal the siamois gene in Xenopus is strongly repressed by Tcf/Lef proteins [44]. A closer inspection revealed repressing activities both in the C- and the N-terminus of Tcf3. For the C-terminal interaction the corepressor CtBP could be identified [45]. To test whether the eye phenotypes depend on CtBP, we injected a truncated Tcf3 version (Tcf3[1-434]; Figure 5A), lacking the CtBP interaction domain. The percentage of eye-less embryos increased to 26% (Figure 5F) compared to 8% for full

length Tcf3. CtBP interaction therefore does not promote the eye phenotypes, but instead reduces them. We next tested the N-terminal repression function of Tcf3, where Gro/Tle corepressors have been identified as corepressors [24]. A deletion version lacking amino acids 62 to 236 (Tcf3□Gro; Figure 5A), which is devoid of the Gro/Tle interaction domain [24], reduced the appearance of strong eye phenotypes to 5% (Figure 5F). In order to better qualify the function of Gro/Tle we concentrated on Tcf3 versions lacking the CtBP interaction domain. In addition, we had observed stronger phenotypes in early embryos, indicating rescue mechanisms in older embryos. We therefore assessed the phenotypes in younger stages. Since eye pigmentation cannot be used as a morphological marker for eye development in early embryos, we performed whole mount in situ hybridization experiments on stage 21 embryos (1 day, 10 hours, 6 somites) using the retinal marker rx2 as a probe (Figure 5B-E). Embryos that developed a weak phenotype (Figure 5C) had smaller eyes than the wild type control (Figure 5B), and rx2 expression was significantly reduced in embryos with a moderate phenotype (Figure 5D) and completely lost in strong phenotypes (Figure 5E). Using these conditions with the CtBP deficient Tcf3(1-434) we observed 90% of embryos with small eye phenotypes (Figure 5F and Additional file 2). We next tested a Tcf3(1-434) version which is devoid of the Gro/Tle interaction domain but still retains the DNA binding and ß-catenin interacting parts of the protein (Tcf3[1-434]□Gro; Figure 5A). This modification strongly reduced the appearance of eye phenotypes to 50% of the injected embryos, most of which showed a weak phenotype, and no eye-less embryos were observed (Figure 5F and Additional File 2). Consequently, impairment of the Gro/Tle interaction considerably reduced the appearance of eye phenotypes in tcf3 misexpression experiments, indicating a crucial contribution of this corepressor. Interestingly, at older stages 21% of the embryos (14/66) overexpressing Tcf3(1-434)□Gro developed ectopic otic vesicles (Additional File 2B,C; arrowheads). All of them formed in the trunk and tail region of the developing embryo, hence, posterior to the endogenous vesicles (Additional File 2C, arrow). These results strongly resemble misexpression experiments of sox3 [46] and Aes can affect sox3 expression within the otic vesicles [47]. Instead of an effect on sox3, the induction of ectopic otic vesicles might however also be caused by a dominant negative effect of the overexpressed truncated Tcf3, thus blocking the repressing function of full length Tcf3. Such an antirepressive effect would be equivalent to ectopic Wnt activation, which we previously could show to induce ectopic otic vesicles [48, 49]. Taken together, Tcf3 function in eye development is modulated by Gro/Tle corepressor interaction.

gro/tle loss-of-function experiments

The eye phenotypes in the gain-of-function experiments indicated a strong link between the Tcf3 repressing function and Gro/Tle proteins. Furthermore, Gro/Tle proteins have previously been implicated in eye development [47, 50]. In order to directly analyse the modulating effect of these corepressors on Tcf3 we next performed Gro/Tle loss-of-function experiments. During embryonic development gro/tle genes are expressed in largely overlapping domains suggesting redundant functions. In mammals four full length genes exist, in fish even six [37]. In order to interfere with the function of all Gro/Tle proteins within one experiment, the short family member Aes has repeatedly been used [47, 50] The rationale behind this strategy is to overexpress a truncated Gro/Tle family member, which then efficiently interacts via its Q-domain with long Gro/Tle proteins. The resulting tetramers therefore will partially lack the C-terminal

domains which are not present in Aes. Since the major protein-protein interaction domain, the WD40 repeats, reside in the C-terminus, inefficient complex formation would be the result. A major criticism towards this strategy is, however, that important interactions also originate from the Q-domain. Aes contains a Q-domain, it is however not clear how efficient this domain can contribute to interactions in mixed complexes. We therefore tested the effect of Aes overexpression on an established Q-domain interaction. For this we selected the Gro/Tle-Six3 interaction, which has been shown to be critical for eye development [50], and performed mammalian two-hybrid experiments. The results showed a stepwise reduction of both Tle1- and Tle4-Six3 complex formation upon increasing Aes concentrations, whereas a control interaction was not affected (Additional File 3). Therefore, Aes overexpression can interfere with both N- and C-terminal interactions of Gro/Tle proteins.

To assess gro/tle loss-of-function phenotypes independent from possible injection-based artefacts, we established heat-inducible transgenic lines (Figure 6A) using the HSE promoter [33]. In addition to an aes transgenic line (HSE:Aes) we also generated a Tle4-Q-domain misexpressing transgenic line (HSE:Q). Q-domain misexpression is expected to similarly interfere with C-terminal interactions of Gro/Tle proteins, but not with those of the Q-domain. Therefore, Aes misexpression could potentially generate more severe phenotypes, depending on the preference of the interactions at the N- or C-terminus of the Gro/Tle proteins. Heat induction of aes at mid-gastrula resulted in the same eye phenotypes as described in previous studies [47, 50]. We categorized these phenotypes into weak, moderate and strong. Embryos with a weak phenotype developed slightly smaller eyes pointing towards the midline (Figure 6C-C”), whereas embryos with a strong phenotype showed cyclopic eyes (Figure 6E-E”). As a moderate phenotype we considered embryos in-between (Figure 6D-D”). Here, additionally to the weak phenotype, the lenses were shifted anteriorly and beginning cyclopia anterior of the forebrain could be observed. In HSE:Aes embryos a total of 24% developed a phenotype (23/97), equally distributed between weak and strong. The HSE:Q line showed a total of 34% phenotypes among the induced embryos (27/79), however, only 5% of the embryos were categorized as strong. Therefore, the interference of the Q-domain was less efficient compared to the aes-misexpressing line, but interestingly the phenotypes were identical. This indicates that during early embryonic development both Aes and Q-domain interfere with the same critical interactions of Gro/Tle proteins, which most probably locate to the C-terminus.

We further analysed the effects of the Aes/Q-mediated loss-of-function approach on gro/tle genes in whole mount in situ hybridization experiments (Figure 6F-K). To be able to distinguish between phenotype groups, we selected embryos at stage 21, where eye development had already begun. rx2 expression (Figure 6I) matched the phenotypes observed in older stages (Figure 6C”-D”). In embryos with a weak/moderate phenotype (Figure 6I) the eyes were smaller compared to the wild type control (Figure 6F) and tilted towards the midline. In strong phenotypes, an additional faint stripe of rx2 expression, that connects the two optic vesicles, was observed in the forebrain (data not shown). These results are in good agreement with the morphologic phenotype observed in older embryos (Figure 6C”-D”). Due to the fact that the connection of the cyclopic eye was observed in the most anterior part of the embryo (Figure 6E”), we analysed if anterior development is impaired. We used the telencephalon marker brain factor 1 (bf1) and found reduced expression in HSE:Aes embryos (Figure 6J). Furthermore, wnt1 expression (Figure 6K) indicated a reduced size of the midbrain. Instead of a defined

expression close to the midline (Figure 6H, arrows), here an indistinct expression pattern throughout the midbrain was observed (Figure 6K, arrows).

Taken together, the aes induced phenotypes show eye defects, which however differ from the tcf3 loss-of-function phenotypes in details. An obvious explanation for the deviating phenotypes is that blocking of Gro/Tle function not only affects Tcf3 but also other Gro/Tle interaction partners important for eye development. One example is Six3, where the effects of aes overexpression have been studied in detail [50]. The Aes/Q misexpression therefore most probably causes a mixed phenotype affecting functions of several Gro/Tle interacting proteins. To test whether they indeed represent loss-of-function phenotypes for gro/tle genes we applied antisense oligonucleotides. Since the combined inactivation of all 6 gro/tle family members is not possible, we concentrated on individual genes, which can only show partial phenotypes. The appearance of eye defects for blocking of individual gro/tle genes would therefore strongly support the Aes/Q results. In order to analyse early expressing family members we selected tle1 [50], tle2b and tle3b [37]. Interestingly the injection of morpholino oligonucleotides revealed strong eye phenotypes for all 3 tle genes. Using the same criteria for the phenotypes as for Aes/Q, 10 to 16% of the embryos showed eye defects (Additional File 4). Highest numbers were observed for tle2b, both in overall numbers (16%) as well as in the proportion of embryos with strong phenotypes (7%, almost half of which were completely eye-less). Combined injection of the morpholino oligonucleotides could further increase the number of phenotypes (27% for tle1 and tle2b). The appearance of eye defects is therefore in perfect agreement with the Aes/Q results. However, details of the phenotypes differed. For example cyclopic eye connections for tle1 morpholinos appeared in the middle of the eyes (Additional File 4C), whereas they were preferentially observed anterior to the forebrain in Aes/Q embryos (Figure 6D").

DISCUSSION

Novel side chains provide higher antisense efficiency for PNAs

For the tcf3 knock down experiments in medaka embryos PNAs were applied. We used phosphonic ester modified mixed PNAs, which previously were shown to be suitable for loss-of-function experiments in medaka [42]. Here again we could demonstrate a specific knock down of gene function. We started with pePNAs with two TML end groups and obtained almost 60% specific phenotypes (400 to 900 µM) (Figure 4A and Additional File 1). At higher concentrations the percentage further increased, however also unspecific toxicity was observed. The pePNA molecules also worked for a splice blocking approach. Although the efficiency was lower compared to the translational blocking experiments, the same tcf3 specific phenotypes appeared (Figure 4A and Additional File 1). Furthermore, a combined injection of both PNAs synergistically improved the overall efficiency of the antisense molecules (74% specific phenotypes).

In a direct comparison with pePNAs the morpholino oligonucleotides resulted in higher efficiency at lower concentrations (71 to 92% phenotypes at 50 and 100 µM, respectively). However, toxic effects also started at lower concentrations (200 µM). Otherwise, the obtained phenotypes were identical for the two antisense molecules (Figure 4B and Additional File 1). However, further modification of the PNA backbone with K-side chains (Figure 2A) considerably improved the PNA efficiency (Figure 4B and Additional File 1). 63

to 92% of the embryos showed tcf3 specific phenotypes at concentrations of 50 to 400 μM (toxicity first appearing at 600 μM). This efficiency is in the same range as that for the morpholino oligonucleotides. The high specificity of this 16mer PNA was clearly demonstrated by the dramatic drop in phenotypes for a 2-nucleotide exchange in the sequence (8 to 16% phenotypes at 100 to 400 μM). Therefore, novel side chain modifications efficiently improved the in vivo antisense function of PNAs.

tcf3 function in medaka embryos

tcf3 genes are of critical importance for the establishment of the antero-posterior (A-P) axis of vertebrates [15, 17]. However, little is known about medaka tcf3 genes. Contrary to the zebrafish, only a single tcf3 gene appeared in our in silico searches and also in previous analyses [41]. Therefore, the prediction for the in situ hybridisation analysis was that the expression domains of the medaka tcf3 should cover those of both zebrafish genes together [18, 19]. Indeed, we could observe such a combined expression first in the embryonic shield (Figure 1A-C) and later in the brain (Figure 1D-H). Also the loss-of-function phenotypes support the presence of a single tcf3 gene in the medaka genome. In zebrafish the hdl mutation results in strong anterior phenotypes, whereas tcf3b inactivation shows mild effects [19]. Combined inactivation of both hdl and tcf3b adds up to a severe phenotype characterized by complete lack of eyes and brain defects [19]. Knock down experiments in medaka resulted either in weakly/moderately affected embryos with reduced eye size, covering the range of phenotypes seen for inactivation of single tcf3 genes in zebrafish, or in strongly affected eye-less embryos corresponding to the complete absence of Tcf3 proteins seen in zebrafish hdl/tcf3b double morphants (Figure 3). The analysis of marker gene expression in the tcf3 knock down embryos verifies the strong effect on the Tcf3/Wnt gradient along the A-P axis [43, 51]. All marker genes tested showed an anterior shift centring around the position of the prechordal plate. Therefore, a single tcf3 gene in medaka combines the function of two zebrafish genes.

Gro/Tle corepressor proteins are critical for tcf3 function

To complement the tcf3 loss-of-function experiments we also performed gain-of-function experiments (Figure 4). These allowed us to analyse the co-repressor dependence of this transcription factor. CtBP has been identified as a critical cofactor during embryonic development [45]. However, for eye development we found Gro/Tle proteins to be more important. Tcf3 variants lacking the Gro/Tle interaction domain showed considerably reduced numbers of eye phenotypes in the gain-of-function experiments (Figure 5F). The critical importance of Gro/Tle proteins for eye development was further supported by different gro/tle loss-of-function experiments, which all resulted in eye phenotypes.

In a first attempt, we concentrated on Aes/Grg5 (Figure 6), a naturally occurring truncated family member of full length Gro/Tle proteins that consists of only the Q and the GP domain [25, 26, 52]. The Q domain allows Aes to oligomerize with full length Gro/Tle proteins, thereby reducing the number of C-terminal interaction domains [21, 29, 50, 53-56]. The GP domain, however, is functionally different from full length Gro/Tle proteins because it does not interact with HDACs [20, 57-59]. It was suggested that by

this interaction Aes turns Gro/Tle oligomers into non-functional complexes, which therefore have a reduced number of C-terminal WD-40 interaction domains and a reduced efficiency to cooperate with HDAC corepressors ([21, 53, 55, 60, 61] and reviewed by Beagle et al. [62]). Furthermore, our mammalian two-hybrid experiments with Six3 indicate that also N-terminal interactions with the Q-domain are blocked by Aes misexpression. Indeed, ectopic expression of Aes in medaka resulted in considerably smaller eyes and otic vesicles and reduced expression of the optic and otic marker genes, suggesting an efficient block of Gro/Tle activity [47, 50]. But in addition to the Gro/Tle blocking functions, Aes is known to exhibit specific functions on its own in certain cellular contexts [58, 59, 63]. The observed phenotypes could therefore be a mixture between gro/tle loss-of-function and aes gain-of-function effects. However, misexpresssion of the Tle4 Q-domain resulted in exactly the same phenotypes as observed for Aes, although the efficiency was lower. Furthermore, also antisense blocking of individual gro/tle genes resulted in reduced eye size of the embryos, indicating that eye formation is a major function of gro/tle genes. Therefore, Aes misexpressing embryos seem to represent almost pure gro/tle loss-of-function phenotypes.

The morphological phenotypes were already visible at early stages (Figure 6C-E) and in situ hybridisation experiments using rx2 confirmed these early effects (Figure 6I). Additional experiments showed a reduction in size of both the forebrain and the midbrain, as indicated by the expression patterns of bf1 and wnt1 (Figure 6J,K). Similar results have been reported for bf1 in WRPW-induced Gro/Tle loss-of-function experiments in Xenopus [64]. Based on the critical importance of Gro/Tle corepressor function for Tcf3, blocking Gro/Tle proteins by Aes should result in phenotypes similar to those seen in tcf3 antisense experiments. Indeed in both cases a dramatic reduction of eye size could be observed. These anterior defects are also in good agreement with the A-P defects seen in Wnt1 overexpression experiments [48]. A final verification of the dominant negative Aes approach was made by knock down of individual medaka gro/tle genes. Although 6 gro/tle genes are present in medaka and are thought to function largely redundantly, we surprisingly observed highly similar phenotypes for knock down of each tle1, tle2b, and tle3b. We observed a clear reduction in eye size, cyclopic eyes as well as eye-less embryos (Additional File 4). These phenotypes closely resembled those of the dominant negative experiments and thus fully support this approach. Taken together, these experiments confirmed the importance of Gro/Tle corepressors for Tcf3 function.

ACKNOWLEDGEMENT

We thank Jochen Wittbrodt for the in situ probe directed against the bf1 gene. The work was supported by the Austrian Research Promotion Agency (FFG, grant 836444) and the Austrian Science Fund (FWF, grant P19571-B11).

REFERENCES

1. Summerton J: Morpholinos and PNAs compared. International Journal of Peptide Research and Therapeutics 2003, 10(3):215-236.

2. Summerton J: Morpholino antisense oligomers: the case for an RNase H-independent structural type. Biochimica et biophysica acta 1999, 1489(1):141-158.

3. Nielsen PE, Egholm M, Berg RH, Buchardt O: Sequence-selective recognition of DNA by strand displacement with a thymine-substituted polyamide. Science 1991, 254(5037):1497-1500.

4. Buchardt O, Egholm M, Berg RH, Nielsen PE: Peptide nucleic acids and their potential applications in biotechnology. Trends in biotechnology 1993, 11(9):384-386.

5. Egholm M, Buchardt O, Christensen L, Behrens C, Freier SM, Driver DA, Berg RH, Kim SK, Norden B, Nielsen PE: PNA hybridizes to complementary oligonucleotides obeying the Watson-Crick hydrogen-bonding rules. Nature 1993, 365(6446):566-568.

6. Ray A, Norden B: Peptide nucleic acid (PNA): its medical and biotechnical applications and promise for the future. FASEB journal : official publication of the Federation of American Societies for Experimental Biology 2000, 14(9):1041-1060.

7. Nielsen PE, Haaima G, Lohse A, Buchardt O: Peptide Nucleic Acids(PNAs) Containing Thymine Monomers Derived from Chiral Amino Acids: Hybridization and Solubility Properties OfD-Lysine PNA. Angewandte Chemie International Edition in English 1996, 35(17):1939-1942.

8. Urtishak KA, Choob M, Tian X, Sternheim N, Talbot WS, Wickstrom E, Farber SA: Targeted gene knockdown in zebrafish using negatively charged peptide nucleic acid mimics. Developmental dynamics : an official publication of the American Association of Anatomists 2003, 228(3):405-413.

9. Dorn S, Aghaallai N, Jung G, Bajoghli B, Werner B, Bock H, Lindhorst T, Czerny T: Side chain modified peptide nucleic acids (PNA) for knockdown of six3 in medaka embryos. In.; 2012.

10. van de Wetering M, Oosterwegel M, Dooijes D, Clevers H: Identification and cloning of TCF-1, a T lymphocyte-specific transcription factor containing a sequence-specific HMG box. Embo J 1991, 10(1):123-132.

11. Arce L, Yokoyama NN, Waterman ML: Diversity of LEF/TCF action in development and disease. Oncogene 2006, 25(57):7492-7504.

12. Behrens J, von Kries JP, Kuhl M, Bruhn L, Wedlich D, Grosschedl R, Birchmeier W: Functional interaction of beta-catenin with the transcription factor LEF-1. Nature 1996, 382(6592):638-642.

13. Kengaku M, Capdevila J, Rodriguez-Esteban C, De La Pena J, Johnson RL, Izpisua Belmonte JC, Tabin CJ: Distinct WNT pathways regulating AER formation and dorsoventral polarity in the chick limb bud. Science 1998, 280(5367):1274-1277.

14. Houston DW, Kofron M, Resnik E, Langland R, Destree O, Wylie C, Heasman J: Repression of organizer genes in dorsal and ventral Xenopus cells mediated by maternal XTcf3. Development 2002, 129(17):4015-4025.

15. Merrill BJ, Pasolli HA, Polak L, Rendl M, Garcia-Garcia MJ, Anderson KV, Fuchs E: Tcf3: a transcriptional regulator of axis induction in the early embryo. Development 2004, 131(2):263-274.

16. Cole MF, Johnstone SE, Newman JJ, Kagey MH, Young RA: Tcf3 is an integral component of the core regulatory circuitry of embryonic stem cells. Genes & development 2008, 22(6):746-755.

17. Pereira L, Yi F, Merrill BJ: Repression of Nanog gene transcription by Tcf3 limits embryonic stem cell self-renewal. Molecular and cellular biology 2006, 26(20):7479-7491.

18. Kim CH, Oda T, Itoh M, Jiang D, Artinger KB, Chandrasekharappa SC, Driever W, Chitnis AB: Repressor activity of Headless/Tcf3 is essential for vertebrate head formation. Nature 2000, 407(6806):913-916.

19. Dorsky RI, Itoh M, Moon RT, Chitnis A: Two tcf3 genes cooperate to pattern the zebrafish brain. Development 2003, 130(9):1937-1947.

20. Arce L, Pate KT, Waterman ML: Groucho binds two conserved regions of LEF-1 for HDAC-dependent repression. BMC cancer 2009, 9:159.

21. Brantjes H, Roose J, van De Wetering M, Clevers H: All Tcf HMG box transcription factors interact with Groucho-related co-repressors. Nucleic acids research 2001, 29(7):1410-1419.

22. Daniels DL, Weis WI: Beta-catenin directly displaces Groucho/TLE repressors from Tcf/Lef in Wnt-mediated transcription activation. Nature structural & molecular biology 2005, 12(4):364-371.

23. Turki-Judeh W, Courey AJ: The unconserved groucho central region is essential for viability and modulates target gene specificity. PloS one 2012, 7(2):e30610.

24. Roose J, Molenaar M, Peterson J, Hurenkamp J, Brantjes H, Moerer P, van de Wetering M, Destree O, Clevers H: The Xenopus Wnt effector XTcf-3 interacts with Groucho-related transcriptional repressors. Nature 1998, 395(6702):608-612.

25. Mallo M, Franco del Amo F, Gridley T: Cloning and developmental expression of Grg, a mouse gene related to the groucho transcript of the Drosophila Enhancer of split complex. Mechanisms of development 1993, 42(1-2):67-76.

26. Schmidt CJ, Sladek TE: A rat homolog of the Drosophila enhancer of split (groucho) locus lacking WD-40 repeats. The Journal of biological chemistry 1993, 268(34):25681-25686.

27. Lindhorst TS, 6020 Innsbruck, AT), Werner, Birgit (Müllerstrasse 13, 6020 Innsbruck, AT), Bock, Holger (Hubangerweg 28, 6051 Götzens, AT),: CHIRAL COMPOUNDS SUBSTITUTED WITH PHOSPHONATE ESTER OR PHOSPHONIC ACID. In.: Ugichem GmbH (Mitterweg 24, 6020 Innsbruck, AT); 2011.

28. Schöllkopf U, Busse U, Lonsky R, Hinrichs R: Asymmetric syntheses via heterocyclic intermediates, XXXI. Asymmetric synthesis of various non-proteinogenic amino acid methyl esters (functionalized in the carbon chain) and amino acids by the bislactim ether method. Liebigs Annalen der Chemie 1986, 1986(12):2150-2163.

29. Chen FM, Benoiton NL: A synthesis of N6,N6,N6-trimethyl-L-lysine dioxalate in gram amounts. Biochemistry and cell biology = Biochimie et biologie cellulaire 1986, 64(3):182-183.

30. Koch T, Hansen HF, Andersen P, Larsen T, Batz HG, Otteson K, Orum H: Improvements in automated PNA synthesis using Boc/Z monomers. The journal of peptide research : official journal of the American Peptide Society 1997, 49(1):80-88.

31. Fink M, Flekna G, Ludwig A, Heimbucher T, Czerny T: Improved translation efficiency of injected mRNA during early embryonic development. Developmental dynamics : an official publication of the American Association of Anatomists 2006, 235(12):3370-3378.

32. Adams B, Dorfler P, Aguzzi A, Kozmik Z, Urbanek P, Maurer-Fogy I, Busslinger M: Pax-5 encodes the transcription factor BSAP and is expressed in B lymphocytes, the developing CNS, and adult testis. Genes & development 1992, 6(9):1589-1607.

33. Bajoghli B, Aghaallaei N, Heimbucher T, Czerny T: An artificial promoter construct for heat-inducible misexpression during fish embryogenesis. Developmental biology 2004, 271(2):416-430.

34. Pomerantz JL, Sharp PA, Pabo CO: Structure-based design of transcription factors. Science 1995, 267(5194):93-96.

35. O'Shea EK, Lumb KJ, Kim PS: Peptide 'Velcro': design of a heterodimeric coiled coil. Current biology : CB 1993, 3(10):658-667.

36. Iwamatsu T: Stages of normal development in the medaka Oryzias latipes. Mechanisms of development 2004, 121(7-8):605-618.

37. Aghaallaei N, Bajoghli B, Walter I, Czerny T: Duplicated members of the Groucho/Tle gene family in fish. Developmental dynamics : an official publication of the American Association of Anatomists 2005, 234(1):143-150.

38. Vancha A, Govindaraju S, Parsa K, Jasti M, Gonzalez-Garcia M, Ballestero R: Use of polyethyleneimine polymer in cell culture as attachment factor and lipofection enhancer. BMC biotechnology 2004, 4(1):23.

39. Ahsan B, Kobayashi D, Yamada T, Kasahara M, Sasaki S, Saito TL, Nagayasu Y, Doi K, Nakatani Y, Qu W et al: UTGB/medaka: genomic resource database for medaka biology. Nucleic acids research 2008, 36(Database issue):D747-752.

40. Kasahara M, Naruse K, Sasaki S, Nakatani Y, Qu W, Ahsan B, Yamada T, Nagayasu Y, Doi K, Kasai Y et al: The medaka draft genome and insights into vertebrate genome evolution. Nature 2007, 447(7145):714-719.

41. Wang D, Manali D, Wang T, Bhat N, Hong N, Li Z, Wang L, Yan Y, Liu R, Hong Y: Identification of pluripotency genes in the fish medaka. International journal of biological sciences 2011, 7(4):440-451.

42. Dorn S, Aghaallaei N, Jung G, Bajoghli B, Werner B, Bock H, Lindhorst T, Czerny T: Side chain modified peptide nucleic acids (PNA) for knock-down of six3 in medaka embryos. BMC biotechnology 2012, 12:50.

43. Chitnis AB, Itoh M: Exploring alternative models of rostral-caudal patterning in the zebrafish neurectoderm with computer simulations. Current opinion in genetics & development 2004, 14(4):415-421.

44. Brannon M, Gomperts M, Sumoy L, Moon RT, Kimelman D: A beta-catenin/XTcf-3 complex binds to the siamois promoter to regulate dorsal axis specification in Xenopus. Genes & development 1997, 11(18):2359-2370.

45. Brannon M, Brown JD, Bates R, Kimelman D, Moon RT: XCtBP is a XTcf-3 co-repressor with roles throughout Xenopus development. Development 1999, 126(14):3159-3170.

46. Koster RW, Kuhnlein RP, Wittbrodt J: Ectopic Sox3 activity elicits sensory placode formation. Mechanisms of development 2000, 95(1-2):175-187.

47. Bajoghli B, Aghaallaei N, Czerny T: Groucho corepressor proteins regulate otic vesicle outgrowth. Developmental dynamics : an official publication of the American Association of Anatomists 2005, 233(3):760-771.

48. Bajoghli B, Aghaallaei N, Jung G, Czerny T: Induction of otic structures by canonical Wnt signalling in medaka. Development genes and evolution 2009, 219(8):391-398.

49. Jung G, Hug M, Halter C, Friesenhengst A, Walzer J, Czerny T: Diffusion of small molecules into medaka embryos improved by electroporation. BMC biotechnology 2013, 13:53.

50. Lopez-Rios J, Tessmar K, Loosli F, Wittbrodt J, Bovolenta P: Six3 and Six6 activity is modulated by members of the groucho family. Development 2003, 130(1):185-195.

51. Kiecker C, Niehrs C: A morphogen gradient of Wnt/beta-catenin signalling regulates anteroposterior neural patterning in Xenopus. Development 2001, 128(21):4189-4201.

52. Miyasaka H, Choudhury BK, Hou EW, Li SS: Molecular cloning and expression of mouse and human cDNA encoding AES and ESG proteins with strong similarity to Drosophila enhancer of split groucho protein. European journal of biochemistry / FEBS 1993, 216(1):343-352.

53. Choi CY, Kim YH, Kwon HJ, Kim Y: The homeodomain protein NK-3 recruits Groucho and a histone deacetylase complex to repress transcription. The Journal of biological chemistry 1999, 274(47):33194-33197.

54. Eberhard D, Jimenez G, Heavey B, Busslinger M: Transcriptional repression by Pax5 (BSAP) through interaction with corepressors of the Groucho family. Embo J 2000, 19(10):2292-2303.

55. Pinto M, Lobe CG: Products of the grg (Groucho-related gene) family can dimerize through the amino-terminal Q domain. The Journal of biological chemistry 1996, 271(51):33026-33031.

56. Yao J, Lai E, Stifani S: The winged-helix protein brain factor 1 interacts with groucho and hes proteins to repress transcription. Molecular and cellular biology 2001, 21(6):1962-1972.

57. Bajoghli B, Aghaallaei N, Soroldoni D, Czerny T: The roles of Groucho/Tle in left-right asymmetry and Kupffer's vesicle organogenesis. Developmental biology 2007, 303(1):347-361.

58. Yu X, Li P, Roeder RG, Wang Z: Inhibition of androgen receptor-mediated transcription by amino-terminal enhancer of split. Molecular and cellular biology 2001, 21(14):4614-4625.

59. Zhang Y, Gao S, Wang Z: Structural and functional analysis of amino-terminal enhancer of split in androgen-receptor-driven transcription. The Biochemical journal 2010, 427(3):499-511.

60. Chen G, Nguyen PH, Courey AJ: A role for Groucho tetramerization in transcriptional repression. Molecular and cellular biology 1998, 18(12):7259-7268.

61. Palaparti A, Baratz A, Stifani S: The Groucho/transducin-like enhancer of split transcriptional repressors interact with the genetically defined amino-terminal silencing domain of histone H3. The Journal of biological chemistry 1997, 272(42):26604-26610.

62. Beagle B, Johnson GV: AES/GRG5: more than just a dominant-negative TLE/GRG family member. Developmental dynamics : an official publication of the American Association of Anatomists 2010, 239(11):2795-2805.

63. Tetsuka T, Uranishi H, Imai H, Ono T, Sonta S, Takahashi N, Asamitsu K, Okamoto T: Inhibition of nuclear factor-kappaB-mediated transcription by association with the amino-terminal enhancer of split, a Groucho-related protein lacking WD40 repeats. The Journal of biological chemistry 2000, 275(6):4383-4390.

64. Tsuji S, Hashimoto C: Choice of either beta-catenin or Groucho/TLE as a co-factor for Xtcf-3 determines dorsal-ventral cell fate of diencephalon during Xenopus development. Development genes and evolution 2005, 215(6):275-284.

FIGURE LEGEND

Figure 1. tcf3 expression in medaka embryonic development.

Whole mount in situ hybridization experiments were performed in wild type embryos at the indicated stages, using a digoxigenin-labelled RNA probe against tcf3. Embryos are shown in dorsal view, anterior at the top. (F-I) Flat mounts; (F'-I') tail view. During gastrulation (A-C) tcf3 is expressed throughout the epiblast and the embryonic body (C-D). In neurula the expression becomes restricted to the head (D,D') from where it spreads caudally and divides into a forebrain, midbrain, and hindbrain section (E;E'). A gap in expression at the mid-hindbrain boundary (F-H, arrowhead) is closed at later stages (H). In later stages, expression is observed throughout the entire body (G-I'). Scale bars 100 µm; A, A-C; F, F-F';G, G-H'. Abbreviations: st, stage.

Figure 2. Sequences of medaka tcf3 antisense molecules and their targets.

(A) Schematic chemical structure of aegPNAs, pePNAs and mixed PNAs (containing both aeg- and pePNA monomers) is shown. Mixed PNAs contain C3 residues. (B) mRNA targets are shown in the 5'-3' orientation, capital letters indicate the coding region. The AUG start codon is underlined. Pre-mRNA represents the unspliced mRNA precursor of the medaka tcf3 gene with exon sequences shown in capital letters. Tcf3MO represents a morpholino oligonucleotide, all other sequences PNAs. aegPNA components are shown with grey overlay, pePNA components with C3 side chains are shown in red letters, pePNA-K components are shown in red overlay. Boxed bases represent mismatches. All PNA and morpholino oligos are shown in 3'-5' orientation. L represents a trimethyl-lysine group.

Figure 3. Loss of function phenotypes for the tcf3 gene in medaka.

Embryos at the 1-cell stage were co-injected with 300 µM Tcf3MO and 1 µg/ml FITC-dextran. The pairs B and F, C and G, D and H each show the same embryo at different

stages (stage 22, A-D; stage 30, E-H). Control embryos (A,E) were co-injected with 1x Yamamoto's and FITC-dextran. Pictures of embryos with a fluorescent signal were taken at the indicated stages. Classification was performed after the onset of eye pigmentation, according to the size of the eye: (B,F) weak, slightly reduced size; (C,G) moderate, severe size reduction; (D,H) strong, eye-less. Embryos at stage 16 (I-K, N-O) are shown in dorsal view, anterior to the top; except for (L,P) which are at stage 17 and shown in lateral view. For genotypic analysis (I-P), whole mount in situ hybridization experiments were performed on MO injected embryos and un-injected wild type controls at stage 16 using digoxigenin-labelled RNA probes against Pax6 (I,M), Pax2 (J,N), Gbx1 (K,O), and Wnt1 (L,P) at stage 17. (I-K, M-O) Broken lines indicate the outlines of the prospective neural domain estimated from the merged expression patterns formed by pax6, pax2 and gbx1 in wild type embryos (I-K). An anterior shift of the expression domains was observed for all four genes. (L,P; arrowhead) wnt1 expression in the mid-hindbrain boundary. Scale bars 100 µm; A, A-H; I, I-K and M-O; L, L and P. Abbreviations: MO, morpholino oligonucleotide.

Figure 4. Knock down efficiencies using modified PNAs.

Quantitative evaluation of tcf3 knock down experiments. Results for injection of antisense molecules at the indicated concentrations. The blue bars represent the percentage of embryos with phenotypes among the surviving embryos, the red bars represents the mortality rate (see also Additional File 1).

Figure 5. tcf3 gain of function phenotypes.

(A) Schematic representation of full length Tcf3, Tcf3 lacking the Gro/Tle interaction domain (Tcf3□Gro), Tcf3 lacking the CtBP binding site (Tcf3[1-434]), and a C-terminal truncated Tcf3 lacking the Gro/Tle interaction domain (Tcf3[1-434]□Gro). (B-F) Embryos at the 1-cell stage were injected with either heat-inducible truncated Tcf3 (Gfp:HSE:Tcf3(1-434); 40 ng/µl) or Tcf3 lacking the Gro/Tle interaction domain (Gfp:HSE:Tcf3(1-434)□Gro; 40 ng/µl). Heat induction was performed at stage 14-15. Gfp positive embryos were selected at stage 22 for subsequent whole mount in situ hybridization experiments using digoxigenin-labelled RNA probes against rx2 (C-F). (B-E) Flat mounts are shown in dorsal view, anterior at the top. Phenotypes were categorized according to their eye size and the expression intensity compared to the control: (C) weak, small eyes, normal expression intensity; (D) small eyes, weak expression; (E), missing eyes and expression. (B) Heat treated wild type control. (F) Quantitative results of the injections using rx2 in situ hybridization. Scale bar 100 µm.

Figure 6. Aes-mediated Gro/Tle loss of function phenotypes.

(A) Schematized presentation of full length Tle protein, the Q-domain, and Aes. For transgenic lines, embryos at the 1-cell stage were injected with 20 ng/µl of DNA (Gfp:HSE:Aes and Gfp:HSE:Q). The F1 generation was heat-induced (10 min, 43.5°C) at stage 15/16. (B-K) Embryos are shown in dorsal view, anterior to the top. (F-K) Flat mounts. (C-D) Phenotypes of the Aes/Q-mediated Gro/Tle loss of function were

categorized according to their eye phenotype into: (C-C") weak, smaller eyes tilted towards the midline; (D-D") moderate, beginning cyclopia anterior; strong (E-E"), cyclopic eye. For whole mount in situ hybridization experiments (F-K), using the indicated digoxigenin-labelled RNA probes, fixation was performed at stage 21; heat treatment occurred as described before. (I) rx2 expression indicates a reduction in eye size, the eyes are tilted at the anterior end towards the midline (arrowheads); (J) Bf1 expression is reduced; (K) Wnt1 expression indicates a reduction in midbrain size and shows an indistinct expression pattern throughout the midbrain (arrows). (B-B", F-H) control embryos were heat-treated wild type embryos. Scale bars 100 μm; B, B-E"; F, F-K.

ADDITIONAL FILES

Additional File 1. Overview of the PNA and MO induced loss of function phenotypes.

Embryos at the 1-cell stage were injected with PNAs or MOs at the indicated concentrations. Phenotypes were categorized according to the size of the eyes into: weak, slightly smaller eyes; moderate, smaller eyes; strong, eye-less. Abbreviations: PNA, peptide nucleic acid; MO, morpholino oligonucleotides.

Additional File 2. Gro/Tle dependence of tcf3 in gain-of-function experiments

Embryos at the 1-cell stage were co-injected with 40 ng/μl of the indicated gfp:HSE:Tcf3 constructs. Heat treatment (10 min, 43.5°C) was applied at stage 14. (A) Statistical overview of the phenotype distribution. Whole mount in situ hybridization experiments for rx2 were performed on embryos at stage 21. (B) dorsal view of a stage 31 embryo with anterior at the top, (C) lateral view with anterior at the left. Arrowheads indicate ectopic otic vesicles, the arrow points to the endogenous otic vesicle. Scale bar 100 μm; B, B and C.

Additional File 3. Mammalian two-hybrid analysis of Aes-mediated Gro/Tle repression.

20 ng of the expression constructs (pMCamVP16, pMCTle4VP16 or pMCTle1VP16) were co-transfected with 70 ng of firefly luciferase reporter construct pLucF24ZF, 20 ng of the expression construct for the six-domain of human Six3 (pMChSix3(85-203)mZFb6) and full length Aes (pKCAes at the indicated concentrations) into HeLa cells. The interaction of the artificial leucine zipper domain "acid" and "base" (Zitat) was used as a control. All three interactions were set 100% in the absence of Aes (acid/base corresponds to a more than 100 fold activation of the luc reporter construct compared to a control without bait, similar induction rates were seen for Tle4/Six3 and Tle1/Six3). Addition of the Aes expression construct at the indicated concentrations did not affect the acid/base interaction (blue bars), but strongly reduced the Tle4/Six3- (red bars) and the Tle1/Six3 interaction (green bars).

Additional File 4. MO-induced gro/tle loss of function phenotypes.

Embryos at the 1-cell stage were co-injected with morpholino oligonucleotides and 1 µg/ml FITC-dextran. Injections were performed using either a single morpholino directed against tle1 (C), tle2b (D,F), and tle3b (E), or combinations directed against tle1+2b (H), tle1+3b (I), tle2b+3b (J), and tle1+2b+3b (K). Single morpholino oligonucleotides were injected at a concentration of 600 µM (C-F) and combinatorial injections (H-K) were performed using 300 µM of each MO. Phenotypes of FITC-dextran positive embryos were observed after the beginning of eye pigmentation at stage 32 (B-F) and stage 28 (G-K). (B,G) Wild type control embryos were injected with 1x Yamamoto's and FITC-dextran. All embryos are shown in dorsal view with anterior at the top. Compared to the wild type controls (B,G), morpholino injected embryos developed smaller eyes that were shifted towards the midline (D,E,J,K) or cyclopic eyes (C,H,I). In rare cases the eyes were lost entirely (E). (A) Phenotypes of FITC-positive embryos were categorized at stage 28-32 into weak and strong phenotypes. Weak phenotypes developed smaller eyes that were shifted towards the midline, whereas strong phenotypes showed cyclopic eyes. Eye-less phenotypes were included into the group of strong phenotypes. *) Included in the group "stong phenotypes". Abbreviations: MO, morpholino oligonucleotide; WT, wild type. Scale bar 100 µM.

Figure 1

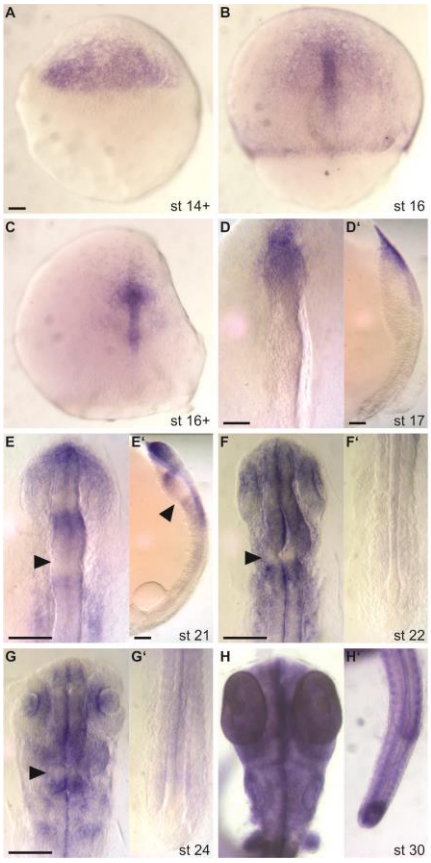

Figure 2

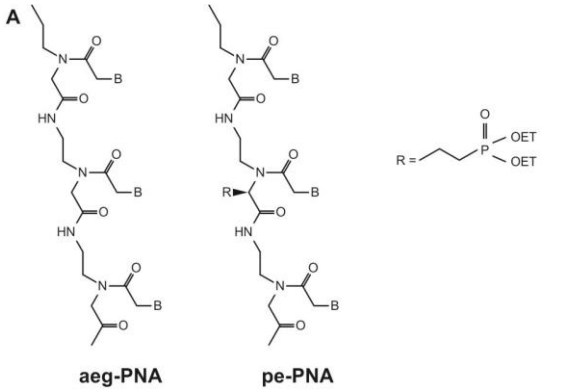

Figure 3

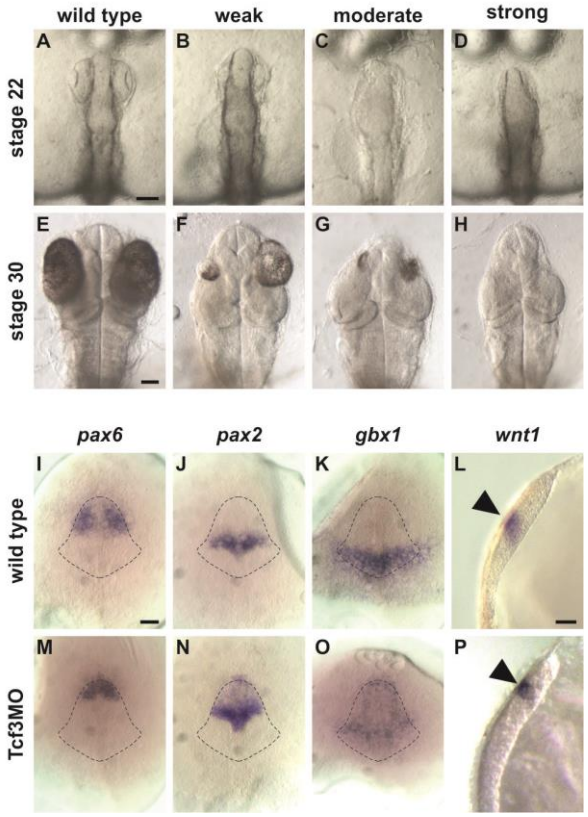

Figure 4

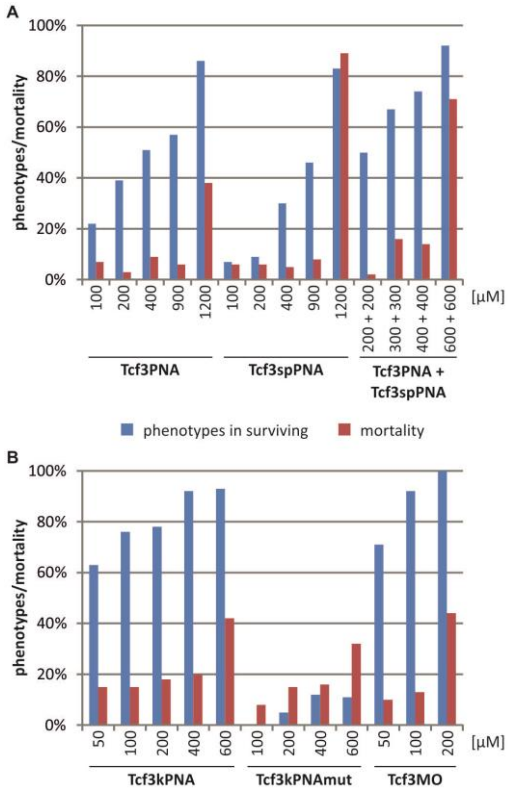

Figure 5

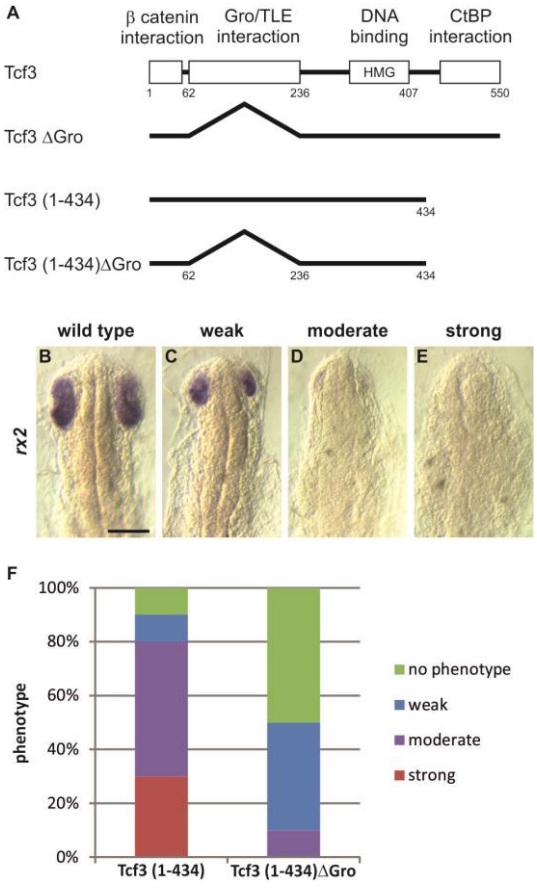

Figure 6

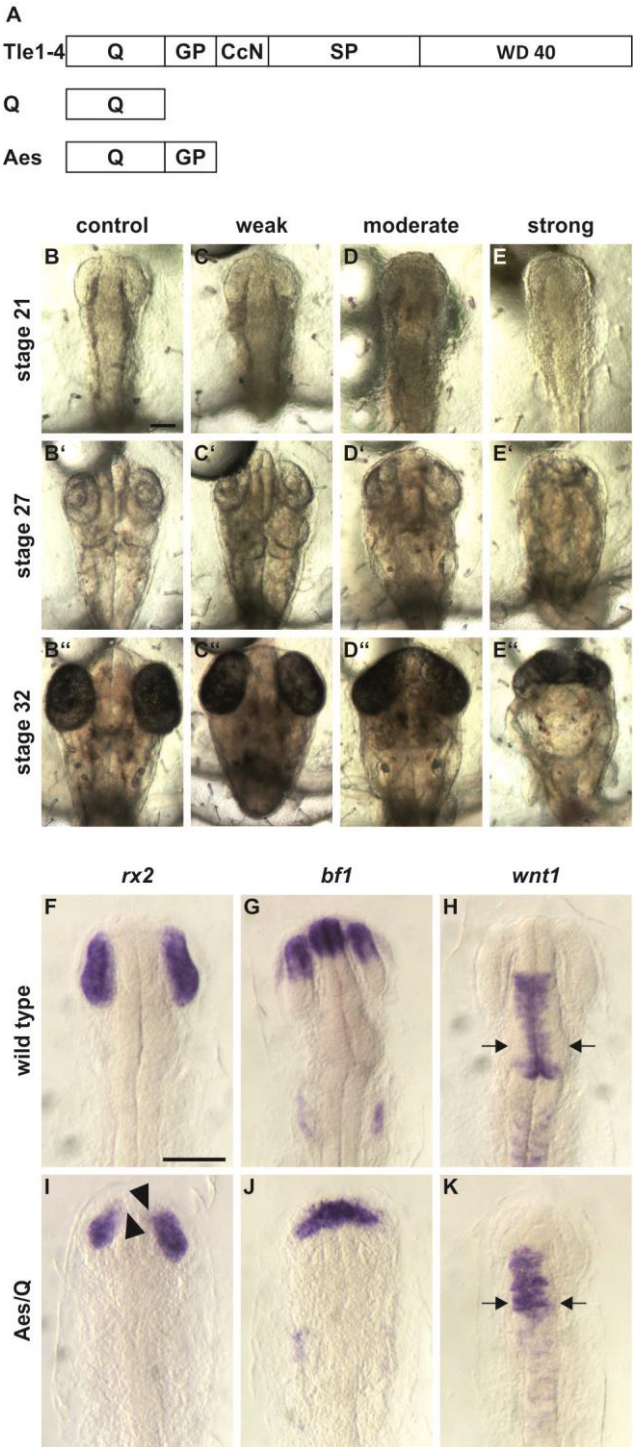
A
Tle1-4
Q
GP
CcN
SP
WD 40
Q
Q
Aes
Q
GP
control
weak
moderate
strong
stage 21
stage 27
stage 32
B
C
D
E
B'
C'
D'
E'
B''
C''
D''
E''
rx2
bf1
wnt1
wild type
Aes/Q
F
G
H
I
J
K

Additional File 1

	concentration [µM]	0	50	100	200	400	600	900	1200	200+200	300+300	400+400	600+600
Tcf3PNA	number of embryos	17		72	72	110	123	52	90				
	dead	1		5	2	10	8	3	34				
	death rate	6%		7%	3%	9%	7%	6%	38%				
	strong phenotype	0		0	2	10	15	3	24				
	moderate phenotype	0		3	7	12	17	10	12				
	weak phenotype	0		12	18	29	33	15	12				
	normal	16		52	43	49	50	21	8				
	phenotypes in surviv.	0%		22%	39%	51%	57%	57%	86%				
Tcf3spPNA	number of embryos	45		32	34	59	101	83	55				
	dead	2		2	2	3	21	7	49				
	death rate	4%		6%	6%	5%	21%	8%	89%				
	strong phenotype	0		0	0	2	11	6	1				
	moderate phenotype	0		0	1	5	8	11	1				
	weak phenotype	0		2	2	10	20	18	3				
	normal	43		28	29	39	41	41	1				
	phenotypes in surviv.	0%		7%	9%	30%	49%	46%	83%				
Tcf3PNA+Tcf3spPNA	number of embryos	37								45	93	121	42
	dead	1								1	15	17	30
	death rate	3%								2%	16%	14%	71%
	strong phenotype	0								2	20	24	2
	moderate phenotype	0								7	18	19	0
	weak phenotype	0								13	14	34	9
	normal	36								22	26	27	1
	phenotypes in surviv.	0%								50%	67%	74%	92%
Tcf3kPNA	number of embryos	19	47	48	45	92	78	42					
	dead	3	7	7	8	18	33	30					
	death rate	16%	15%	15%	18%	20%	42%	71%					
	strong phenotype	0	15	6	6	26	21	7					
	moderate phenotype	0	6	6	11	26	10	0					
	weak phenotype	0	4	19	12	16	11	0					
	normal	16	15	10	8	6	3	5					
	phenotypes in surviv.	0%	63%	76%	78%	92%	93%	58%					
Tcf3kPNAmut	number of embryos	25		24	46	49	53						
	dead	3		2	7	8	17						
	death rate	12%		8%	15%	16%	32%						
	strong phenotype	0		0	0	1	0						
	moderate phenotype	0		0	0	1	1						
	weak phenotype	0		0	2	3	3						
	normal	22		22	37	36	32						
	phenotypes in surviv.	0%		0%	5%	12%	11%						
Tcf3MO	number of embryos	9	171	112	34								
	dead	1	17	14	15								
	death rate	11%	10%	13%	44%								
	strong phenotype	0	65	66	16								
	moderate phenotype	0	19	19	2								
	weak phenotype	0	25	5	1								
	normal	8	45	8	0								
	phenotypes in surviv.	0%	71%	92%	100%								

Additional File 2

A

	rx2	
	Tcf3(1-434)	Tcf3(1-434)ΔGro
Embryos	10	10
Weak phenotypes	1	4
Moderate phenotypes	5	1
Strong phenotypes	3	
Total phenotypes	90%	50%

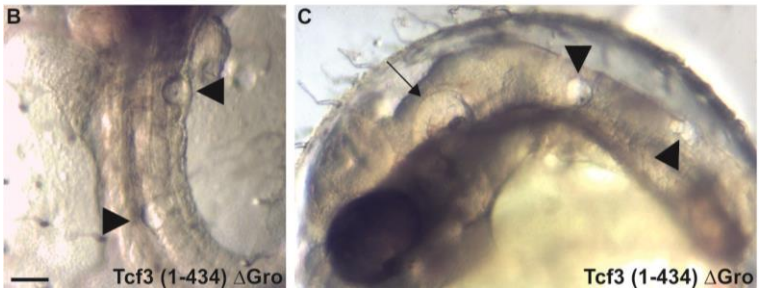

Additional File 3

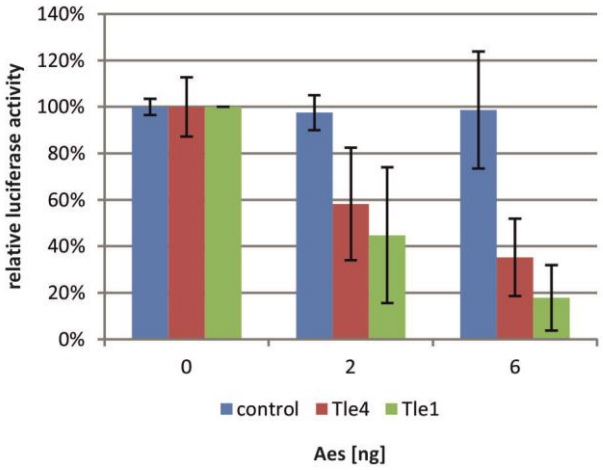

Additional File 4

A

Morpholino Concentration	*tle 1* 600 µM	*tle 2b* 600 µM	*tle 3b* 600 µM	*tle 1+2b* 300 µM each	*tle 1+3b* 300 µM each	*tle 2b+3b* 300 µM each	*tle 1+2b+3b* 300 µM each
Embryos	95	267	117	55	115	45	58
Dead	11	30	6	11	16	5	4
Mortality	12%	11%	5%	20%	14%	11%	7%
Weak	4	12	1	7	16	3	1
Moderate	2	11	10	0	1	3	5
Strong	2	16	2	5	4	0	3
Eye-less*)	0	7	1	3	3	0	0
Eye phenotypes in surviving embryos	10%	16%	12%	27%	21%	15%	17%

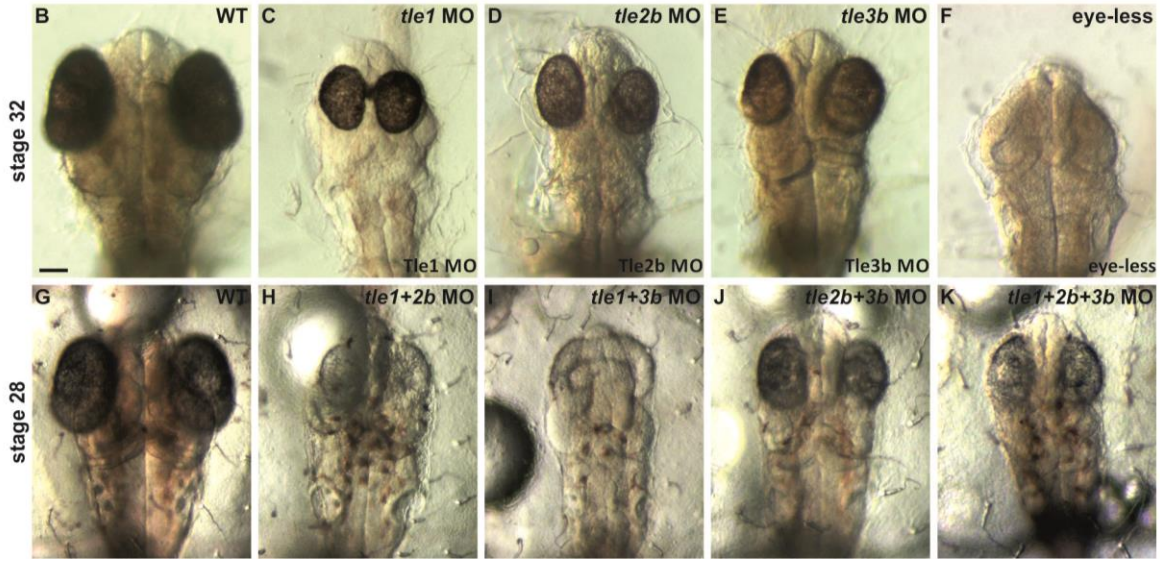

Jung *et al. BMC Biotechnology* 2013, **13**:53
http://www.biomedcentral.com/1472-6750/13/53

BMC Biotechnology

RESEARCH ARTICLE Open Access

Diffusion of small molecules into medaka embryos improved by electroporation

Gerlinde Jung[1], Markus Hug[1], Christian Halter[2], Andrea Friesenhengst[1], Johann Walzer[2] and Thomas Czerny[1*]

Abstract

Background: Diffusion of small molecules into fish embryos is essential for many experimental procedures in developmental biology and toxicology. Since we observed a weak uptake of lithium into medaka eggs we started a detailed analysis of its diffusion properties using small fluorescent molecules.

Results: Contrary to our expectations, not the rigid outer chorion but instead membrane systems surrounding the embryo/yolk turned out to be the limiting factor for diffusion into medaka eggs. The consequence is a bi-phasic uptake of small molecules first reaching the pervitelline space with a diffusion half-time in the range of a few minutes. This is followed by a slow second phase (half-time in the range of several hours) during which accumulation in the embryo/yolk takes place. Treatment with detergents improved the uptake, but strongly affected the internal distribution of the molecules. Testing electroporation we could establish conditions to overcome the diffusion barrier. Applying this method to lithium chloride we observed anterior truncations in medaka embryos in agreement with its proposed activation of Wnt signalling.

Conclusions: The diffusion of small molecules into medaka embryos is slow, caused by membrane systems underneath the chorion. These results have important implications for pharmacologic/toxicologic techniques like the fish embryo test, which therefore require extended incubation times in order to reach sufficient concentrations in the embryos.

Keywords: Medaka, Small molecules, Diffusion, Toxicology, Electroporation, LiCl

Background

Japanese medaka (*Oryzias latipes*) are small egg-laying freshwater fish that are native to brackish waters and rice paddies in South-East Asia. Economic husbandry, high fecundity, and ex utero development make them a popular vertebrate model organism in developmental biology and molecular genetics and their transparent chorion facilitates non-invasive observation. Furthermore, they are very hardy and highly resistant to common fish diseases (reviewed in [1]). These properties make medaka ideal for testing of toxic substances [2-5].

Toxicity tests are conducted to evaluate the adverse effects of chemicals or biological substances on organisms and are mainly performed by animal experiments. Even if testing of cosmetic and personal care products has been reduced over the last years, there remain numerous chemicals, such as pharmaceuticals or food additives, where animal tests are necessary. On the other hand, several programs like the OECD HPV (High Production Volume) Program or the European Union REACH (Registration, Evaluation, Authorization and Restriction of Chemicals) initiative were introduced to regulate the chemical industry globally (reviewed in [6]). They require extensive test regimes for most chemicals. Without further alternatives, these new regulations would therefore dramatically increase the number of animal experiments, particularly for mammals and birds.

Historically, fish toxicity testing plays an important role in ecotoxicology and aquatic toxicology. It is however a controversial question, whether adult fish can be a replacement for mammals and birds, because they may experience the same levels of pain and distress. One alternative is the use of embryos [7,8]. In the fish embryo toxicity (FET) test, newly fertilized eggs are exposed to a chemical for 48 hours and various lethal and sub-lethal endpoints are recorded as described by Lammer and

* Correspondence: thomas.czerny@fh-campuswien.ac.at
[1]Department for Applied Life Sciences, University of Applied Sciences, FH Campus Wien, Helmut-Qualtinger-Gasse 2, A-1030, Vienna, Austria
Full list of author information is available at the end of the article

colleagues [9]. Due to their high fecundity and the synchronous extra-uterine development of the transparent embryos, fish are particularly well suited for such a strategy. Most FET tests have been conducted with zebrafish but inter-species comparison with fathead minnow and medaka demonstrated applicability also for other species [10]. Furthermore, fish embryos are suitable for adaption to high throughput protocols [11].

Contrary to zebrafish, medaka embryonic development is relatively long, thus providing extended time for testing. In combination with their hardiness, medaka embryos therefore represent an ideal system for toxicologic/pharmacologic testing. During FET tests the substances have to diffuse into the developing embryo. Medaka embryos are surrounded by an acellular envelope, the chorion, which protects the developing embryo from environmental influences. Once fertilized, the chorion turns into a rigid structure [12] and might therefore act as an effective barrier that protects the embryo also against chemicals.

Compared to zebrafish, we found a substantially reduced sensitivity for chemicals like lithium chloride for medaka. Closer inspection revealed a limiting diffusion rate of membranes positioned closely to the embryo. Contrary to our expectations, the rigid outer chorion is readily passed by small molecules. In an effort to overcome these problems, we tested the addition of detergents. This effectively improved diffusion, but also affected the internal distribution of the chemicals. Electroporation also enhanced the uptake of fluorescent tracer molecules. When applied to Wnt-signalling, electroporation facilitated the transfer of the GSK-3 inhibitor lithium, thereby inducing deficiencies in medaka anterior-posterior development, similar to those reported for zebrafish [13].

Methods

Fish stocks and maintenance

Japanese medaka from the wild-type cab strain were used for this study. Adult fish were maintained at 26°C with an artificial 14 hours light and 10 hours dark cycle. Stages were determined according to Iwamatsu [14].

Dechorionation using hatching enzyme

For dechorionation, the embryos were placed in a small drop of water on a plastic surface. Excess liquid was removed and hatching enzyme was added (10 μl hatching enzyme per 15 embryos). The embryos were incubated at 27°C until holes appeared in the chorion. The remaining chorion was removed using forceps and the embryos were kept in ERM (17 mM NaCl; 0.4 mM KCl; 0.27 mM $CaCl_2$; 0.65 mM $MgSO_4$) in dishes coated with agarose.

Hatching enzyme was prepared as follows: embryos with visible hatching glands were homogenized in pre-cooled PBS (0.75 μl PBS per embryo), incubated over night at 4°C and debris was removed by centrifugation (15.000 rpm, 4°C, 10 minutes). The hatching enzyme solution was stored in aliquots at −20°C.

Diffusion experiments

Sodium fluorescein (Roth; 10 mg/ml), rhodamine B (Roth; 10 ng/ml) and acridine orange (Roth; 1 μg/ml) solutions were prepared in 1x Yamamoto's medium (0.128 M NaCl; 0.27 mM KCl; 0.14 mM $CaCl_2$; 0.24 mM $NaHCO_3$). Four embryos were incubated in 50 μl staining solution for 40 minutes (if not mentioned otherwise) at 27°C protected from light. Standard post incubation washes were performed with 0.5 ml ERM at room temperature on a shaker. The embryos were washed 3 times with fresh ERM in the first seven minutes and subsequently 10, 20, 30 and 60 minutes after the incubation.

For yolk injections, sodium fluorescein (10 mg/ml) was injected into the yolk using a microinjector (Eppendorf) and borosilicate glass capillaries (Clark Electromedical Instruments).

For methylene blue diffusion, 0.001% methylene blue in 1x ERM was used. The embryos were incubated for 10 minutes at 27°C. Standard washing steps were performed as described above.

Quantification of fluorescence intensity

Embryos were examined *in vivo* by fluorescence microscopy using a Nikon Eclipse TS100 inverted microscope equipped with an Infinity 2 camera. Pictures with defined exposure times were taken and the fluorescence intensity was quantified from the pictures with the ImageJ software [15]. The quantification of internal concentrations was performed by measuring the fluorescence intensity at different time points of washing and extrapolating back to time zero (start of washing).

As a reference we used empty cellulose sulphate beads with an average diameter of 730 μm [16], which were soaked with different concentrations of the fluorescent dyes for several days to reach equilibration. The beads were shortly washed and then transferred into mineral oil, where they were immediately quantified as described above.

Electroporation

Electroporation of medaka embryos was performed in 1× Yamamoto's medium. Prior to electroporation the embryos were pre-incubated with the staining solution for 40 minutes in Gene Pulser® disposable Cuvettes with 0.4 cm gap width (Bio-Rad) at 27°C and then electroporated in the same cuvettes. For better comparison, the control experiments were also performed in cuvettes omitting the electroporation pulses. Electroporation was performed with a home-made device

Jung *et al. BMC Biotechnology* 2013, **13**:53
http://www.biomedcentral.com/1472-6750/13/53

consisting of a function generator (sine wave with added DC-voltage and variable modulation depth), a pulse generator (generating a defined number of pulses with varying length), a switch (regulated by the pulse generator, controlling the output of the function generator to the amplifier) and an amplifier connected to the cuvette filled with 100 µl 1× Yamamoto's medium. An oscilloscope was used to display the signals. The conditions for the experiments were: modulation frequency 1 to 10^5 Hz, modulation depth 1; voltage 5 to 50 V; 1 to 3 pulses with intervals of varying length.

For the experiments mimicking chorion diffusion alone, dead embryos were prepared as follows: fifty embryos at stage 17 were electroporated in 400 µl 1× Yamamoto's medium using 3 pulses of 60 ms with 200 ms interval, 60 V, 0.5 A and 35 kHz, followed by 30 minutes incubation in 1× ERM at 27°C.

Lithium chloride

Embryos at stage 14 were incubated in 100 µl 0.4 M lithium chloride (Roth) solution for 10 minutes at 27°C, followed by electroporation using the following settings: modulation frequency 330 Hz; voltage 15 V; pulse time 100 ms; 1 pulse. After diffusion and electroporation the embryos were washed as described before. Embryos were examined *in vivo* by light microscopy using a Zeiss Stemi 2000-C microscope equipped with an AxioCam HRc camera.

Results

We previously tested the effects of the Wnt signalling pathway on medaka anterior-posterior development by overexpressing *wnt1* [17]. Another well-established way to activate this pathway is the application of the GSK-3 inhibitor lithium [18]. However, when we used conditions established for zebrafish embryos [13] no effects could be observed. Except at very high concentrations (above 1 M) where a low number of embryos showed phenotypes. We therefore reasoned that the diffusion through the chorion into the embryos was not efficient. In order to understand this problem in more detail and to find possible solutions, we started analysing the diffusion properties of the embryo's chorion and membranes. As small and easily quantifiable molecular tracers we selected fluorescing substances.

Diffusion into medaka embryos

We compared several fluorescing small molecules. Depending on their molecular properties, they were effective at variable concentrations and differed in their distribution within the egg (embryo/yolk). We finally selected fluorescein, which showed enrichment within the embryo (see below) and therefore appeared well suited as a model for small molecules affecting embryonic development. To quantify the uptake, we compared fluorescence spectroscopic determination of egg extracts and quantification of live embryos under a fluorescence microscope (measurement of pixel intensity of microscopic pictures, for details see Materials and Methods). Although the spectroscopic measurements were more sensitive, we selected the microscopic determination of fluorescence intensity as a standard quantification method. This allowed us to follow the same individuals during different stages of development and thereby to qualify tissue distribution, phenotypic alterations and survival of the embryos.

To determine the optimal conditions, the embryos were incubated in the staining solution at 27°C with variable concentrations of fluorescein for different durations. Best quantifiable results were obtained after 40 min incubation with 10 mg/ml fluorescein and 30 min washing time. Even at considerable higher concentrations (100 mg/ml), fluorescein did not cause any phenotypic alterations in the embryos. These conditions allowed sensitive quantification of the internalized dye over a wide linear range and the settings were therefore applied to all further diffusion experiments. We first analysed the uptake of fluorescein during medaka embryonic development. At the 1-cell stage the internalized fluorescein was localized almost exclusively in the zygote (Figure 1A) and remained in the proliferating cells during early development (Figure 1B). Also later, fluorescence was detected preferentially in the embryo (Figure 1C). For incubation shortly before hatching the signal became enriched in the embryonic liver (Figure 1D). Measurement of the pixel intensity showed a relatively constant fluorescein uptake throughout all developmental stages, except from the 4-cell stage to early morula where the signal slightly increased (Figure 1E).

We also looked at the fate of fluorescein. For this, embryos at the 1-cell stage were treated as described before, but the fluorescence signal was determined after 4 days of incubation in ERM. This extensive washing removed the majority of fluorescein. However, residual fluorescence was detected in the gallbladder and the liver. Even in bright field pictures (Additional file 1) yellow staining of fluorescein can be seen in the gallbladder. Therefore, the fate of fluorescein in older medaka embryos is comparable to that of mammals [19].

Diffusion barriers within the medaka egg

Overall, the amount of internalized fluorescein was relatively low. After 40 minutes of in-diffusion between 3 and 9 µg/ml (uniform distribution assumed) were detected in the embryo which represents less than 0.1% of the external concentration (10 mg/ml). Due to the high concentration in the supernatant the internal fluorescein concentration could not be quantitated during in-diffusion. In order to learn more about the kinetics we therefore analysed the out-diffusion. Several fast washing

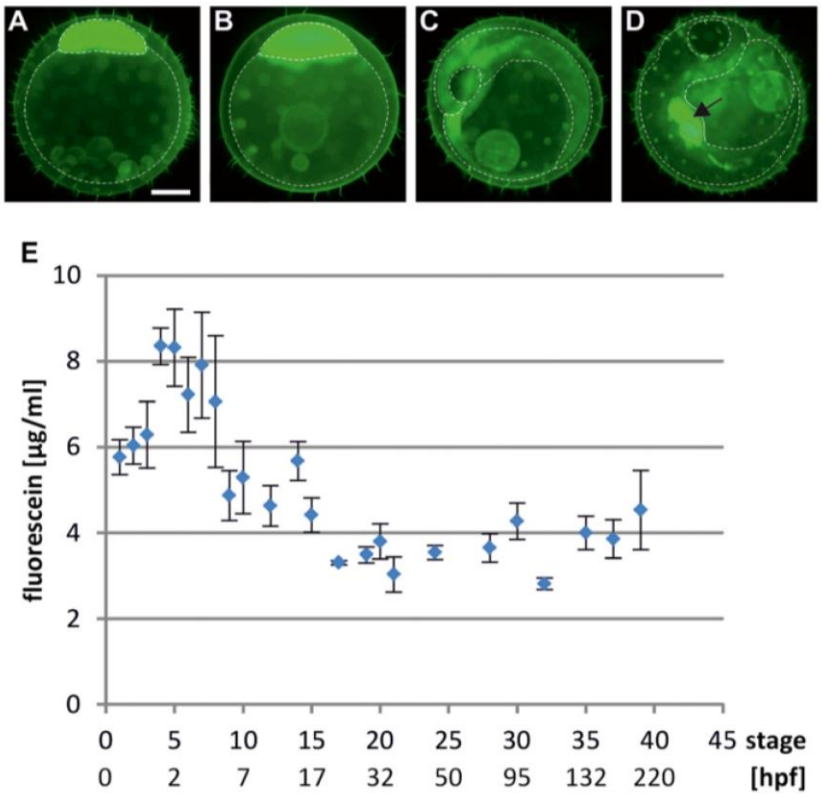

Figure 1 Diffusion of the small molecule fluorescein into the medaka embryo. Embryos at various stages were incubated with 10 mg/ml fluorescein for 40 minutes at 27°C. Pictures were taken after 30 minutes of washing and the fluorescence intensity was measured. The dotted lines demarcate the outlines of: (**A**,**B**) yolk and blastoderm, and (**C**,**D**) yolk and embryo. Embryos are shown in lateral view. Black arrow indicates the liver and gall bladder. (**A**-**D**) Distribution of fluorescein uptake during four representative embryonic stages: **A**, stage 2a; **B**, stage 8; **C**, stage 26; **D**, stage 38. The internal concentration of fluorescein (average distribution in embryo/yolk assumed) for different embryonic stages is shown in (**E**). Scale bar 250 µM. Abbreviations: hpf, hours post fertilization.

steps directly after the incubation were necessary to remove excess material from the surface of the eggs. First reproducible results were obtained after 7 min of washing (including a 3-fold exchange of the supernatant). Additional measuring points after 20, 30, 60, 90 and 120 minutes revealed two phases for diffusion: a fast loss of signal during the first 30 minutes, followed by a slower second phase (Figure 2A). Calculation of the diffusion half-times for fluorescein resulted in 4 minutes for the first, and 2.4 hours for the second phase.

Based on the bi-phasic out-diffusion observed for fluorescein, we questioned which structures of the medaka egg are responsible for the diffusion kinetics. The egg is shielded by a rigid acellular envelope, the chorion, which represents a prime candidate for a diffusion barrier [3]. However, inside the chorion the embryo and the yolk are covered by additional extra-embryonic membrane systems, which could also affect diffusion. In order to differentiate between these possibilities we manipulated the eggs. In eggs with dead embryos the yolk and membranes shrink to a small ball within the chorion (Figure 2B,C). The quantified fluorescence signal in the egg therefore mainly depends on the diffusion through the chorion. In order to qualify the diffusion properties of the membrane systems covering embryo and yolk, we used hatching enzyme to dechorionate the eggs (Figure 2B,D; for experimental details see Methods).

Quite unexpectedly, diffusion of fluorescein into dead embryos resulted in strong fluorescence (Figure 2C'), indicating that the chorion is readily passed by small molecules. Quantification of the signals (Figure 2E, for details see Methods) showed that the interior concentration almost reached saturation after 40 minutes (50% after 20 minutes). On the other hand, diffusion into dechorionated embryos was extremely slow, resulting in an average concentration similar to that for intact eggs (<0.1%) after 40 minutes (some of the dechorionated embryos showed high signals, which was however due to

Jung *et al. BMC Biotechnology* 2013, **13**:53
http://www.biomedcentral.com/1472-6750/13/53

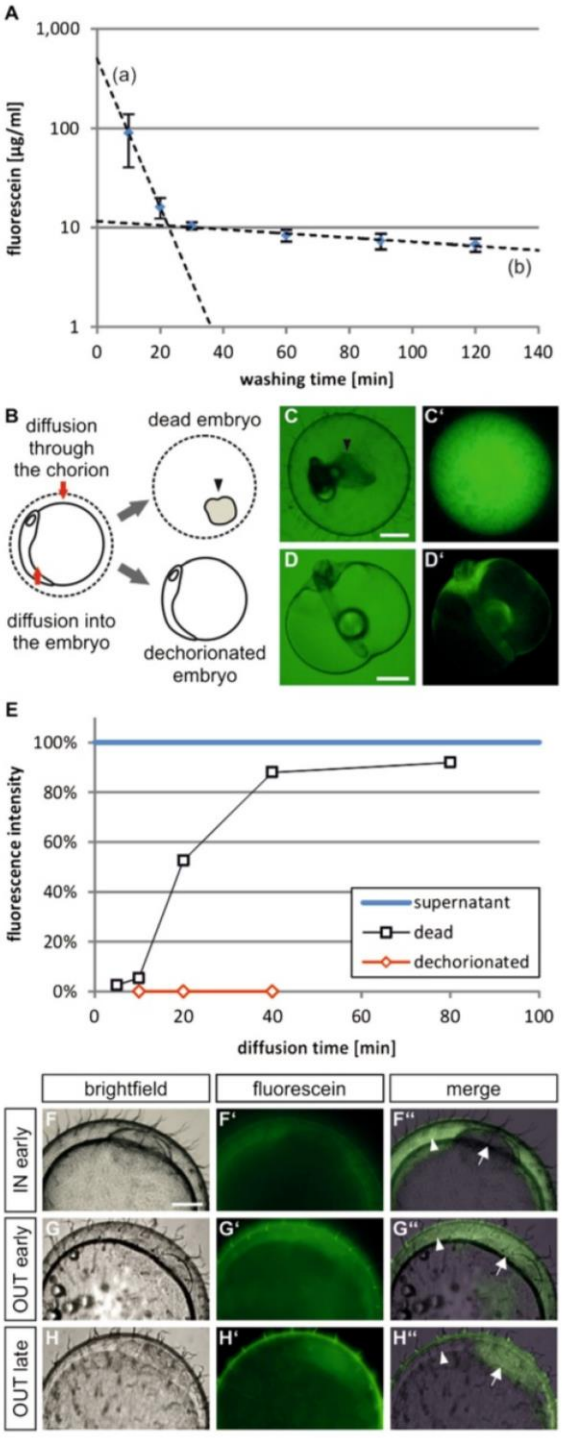

Figure 2 (See legend on next page.)

(See figure on previous page.)
Figure 2 Diffusion barriers within the medaka egg. Stage 17 embryos were incubated with 10 mg/ml fluorescein for 40 minutes at 27°C and internal concentrations were determined at different time points of washing (**A**; mean values of 8–10 eggs are shown +/− SEM). (**A**) Dotted lines indicate the bi-phasic out-diffusion: (**a**) fast loss of the signal (first 2 measuring points), (**b**) slower second phase (best-fit of last 4 measuring points). (**B**, left side) shows a schematic view of an egg and the consecutive diffusion steps (red arrows). (**C**) Bright field picture of a dead embryo, representing diffusion through the chorion; the black arrow head indicates the shrunken embryo/yolk with the surrounding membranes. (**D**) Dechorionated embryo at stage 22 in dorsal view with anterior being at the top, (**C'**, **D'**) corresponding fluorescent images. (**E**) Concentrations of fluorescein in dead or dechorionated embryos after different incubation times. The concentration of the supernatant (blue) was set to 100%. Several measuring points (7, 20 and 30 min) were taken and the initial concentration at the onset of the washing calculated by extrapolation (compare **A**). (**F**-**H**) Eggs in brightfield, fluorescence and merged pictures. (**F**-**F"**) Distribution of fluorescein after 10 minutes of in-diffusion (IN early) and 2 minutes of washing (1 mg/ml fluorescein). (**G**-**G"**) Out-diffusion after 40 minutes of incubation (10 mg/ml fluorescein) and 5 minutes washing (OUT early) and (**H**-**H"**) same conditions as in (**G**) but 30 minutes of washing time. Scale bar 250 μM.

disruption of the fragile membranes). Therefore, not the chorion, but membrane systems within the medaka egg represent the main diffusion barrier for small molecules. These data would predict that diffusion of small molecules into intact embryos should rapidly proceed through the chorion into the perivitelline space, but would then be stopped at inner membranes. To test this hypothesis also with life embryos, we looked at eggs shortly exposed to fluorescein (10 minutes), which should be sufficient to reach high signal levels in the perivitelline space, but not in the embryo. Indeed, after a short washing step (2 minutes) the expected distribution was visible (Figure 2F-F"). Based on the previous experiments (Figure 1), the cells of the embryo should however show a signal when exposed for longer times (40 minutes). After a short washing step fluorescein should therefore be detectable in both the perivitelline space and the embryo (Figure 2G-G"; white arrowhead and arrow, respectively). During extended washing fluorescein should rapidly disappear from the perivitelline space (fast out-diffusion), but a signal would be retained in the embryo (slow out-diffusion). The expected results could be observed (Figure 2H-H"). In order to verify this model also with another small molecule we tested methylene blue. As seen for fluorescein, methylene blue rapidly (after 10 minutes of incubation) accumulated in the perivitelline space (Additional file 2A). Longer washing times (20 minutes) quickly removed methylene blue again, but no signals were detectable in the cells of the embryo (Additional file 2B).

An internal diffusion barrier is also in perfect agreement with the bi-phasic out-diffusion profile (Figure 2A). The first phase represents loss of fluorescein from the perivitelline space (line a) and the second phase (line b) is caused by the considerably slower diffusion out of the embryo/yolk (resulting in a low steady state concentration in the perivitelline space). The half-time calculated for the initial out-diffusion (4 minutes) roughly fits to that of in-diffusion through the chorion (20 minutes; a factor of 5 differing the values can be explained by the larger interior volume of dead embryos compared to that of the perivitelline space). Therefore, the slow diffusion of small molecules into medaka embryos is caused by membrane systems close to the embryo and dechorionation does not improve the uptake.

Detergents affect membrane behaviour

In an attempt to overcome this diffusion barrier, we first focussed on the injection of the small molecules. Injection into single cells of the embryo is well established for early stages of development, leading to a rapid distribution in all cells of the embryo. During later development injection into large internal cavities, like the neural tube, would be an option. However this is again limited to certain stages. In order to accomplish uniform diffusion into the embryos, we tested injection into the yolk, a method that is often performed in zebrafish. Within 30 minutes the injected fluorescein evenly distributed throughout the yolk (Additional file 3A-C and F-G). However, the detection of signals in the embryo was only possible after 4 hours (Additional file 3D,K) and the obtained concentrations were low. Furthermore, yolk injection in medaka results in low reproducibility, due to rapid clogging of the injection needles by the sticky yolk.

Next we tested incubation of the embryos with detergents. Contrary to ionic detergents like SDS, which appeared highly toxic, Triton X-100 worked well. The embryos tolerated concentrations up to 0.01% (40 minutes incubation) without showing phenotypes. At 0.03% Triton X-100, the survival was reduced to 69% and for 0.1% Triton to 25%, but no obvious phenotypes were detectable in the surviving embryos. Co-incubation with 0.03% Triton X-100 increased the fluorescein uptake of the eggs by a factor of 6 compared to control embryos treated with ERM (Figure 3A,D; 30 minutes of washing; note that different exposure times were used for the pictures). Interestingly, extended washing did not reduce the intensity of the fluorescent signal of detergent treated embryos (Figure 3D-F), indicating that the dye became trapped in the embryo/yolk. The signal intensity therefore increased to 20 fold after 60 minutes and to more than 80 fold after 24 hours (Figure 3B,E and C,F) compared to the control embryos at the same time points. Furthermore, Triton-treated eggs showed signals throughout the embryo

Jung *et al. BMC Biotechnology* 2013, **13**:53
http://www.biomedcentral.com/1472-6750/13/53

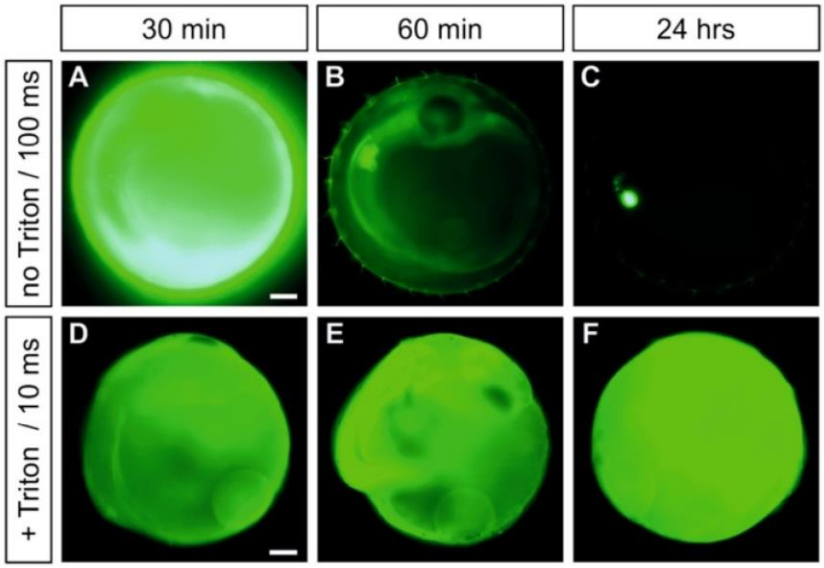

Figure 3 Incubation with detergents. 3 day old embryos incubated for 40 minutes with fluorescein (10 mg/ml) at different time points of washing without addition (**A**-**C**; no Triton), or together with 0.03% Triton X-100 (**D**-**F**; + Triton). Embryos are shown in lateral view, anterior to the top. Note that pictures (**A**-**C**) were taken with 100 ms exposure time, whereas (**D**-**F**) with 10 ms. The accumulation of fluorescein in the liver/gallbladder at later stages can be seen in (**C**). Scale bar 250 μM.

and the yolk (Figure 3D-F), whereas fluorescein was clearly enriched in the embryos of non-treated eggs (Figure 3B and Figure 1A-D). Therefore, addition of Triton X-100 improves the uptake of small molecules into the egg, but also affects their distribution between compartments, making the assessment of pharmacologic/toxicologic properties difficult.

Electroporation improves small molecule uptake into embryos

Another method for enhanced transport across membranes is electroporation. Hostetler and colleagues used direct current-shifted radio frequency pulses to generate transgenic medaka fish [20]. We used the same conditions as a starting point (modulation frequency, 35 kHz; voltage, 25 V; pulse duration, 10 ms; using 3 pulses with 1 second pulse interval) and measured the fluorescence intensity of fluorescein in electroporated stage 17 embryos. Due to the fact that fluorescein readily passes the chorion, we incubated the eggs prior to electroporation for 40 minutes with the staining solution. As a result high concentrations of the dye accumulated in the perivitelline space (compare Figure 2F"). To overcome the rate limiting membrane systems we applied electric pulses varying the voltage and pulse duration over a wide range. Finally, we obtained optimal fluorescence intensity and survival at 15 V and 5 seconds pulse duration (Figure 4A and Additional file 4). In contrast to Hostetler and colleagues, these conditions represent a single pulse of extended length, but with comparable low voltage. Additional pulses did not improve fluorescein uptake into the embryos. Nevertheless, other combinations, such as high voltage with short pulses also resulted in significantly higher fluorescence intensity than diffusion alone. However, the combination of long pulses with high voltage was impossible to apply due to a reduced survival rate. The same conditions were also applicable for younger (Figure 4B') and older embryos (Figure 4C').

In order to verify that electroporation improves the rate limiting diffusion through inner membrane systems, we performed the same experiments with dead and dechorionated embryos (Figure 5). Electroporation did not change the signal intensity of fluorescein in dead embryos, indicating that it has no effect on the uptake through the chorion (Figure 5A,C,F), whereas dechorionated embryos showed a nearly 15-fold increase of dye intensity after electroporation (Figure 5A,D,G). Therefore, similar to whole embryos (Figure 5A,B,E), the dechorionated embryos still contain membranes acting as diffusion barriers, which can be made permeable by electroporation.

The electroporation experiments presented so far had been performed with modulation frequencies of 35 kHz. We next varied this frequency and found considerable differences in signal intensity. The optimum for fluorescein uptake appeared at 330 Hz (Figure 6A). In order to

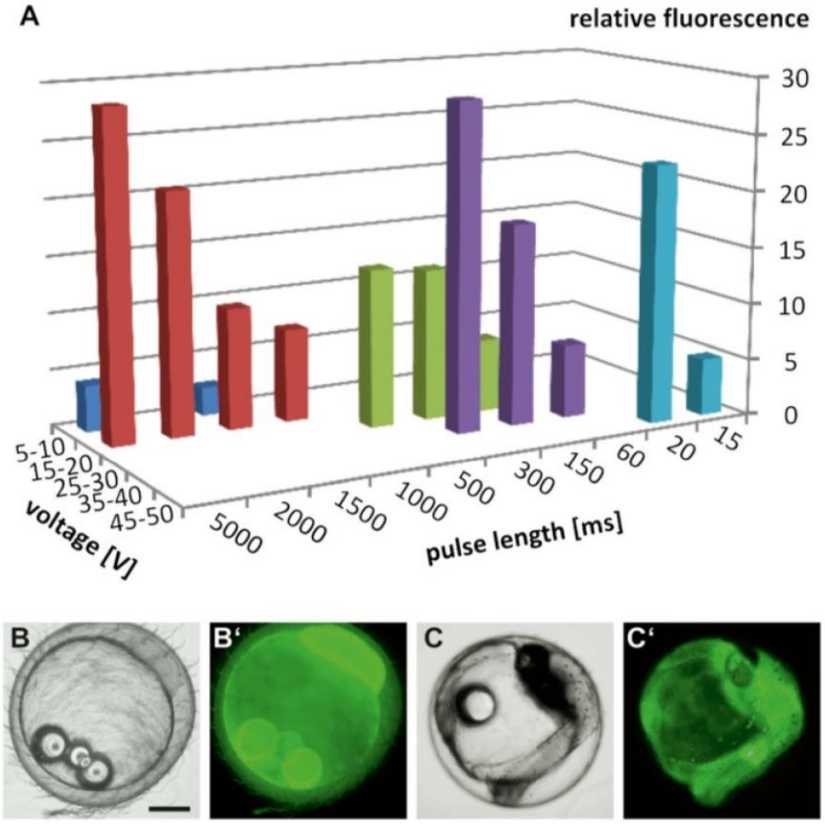

Figure 4 Optimization of electroporation conditions. (**A**) Embryos at stage 17 were incubated with 10 μg/ml fluorescein for 40 minutes at 27°C. Subsequent electroporation was performed at 35 kHz with varying voltages and pulse lengths. Relative fluorescence indicates fold quantified signal compared to that of non-electroporated, but otherwise equally treated reference embryos. Similar results were obtained for early (**B**, **B'**, stage 4) and late (**C**, **C'**, stage 31) embryos. Embryos are shown in lateral (**B**,**B'**) and dorso-lateral (**C**,**C'**) view. Scale bar 250 μM.

extend the results to other small molecules, we selected two additional dyes (rhodamine B and acridine orange) which differ in their molecular properties from fluorescein. Thus rhodamine B becomes strongly enriched in the yolk (Figure 6B-D). Contrary to most other dyes we tested, washing only partly removed the dye from the egg, where it remained trapped in the yolk. Acridine orange showed a more uniform distribution being present both in the yolk and the embryo (Figure 6E-G). At later stages, strong fluorescence was observed in the gallbladder/liver (Figure 6G). It therefore exhibits properties in-between fluorescein and rhodamine B. As for fluorescein, we performed electroporation experiments with rhodamine B and acridine orange. Compared to diffusion alone electroporated embryos always showed an extended uptake of the molecules, demonstrating the potential of electroporation also for other small molecules. Taken together, electroporation enhances the uptake of different small molecules into medaka embryos.

Lithium induces deficiencies in anterior-posterior development

After the analysis of the diffusion properties of medaka eggs and the establishment of electroporation as a tool to improve the uptake, we tested the procedure for our initial experiments with lithium chloride. For this we used 0.4 M lithium chloride, a concentration comparable to the one used in zebrafish experiments [13]. Also the incubation time (10 minutes) was in agreement with the zebrafish experiments. Diffusion alone at stage 14 (40% epiboly) resulted in normal development (Figure 7A). However, more than 60% of the embryos that were electroporated (15 V, 330 Hz, 100 ms, 1 pulse) in the presence of lithium chloride showed clear deficiencies in anterior-posterior development (Figure 7A), with 24% developing a weak phenotype and 39% a strong phenotype (Figure 7A and Additional file 5). As a strong phenotype we classified all embryos that showed severe axis truncation anterior to the midbrain, resulting in missing eyes and forebrain (Figure 7D,G), whereas in weak

Jung *et al. BMC Biotechnology* 2013, **13**:53
http://www.biomedcentral.com/1472-6750/13/53

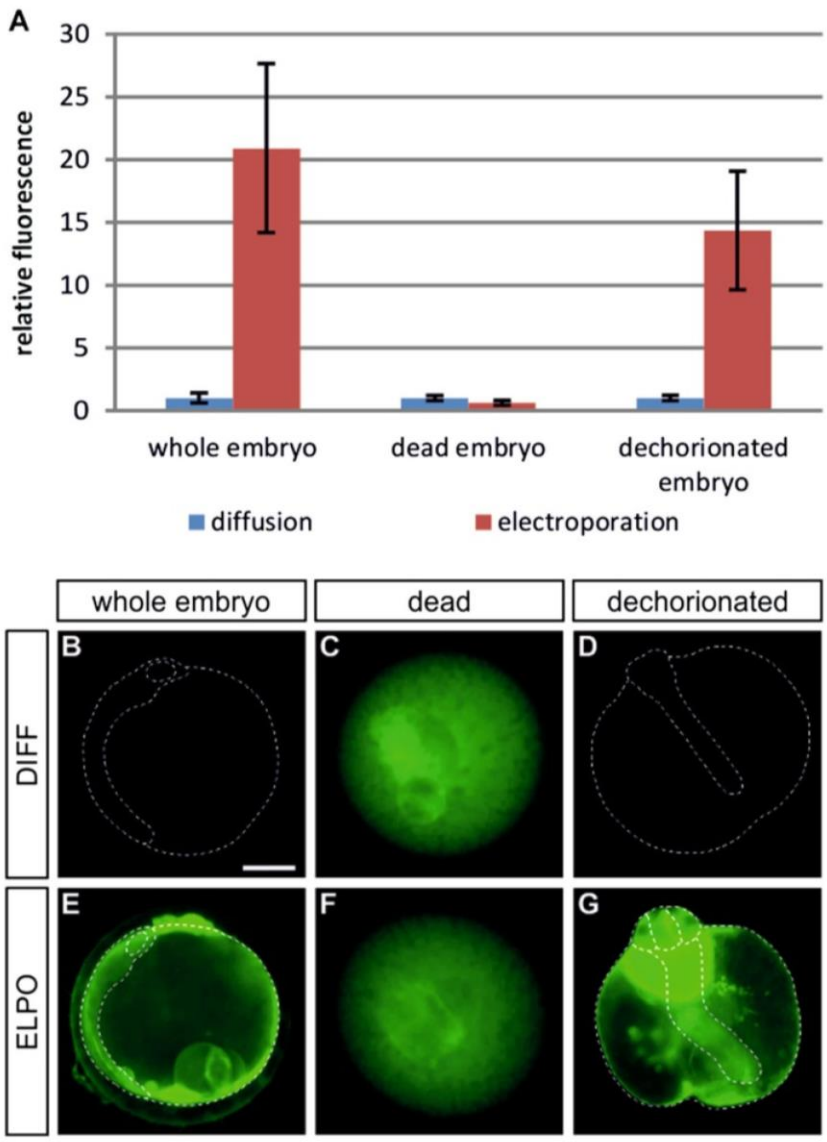

Figure 5 Electroporation affects the transfer of fluorescein through inner membranes, but not the chorion. Embryos were incubated with 10 µg/ml fluorescein for 40 minutes (**A**, blue bars; **B**-**D**); subsequent electroporation (**A**, red bars; **E**-**G**) was performed using 35 kHz, 15 V, 5000 ms, 1 pulse. Pictures were taken after 30 minutes washing time. Embryos are shown in lateral (**B**,**E**) and dorsal (**D**,**G**) view with anterior to the top. Scale bar 250 µM. Abbreviations: ELPO, electroporation; DIFF, diffusion.

phenotypes only the eyes were affected (Figure 7C,F). Furthermore, we observed the formation of enlarged and ectopic otic vesicles (Additional file 6), which again is in good agreement with the phenotypes seen for *wnt1* overexpression [17]. Control embryos that were electroporated and not treated with lithium chloride developed normally, but showed an elevated mortality rate (Figure 7A and Additional file 5). Nevertheless, electroporation could be established as a tool to enhance the uptake of small molecules into medaka embryos in order to study effects on development.

Discussion

Several studies have been performed to qualify the effect of small molecules on fish embryos [21-23]. In addition, toxicological applications like the FET test are discussed as an alternative to experiments with mammals and birds [8]. The uptake of substances by the embryos has

Jung *et al. BMC Biotechnology* 2013, **13**:53
http://www.biomedcentral.com/1472-6750/13/53

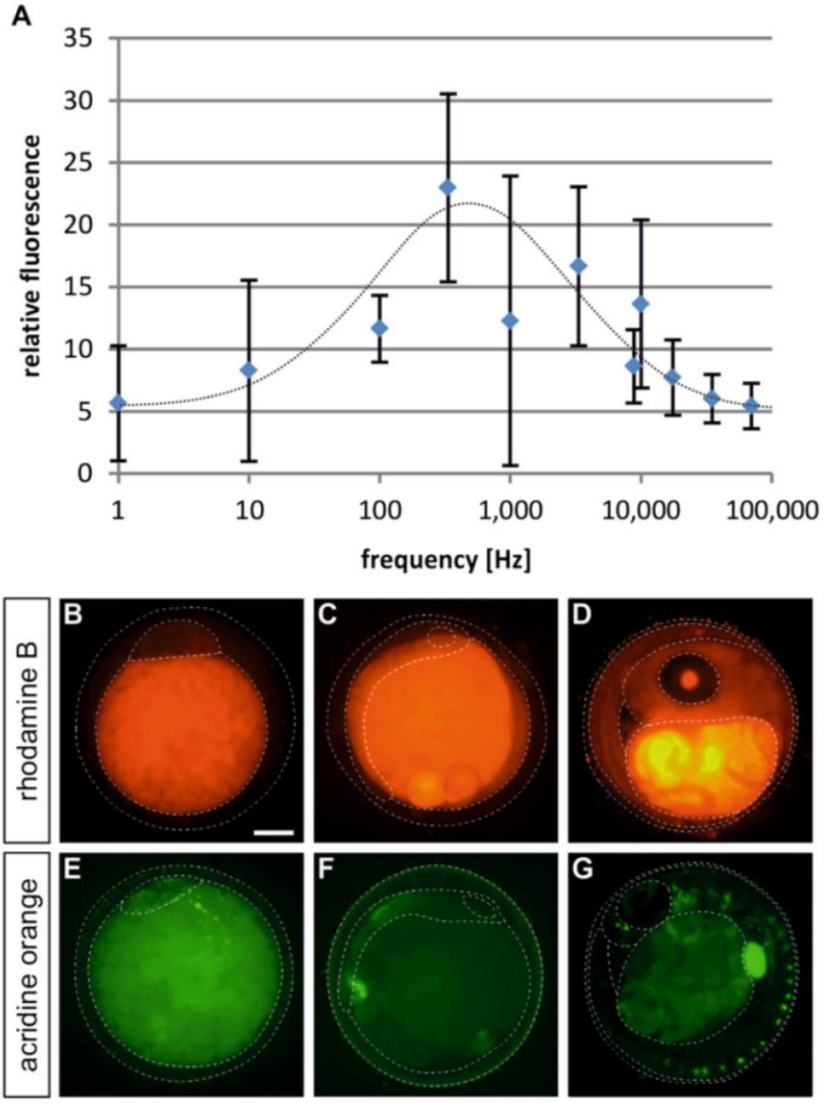

Figure 6 Electroporation of rhodamine B and acridine orange. (**A**) Optimisation of the modulation frequency of electroporation. The electroporation was performed at 15 V; 5000 ms; 1 pulse using variable frequencies. Relative fluorescence indicates fold fluorescein signal measured compared to non-electroporated, but otherwise equally treated reference embryos. For extension to other small molecules, the embryos were incubated with 10 ng/ml rhodamine B (**B**-**D**) and 1 μg/ml acridine orange (**E**-**G**) at stage 2a (**B**,**E**), stage 17 (**C**,**F**) and stage 36 (**D**,**G**) for 40 minutes at 27°C. Electroporation was performed using 330 Hz; 15 V; 5000 ms; 1 pulse. The dotted lines demarcate the outlines of: (**B**,**E**) yolk and blastoderm, and (**C**,**D**,**F**,**G**) yolk and embryo. Embryos are shown in lateral view. Scale bar 250 μM.

been recognized as a critical factor in these experiments [24,25]. However, little is known about the diffusion properties of the chorion and other membrane systems covering fish embryos. We used fluorescing substances as a model to study the diffusion of small molecules into medaka embryos. Combined with fluorescence microscopy quantification this offers a number of advantages over conventional techniques like radioactive labelling. Firstly, individual embryos can be followed over the time and quantified repeatedly. Secondly, the internal distribution of the molecules in the embryo due to the physicochemical nature of the molecules can be examined and compared at different stages of development. Alterations in the compartment specific distribution, as for example after incubation with detergents (Figure 3), are highly important for the assessment of pharmacokinetic

Jung *et al. BMC Biotechnology* 2013, **13**:53
http://www.biomedcentral.com/1472-6750/13/53

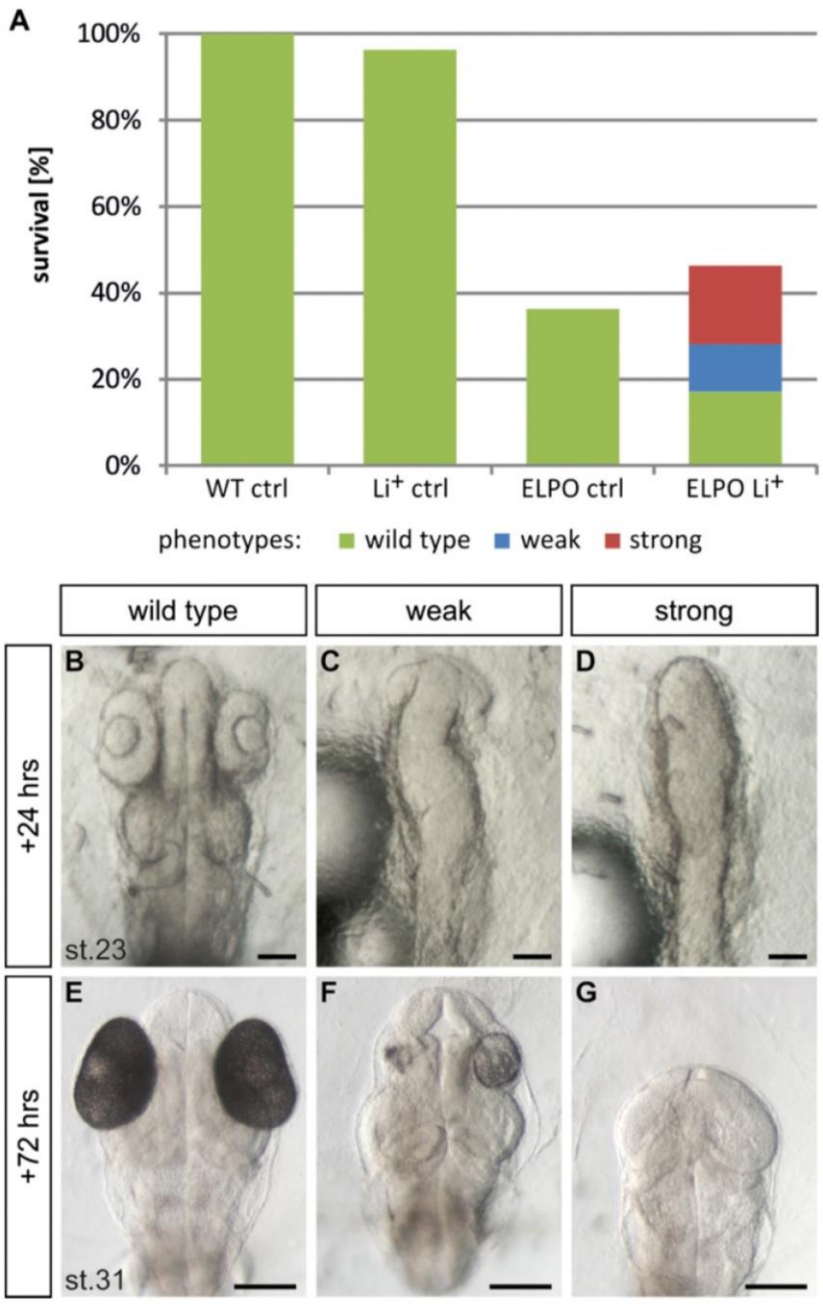

Figure 7 Lithium induction causes deficiencies in anterior-posterior development. Embryos at 40% epiboly were exposed to 0.4 M LiCl for 10 minutes at 27°C. Subsequent electroporation was performed at 330 Hz; 15 V; 100 ms; 1 pulse. 24 hours after the induction (+24 hrs) the phenotypes were clearly detectable and finally categorized after 72 hours (+72 hrs) as: wild type (green; **B**, **E**), weak (blue; **C**, **F**) and strong phenotypes (red; **D**, **G**). (**A**) The control (Li^+ ctrl) shows equally treated but non-electroporated embryos, electroporation control embryos (ELPO ctrl) were electroporated, but not exposed to LiCl. Electroporated embryos with LiCl (ELPO Li^+) showed phenotypes indicated by colours. Embryos are shown in dorsal view with anterior to the top. Scale bar 100 μM.

properties of drugs. Thirdly, metabolic processing can be followed (e.g. as for the accumulation of fluorescein and acridine orange in the liver/gallbladder). And finally, the distribution in different compartments due to variable diffusion rates can be detected, as the accumulation in the perivitelline space (Figure 2F-H").

We used fluorescein, rhodamine B, acridine orange, and lithium chloride for our experiments. They represent small molecules which cover a large spectrum of different properties from charged (lithium chloride) to non-charged (acridine orange). The substances exhibited varying distributions in medaka eggs, indicating differences in their hydrophobic properties (rhodamine B being most strongly enriched in the yolk). Nevertheless, all substances showed low diffusion rates into medaka embryos. In contrast to zebrafish, medaka eggs contain a hard chorion. Based on suggestions from the literature [3], we therefore suspected the chorion to represent a diffusion barrier, shielding the embryos from their chemical environment. Following sperm entry, a calcium wave moves along the surface and the chorion matures [26], thereby reaching maximum hardness approximately 6 hours after fertilization [12]. We therefore expected a dramatic reduction of the diffusion rate after chorion hardening. However, no differences appeared in the experiments (Figure 1E). As the chorion permeability is connected to calcium ions [27,28] we incubated the embryos right after fertilization in a calcium-free medium [29], with different pH values and even tried incubation in distilled water. However, the uptake of fluorescein into the embryos did not improve (data not shown). Therefore, conditions affecting chorion hardening did not alter the diffusion rates into the egg, neither did dechorionation of the embryos (Figure 2D', E). Instead we observed a rapid diffusion through the chorion into dead embryos (Figure 2C'.E). The fact that inner membrane systems and not the chorion represent the main diffusion barrier in medaka eggs was further supported by the fast accumulation of signals in the perivitelline space (early in-diffusion; Figure 2F-F") and the rapid loss of this signal during out-diffusion (Figure 2G-H"). On the contrary, accumulation in the embryo needed extensive in-diffusion times, but once achieved stayed considerably longer than that of the perivitelline space (Figure 2F-H"). The result is a bi-phasic progression of diffusion (Figure 2A), caused by a strong diffusion barrier positioned closer to the embryo than the chorion. During blastula stage, the egg can be subdivided into three distinct cell lineages. One lineage consists of the pluripotent deep layer blastomeres (DEL), which produce the future embryo proper. The second domain consists of a syncytium of multiple nuclei, called the yolk syncytial layer (YSL). The third domain is the envelope layer (EVL), a thin cell layer which covers the DEL and will eventually form the periderm [30]. Both the second and the third domain are extra-embryonic. According to our results, the EVL/periderm would be a candidate to block the diffusion into the egg.

These results have important implications for pharmacologic and toxicologic experiments with medaka embryos. Due to the bi-phasic diffusion process, the substance is initially enriched in the perivitelline space (diffusion half-time in the range of a few minutes). Subsequently, the slow diffusion into the embryo/yolk starts (diffusion half-time in the range of several hours). Therefore extended exposure to the test substances is necessary to evaluate pharmacologic/toxicologic consequences on embryonic development. Due to the slow accumulation in the embryo, effects on the first hours of development (e.g. early teratogenic properties) will not be detectable without enhanced transfer.

Assuming that the main diffusion barrier is a membrane system, it should be possible to increase its permeability by addition of detergents. Indeed, addition of Triton X-100 improved the uptake of fluorescein dramatically, but severely affected the membrane systems of the embryo (see Figure 3). Also injection into the yolk turned out to be inefficient. A possibility to make membranes permeable is electroporation. We applied current shifted radio frequency pulses [20] and could optimize the conditions to substantially increase the dye uptake compared to diffusion alone. Also other electroporation techniques like nanosecond pulsed electric fields have been tested for this purpose [31]. Such techniques would not only be of interest for small molecules, but also for the transfer of DNA or RNA. Indeed, Hostetler and colleagues initially proposed this technique to obtain transgenic medaka fish. In our hand the method worked effectively for small molecules, however, we failed with DNA. Closer inspection revealed that not even fluorescence labelled oligonucleotides (MW 6000) could pass the chorion, suggesting a size exclusion for the pores of the chorion in that range (data not shown). Electroporation did not improve this transfer. We also used DNA expression constructs containing gfp and luciferase for more sensitive assays, but failed to detect any marker gene expression in intact electroporated embryos. Only after dechorionation we could successfully transfer DNA into the embryos by electroporation (detection of gfp expression; data not shown). However, the survival of dechorionated embryos is extremely low during electroporation, making the method inapplicable for routine experiments. Injection of DNA into the perivitelline space and subsequent electroporation would be an option. However, direct injection of DNA into the zygote represents a simple alternative.

Having established electroporation for the uptake of small molecules into the living medaka embryo, we then

returned to our initial question, the application of lithium to medaka development. The effects of lithium on developmental processes have been shown in several organisms. Already more than 60 years ago it was known that amphibian embryos developed severe anterior truncations when exposed to lithium during gastrulation (reviewed in [18]). This dorsalization effect was explained by the finding that lithium inhibits GSK-3β, a key component of the Wnt signalling pathway [32,33]. Indeed, diffusion and subsequent electroporation led to axis truncations in medaka embryos, similar to those observed upon ectopic expression of *wnt1* [17]. The embryos either failed to develop anteriorly to the midbrain (Figure 7D,G), lacking eyes and the forebrain (strong phenotype), or they developed eyes with reduced size (Figure 7C,F; weak phenotype). Electroporation therefore effectively improves the transfer of small molecules into medaka embryos. Hence, this method can be used to enhance the uptake of chemicals. Examples of such applications are specific inducers or repressors of signalling pathways to study embryonic development. For these experiments timing represents an important parameter. Slow diffusion and consequently slow accumulation prevents an exact timing of the effective concentration in the embryo. Electroporation strongly increases the internal concentration within a single step as exemplified for lithium chloride (the timing of Wnt signalling pathway activation critically affects the observed phenotypes; [17]).

Conclusion

During our experiments we found that membrane layers surrounding the medaka embryo represent a diffusion barrier for small molecules, whereas the hard outer chorion is readily passed. The slow diffusion has to be considered when toxicologic or pharmacologic experiments are performed with medaka embryos. A possible way to overcome this problem is electroporation, which substantially improves the uptake of small molecules. We thus were able to induce medaka embryos with the GSK-3 inhibitor lithium and could show that the resulting activation of the Wnt signalling pathway causes deficiencies in anterior-posterior development.

Additional files

Additional file 1: Fluorescein enrichment in the gallbladder/liver. Embryos at the 1-cell stage were incubated with 10 mg/ml fluorescein for 40 minutes at 27°C. Standard washing steps were performed and pictures were taken after 3 days (stage 31). Embryos are shown in lateral view with anterior to the left. (A) Fluorescence and (B) bright field pictures of the eggs, arrow heads indicate staining in the gallbladder. Scale bar 250 μM.

Additional file 2: Methylene blue diffusion into embryos. Embryos at the 1-cell stage were incubated with 0.001% methylene blue in 10× ERM for 10 minutes at 27°C. Standard washing steps were performed and brightfield pictures were taken after 10 (A) and 20 minutes (B) of washing. Embryos are shown in lateral view; the blastomeres are on the top. Scale bar 250 μM. Abbreviations: DIFF, diffusion.

Additional file 3: Yolk injection. Embryos at the 1-cell stage (upper row) and stage 30 (lower row) were injected with 10 mg/ml fluorescein. Embryos are shown in lateral view, blastomeres (A-D) or anterior (E-J) to the top right. The yolk and embryo are demarcated by the dotted lines, the outlines of the chorion by continuous white lines. Incubation time after yolk-injection is indicated by the time designation at the bottom left. In both early (D) and late (I) yolk-injected embryos weak fluorescence (D; arrow head) was only detected after 4 hours within the embryo. Older embryos showed clear enrichment of fluorescein within the gallbladder/liver (I,J; arrow). Scale bar 250 μM. Abbreviations: min, minutes; hrs, hours.

Additional file 4: Results of electroporation optimization experiments. Embryos at stage 17 were incubated with 10 μg/ml fluorescein for 40 minutes at 27°C. Subsequent electroporation was performed at 15 kHz with varying voltages and pulse lengths. Fluorescence intensity is shown in the top row and was normalized to the values measured for the diffusion control. Survival: percentage of surviving embryos after 20 minutes of washing. In order to obtain more significant results, experiments with similar conditions (voltage) were combined.

Additional file 5: Electroporation of lithium incubated embryos. Embryos at 40% epiboly were incubated with 0.4 μM lithium chloride for 10 minutes at 27°C. Thereafter, embryos were either directly transferred into ERM (Diffusion), or electroporation was performed at 330 Hz, 15 V, 100 ms using a single pulse (Electroporation). Phenotypes were categorized into strong (eyes were missing) and weak (only small eyes developed) 72 hours after induction. *) Ectopic otic vesicles were observed only in embryos developing a strong phenotype and were not considered in the calculation of the percentage of phenotypes in surviving embryos.

Additional file 6: Ectopic otic vesicles in lithium induced embryos. Embryos at 40% epiboly were exposed to 0.4 M LiCl for 10 minutes at 27°C followed by electroporation at 330 Hz; 15 V; 100 ms; 1 pulse (longer pulse lengths resulted in reduced survival of the embryos). Embryo is shown in dorsal view with anterior to the top 72 hours after the induction, black arrowheads indicate ectopic otic vesicles. Scale bar 100 μM.

Competing interests

The authors declare that they have no competing interests.

Authors' contributions

GJ carried out the majority of diffusion experiments, the electroporation experiments with lithium and drafted the manuscript. MH performed all other electroporation experiments. AF participated in the diffusion experiments. CH and JW build the electroporation apparatus. TC was responsible for coordination of the experiments and writing of the manuscript. All authors read and approved the final manuscript.

Acknowledgement

The work was supported by the Austrian Science Fund (FWF, grant P19571-B11) and the City of Vienna (MA23 – project 10-20).

Author details

[1]Department for Applied Life Sciences, University of Applied Sciences, FH Campus Wien, Helmut-Qualtinger-Gasse 2, A-1030, Vienna, Austria. [2]Department for Engineering, University of Applied Sciences, FH Campus Wien, Favoritenstrasse 226, A-1100, Vienna, Austria.

Received: 14 February 2013 Accepted: 17 June 2013
Published: 1 July 2013

References

1. Wittbrodt J, Shima A, Schartl M: **Medaka–a model organism from the far East.** *Nat Rev Genet* 2002, **3**(1):53–64.

2. Pastva SD, Villalobos SA, Kannan K, Giesy JP: **Morphological effects of Bisphenol-A on the early life stages of medaka (Oryzias latipes).** *Chemosphere* 2001, **45**(4–5):535–541.
3. Villalobos SA, Hamm JT, Teh SJ, Hinton DE: **Thiobencarb-induced embryotoxicity in medaka (Oryzias latipes): stage-specific toxicity and the protective role of chorion.** *Aquat Toxicol* 2000, **48**(2–3):309–326.
4. Kordes C, Rieber EP, Gutzeit HO: **An in vitro vitellogenin bioassay for oestrogenic substances in the medaka (Oryzias latipes).** *Aquat Toxicol* 2002, **58**(3–4):151–164.
5. Kang IJ, Yokota H, Oshima Y, Tsuruda Y, Oe T, Imada N, Tadokoro H, Honjo T: **Effects of bisphenol a on the reproduction of Japanese medaka (Oryzias latipes).** *Environ Toxicol Chem* 2002, **21**(11):2394–2400.
6. Scialli AR: **The challenge of reproductive and developmental toxicology under REACH.** *Regul Toxicol Pharmacol* 2008, **51**(2):244–250.
7. Embry MR, Belanger SE, Braunbeck TA, Galay-Burgos M, Halder M, Hinton DE, Leonard MA, Lillicrap A, Norberg-King T, Whale G: **The fish embryo toxicity test as an animal alternative method in hazard and risk assessment and scientific research.** *Aquat Toxicol* 2010, **97**(2):79–87.
8. Strahle U, Scholz S, Geisler R, Greiner P, Hollert H, Rastegar S, Schumacher A, Selderslaghs I, Weiss C, Witters H, *et al*: **Zebrafish embryos as an alternative to animal experiments–a commentary on the definition of the onset of protected life stages in animal welfare regulations.** *Reprod Toxicol* 2012, **33**(2):128–132.
9. Lammer E, Carr GJ, Wendler K, Rawlings JM, Belanger SE, Braunbeck T: **Is the fish embryo toxicity test (FET) with the zebrafish (Danio rerio) a potential alternative for the fish acute toxicity test?** *Comp Biochem Physiol C Toxicol Pharmacol* 2009, **149**(2):196–209.
10. Braunbeck T, Boettcher M, Hollert H, Kosmehl T, Lammer E, Leist E, Rudolf M, Seitz N: **Towards an alternative for the acute fish LC(50) test in chemical assessment: the fish embryo toxicity test goes multi-species – an update.** *ALTEX* 2005, **22**(2):87–102.
11. Yang L, Ho NY, Alshut R, Legradi J, Weiss C, Reischl M, Mikut R, Liebel U, Muller F, Strahle U: **Zebrafish embryos as models for embryotoxic and teratological effects of chemicals.** *Reprod Toxicol* 2009, **28**(2):245–253.
12. Yamagami K, Hamazaki TS, Yasumasu S, Masuda K, Iuchi I: **Molecular and cellular basis of formation, hardening, and breakdown of the egg envelope in fish.** *Int Rev Cytol* 1992, **136**:51–92.
13. Stachel SE, Grunwald DJ, Myers PZ: **Lithium perturbation and goosecoid expression identify a dorsal specification pathway in the pregastrula zebrafish.** *Development* 1993, **117**(4):1261–1274.
14. Iwamatsu T: **Stages of normal development in the medaka Oryzias latipes.** *Mech Dev* 2004, **121**(7–8):605–618.
15. Schneider CA, Rasband WS, Eliceiri KW: **NIH Image to ImageJ: 25 years of image analysis.** *Nat Methods* 2012, **9**(7):671–675.
16. Ortner V, Kaspar C, Halter C, Tollner L, Mykhaylyk O, Walzer J, Gunzburg WH, Dangerfield JA, Hohenadl C, Czerny T: **Magnetic field-controlled gene expression in encapsulated cells.** *J Control Release* 2012, **158**(3):424–432.
17. Bajoghli B, Aghaallaei N, Jung G, Czerny T: **Induction of otic structures by canonical Wnt signalling in medaka.** *Dev Genes Evol* 2009, **219**(8):391–398.
18. Kao KR, Elinson RP: **The legacy of lithium effects on development.** *Biol Cell* 1998, **90**(8):585–589.
19. Schmidt R, Buscher HP: **Hepatic uptake of fluorescein, investigated by video fluorescence microscopy and digital image analysis.** *J Hepatol* 1991, **13**(2):208–212.
20. Hostetler HA, Peck SL, Muir WM: **High efficiency production of germ-line transgenic Japanese medaka (Oryzias latipes) by electroporation with direct current-shifted radio frequency pulses.** *Transgenic Res* 2003, **12**(4):413–424.
21. Modra H, Vrskova D, Macova S, Kohoutkova J, Hajslova J, Haluzova I, Svobodova Z: **Comparison of diazinon toxicity to embryos of Xenopus laevis and Danio rerio; degradation of diazinon in water.** *Bull Environ Contam Toxicol* 2011, **86**(6):601–604.
22. Osterauer R, Kohler HR: **Temperature-dependent effects of the pesticides thiacloprid and diazinon on the embryonic development of zebrafish (Danio rerio).** *Aquat Toxicol* 2008, **86**(4):485–494.
23. Oxendine SL, Cowden J, Hinton DE, Padilla S: **Adapting the medaka embryo assay to a high-throughput approach for developmental toxicity testing.** *Neurotoxicology* 2006, **27**(5):840–845.
24. Hamm JT, Wilson BW, Hinton DE: **Increasing uptake and bioactivation with development positively modulate diazinon toxicity in early life stage medaka (Oryzias latipes).** *Toxicol Sci* 2001, **61**(2):304–313.
25. Harvey B, Kelley RN, Ashwood-Smith MJ: **Permeability of intact and dechorionated zebra fish embryos to glycerol and dimethyl sulfoxide.** *Cryobiology* 1983, **20**(4):432–439.
26. Gilkey JC, Jaffe LF, Ridgway EB, Reynolds GT: **A free calcium wave traverses the activating egg of the medaka.** *Oryzias latipes. J Cell Biol* 1978, **76**(2):448–466.
27. Masuda K, Luchi I, Yamagami K: **Analysis of Hardening of the Egg Envelope (Chorion) of the Fish, Oryzias latipes.** *Dev Growth Differ* 1991, **33**(1):75–83.
28. Masuda K, Murata K, Iuchi I, Yamagami K: **Some Properties of the Hardening Process in Chorions Isolated from Unfertilized Eggs of Medaka, Oryzias latipes.** *Dev Growth Differ* 1992, **34**(5):545–551.
29. Iwamatsu T, Shibata Y, Kanie T: **Changes in chorion proteins induced by the exudate released from the egg cortex at the time of fertilization in the teleost, Oryzias latipes.** *Dev Growth Differ* 1995, **37**(6):747–759.
30. Kimmel CB, Warga RM, Schilling TF: **Origin and organization of the zebrafish fate map.** *Development* 1990, **108**(4):581–594.
31. Tominaga N, Kono S, Yamaguchi A, Akiyama H, Arizono K: **A novel material incorporation technique for medaka (Oryzias latipes) eggs using nanosecond pulsed electric fields.** *Biosci Biotechnol Biochem* 2009, **74**(6):1279–1282.
32. Klein PS, Melton DA: **A molecular mechanism for the effect of lithium on development.** *Proc Natl Acad Sci U S A* 1996, **93**(16):8455–8459.
33. Stambolic V, Ruel L, Woodgett JR: **Lithium inhibits glycogen synthase kinase-3 activity and mimics wingless signalling in intact cells.** *Curr Biol* 1996, **6**(12):1664–1668.

doi:10.1186/1472-6750-13-53
Cite this article as: Jung *et al.*: Diffusion of small molecules into medaka embryos improved by electroporation. *BMC Biotechnology* 2013 **13**:53.

Additional file 1. Fluorescein enrichment in the gallbladder/liver

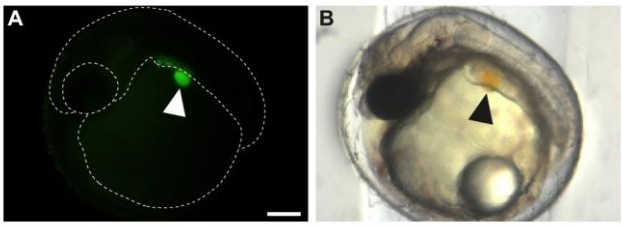

Additional file 2. Methylene blue diffusion into embryos

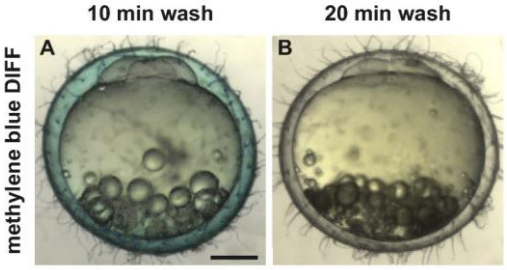

Additional file 3. Yolk injection

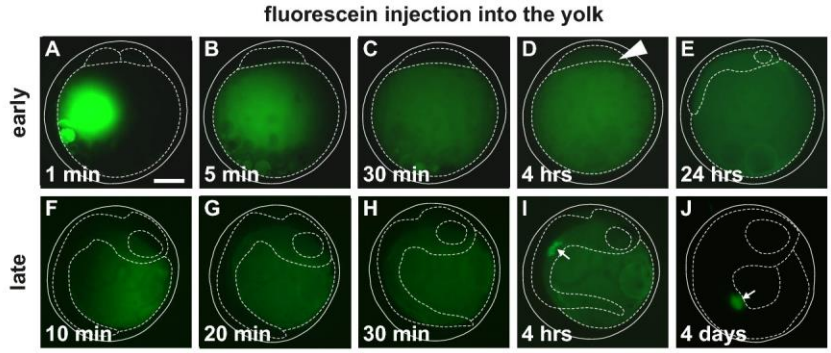

Additional file 4. Results of electroporation optimization experiments.

	Burst duration [ms] / Voltage [V]	15	20	60	150	300	500	1,000	1,500	2,000	5,000
Relative fluorescence	5-10								3		4
	15-20							8	11	21	29
	25-30				6	13	14				
	35-40			6	18	29					
	45-50	5	23	10							
Survival	5-10								88%		92%
	15-20								50%		80%
	25-30				83%	82%	100%				
	35-40			83%	100%	33%					
	45-50	98%	50%	75%		33%					

Additional file 5. Electroporation of lithium incubated embryos.

	Diffusion		Electroporation	
Lithium chloride	**0 µM**	**0.4 µM**	**0 µM**	**0.4 µM**
Embryos	23	48	36	36
Dead	0	1	12	10
Mortality	0%	2%	33%	28%
Strong phenotype	0	0	0	7
Weak phenotype	0	0	0	7
Ectopic otic vesicles*)	0	0	0	4
Normal development	23	47	24	12
Phenotypes in surviving embryos	**0%**	**0%**	**0%**	**54%**

Additional file 6. Ectopic otic vesicles in lithium induced embryos

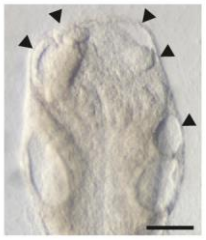

Dorn *et al. BMC Biotechnology* 2012, **12**:50
http://www.biomedcentral.com/1472-6750/12/50

BMC Biotechnology

RESEARCH ARTICLE Open Access

Side chain modified peptide nucleic acids (PNA) for knock-down of *six3* in medaka embryos

Sebastian Dorn[1†], Narges Aghaallaei[1†], Gerlinde Jung[2†], Baubak Bajoghli[1,3], Birgit Werner[4], Holger Bock[4], Thomas Lindhorst[4] and Thomas Czerny[1,2*]

Abstract

Background: Synthetic antisense molecules have an enormous potential for therapeutic applications in humans. The major aim of such strategies is to specifically interfere with gene function, thus modulating cellular pathways according to the therapeutic demands. Among the molecules which can block mRNA function in a sequence specific manner are peptide nucleic acids (PNA). They are highly stable and efficiently and selectively interact with RNA. However, some properties of non-modified aminoethyl glycine PNAs (aegPNA) hamper their *in vivo* applications.

Results: We generated new backbone modifications of PNAs, which exhibit more hydrophilic properties. When we examined the activity and specificity of these novel phosphonic ester PNAs (pePNA) molecules in medaka (*Oryzias latipes*) embryos, high solubility and selective binding to mRNA was observed. In particular, mixing of the novel components with aegPNA components resulted in mixed PNAs with superior properties. Injection of mixed PNAs directed against the medaka *six3* gene, which is important for eye and brain development, resulted in specific *six3* phenotypes.

Conclusions: PNAs are well established as powerful antisense molecules. Modification of the backbone with phosphonic ester side chains further improves their properties and allows the efficient knock down of a single gene in fish embryos.

Keywords: PNA, Knock down, Medaka, Six3

Background

Antisense oligonucleotides are designed for sequence specific binding of complementary regions on their target mRNA. The binding either results in mRNA cleavage, caused by the activation of endonucleases RNase H or L [1], or in the inhibition of translation [2]. Different modifications of the nucleic bases or the backbone were introduced to improve their activity and biological stability. In morpholino antisense molecules, the ribose is replaced by morpholino rings and non-ionic phosphorodiamidate is used instead of phosphodiester linkages [3]. Their binding strength closely resembles that of RNA or DNA molecules, therefore, molecules with a length of 25 nucleotides are used for efficient transcriptional blockage. For translational blocking the 5' untranslated region or the region around the start codon of the target mRNA are selected [4]. Morpholino oligomers can also be used for efficient blocking of the splice machinery [5]. The highly specific effect of morpholino oligomers on gene silencing could be demonstrated in sea urchins [6], Xenopus [7], Zebrafish [8] and Medaka [9]. Today morpholino oligos represent the gold standard for gene specific knock down in many species.

In 1991 Nielsen and colleagues created peptide nucleic acids (PNA) which instead of the phosphate ribose ring of DNA contain a polyamide backbone of N-(2-aminoethyl)-glycine (aeg) units [10]. aegPNAs bind to complementary RNA or DNA in a sequence-specific manner [11,12]. The chemical structure is responsible for a high stability against proteases, nucleases as well as thermal and pH fluctuations [13]. The entire neutral charge of the molecule decreases

* Correspondence: thomas.czerny@fh-campuswien.ac.at
†Equal contributors
[1]Department for Biomedical Sciences, University of Veterinary Medicine, Veterinärplatz 1, A-1210, Vienna, Austria
[2]Department for Applied Life Sciences, University of Applied Sciences, FH Campus Wien, Helmut-Qualtinger-Gasse 2, A-1030, Vienna, Austria
Full list of author information is available at the end of the article

Dorn *et al. BMC Biotechnology* 2012, **12**:50
http://www.biomedcentral.com/1472-6750/12/50

the electrostatic repulsion, which results in high hybridization affinity with RNA and DNA. Consequently short probe lengths (13–18 bases) are sufficient for selective binding, thereby reducing the probability for forming secondary structures [13-15]. In addition, the introduction of mismatches has a stronger effect on the stability of PNA/DNA interactions in comparison to DNA/DNA duplexes, demonstrating the high specificity of PNAs [16]. Several *in vitro* techniques make use of the extraordinary affinity of PNAs [17,18]. *In vivo* techniques also strongly benefit from the highly specific binding to mRNAs, however, so far unmodified aegPNAs have not been successful in injection experiments for gene specific knock down in animal models [19]. One problem for the application of PNAs is the low solubility due to the absence of charges. Introduction of negative charges by forming hetero-oligomers of alternating trans-4-hydroxy-L-proline/phosphonate polyamides with DNA bases (HypNA-pPNA) allowed specific down regulation of target genes in zebrafish embryos [20]. In addition, various end-modifications of PNAs have been developed, which mainly address the improvement of their cell delivery [21,22].

Here we tested the modification of the PNA backbone in order to keep the conformation most similar to the well established original aegPNAs. The resulting pePNAs contain phosphonic ester side chains in an otherwise non-modified polyamide backbone. The neutral pePNAs are highly soluble, but keep the high affinity and specificity of aegPNAs. In particular mixed versions of pe- and aegPNA components show favourable properties. We demonstrate the efficiency of these new antisense molecules by blocking gfp expression and *in vivo* down regulation of *six3* gene function in medaka embryos.

Results and discussion

Synthesis of novel peptide nucleic acids

aegPNAs bind corresponding RNA sequences with high affinity and specificity, however, unfavourable properties like their low solubility hamper their application *in vivo*. By employing the building blocks shown in Additional file 1: Figure S1, we introduced phosphonic ester side chains into the otherwise non-modified backbone of aegPNAs. As a result novel phosphonic ester PNA variants (pePNA) were obtained (see Figure 1).

First we investigated the properties of a 15mer pePNA. The oligomer exhibited good solubility in water and we were able to prepare highly concentrated stock solutions (10 mM). However, it turned out that pePNAs capped with acetyl at the C-terminus tend to form stable foam after sonification at this concentration. A possible explanation might be the large number of phosphonic esters residues, which introduce a highly polar but not ionic character into the oligomer. The tendency to form foams was not observed when the pePNAs were permanently charged with trimethyl-lysine (TML) at the C-terminus prior to capping with acetyl (see Additional file 1: Figure S1).

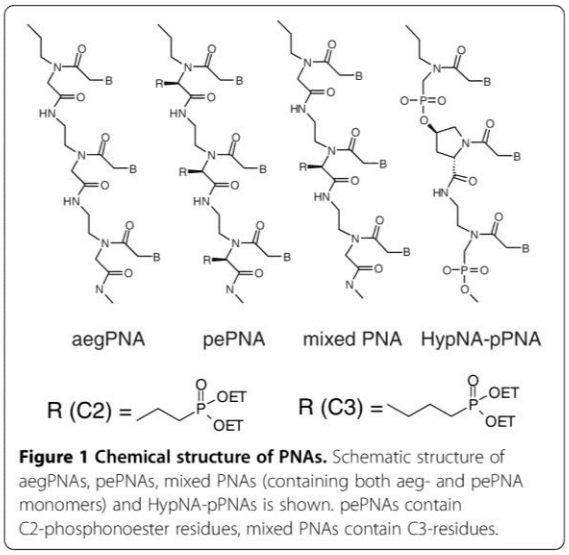

Figure 1 Chemical structure of PNAs. Schematic structure of aegPNAs, pePNAs, mixed PNAs (containing both aeg- and pePNA monomers) and HypNA-pPNAs is shown. pePNAs contain C2-phosphonoester residues, mixed PNAs contain C3-residues.

pePNAs efficiently block translation of *gfp* mRNA

In order to establish conditions for the application of pePNA molecules for antisense approaches we established an assay for translation blocking. Cell culture based assays include the problem of the transport of PNAs (or PNA/DNA duplexes) into the cells [23]. To use an unbiased strategy we therefore used injection into fish embryos. The pePNAs were co-injected together with *gfp* mRNA into medaka embryos at the one-cell stage. As target sequence within the *gfp* mRNA we selected a region directly after the AUG (see Figure 2), which previously had been used for knock down strategies with morpholino oligos [9]. The embryos continued development and 24 hours later the gfp signal was observed under the fluorescence microscope. According to the gfp expression level, the embryos were categorized into 4 groups with strong, moderate, weak and no gfp signal, respectively (Figure 3A-D). To consider the small variations of the injection procedure, we calculated an overall number of gfp signal intensity for all embryos, which is based on different weights for the individual groups of embryos. For this calculation, strong embryos were weighted with 100%, embryos of the moderate group with 30%, those of the weak group with 10% and those showing no gfp signal were counted with 0%. From this an average number for all embryos was derived and then corrected by those for the injection of mRNA alone. The resulting value represents the average gfp intensity in % (mRNA alone results in 100%).

Dorn *et al. BMC Biotechnology* 2012, **12**:50
http://www.biomedcentral.com/1472-6750/12/50

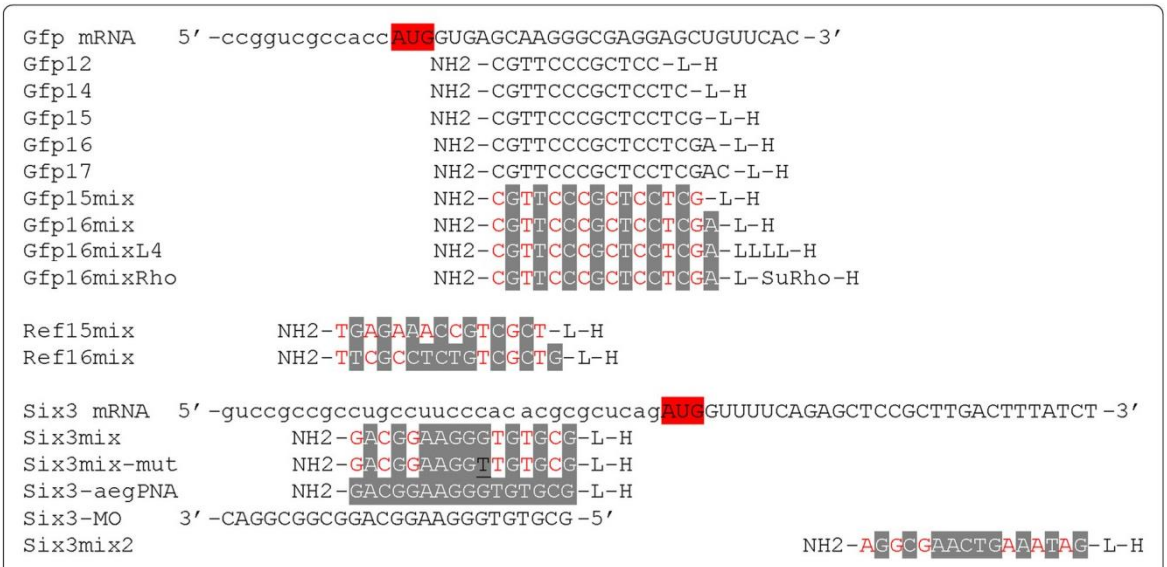

Figure 2 Sequences of the antisense molecules and their targets. The mRNA targets are shown in the 5′-3′ orientation, capital letters indicate the coding region. The AUG start codon is marked by red overlay. A morpholino oligo is indicated by MO (Six3-MO). All other sequences represent PNAs, pePNA-C2 components are shown in black, pePNA-C3 components in red and aegPNAs components are marked by gray overlay. Underlined bases (black) represent mismatches. All PNA and morpholino oligos are shown in the 3′-5′ (NH2-H for PNAs) orientation. L means trimethyl-lysine and LLLL a combination of 4 such residues. SuRho indicates sulforhodamine B.

We first compared the efficiency of different lengths of the oligomers (12mer, 14mer, 16mer and 17mer; for sequence information see Figure 2). The pePNAs (200 μM) were co-injected with 10 ng/μl *gfp* mRNA. Although all PNA lengths were able to reduce the gfp signal in the embryos (Figure 3E and Additional file 2: Table S1), the strongest effect was observed for the 16mer PNA (Gfp16; reduction to 28% average gfp intensity).

To investigate the influence of the steric hindrance of the phosphonic ester residues, we synthesized a second set of 15 and 16mers. In this set an additional methylene group was introduced into the side chain (R-C3 instead of R-C2; see Figure 1) to elongate the alkyl spacer between the phosphonic esters and the oligomer backbone. Furthermore, the number of side chains was reduced, forming a hybrid oligomer of pe- and aegPNA components. We hypothesised an increased binding efficiency of these mixed PNAs and indeed found a high melting point (66.9°C) for Gfp16mix with complementary DNA. On the contrary a corresponding pure pePNA (Gfp17) showed a considerably lower melting point of 57.8°C (although containing one additional nucleotide compared to Gfp16mix). The presence of the aegPNA monomers in the molecules thus increased the binding affinity and this consequently resulted in a stronger reduction of the gfp signal compared to C2-pePNAs (data not shown). We therefore increased the amount of *gfp* mRNA for the co-injection assay to 20 ng/μl. This resulted in stronger gfp intensity, which allowed us to better evaluate the improved antisense effect of the mixed PNAs. At a concentration of 200 μM, a 15mer PNA with a mixed backbone (Gfp15mix) showed a reduction to 59% of the gfp fluorescence intensity. This result could be improved when a 16mer mixed PNA (Gfp16mix) was injected (41%), demonstrating a superior effect of 16mer PNAs also for mixed backbones. Similar effects were observed for a mixed PNA containing 4 TML residues (Gfp16mixL4). At higher concentrations of 400 μM or 600 μM the average gfp intensity was reduced to minimum levels of 12%. As a control for the specificity of the PNAs, we used a reference PNA with a completely unrelated sequence (Ref15mix). The gfp level in this control experiment was similar to the group of injected embryos without adding PNAs (Figure 3F). Furthermore, we did not observe any toxicity of the PNAs in the fish embryos at higher concentrations (up to 600 μM; see death rates in Additional file 3: Table S2).

Uniform distribution of PNA molecules in medaka embryos

To get more information about the fate of the PNAs in the embryos, we injected a sulforhodamine labeled mixed PNA variant (Gfp16mixRho; for sequence information see Figure 2). After injection at the one-cell stage the PNA distributed equally into the dividing blastomeres

Dorn *et al. BMC Biotechnology* 2012, **12**:50
http://www.biomedcentral.com/1472-6750/12/50

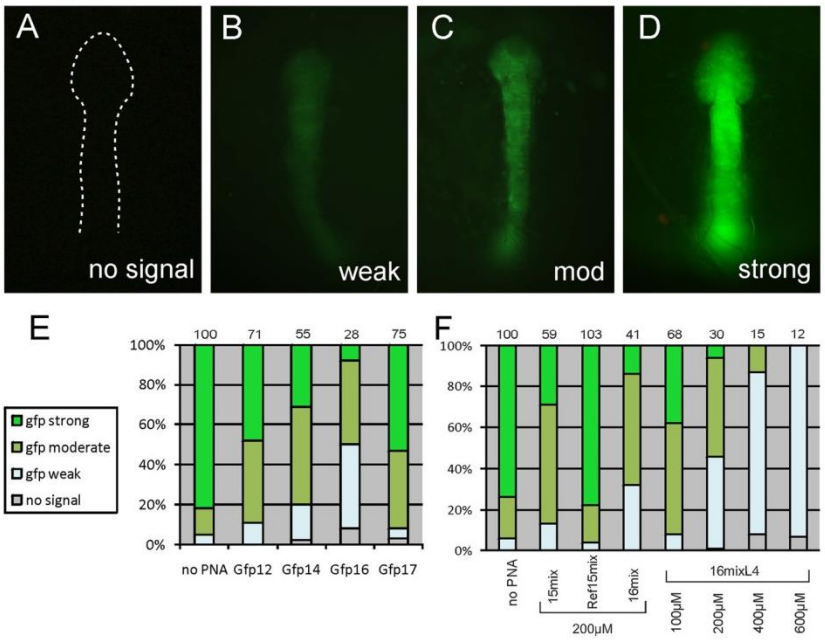

Figure 3 Translational blocking of pePNAs after injection of gfp mRNA into medaka embryos. The pePNAs were coinjected with gfp mRNA into medaka embryos at the one cell stage. 24 hours later the intensity of the gfp fluorescence was qualified as weak (**B**), moderate (**C**; mod) or strong (**D**). (**A**) Shows an uninjected embryo (no signal, corresponding to a complete knock down of gfp). The embryos are shown in a dorsal view, anterior to the top. A graph summarizing the experiments for optimisation of the PNA length is shown in (**E**). The names of the PNAs are explained in Figure 2. The embryos were injected with a mixture of 10 ng/µl gfp mRNA and 200 µM PNAs preincubated for 30 minutes on ice. After 24 hours the embryos were divided into groups according to their gfp signal intensity. Above the columns the calculated average gfp intensity in percent is indicated (see text for calculation). Similarly the results for mixed PNAs are shown in (**F**). Injections and evaluations were performed as in (**E**), except that 20 ng/µl mRNA were used. Note that the increased amount of mRNA results in higher numbers of average gfp intensity for comparable antisense function.

(Additional file 4: Figure S2). A uniform distribution of the PNA in the embryo could also be observed at later stages, no signals were detected in the yolk. Using this labeled PNA we were able to exactly quantify the injection volume and the final concentration of the PNAs in the embryo. As a reference we used small beads (average 730 µm), which were soaked for several days with a defined concentration of the PNA. A comparison of the fluorescence signals of these beads with the injected embryos allowed us to determine the injection volume to 11.3 nl on average. Injection of antisense molecules at 100 µM consequently resulted in a concentration of 25 µM in the embryonic cells (the volume of the embryo was determined at the four-cell stage at 33 nl, for calculations see Methods section). Here uniform distribution within the cells was assumed.

Knock down of the *six3* gene in medaka embryos by mixed PNAs

The Gfp-PNA molecules were tested in an *in vivo* setting, but the mixing of gfp-antisense PNAs with the *gfp* mRNA in the injection solution could lead to PNA/RNA hybridization prior to injection into the embryos. To avoid this possibility, we decided to test the targeting specificity of the PNAs in a complex *in vivo* environment, with a large excess of non-target mRNA. We therefore selected the endogenous *six3* gene as a target for PNA knock down experiments.

Six3 is part of the Six family of proteins, whose members are characterized by the presence of an N-terminal Six domain and a homeodomain [24]. Six genes are highly conserved across the animal kingdom. In *Drosophila* the *six3* homologue *optix* fulfills important functions in the development of the visual system [25]. In vertebrates, *six3* and *six6* are expressed in developing areas of the lens, neural retina, retinal-pigmented epithelium, nasal placodes, optic chiasm and forebrain. They take over important tasks in forming the rostral brain and the eye, especially the retina and the lens [26-28]. The critical function in eye development could also be demonstrated in medaka where inactivation of *six3* by morpholino knock-down resulted in lack of forebrain and eye structures [9].

Dorn *et al. BMC Biotechnology* 2012, **12**:50
http://www.biomedcentral.com/1472-6750/12/50

Based on the results of the gfp experiments we synthesized a 16mer mixed C3-PNA for the knock down experiments (referred to as Six3mix; for sequence information see Figure 2). The chosen sequence is a subset of a published morpholino 25mer directed against the *six3* 5'-region, directly upstream of the start codon [9]. After injection of the Six3mix-PNA a variety of eye and forebrain phenotypes were observed, in good agreement with previous results obtained for morpholino oligos in medaka embryos [9]. Based on the eye and forebrain phenotypes and in agreement with the literature [9] we divided these embryos into three groups. Embryos with a weak phenotype showed a size reduction of the eyes, which at the anterior part pointed towards the midline (Figure 4A arrows). Embryos with a cyclopic eye phenotype or strongly reduced eye size were characterized as moderate phenotype and embryos with almost no eye and forebrain formation were determined as strong phenotype (Figure 4A). The eye and forebrain phenotypes in Six3mix-PNA injected embryos were then confirmed by analyzing the expression of the winged-helix transcription factor *bf1*. It has been shown that *bf1* is essential for forebrain and eye development [29-31] and is regulated by Six3 [32]. As expected the *bf1* expression was strongly reduced in Six3mix-PNA injected embryos, especially in those with strong eye and forebrain phenotypes (Figure 4B).

The frequency of the obtained phenotypes was dependent on the Six3mix-PNA concentration. Whereas at lower concentrations (e.g. 50 μM) only 10% of the surviving embryos showed a weak phenotype, at higher concentrations (e.g. 400 μM) up to 95% of the surviving embryos exhibited eye and forebrain phenotypes (Figure 4A,C). A further increase of the PNA concentration to 900 μM only slightly improved the proportion of strong phenotypes, however, the frequency of mortality increased dramatically (82%; 51 of 62 injected embryos) indicating toxic effects of mixed PNAs at higher concentrations.

A critical question was how the introduced side chain modifications of the pePNA components affected the *in vivo* knock down efficiency compared to unmodified aegPNAs. Contrary to negative results reported for unmodified aegPNAs in fish embryos [19], we observed gene specific phenotypes in the injected embryos. However, mixed PNAs were more efficient than aegPNAs when compared directly (aeg- and mix-PNAs of the same length and sequence were used, both modified with TML at the C-teminus; see Figure 2). At 400 μM, where Six3mix-PNAs showed *six3* specific phenotypes in 95% of the surviving embryos, injection of Six3-aegPNAs resulted in only 54% affected embryos (Figure 4D and Additional file 5: Table S3). Furthermore, the fraction of strong phenotypes was largely reduced compared to Six3mix-PNAs (16% strong phenotypes for Six3-aegPNA versus 65% for Six3mix-PNA; calculated from Additional file 5: Table S3; see also Figure 4D). Finally, also the toxicity of aegPNAs was higher compared to mixed PNAs (compare death rates in Additional file 5: Table S3). At higher concentrations (600 μM) the results for the two PNA types was similar, however here the high death rate (>50%) indicates already considerable toxicity for both PNAs.

To examine the selectivity and the toxicity of the modified PNAs, we compared the frequency of the mortality and the obtained eye phenotypes in Six3mix-PNA injected embryos with two other control groups. First we injected a mixed PNA of the same length, but with a completely unrelated sequence (Ref16mix-PNA). Although the frequency of dead embryos slightly increased up to 400 μM PNA concentration, the surviving embryos did not show any malformations (Figure 4A; Ref16mix-PNA 400 μM). As a second control experiment to evaluate the selectivity of the antisense function we synthesized a 16mer mixed PNA with a single mismatch (Six3mix-mut-PNA; for sequence information see Figure 2). Although the mutant PNA also resulted in *six3* specific phenotypes, the frequency of embryos with eye and forebrain phenotype was strongly reduced (Figure 4D and Additional file 5: Table S3), suggesting that a single point mutation strongly affects the target selection of the mixed PNAs. This property offers the possibility to design highly specific antisense molecules that are able to select between individual allelic sequences, differing by single point mutations.

We next compared the Six3mix-PNAs directly with morpholino oligos, which represent the standard antisense molecules used for gene specific knock down in fish embryos [8]. We used a published target sequence for the medaka *six3* gene [9], which overlaps with our PNA sequences (for sequence information see Figure 2). We carefully compared the phenotypes at different embryonic stages. Morphologically, Six3mix-PNA injected embryos were not distinguishable from those injected with the morpholino oligo (data not shown), but they already appeared at lower concentrations compared to the PNAs (between 50 and 100 μM; see Additional file 5: Table S3). The appearance of unspecific phenotypes is well established for high concentrations of morpholino oligos [33]. We observed such phenotypes at concentrations of 200 μM, which already result in a high mortality rate of 90% (see Figure 4E and Additional file 5: Table S3). Again these unspecific phenotypes were highly similar to those observed for high doses of PNAs (a typical embryo is shown in Figure 4A), suggesting similar unspecific effects of both antisense molecules in the central nervous system and the eyes. For both morpholino oligos and PNAs the unspecific phenotypes only appeared

Dorn *et al. BMC Biotechnology* 2012, **12**:50
http://www.biomedcentral.com/1472-6750/12/50

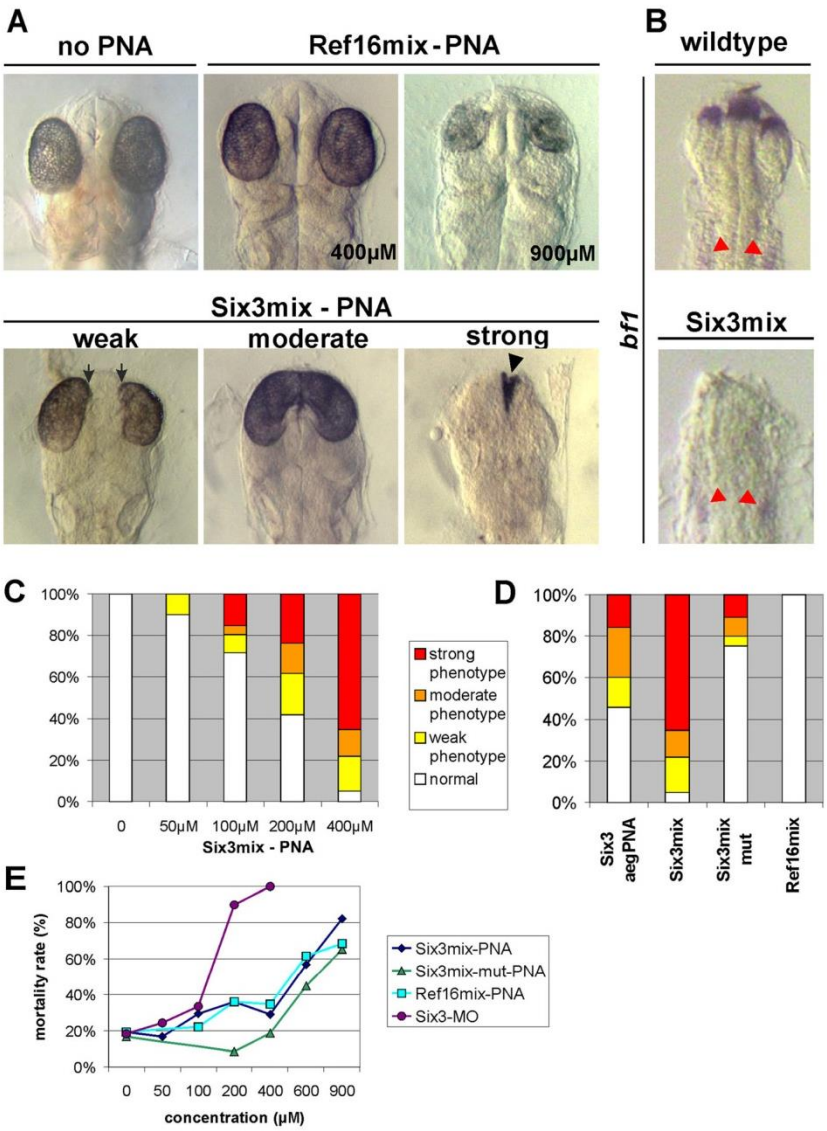

Figure 4 Injection of medaka embryos with Six3-PNAs. A wild-type embryo (no PNA injection) at 3 days is shown in (**A**). Embryos injected with 400 µM Ref16mix-PNA are indistinguishable from wild-type embryos; at 900 µM unspecific phenotypes were detected (both in A). The Six3mix-PNA injected embryos were evaluated 3 days after injection at stage 29. The phenotypes were divided into weak, moderate and strong (for criteria see text). Arrows indicate the anterior parts of the eyes pointing to the midline in weak phenotypes. The black arrowhead indicates remnants of the eye structures. All embryos in (**A**) are at stage 29 (34 somites). In (**B**) the expression of the *bf1* gene in wild-type and strongly affected embryos injected with Six3mix-PNAs is shown (both at stage 22; 9 somites). Note the presence of *bf1* expression in the otic vesicles, both in wild-type as well as in Six3mix-PNA injected embryos (marked by red arrowheads). Dorsal views of the anterior part of the embryos are shown. The quantitative evaluation of the *six3* knock down experiments is shown in (**C**) and (**D**) for the indicated PNA molecules. The percentages of phenotypes for the diagrams were calculated from the surviving embryos. PNAs shown in (**D**) were injected at 400 µM. (**E**) Shows the mortality rate of embryos injected at the indicated concentration (survival was examined 24 hrs after injection, see also Additional file 5: Table S3).

at concentrations which already cause high mortality rates (200 µM for morpholino oligos and 600-900 µM for mix-PNAs). In addition they were clearly distinguishable from the *six3*-specific phenotypes and also appeared in embryos injected with high amounts of the control PNA Ref16mix, these embryos however lacked any *six3* specific phenotypes. To further extend the comparison, we performed a series of in situ hybridisation experiments.

No differences were detectable between morpholino and mix-PNA injected embryos (see Additional file 6: Figure S3). Therefore, both types of antisense molecules generate the same range of *six3*-specific phenotypes in medaka embryos and also lead to highly similar unspecific effects at high doses. Similar to previous observations [3], we saw a higher efficiency of morpholino oligos at low concentrations. Morpholino oligos show a lower affinity for RNA compared to PNAs of the same length [34]. Our modification of aegPNAs into mixed PNAs resulted in enhanced knock down efficiency and interestingly, also in reduced affinity (see melting point determinations above). Therefore properties different from the affinity must account for the high efficiency of morpholino oligos, however, also the toxicity of these molecules peaks at substantially lower concentrations compared to the mixed PNAs (see Figure 4E).

To further demonstrate the specificity of the *six3* knock down, we injected a completely unrelated 16mer mix-PNA, directed against a sequence downstream of the *six3* AUG (Six3mix2; see Figure 2). The efficiency of this PNA was weak, since no phenotypes were observed at lower concentrations, however at 600 μM the expected typical *six3*-phenotypes appeared (see Additional file 5: Table S3). Therefore, two independent mixed PNAs directed against the *six3* mRNA resulted in the same gene-specific phenotypes, which are indistinguishable from those caused by morpholino oligos. Finally we performed a rescue experiment. For this purpose we generated mRNA of the human *six3* gene, which does not contain the targeted sequences of the medaka *six3*. At higher concentrations (25 and 50 ng/μl), injection of this mRNA causes specific phenotypes (enlarged eyes and ectopic retina, data not shown), we therefore switched to lower concentrations of 5 and 10 ng/μl. In a control experiment co-injection of *gfp*-mRNA with 400 μM Six3mix-PNA resulted in the expected phenotypes (see Additional file 7: Figure S4). However co-injection of *hSix3*-mRNA strongly reduced the overall number of *six3*-phenotypes (from 52% for the control embryos to 14 and 11%, respectively). Furthermore, no strong and moderate phenotypes appeared in these embryos any more. Therefore, the rescue experiments further demonstrate the specificity of the *six3* knock down by the mixed PNAs.

Conclusions

PNAs are highly efficient antisense molecules, which bind their mRNA target sequences with high affinity. However, some properties make their application *in vivo* difficult. Contrary to previous observations [19] we show here that unmodified aegPNAs can be used for the specific knock down of genes in living animals. However, the introduction of phosphonic ester side chains to the backbone improves the properties of the PNAs considerably. The increased hydrophilicity resulted in high solubility and the modified pePNAs worked efficiently in translational blocking of mRNA. The combination with aegPNAs in mixed molecules combined the favourable hydrophilic properties of the pePNAs with the superior binding affinity of aegPNAs. As a result, we could demonstrate an efficient and highly specific knock down of a single medaka gene *in vivo*.

Methods

PNA synthesis

PNA monomer building blocks are commercially available. Optical pure (R-configuration according to CIP rules) pePNA monomer building blocks were synthesized according to a route reported previously [35-37]. N^2-Boc-N^6, N^6, N^6-trimethyl-(L)-lysine iodide (TML) as building block was prepared as published by Chen and Benoiton [38]. A schematic presentation of the building blocks is shown in Additional file 1: Figure S1. Ethyl esters of phosphonic acid are highly stable under physiologic conditions and against esterases [39]. All PNAs were synthesized on a fully automated solid phase synthesizer (Multisynthec Syro) according to a protocol developed by Koch [40]. aegPNAs (Six3-aegPNA) were synthesized by Eurogentec.

The PNAs were dissolved in nuclease free water by repeatedly shaking and vortex ting. Finally they were gently sonicated for 2 minutes with repeated pulses. Subsequently the PNAs were divided into aliquots of 100 μl (2 mM final concentration) and kept at −80°C.

Measurement of melting points

The melting points of PNA-DNA duplexes were determined in Dulbecco's PBS (1x) without Ca & Mg with a Thermo Genesys 10s UV−vis Spectrometer and a heated cuvette (Haake F3 S water bath).

Microinjection into medaka embryos

Embryos of the medaka Cab strain were used for all experiments. Stages were determined according to Iwamatsu [41]. For the gfp experiments, first mRNA of *gfp* was *in vitro* transcribed using the T7 High Yield Message Marker Kit (Ambion) according to the manufacturer's instructions. The injection solution containing *gfp* mRNA (10 or 20 ng/μl), PNAs (50-600 μM) and Ribo-Lock RNase inhibitor (2units/μl; Fermentas) were mixed on ice and then injected into embryos at the one-cell stage. Injection of *six3* antisense molecules was done at concentrations of 50–1200 μM PNAs or morpholino oligos. After injection the embryos were incubated at normal conditions (1x ERM buffer at 27°C).

Quantification of the PNA concentration in the embryos

Sulforhodamine labeled PNAs (Gfp16mixRho) were injected at concentrations of 50 μM, 100 μM, 500 μM and 900 μM at the one-cell stage. At the four-cell stage pictures were made under the fluorescence microscope at standardised exposure times (1 ms, 10 ms, 100 ms and 1000 ms) and quantified using the ImageJ programme (background values were subtracted from all samples and only intensities within a linear range were considered for the quantification). For comparison, cellulose sulphate beads with an average diameter of 730 μm were soaked several days with the labeled PNA, shortly washed and then treated the same way under the fluorescence microscope. The volume of the embryo at the four-cell stage was determined by measuring the average diameter of the blastomeres (250 μm) resulting in a volume of 33 nl for the embryo. Using the volumes of the beads and the embryos the internal concentration of the PNA in the embryos could be calculated and resulted in an average value of 25.7 μM for injections with 100 μM PNA (injections were performed in a reproducible manner). The average injection volume therefore was 11.3 nl. All experiments were done in 5 fold repetitions.

Whole-mount in situ hybridization

Whole-mount in situ hybridization using DIG-labeled probes was performed as described previously [42].

Additional files

Additional file 1: Figure S1. Building blocks used for the chemical synthesis.

Additional file 2: Table S1. Optimisation of the PNA length. The names of the PNAs are explained in Figure 2. The embryos were injected with a mixture of 10 ng/μl gfp mRNA and 200 μM PNAs preincubated for 30 minutes on ice. After 24 hours the embryos were divided into groups according to their gfp signal intensity. The average gfp intensity of the surviving embryos was then calculated as described in the text.

Additional file 3: Table S2. Antisense function of mixed PNAs on gfp mRNA. Injections and evaluations were performed as described in Table 1, except that 20 ng/μl mRNA was used. Note that the increased amount of mRNA results in higher numbers of average gfp intensity for comparable antisense function.

Additional file 4: Figure S2. Distribution of mix-PNAs in the embryo. Medaka embryos injected with 100 μM solution of Gfp16mixRho are shown in the 2-cell stage (A) and stage 24 (16 somites; B). A dashed line indicates the outline of the yolk. A lateral view of the embryo is shown in B.

Additional file 5: Table S3. *Six3* knock down by PNAs. PNAs and morpholino oligos were injected at the indicated concentrations and the embryos evaluated after 3 days at stage 29 according to the severity of the phenotype. "Phenotypes in surviving" indicates the percentage of surviving embryos showing *six3* phenotypes.

Additional file 6: Figure S3. Comparison of mixed PNA and morpholino phenotypes. Embryos were injected with 400 μM Six3mix-PNA (PNA) or 100 μM Six3-MO (MO) and at stage 20 analysed by in situ hybridisation with probes for *pax2* and *rx2*. Typical results are shown for each group of weak, moderate and strong phenotypes, wildtype (WT) embryos are shown as a reference. An arrowhead marks *pax2* expression in the mid-hindbrain boundary, note the reduced expression in the strong group. The eye vesicles in the weak group are smaller compared to wildtype embryos, in the moderate group their size is further reduced, in the strong group no eye vesicles were detectable.

Additional file 7: Figure S4. Rescue of Six3mix-PNA injected embryos. Embryos were injected with 400 μM Six3mix-PNA (PNA) together with *gfp*-mRNA (10 ng/μl) or *hSix3*-mRNA (5 and 10 ng/μl). The phenotypes were then determined according to criteria described in the text. "Phenotypes in surviving" indicates the percentage of surviving embryos showing *six3* phenotypes.

Competing interests

The authors declare that they have no competing interests.

Authors' contributions

SD and GJ performed the injections with six3 antisense molecules, NA and BB performed the gfp knock down experiments. BW, HB and TL synthesized the PNAs. SD, NA and BB drafted the manuscript. TC conceived of the study and participated in its design and was responsible for coordinating and writing the manuscript. All authors read and approved the final manuscript.

Acknowledgements

We thank Jochen Wittbrodt for in situ probes directed against the *bf1* gene. The work was supported by the Austrian Research Promotion Agency (FFG, grant 811026/10448) and the Austrian Science Fund (FWF, grant P19571-B11).

Author details

[1]Department for Biomedical Sciences, University of Veterinary Medicine, Veterinärplatz 1, A-1210, Vienna, Austria. [2]Department for Applied Life Sciences, University of Applied Sciences, FH Campus Wien, Helmut-Qualtinger-Gasse 2, A-1030, Vienna, Austria. [3]Current address: Director's Research Unit, European Molecular Biology Laboratory (EMBL), Meyerhofstrasse 1, 69117, Heidelberg, Germany. [4]Ugichem GmbH, Mitterweg 24, A-6020, Innsbruck, Austria.

Received: 23 February 2012 Accepted: 31 July 2012
Published: 17 August 2012

References

1. Opalinska JB, Gewirtz AM: **Therapeutic potential of antisense nucleic acid molecules.** *Sci STKE* 2003, **2003**(206):pe47.
2. Wacheck V, Zangemeister-Wittke U: **Antisense molecules for targeted cancer therapy.** *Crit Rev Oncol Hematol* 2006, **59**(1):65–73.
3. Summerton J: **Morpholino antisense oligomers: the case for an RNase H-independent structural type.** *Biochim Biophys Acta* 1999, **1489**(1):141–158.
4. Corey DR, Abrams JM: **Morpholino antisense oligonucleotides: tools for investigating vertebrate development.** *Genome Biol* 2001, **2**(5):1015.
5. Morcos PA: **Achieving targeted and quantifiable alteration of mRNA splicing with Morpholino oligos.** *Biochem Biophys Res Commun* 2007, **358**(2):521–527.
6. Howard EW, Newman LA, Oleksyn DW, Angerer RC, Angerer LM: **SpKrl: a direct target of beta-catenin regulation required for endoderm differentiation in sea urchin embryos.** *Development* 2001, **128**(3):365–375.
7. Heasman J, Kofron M, Wylie C: **Beta-catenin signaling activity dissected in the early Xenopus embryo: a novel antisense approach.** *Dev Biol* 2000, **222**(1):124–134.
8. Nasevicius A, Ekker SC: **Effective targeted gene 'knockdown'in zebrafish.** *Nat Genet* 2000, **26**(2):216–220.
9. Carl M, Loosli F, Wittbrodt J: **Six3 inactivation reveals its essential role for the formation and patterning of the vertebrate eye.** *Development* 2002, **129**(17):4057.
10. Nielsen PE, Egholm M, Berg RH, Buchardt O: **Sequence-selective recognition of DNA by strand displacement with a thymine-substituted polyamide.** *Science* 1991, **254**(5037):1497.
11. Wittung P, Nielsen PE, Buchardt O, Egholm M, Norde B: **DNA-like double helix formed by peptide nucleic acid.** *Nature* 1994, **368**:561–563.
12. Nielsen PE, Egholm M: **An introduction to peptide nucleic acid.** *Curr Issues Mol Biol* 1999, **1**(2):89–104.

13. Buchardt O, Egholm M, Berg RH, Nielsen PE: **Peptide nucleic acids and their potential applications in biotechnology.** *Trends Biotechnol* 1993, **11**(9):384–386.
14. Egholm M, Buchardt O, Christensen L, Behrens C, Freier SM, Driver DA, Berg RH, Kim SK, Norden B, Nielsen PE: **PNA hybridizes to complementary oligonucleotides obeying the Watson Crick hydrogen-bonding rules.** *Nature* 1993, **365**:566–568.
15. Ray A, Nordén B: **Peptide nucleic acid (PNA): its medical and biotechnical applications and promise for the future.** *FASEB J* 2000, **14**(9):1041.
16. Nielsen PE: **PNA technology.** *Mol Biotechnol* 2004, **26**(3):233–248.
17. Germini A, Rossi S, Zanetti A, Corradini R, Fogher C, Marchelli R: **Development of a peptide nucleic acid array platform for the detection of genetically modified organisms in food.** *J Agric Food Chem* 2005, **53**(10):3958–3962.
18. Nagai Y, Miyazawa H: **Genetic heterogeneity of the epidermal growth factor receptor in non–small cell lung cancer cell lines revealed by a rapid and sensitive detection system, the peptide nucleic acid-locked nucleic acid PCR clamp.** *Cancer Res* 2005, **65**(16):7276.
19. Wickstrom E, Choob M, Urtishak KA, Tian X, Sternheim N, Talbot S, Archdeacon J, Efimov VA, Farber SA: **Sequence specificity of alternating hydroyprolyl/phosphono peptide nucleic acids against zebrafish embryo mRNAs.** *J Drug Target* 2004, **12**(6):363–372.
20. Urtishak KA, Choob M, Tian X, Sternheim N, Talbot WS, Wickstrom E, Farber SA: **Targeted gene knockdown in zebrafish using negatively charged peptide nucleic acid mimics.** *Dev Dyn* 2003, **228**(3):405–413.
21. Mäe M, Andaloussi SE, Lehto T, Langel Ü: **Chemically modified cell-penetrating peptides for the delivery of nucleic acids.** *Expert Opinion on Drug Delivery* 2009, **6**(11):1195–1205.
22. Shiraishi T, Hamzavi R, Nielsen PE: **Subnanomolar antisense activity of phosphonate-peptide nucleic acid (PNA) conjugates delivered by cationic lipids to HeLa cells.** *Nucleic Acids Res* 2008, **36**(13):4424.
23. Doyle DF, Braasch DA, Simmons CG, Janowski BA, Corey DR: **Inhibition of gene expression inside cells by peptide nucleic acids: effect of mRNA target sequence, mismatched bases, and PNA length.** *Biochemistry* 2001, **40**(1):53–64.
24. Kawakami K, Sato S, Ozaki H, Ikeda K: **Six family genes—structure and function as transcription factors and their roles in development.** *Bioessays* 2000, **22**(7):616–626.
25. Cheyette BNR, Green PJ, Martin K, Garren H, Hartenstein V, Zipursky SL: **The Drosophila sine oculis locus encodes a homeodomain-containing protein required for the development of the entire visual system.** *Neuron* 1994, **12**(5):977–996.
26. Oliver G, Mailhos A, Wehr R, Copeland NG, Jenkins NA, Gruss P: **Six3, a murine homologue of the sine oculis gene, demarcates the most anterior border of the developing neural plate and is expressed during eye development.** *Development* 1995, **121**(12):4045.
27. Jean D, Ewan K, Gruss P: **Molecular regulators involved in vertebrate eye development.** *Mech Dev* 1998, **76**(1–2):3–18.
28. López-Ríos J, Tessmar K, Loosli F, Wittbrodt J, Bovolenta P: **Six3 and Six6 activity is modulated by members of the groucho family.** *Development* 2003, **130**(1):185.
29. Xuan S, Baptista CA, Balas G, Tao W, Soares VC, Lai E: **Winged helix transcription factor BF-1 is essential for the development of the cerebral hemispheres.** *Neuron* 1995, **14**(6):1141–1152.
30. Huh SO, Hatini V, Marcus RC, Li SC, Lai E: **Dorsal-ventral patterning defects in the eye of BF-1-deficient mice associated with a restricted loss of shh expression.** *Dev Biol* 1999, **211**(1):53–63.
31. Toresson H, Martinez-Barbera JP, Bardsley A, Caubit X, Krauss S: **Conservation of BF-1 expression in amphioxus and zebrafish suggests evolutionary ancestry of anterior cell types that contribute to the vertebrate telencephalon.** *Dev Genes Evol* 1998, **208**(8):431–439.
32. Lagutin OV, Zhu CC, Kobayashi D, Topczewski J, Shimamura K, Puelles L, Russell HRC, McKinnon PJ, Solnica-Krezel L, Oliver G: **Six3 repression of Wnt signaling in the anterior neuroectoderm is essential for vertebrate forebrain development.** *Genes Dev* 2003, **17**(3):368.
33. Robu ME, Larson JD, Nasevicius A, Beiraghi S, Brenner C, Farber SA, Ekker SC: **p53 activation by knockdown technologies.** *PLoS genetics* 2007, **3**(5):e78.
34. Summerton J: **Morpholinos and PNAs compared.** *Lett Pept Sci* 2004, **10**:215–236.
35. Schöllkopf U, Busse U, Lonsky R, Hinrichs R: **Asymmetric syntheses via heterocyclic intermediates, XXXI. Asymmetric synthesis of various non proteinogenic amino acid methyl esters (functionalized in the carbon chain) and amino acids by the bislactim ether method.** *Liebigs Ann Chem* 1986, **1986**(12):2150–2163.
36. Nielsen PE, Haaima G, Lohse A, Buchardt O: **Peptide Nucleic Acids (PNAs) Containing Thymine Monomers Derived from Chiral Amino Acids: Hybridization and Solubility Properties of D Lysine PNA.** *Angewandte Chemie International Edition in English* 1996, **35**(17):1939–1942.
37. Lindhorst T, Werner B, Bock H: **Chiral compounds substituted with phosphonate acid ester functions or phosphonic acid functions.** *US Patent App* 2007, **20**:478. 100/022.
38. Chen FM, Benoiton NL: **A synthesis of N6, N6, N6-trimethyl-L-lysine dioxalate in gram amounts.** *Biochem Cell Biol* 1986, **64**(3):182–183.
39. Landt M, Everard RA, Butler LG: **5'-Nucleotide phosphodiesterase: features of the substrate binding site as deduced from specificity and kinetics of some novel substrates.** *Biochemistry (N Y)* 1980, **19**(1):138–143.
40. Koch T, Hansen HF, Andersen P, Larsen T, Batz HG, Otteson K, Orum H: **Improvements in automated PNA synthesis using Boc/Z monomers.** *J Pept Res* 1997, **49**(1):80–88.
41. Iwamatsu T: **Stages of normal development in the medaka Oryzias latipes.** *Mech Dev* 2004, **121**:605–618.
42. Aghaallaei N, Bajoghli B, Walter I, Czerny T: **Duplicated members of the Groucho/Tle gene family in fish.** *Dev Dyn* 2005, **234**(1):143–150.

doi:10.1186/1472-6750-12-50
Cite this article as: Dorn *et al.*: Side chain modified peptide nucleic acids (PNA) for knock-down of *six3* in medaka embryos. *BMC Biotechnology* 2012 **12**:50.

Additional file 1. Figure S1. Building blocks used for the chemical synthesis.

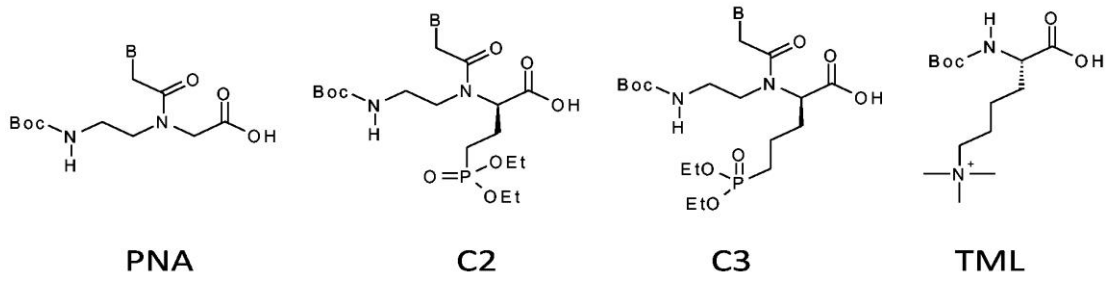

Additional file 2. Table S1. Optimisation of the PNA length.

coinjected PNA	no PNA	Gfp12	Gfp14	Gfp16	Gfp17
injected embryos	72	71	71	71	67
dead	11	7	10	5	6
death rate	15%	10%	14%	7%	9%
gfp signal strong	50	31	19	5	32
gfp signal moderate	8	26	30	28	24
gfp signal weak	3	7	11	28	3
no gfp signal	0	0	1	5	2
average gfp intensity	100%	71%	55%	28%	75%

Additional file 3. Table S2. Antisense function of mixed PNAs on gfp mRNA.

coinjected PNA	no PNA	Gfp15 mix	Ref15 mix	Gfp16 mix	Gfp16mixL4			
concentration		200µM	200µM	200µM	100µM	200µM	400µM	600µM
injected embryos	195	47	138	48	29	157	44	32
dead	22	2	15	4	3	18	6	2
death rate	11%	4%	11%	8%	10%	11%	14%	6%
gfp signal strong	129	13	96	6	10	8	0	0
gfp signal moderate	34	26	22	24	14	66	5	0
gfp signal weak	10	6	5	14	2	63	30	28
no gfp signal	0	0	0	0	0	2	3	2
average gfp intensity*	100%	59%	103%	41%	68%	30%	15%	12%

Additional file 4. Figure S2. Distribution of mix-PNAs in the embryo.

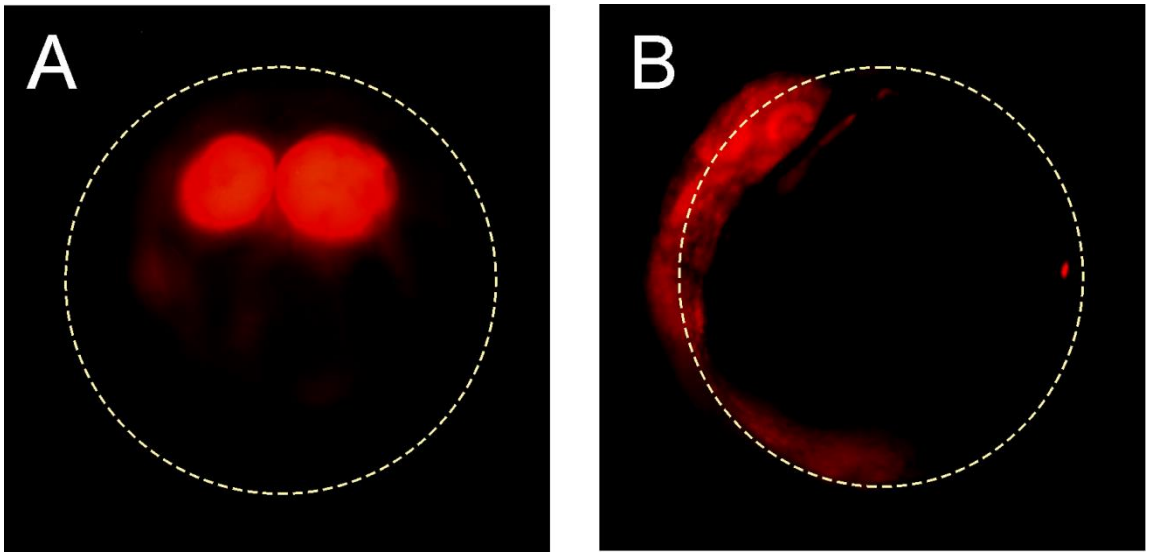

Additional file 5. Table S3. Six3 knock down by PNAs.

concentration	0	50µM	100µM	200µM	400µM	600µM	900µM
Six3mix-PNA							
number of embryos	83	36	65	86	142	67	62
dead	16	6	19	31	41	38	51
death rate	19%	17%	29%	36%	29%	57%	82%
strong phenotype	0	0	7	13	66	12	8
medium phenotype	0	0	2	8	13	7	2
weak phenotype	0	3	4	11	17	4	0
normal	67	27	33	23	5	6	1
phenotypes in surviv.	0%	10%	28%	58%	95%	79%	91%
Six3mix2-PNA							
number of embryos	83				21	31	50
dead	16				6	18	35
death rate	19%				29%	58%	70%
strong phenotype	0				0	5	4
medium phenotype	0				0	4	3
weak phenotype	0				0	3	0
normal	67				15	1	8
phenotypes in surviv.	0%				0%	92%	47%
Six3-aegPNA							
number of embryos	106		68	40	142	129	
dead	11		12	18	72	70	
death rate	10%		18%	45%	51%	54%	
strong phenotype	0		0	2	11	12	
medium phenotype	0		3	8	17	23	
weak phenotype	0		5	5	10	9	
normal	95		48	7	32	16	
phenotypes in surviv.	0%		14%	68%	54%	73%	
Six3mixmut-PNA							
number of embryos	96			104	124	105	112
dead	16			9	23	47	73
death rate	17%			9%	19%	45%	65%
strong phenotype	0			6	11	10	14
medium phenotype	0			7	9	5	1
weak phenotype	0			6	5	5	2
normal	80			76	76	38	22
phenotypes in surviv.	0%			20%	25%	34%	44%
Ref16mix-PNA							
number of embryos	83		27	25	26	39	19
dead	16		6	9	9	24	13
death rate	19%		22%	36%	35%	62%	68%
strong phenotype	0		0	0	0	0	0
medium phenotype	0		0	0	0	0	0
weak phenotype	0		0	0	0	0	0
normal	67		21	16	17	15	6
phenotypes in surviv.	0%		0%	0%	0%	0%	0%
Six3-MO							
number of embryos	66	29	27	59	17		
dead	12	7	9	53	17		
death rate	18%	24%	33%	90%	100%		
strong phenotype	0	12	11	6	0		
medium phenotype	0	6	7	0	0		
weak phenotype	0	2	0	0	0		
normal	54	2	0	0	0		
phenotypes in surviv.	0%	91%	100%	100%			

Additional file 6. Figure S3. Comparison of mixed PNA and morpholino phenotypes.

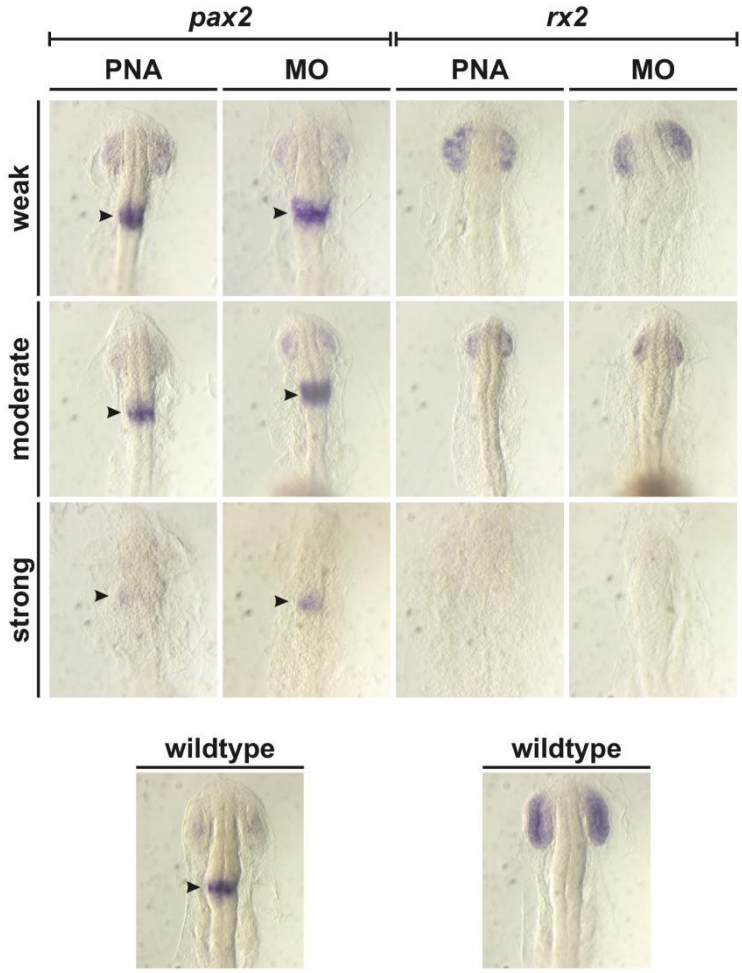

Additional file 7. Figure S4. Rescue of Six3mix-PNA injected embryos.

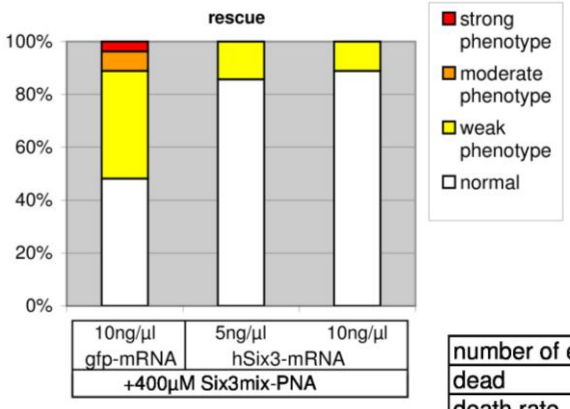

	Six3mix-PNA +		
	gfp-mRNA 10ng/µl	hSix3 mRNA 5ng/µl	10ng/µl
number of embryos	39	20	39
dead	12	6	12
death rate	31%	30%	31%
strong phenotype	1	0	0
moderate phenotype	2	0	0
weak phenotype	11	2	3
normal	13	12	24
phenotype in surviv.	52%	14%	11%

Dev Genes Evol
DOI 10.1007/s00427-009-0302-z

ORIGINAL ARTICLE

Induction of otic structures by canonical Wnt signalling in medaka

Baubak Bajoghli · Narges Aghaallaei · Gerlinde Jung · Thomas Czerny

Received: 7 April 2009 / Accepted: 30 August 2009

Abstract The Wnt family of signalling proteins is known to participate in multiple developmental decisions during embryogenesis. We misexpressed *Wnt1* in medaka embryos and observed anterior truncations, similar to those described for ectopic activation of canonical Wnt signalling in other species. Interestingly, when we induced a heat-shock *Wnt1* transgenic line exactly at 30% epiboly, we observed multiple ectopic otic vesicles in the truncated embryos. The vesicles then fused, forming a single large ear structure. These "cyclopic ears" filled the complete anterior region of the embryos. The ectopic induction of otic development can be explained by the juxtaposition of hindbrain tissue with anterior ectoderm. Fibroblast growth factor (Fgf) ligands are thought to mediate the otic-inducing properties of the hindbrain. However, signals different from Fgf3 and Fgf8 are necessary to explain the formation of the ectopic ear structures, suggesting that Wnt signalling is involved in the otic induction process in medaka.

Keywords Wnt1 · Otic induction · Cyclopic ear · Medaka

Communicated by T. Hollemann

Baubak Bajoghli and Narges Aghaallaei contributed equally to this work.

Electronic supplementary material The online version of this article (doi:10.1007/s00427-009-0302-z) contains supplementary material, which is available to authorized users.

B. Bajoghli · N. Aghaallaei · T. Czerny (✉)
Department for Biomedical Sciences,
University of Veterinary Medicine,
Veterinärplatz 1,
1210 Vienna, Austria
e-mail: thomas.czerny@vu-wien.ac.at

G. Jung · T. Czerny
Department for Applied Life Sciences,
University of Applied Sciences,
FH Campus Wien, Viehmarktgasse 2A,
1030 Vienna, Austria

Present Address:
B. Bajoghli · N. Aghaallaei
Max-Planck Institute of Immunobiology,
Stuebeweg 51,
79108 Freiburg, Germany

Published online: 16 September 2009

Introduction

In teleost fish, the inner ear originates from an ectodermal placode located at the level of rhombomere 4 (r4) of the hindbrain, and the otic placode then cavitates to form the otic vesicle (reviewed in Whitfield et al. 2002). Classical transplantation experiments demonstrated a prominent role of the hindbrain in the otic induction process. In zebrafish, grafting hindbrain tissue to the ventral side of the embryo induces ectopic otic vesicles (Woo and Fraser 1998). Members of the fibroblast growth factor (Fgf) family of secreted ligands are the best candidates for otic-inducing factors (reviewed in Riley and Phillips 2003; Whitfield et al. 2002), but the role of other modulating factors such as Wnt signalling in this process is not clear.

Experiments with lithium chloride treatment by Gutknecht and Fritzsch (1990) in *Xenopus* embryos led to multiple expanded otic vesicles. Since lithium is a potent inhibitor of GSK3; these experiments can be interpreted as a first indication of otic-inducing effects by canonical Wnt signalling. A model for induction of the chick inner ear was proposed in which *Fgf19* cooperates with *Wnt8c* to induce ectopic otic placodes (Ladher et al. 2000). Neither *Fgf19* nor *Wnt8c* was able to induce the expression of all otic markers in explants of uncommitted ectoderm, whereas a combination of both genes strongly induced the full range of markers genes. Loss of *Wnt8* function experiments in zebrafish suggest

that otic placode induction occurs normally in the absence of *Wnt8* expression (Phillips et al. 2004). In that study, morpholino knockdown of the *Wnt8* gene and misexpression of the Wnt antagonist *dickkopf 1* failed to block otic induction. Phillips and colleagues proposed that Wnt serves to regulate the temporal expression of *Fgf3* and *Fgf8* in the hindbrain, hence playing an indirect role in otic induction (Phillips et al. 2004). Furthermore, Wnt signalling was proposed to affect the preplacodal state in chicks (Bailey and Streit 2006), and in mice, it was suggested to be required after Fgf-dependent induction to maintain otic fate (Ohyama et al. 2006). Here, we address the question whether Wnt signalling is involved in otic induction in medaka fish. We demonstrate that ectopic activation of this pathway affects otic development at the time of induction by juxtaposing regions normally separated in the embryo. This is in good agreement with hindbrain tissue as a source for otic-inducing signals. However our experiments suggest that signals in addition to Fgf3 and Fgf8 induce the formation of ectopic ear structures in medaka.

Materials and methods

Fish strain and transgenic lines

Embryos of the medaka Cab inbred strain were used for all experiments. Stages were determined according to Iwamatsu (2004). All studies on heat-inducible *Wnt1*-transgenic embryos were carried out using three independent lines described previously (Bajoghli et al. 2007).

Embryo injections

Medaka embryos were microinjected into single blastomeres at the one- to two-cell stage. mRNA of mouse *Wnt1* was injected at 200 ng/μl. For transient experiments, a heat-inducible *Wnt1* construct (Bajoghli et al. 2007) was injected at 10 ng/μl together with *I-SceI* meganuclease.

Isolation of medaka *EphA4* and *Hoxb1a* probes

The primers used for the RT-PCR were as follows: for *EphA4*, 5- GAAAAGAACATCCCCATTCG-3 and 5-GAGTTGCG TTCCTCATATCCT-3; for *Hoxb1a*, 5-ATGGAAAACATG AACTCCTTTG-3 and 5-GTGCGGGACCGTTAGGTA-3. The DNA fragments were cloned into the pGEM-Teasy vector (Promega).

Whole-mount in situ hybridisation

Whole-mount in situ hybridisation was performed as described previously using DIG- or FITC-labelled probes (Aghaallaei et al. 2005).

Results

To elucidate the function of Wnt signalling during medaka otic induction, we decided to use gain-of-function analysis. Wnt1, Wnt8 and Wnt3a proteins define a functional class of Wnt ligands (Torres et al. 1996), which preferentially stimulate the canonical Wnt pathway (reviewed by Logan and Nusse 2004). We selected *Wnt1* for our misexpression experiments. Injection of *Wnt1* mRNA into medaka embryos resulted in a posteriorised phenotype characterised by severe truncations of anterior structures (Fig. 1b). Similar phenotypes have been observed upon ectopic activation of canonical Wnt signalling in various vertebrate species (Kelly et al. 1995; Stachel et al. 1993; van de Water et al. 2001; Yamaguchi and Shinagawa 1989). Since Wnt signalling has multiple functions during early embryonic development depending on the time window (Liu et al. 2005), we switched to induced expression using a heat-shock-inducible system (Bajoghli et al. 2004). Activation of the injected heat-shock *Wnt1* construct at early gastrulation resulted in the same posteriorisation phenotype seen for mRNA. However, 18% of the embryos (13 of 70) showed enlarged otic vesicles (data not shown), and in addition, 7% of the embryos (five of 70) exhibited small ectopic otic vesicles located anteriorly to the endogenous otic vesicle (Fig 1c, arrow). When we repeated these experiments with an expression construct for the zebrafish *Wnt8* gene, we also observed ectopic otic vesicles in 20% of the embryos (11 of 56; data not shown). These experiments are consistent with data for injection of a *Wnt8* expression construct in zebrafish (Phillips et al. 2004). In order to overcome the mosaic nature of the injection technique, we repeated the experiments with a heat-shock *Wnt1* transgenic medaka line (Bajoghli et al. 2007). In agreement with transient misexpression, uniform activation of *Wnt1* in the whole embryo at early gastrulation led to posteriorisation. However, instead of the isolated ectopic vesicles observed before, one large vesicle appeared in the *Wnt1*-transgenic embryos, covering the complete anterior region starting from the position of the endogenous otic vesicles (Fig 1d). At later stages, the vesicle forms inner ear structures and contains multiple otoliths (Supplementary Fig. S1). We confirmed the identity of this ectopic otic structure by marker gene expression. The expression patterns of *Starmaker* (Fig. 1f), *Eya1* and *Six1* identified the structures as otic vesicles (Supplementary Fig. S1). Due its similarity with cyclopic eyes, we named this phenotype "cyclopic ear".

In order to learn more about the effect of timing, we performed a time-course experiment by systematically varying the time of heat-shock activation in *Wnt1* transgenic embryos from 30% epiboly to the three-somite stage (Fig. 2a). The experiments indicate a strict time dependence on the extent of the anterior truncations. Early activation of Wnt signalling leads to a severe truncation of the body axis

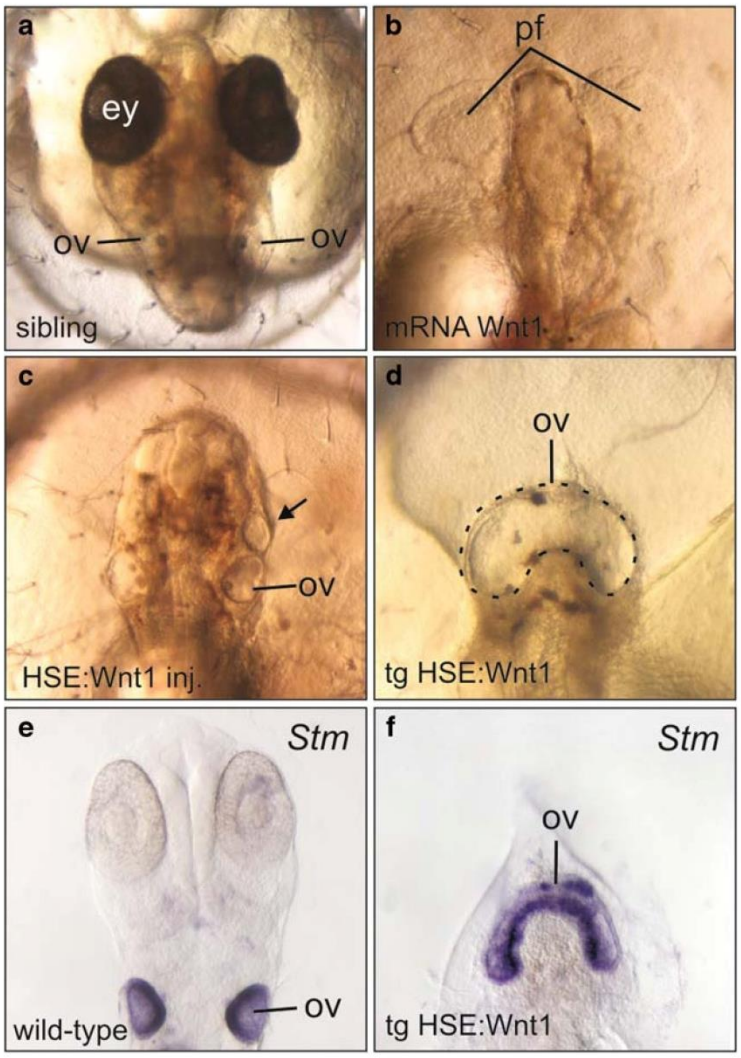

Fig. 1 Activation of the canonical Wnt pathway in medaka embryos. Dorsal views of embryos at 2dpf (**a**, **c**, **d**) and 5dpf (**b**). A non-transgenic sibling (**a**) is compared to embryos with transient injections of *Wnt1* mRNA (**b**), a heat-inducible *Wnt1* construct (**c**) and *Wnt1*-transgenic lines (**d**). Starmaker is strongly expressed in normal otic vesicles (**e**) and in cyclopic ear structures (**f**). An ectopic otic vesicle is indicated by an *arrow*. The heat-shock treatment was performed for 2 h at 39°C for **c**, **d** and **f** and 3 h at 30% for **a**. *ey* eye, *ov* otic vesicle, *pf* pectoral fin

at the level of the hindbrain, whereas posterior parts of the embryos are not affected. The extent of the axis truncations does not differ dramatically between the one cell stage (mRNA injection, see Fig 1b) and early gastrulation (Fig. 2a). However between early and late gastrulation, the truncations are gradually reduced, with midbrain structures appearing at heat shocks at 60% epiboly and forebrain structures at 80% epiboly. Ectopic Wnt activation at neurula stages only affects eye development, whereas embryos heat-shocked during somitogenesis appear normal. These phenotypes would correlate with the timing of neural plate induction by the migrating mesoderm, which might be blocked at different time points by the ectopic Wnt signals. The gradual loss of anterior structures can also be observed with hindbrain marker gene expression (see below).

In the time-course experiment, the cyclopic ear phenotype was only observed when Wnt signalling was induced at 30% epiboly. Slightly later activation of the pathway at 40% epiboly generates embryos with normal otic vesicle morphology. In previous work, we identified early gastrulation as a critical phase for otic induction in medaka (Aghaallaei et al. 2007). The ectopic Wnt activity therefore affects otic development during the induction phase.

To examine whether the effect of Wnt signalling is dosage dependent, we varied the time of heat treatment in embryos at early gastrulation from 5 min to 2 h. We used the Gfp signals originating from the bidirectional heat-shock promoter as a marker for the expression level (Fig. 2b). Interestingly, all embryos heat-treated for more than 10 min showed the same phenotype; the only

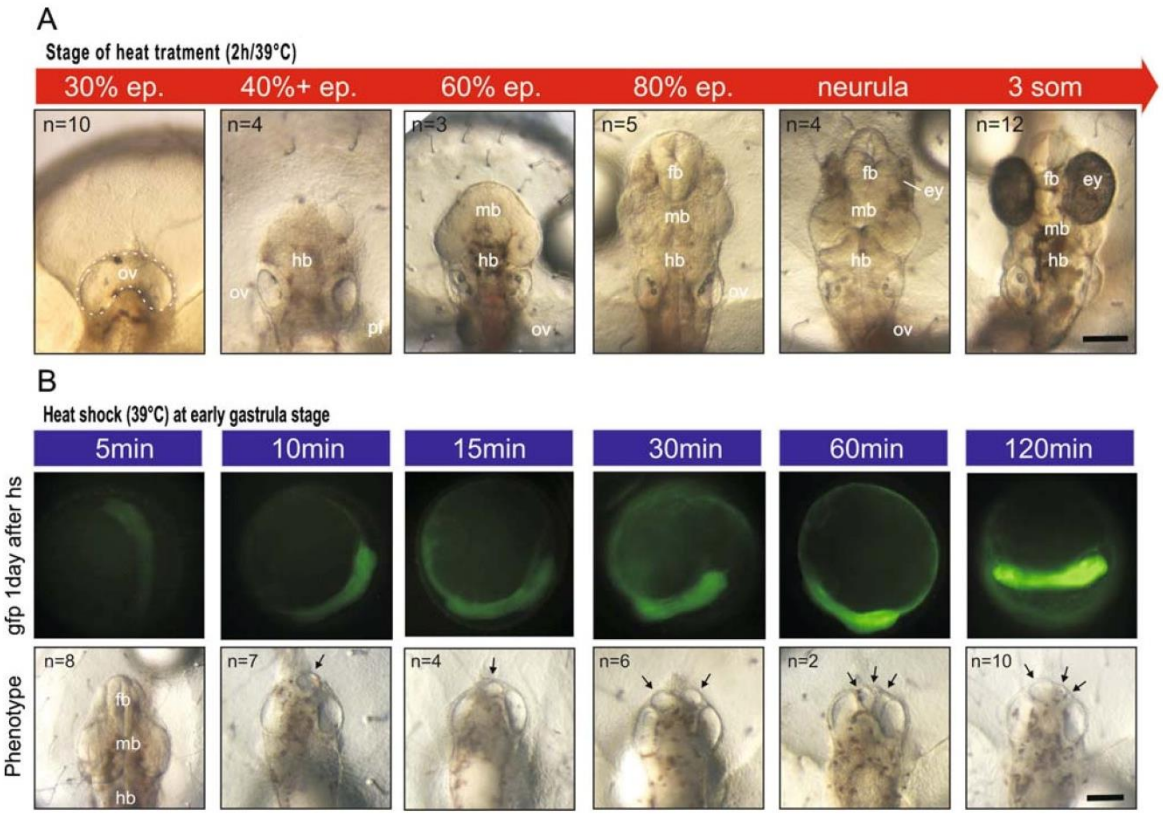

Fig. 2 Temporal and dosage effects of *Wnt1* activation during early development. Dorsal views of *Wnt1*-transgenic embryos. **a** The heat shock was performed at different stages for 2 h at 39°C. **b** *Wnt1*-transgenic embryos were heat-shocked at early gastrulation for different durations. The Gfp activity 1 day after heat shock was used as a marker. Ectopic otic vesicles are indicated by *arrows*. *n* the number of examined embryos, *ep.* epiboly, *ey* eye, *fb* forebrain, *md* midbrain, *hb* hindbrain, *ov* otic vesicle

difference was the number of ectopic otic vesicles, which increased upon longer heat treatment (Fig. 2b, arrows).

Next, we performed a time-lapse analysis. The experiments revealed that the cyclopic ear phenotype is an "end-product" of the fusion of the endogenous otic vesicles with several small ectopic structures into a single otic vesicle (Fig. 3, yellow arrows). The fusion of the vesicles started immediately after their formation (1-day-old embryos) and ended when the embryos where 3 days old and further development was arrested. Our observations show that the fusion process is dynamic and does not occur in a reproducible manner. However, the number of ectopic otic vesicles at the beginning is *Wnt1* dosage dependent.

To understand the molecular events responsible for the cyclopic ear phenotype, we analysed the expression pattern of some hindbrain and otic marker genes (for schematic presentation, see supplementary Fig. 2S online). For this purpose, one group of *Wnt1*-transgenic embryos (group A) was induced at 30% epiboly. For comparison, another group of *Wnt1*-transgenic embryos (group B) was induced at 50% epiboly, which did not develop ectopic otic vesicles. The embryos were fixed at a preplacodal stage (two-somite stage). For analysis of the hindbrain structures, we used probes directed against *EphA4* and *Hoxb1a*, expressed in r3/r5 and r4, respectively (see "Materials and methods"; Fig 4a). The expression patterns of the hindbrain marker genes confirmed the truncations of the anteroposterior axis in the *Wnt1* transgenic embryos. In group B embryos, r3 and all structures posterior to this rhombomere appeared normal (Fig. 4c, f, i, r), whereas in group A embryos, the last distinguishable rhombomere was r5 (Fig. 4b, e, h). Interestingly, the expression patterns of the marker genes suggest that the remaining anterior structures of the embryos are of one uniform fate. In group A embryos, this region anterior to r5 expressed *Hox1a*, *Fgf8* and *Fgf3* (Fig. 4b, e, h), which would be consistent with an r4 fate. In group B embryos, the region anterior to r3 expressed *Fgf8* (Fig. 4f), indicating an r2 fate. However, we also found expression of *Fgf3* and *Engrailed 2* (*En2*; Fig. 4i, r), normally not expressed in r2. In wild-type embryos, these

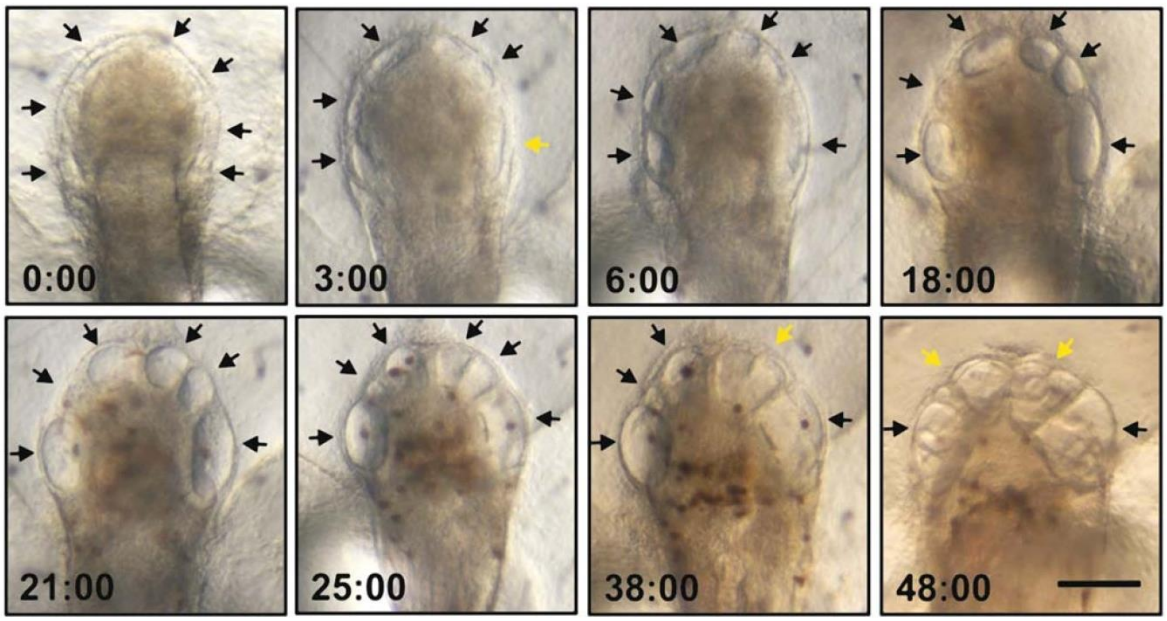

Fig. 3 Time-lapse analysis of the cyclopic ear phenotype. The otic vesicle morphology was analysed in *Wnt1*-transgenic embryos from stage 20 to stage 30. Heat shock was performed at 30% epiboly for 2 h at 39°C. Ectopic otic vesicles are indicated by *black arrows*. The fusion of vesicles is indicated by *yellow arrows*

two genes are expressed in the more anteriorly positioned midbrain–hindbrain boundary (mhb). The fate of the region anterior to r3 in group B embryos therefore remains unclear.

A combination of local competence factors together with signals from a distance is thought to induce otic structures in vertebrates (Riley and Phillips 2003; Whitfield et al. 2002). Fgf ligands are thought to mediate the signals originating from r4 (Maves et al. 2002; Phillips et al. 2001), and *Dlx3b* and *Foxi1* are the best candidates for the competence factors (Esterberg and Fritz 2009; Lee et al. 2003; Solomon et al. 2004). *Dlx3b* is a preplacodal marker gene (Liu et al. 2003) initially expressed in a horseshoe-shape surrounding the entire neural plate (Supplementary Fig. S3; Hochmann et al. 2007; Kaji and Artinger 2004). Due to the anterior truncations, the neural plate was shortened in the *Wnt1* embryos, but *Dlx3b* expression in the adjacent ectoderm remained in both groups (Fig. 4k, l and Supplementary Fig. S3). In group A embryos, the expression was upregulated in the anterior region (Fig. 4k), anticipating the development of the ectopic otic structures. In group B, strong *Dlx3b* expression was restricted to regions flanking r4, coinciding with the normal position of otic structures (Fig. 4l). The forkhead-domain containing transcription factor *Foxi1* is expressed in two domains positioned laterally to the neural plate (Hochmann et al. 2007), which we also found in group B embryos (Fig. 4o). Interestingly we detected strong *Foxi1* expression in group A embryos at the position where the ectopic otic structures develop (Fig. 4n), contrary to group B embryos, which do not show any *Foxi1* expression in this region (Fig. 4o).

Sox3 is a marker for both the epibranchial and the otic preplacodal region, whereas *Pax2* marks otic tissue specifically (Nikaido et al. 2007). In order to see whether the ectopic placodes of *Wnt1* expressing embryos are restricted to otic development, we analysed group A embryos for expression of the two marker genes (Supplementary Fig. S4). We found both genes activated in overlapping anterior regions, indicating a clear bias towards ear development. This is in agreement with data from chick and mouse experiments, where Wnt signalling was found to partition the progenitor region, positively into inner ear and negatively into epibranchial placodes (Freter et al. 2008; Ohyama et al. 2006). Group B embryos did not show expression of either marker gene in the anterior region (data not shown).

Discussion

Ectopic expression of *Wnt1* during early development of vertebrates is known to result in anterior truncations (Christian and Moon 1993). The heat-shock transgenic line allowed us to perform highly specific time-course experiments for ectopic *Wnt1* activity in medaka fish. By

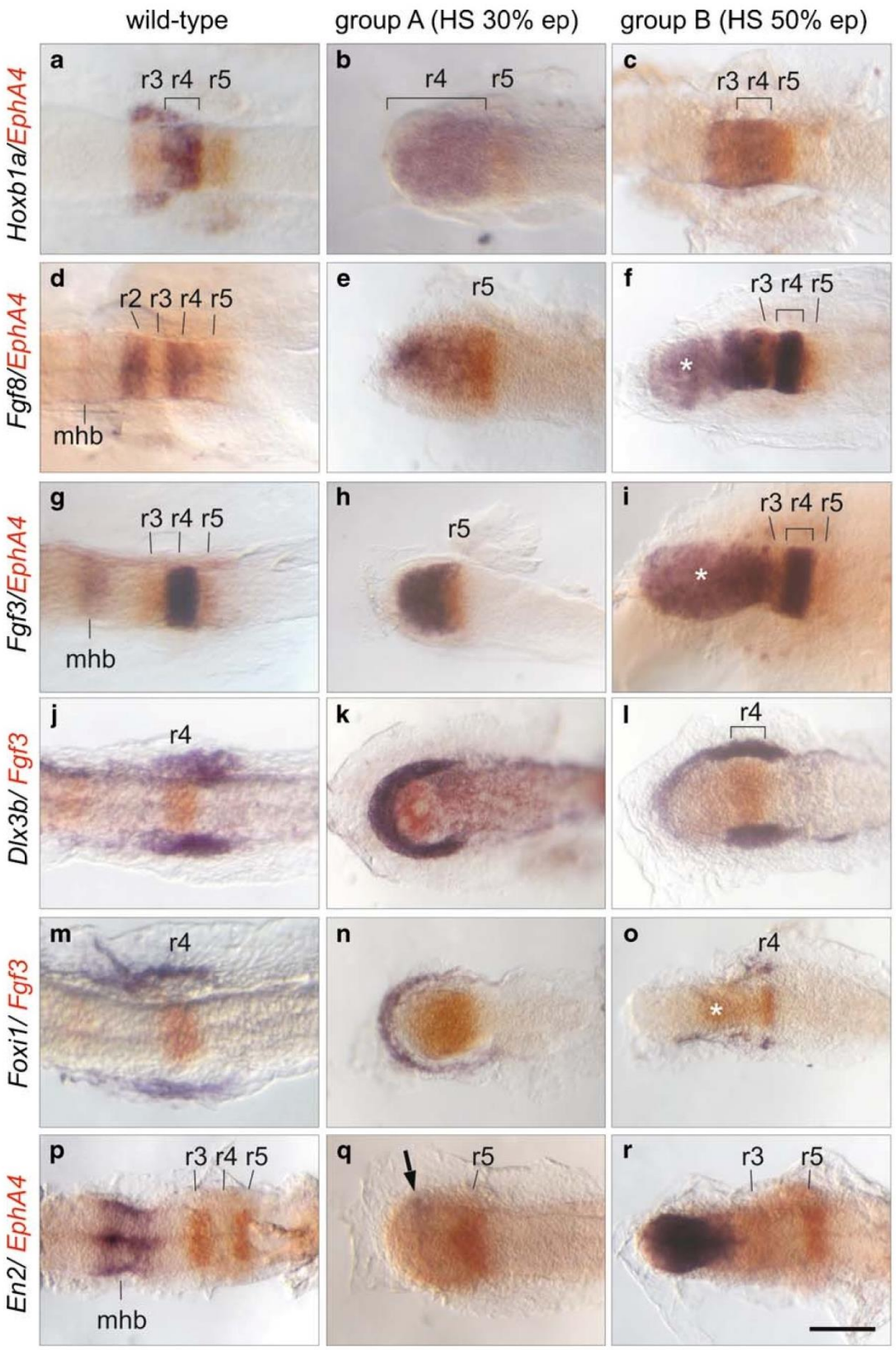
wild-type
group A (HS 30% ep)
group B (HS 50% ep)
Hoxb1a/EphA4
Fgf8/EphA4
Fgf3/EphA4
Dlx3b/ Fgf3
Foxi1/ Fgf3
En2/ EphA4
a
b
c
d
e
f
g
h
i
j
k
l
m
n
o
p
q
r
r3 r4 r5
r4 r5
r5
r2 r3 r4 r5
mhb
r4
r3 r5

Fig. 4 Analysis of hindbrain and otic marker genes in the *Wnt1*-transgenic lines. Dorsal views of embryos at two somites (**a**–**r**). Anterior is to the *left*. The positions of rhombomeres (*r*) and the mid-hindbrain boundary (*mhb*) are indicated. The heat shock of *Wnt1*-transgenic embryos was performed at 30% epiboly in group A and 50% epiboly in group B, respectively. The *asterisks* indicate anterior expression of *Fgf3* and *Fgf8*, respectively, in group B embryos, despite the fact that they lack ectopic ear structures. The *arrow* indicates weak *En2* expression. *mhb.* mid-hindbrain boundary

systematically varying the time of activation, we observed a strict dependence of timing on the extent of the anterior truncations (Fig. 2a). These phenotypes can be interpreted by a gradient of Wnt signalling being responsible for patterning the anteroposterior axis (Kiecker and Niehrs 2001). The critical influence of timing in our experiments is in good agreement with lithium exposure experiments (Yamaguchi and Shinagawa 1989).

Induction of canonical Wnt signalling in the transgenic embryos at 30% epiboly resulted in a novel phenotype. Extensive otic tissue developed and finally covered the complete anterior region of the embryos. Interestingly, these effects on otic induction seemed to be uncoupled from the axis truncations. Injection of both *Wnt1* mRNA and DNA resulted in truncations, but only the uniform misexpression at 30% epiboly in the transgenic line produced the cyclopic ear phenotype. In addition, the number of ectopic otic vesicles was dose dependent, whereas the axis truncations appeared indistinguishable from low to high *Wnt1* doses (Fig. 2b). In the zebrafish model system, activation of canonical Wnt signalling at the midblastula transition did not produce ectopic otic vesicles. This experiment was used as an argument against a role of canonical Wnt signalling in otic induction (Phillips et al. 2004). In support of these data, we also failed to induce ectopic otic tissue with constitutive active DNA constructs in medaka. However, in contrast to the latter study, we demonstrate a strict time dependence for Wnt signalling in the otic induction process, namely at 30% epiboly.

Fgf signalling plays a major role in otic induction (reviewed in Riley and Phillips 2003; Whitfield et al. 2002), and we recently could demonstrate an inducing effect of *Fgf8* misexpression during early gastrulation in medaka. In these experiments, the formation of ectopic otic vesicles was further boosted by coexpression of the competence factors *Dlx3b* and *Foxi1* (Aghaallaei et al. 2007). Here we compared groups of *Wnt1*-transgenic embryos induced at 30% epiboly (group A), with those induced at 50% epiboly (group B). In both groups of *Wnt1*-transgenic embryos, we found similar expression of *Fgf8* (Fig. 4e, f); however, only group A embryos developed ectopic otic structures. *Fgf3* expression was stronger in the anterior region of group A embryos (Fig. 4h, k, n) and weaker and more variable in group B (Fig. 4i, l, o). In addition, we observed *Dlx3b* activity in both groups (Fig. 4k, l and Supplementary Fig. S3). Therefore Fgf signalling activity and *Dlx3b* expression, representing two prerequisites for otic induction, were present in the anterior regions of both groups. However, in group B embryos, no *Foxi1* expression was detected in this region (Fig. 4o), contrary to group A (Fig. 4n). The differential *Foxi1* expression in the two groups of embryos could be critical for the induction of ectopic otic development (Fig. 4n, o). Indeed we previously found a central role for this competence factor in the preplacodal gene regulatory network in medaka (Aghaallaei et al. 2007). Loss-of-function experiments in zebrafish also confirm a critical role of *Foxi1* (Lee et al. 2003; Solomon et al. 2003).

The main result of pulsed Wnt activation is the truncation of anterior structures. In order to study the role of canonical Wnt signalling on inner ear formation, it would be ideal to uncouple the effects on the otic induction process from those on axis formation. However, this is not possible with our experimental approach. Due to the axis truncations, an expanded r4 region is positioned next to the anterior expression domains of *Dlx3b* and *Foxi1* in group A embryos. The close contact between this rhombomere and ectoderm positive for the competence factors is a hallmark of normal otic development. The ectopic activation of *Foxi1* in group A embryos could be mediated by signals of this r4 region. In agreement with this, we previously described the activation of *Foxi1* by *Fgf8* in medaka embryos (Aghaallaei et al. 2007). However, we found equal expression of *Fgf8* in both group A and group B embryos (Fig. 4e, f). Anterior *Fgf3* expression was variable in group B (Fig. 4i, l, o), but since none of these embryos developed ectopic ear structures, *Fgf3* expression is unlikely to be responsible for the differences. Therefore signals in addition to these Fgf ligands seem to be essential for the ectopic otic development in group A embryos. Alternatively, signals could be secreted from the hindbrain structures in group B embryos, which block the formation of otic tissue, but instead promote the midbrain–hindbrain boundary gene *Engrailed 2*. Interestingly, recent experiments with retinoic acid (RA) signalling in zebrafish revealed widespread ectopic otic induction upon excess activation of this pathway (Hans and Westerfield 2007). *Foxi1* was ectopically activated in these embryos, whereas other marker genes for otic induction were not altered significantly. It is therefore possible that a genetic network of different signalling pathways (Fgf/RA/Wnt) controls otic induction and in particular *Foxi1*. Further experiments will be necessary to clarify the role of Wnt signalling in this process.

Acknowledgements We thank Jochen Wittbrodt and Mirana Ramialison for the medaka *Starmaker* probe, which was kindly provided before publishing. The work was supported by the Austrian Science Fund (FWF, grant 19571-B11).

References

Aghaallaei N, Bajoghli B, Walter I, Czerny T (2005) Duplicated members of the Groucho/Tle gene family in fish. Dev Dyn 234:143–50

Aghaallaei N, Bajoghli B, Czerny T (2007) Distinct roles of Fgf8, Foxi1, Dlx3b and Pax8/2 during otic vesicle induction and maintenance in medaka. Dev Biol 307:408–20

Bailey AP, Streit A (2006) Sensory organs: making and breaking the pre-placodal region. Curr Top Dev Biol 72:167–204

Bajoghli B, Aghaallaei N, Heimbucher T, Czerny T (2004) An artificial promoter construct for heat-inducible misexpression during fish embryogenesis. Dev Biol 271:416–30

Bajoghli B, Aghaallaei N, Soroldoni D, Czerny T (2007) The roles of Groucho/Tle in left-right asymmetry and Kupffer's vesicle organogenesis. Dev Biol 303:347–61

Christian JL, Moon RT (1993) Interactions between Xwnt-8 and Spemann organizer signaling pathways generate dorsoventral pattern in the embryonic mesoderm of Xenopus. Genes Dev 7:13–28

Esterberg R, Fritz A (2009) dlx3b/4b are required for the formation of the preplacodal region and otic placode through local modulation of BMP activity. Dev Biol 325:189–99

Freter S, Muta Y, Mak SS, Rinkwitz S, Ladher RK (2008) Progressive restriction of otic fate: the role of FGF and Wnt in resolving inner ear potential. Development 135:3415–24

Gutknecht D, Fritzsch B (1990) Lithium can transform ear placodes of Xenopus into multiple otic vesicles connected by tubes. Naturwissenschaften 77:235–7

Hans S, Westerfield M (2007) Changes in retinoic acid signaling alter otic patterning. Development 134:2449–58

Hochmann S, Aghaallaei N, Bajoghli B, Soroldoni D, Carl M, Czerny T (2007) Expression of marker genes during early ear development in medaka. Gene Expr Patterns 7:355–62

Iwamatsu T (2004) Stages of normal development in the medaka Oryzias latipes. Mech Dev 121:605–18

Kaji T, Artinger KB (2004) dlx3b and dlx4b function in the development of Rohon-Beard sensory neurons and trigeminal placode in the zebrafish neurula. Dev Biol 276:523–40

Kelly GM, Erezyilmaz DF, Moon RT (1995) Induction of a secondary embryonic axis in zebrafish occurs following the overexpression of beta-catenin. Mech Dev 53:261–73

Kiecker C, Niehrs C (2001) A morphogen gradient of Wnt/beta-catenin signalling regulates anteroposterior neural patterning in Xenopus. Development 128:4189–201

Ladher RK, Anakwe KU, Gurney AL, Schoenwolf GC, Francis-West PH (2000) Identification of synergistic signals initiating inner ear development. Science 290:1965–7

Lee SA, Shen EL, Fiser A, Sali A, Guo S (2003) The zebrafish forkhead transcription factor Foxi1 specifies epibranchial placode-derived sensory neurons. Development 130:2669–79

Liu D, Chu H, Maves L, Yan YL, Morcos PA, Postlethwait JH, Westerfield M (2003) Fgf3 and Fgf8 dependent and independent transcription factors are required for otic placode specification. Development 130:2213–24

Liu F, van den Broek O, Destree O, Hoppler S (2005) Distinct roles for Xenopus Tcf/Lef genes in mediating specific responses to Wnt/beta-catenin signalling in mesoderm development. Development 132:5375–85

Logan CY, Nusse R (2004) The Wnt signaling pathway in development and disease. Annu Rev Cell Dev Biol 20:781–810

Maves L, Jackman W, Kimmel CB (2002) FGF3 and FGF8 mediate a rhombomere 4 signaling activity in the zebrafish hindbrain. Development 129:3825–37

Nikaido M, Doi K, Shimizu T, Hibi M, Kikuchi Y, Yamasu K (2007) Initial specification of the epibranchial placode in zebrafish embryos depends on the fibroblast growth factor signal. Dev Dyn 236:564–71

Ohyama T, Mohamed OA, Taketo MM, Dufort D, Groves AK (2006) Wnt signals mediate a fate decision between otic placode and epidermis. Development 133:865–75

Phillips BT, Bolding K, Riley BB (2001) Zebrafish fgf3 and fgf8 encode redundant functions required for otic placode induction. Dev Biol 235:351–65

Phillips BT, Storch EM, Lekven AC, Riley BB (2004) A direct role for Fgf but not Wnt in otic placode induction. Development 131:923–31

Riley BB, Phillips BT (2003) Ringing in the new ear: resolution of cell interactions in otic development. Dev Biol 261:289–312

Solomon KS, Kudoh T, Dawid IB, Fritz A (2003) Zebrafish foxi1 mediates otic placode formation and jaw development. Development 130:929–40

Solomon KS, Kwak SJ, Fritz A (2004) Genetic interactions underlying otic placode induction and formation. Dev Dyn 230:419–33

Stachel SE, Grunwald DJ, Myers PZ (1993) Lithium perturbation and goosecoid expression identify a dorsal specification pathway in the pregastrula zebrafish. Development 117:1261–74

Torres M, Gomez-Pardo E, Gruss P (1996) Pax2 contributes to inner ear patterning and optic nerve trajectory. Development 122:3381–91

van de Water S, van de Wetering M, Joore J, Esseling J, Bink R, Clevers H, Zivkovic D (2001) Ectopic Wnt signal determines the eyeless phenotype of zebrafish masterblind mutant. Development 128:3877–88

Whitfield TT, Riley BB, Chiang MY, Phillips B (2002) Development of the zebrafish inner ear. Dev Dyn 223:427–58

Woo K, Fraser SE (1998) Specification of the hindbrain fate in the zebrafish. Dev Biol 197:283–96

Yamaguchi Y, Shinagawa A (1989) Marked alteration at midblastula transition in the effect of lithium on formation of the larval body pattern of Xenopus laevis. Dev Growth Differ 31:531–541

Supplementary Fig. S1: Experimental strategies used for Fig.4.

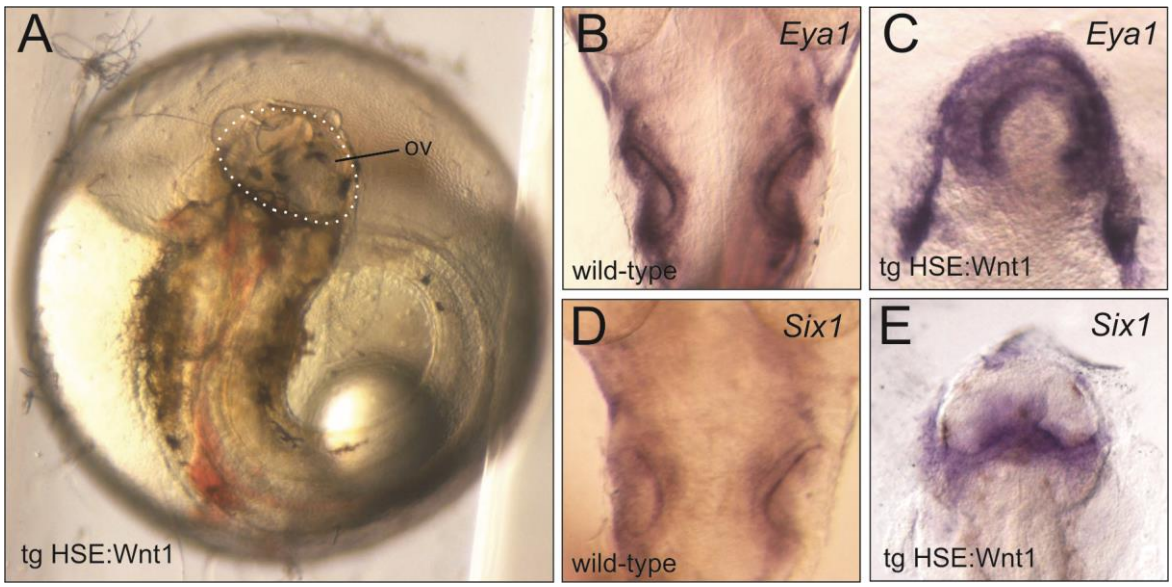

Supplementary Fig. S2: Expression of late otic marker genes in cyclopic ear embryos.

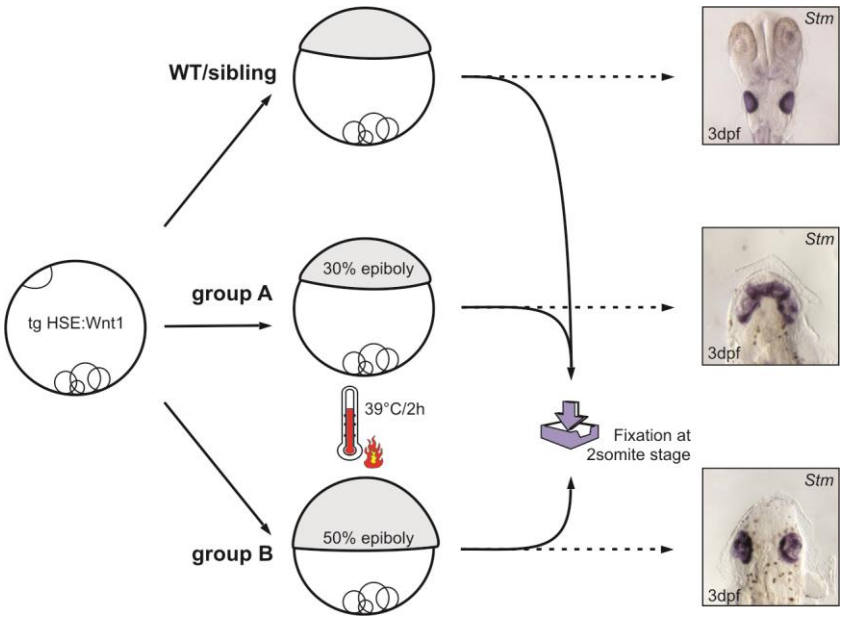

Supplementary Fig. S3: Expression of *Dlx3b* and *Fgf8* at late gastrulation in *Wnt1*-transgenic lines.

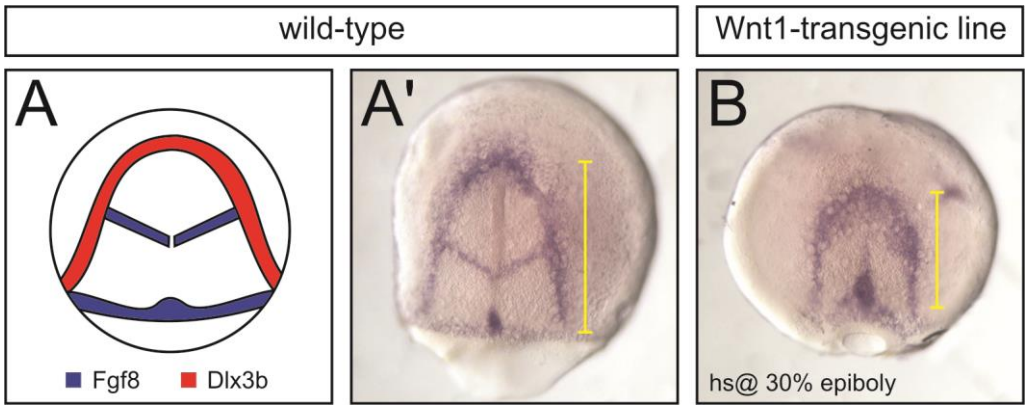

Supplementary Fig. S4: Bias towards otic development in the anterior preplacodal region.

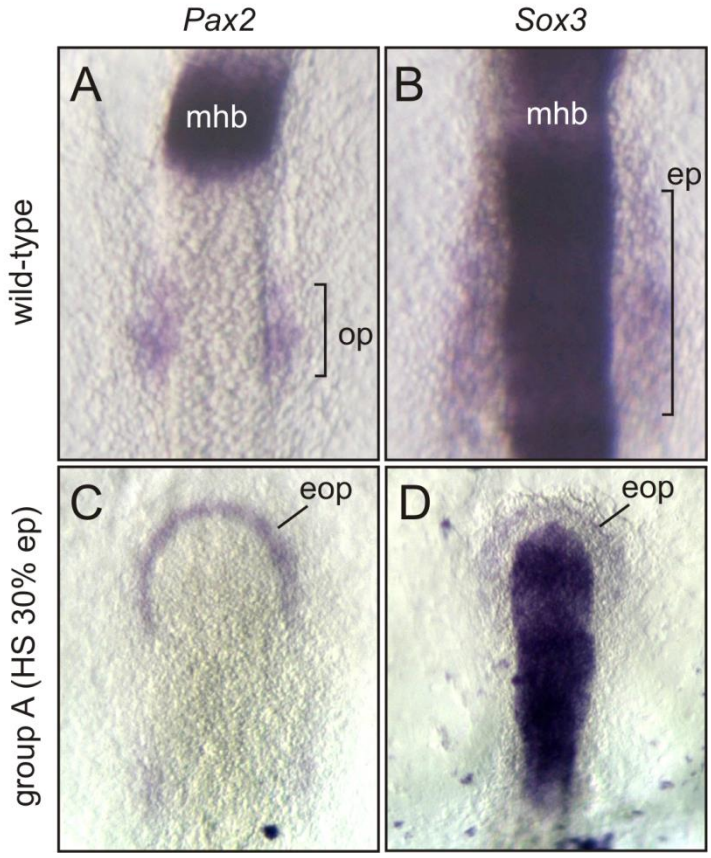

VITA

DI(FH) Gerlinde Jung

Porzellangasse 50/27, 1090 Wien
T: +43-676-4314041
@: gerlinde.jung@gmail.com

Personal information

Date of birth:	May 12, 1979, Wels
Citizenship:	Austria
Marital status:	Single

Education

2007 - present	PhD studies in Molecular Biology, University of Vienna. Dissertation topic: „ Analysis of *Tle* Genes in Medaka Embryonic Development”
2002 - 2006	Master studies in Biotechnology, University of Applied Sciences FH Campus Wien; degree with distinction. Topic of the diploma thesis: “Modulation of Endocytic Activity of Transport Receptors”
1997 - 2002	Medical studies (premedical studies), University of Vienna
1990 - 1997	High School, BG/BRG Perchtoldsdorf, 2380 Perchtoldsdorf
1985 - 1990	Primary School and High School, Tyska Skolan Stockholm, Sweden

Employment history

2013 – present **Quality Specialist**, Baxter Bioscience
Quality Assurance/Exception Management

2006 - 2012 **Scientific researcher** at the University of Applied Sciences, FH Campus Wien, Dr. Thomas Czerny.

- Independent planning and handling of projects.
- Techniques: Microinjection, *in situ* hybridization, cloning, cell culture, mammalian two hybrid, PCR.
- Management of the divisions Fish facility and Microscopy.
- Supervision of 3 master students and 5 bachelor students.
- Planning and design of a new laboratory and its relocation (Marxbox, 1030 Wien). Maintenance, design and installation of a fish facility.

- Independent planning and management of laboratory courses for students.

2005 - 2006 **Diploma student**, Department of Molecular Genetics, Medical University of Vienna, Dr. Wolfgang J. Schneider.

- Isolation and analysis of proteins and antibodies.
- Techniques: Protein/DNA/RNA extraction, Western Blot, cloning, PCR, real time PCR, cell culture, immunofluorescence.

2004 **Internship**, Institute for Veterinary Disease Control of the Austrian Agency for Health and Food Safety (AGES).

- Isolation and analysis of samples deriving from veterinary and human origin (August – September).
- Techniques: DNA/RNA extraction, PCR, real time PCR, sequencing.

2000 - 2002 **Consultant**, Call Center T-Mobile Austria.

- Customer care and technical advice.

1997 - 2000 **Assistant**, Ordination Dr. Ilse Gund-Jung; general medicine and psychotherapy.

- Assistance and maintenance in the office.
- Specimen management and their scientific analysis.

Professional Qualifications

Languages	English (Level C2), Swedish (Advanced) French, Italian (Basics)
Computer skills	Graphics editing software: Photoshop, CorelDRAW, ImageJ, AxioVision, INFINITY Capture Database research: Pubmed, NCBI, ExPASy, Ensembl Software for molecular biology: VectorNTI, BLAST
Driving license	Class B

Teaching activities

Tutor	Dissecting Course 1 and 2; Department of Anatomy, Medical University of Vienna
Tutor	Cyto- and Developmental Genetics: „The fish model system“; University of Vienna
Tutor	Macromolecular Analytics RNA; FH Campus Wien
Tutor	Forward and Reverse Genetics; FH Campus Wien

Publications

Saarela J, Jung G, Hermann M, Nimpf J, Schneider WJ. **The patatin-like lipase family in Gallus gallus. *BMC Genomics*.** 2008 Jun 12;9:281.

Bajoghli B, Aghaallaei N, Jung G, Czerny T. **Induction of otic structures by canonical Wnt signalling in medaka.** *Dev Genes Evol.* 2009 Aug;219(8):391-8.

Dorn S, Aghaallaei N, Jung G, Bajoghli B, Werner B, Bock H, Lindhorst T, Czerny T: **Side chain modified peptide nucleic acids (PNA) for knock-down of six3 in medaka embryos**. *BMC Biotechnol*, **12**(1):50.

Jung, G., Hug, M., Halter, C., Friesenhengst, A., Walzer, J. and Czerny, T. (2013). "**Diffusion of small molecules into medaka embryos improved by electroporation.**" *BMC Biotechnol,* **13**: 53.

Jung G., Dorn S., Aghaallaei N., Bajoghli B., Bock H., Werner B., Lindhorst T., Czerny T.: **The function of Tcf3 in medaka embryos: efficient knock down with pePNAs.** Manuscript in preparation.

Conferences

The hepato-oocyte-embryo axis: lipolytic enzymes in the chicken. *J. Saarela, G. Jung, J. Nimpf, W.J. Schneider;* **14. Jahrestagung der Austrian Atherosclerosis Society (AAS), Österreich St.Gilgen**

Side chain modified peptide nucleic acids (PNA) for knock-down of *six3* in medaka embryos. *Dorn S., Aghaallaei N., Jung G., Bajoghli B., Werner B., Bock H., Lindhorst T.,Czerny T.* **4th ÖGMBT Annual Meeting, Graz, Austria, 17th-19th September 2012**